The Axial Behaviour of Piled Foundations in Liquefiable Soil

Mark Stringer

Peterhouse

A thesis submitted for the degree of

Doctor of Philosophy

Department of Engineering

University of Cambridge

Declaration

I hereby declare that, except where specific reference is made to the work of others, the contents of this dissertation are wholly a result of my own original work and includes nothing which is the outcome of work done in collaboration. No part of this dissertation has been submitted to be considered for any other degree or qualification at this, or any other University. This dissertation is presented in less than 65,000 words and fewer than 150 figures and tables.

Mark Stringer

May 2012

Abstract

Understanding the mechanisms by which any engineering structure resists load is an essential requirement for its consistent and reliable design. The axial resistance which can be mobilised by piled foundations in liquefiable soils when subjected to strong shaking remains highly uncertain, and a number of piled foundations have failed in strong earthquakes as recently as 2011 . The lack of visible foundation distress in many such cases indicates that failure can occur as a result of the loss of axial capacity during an earthquake, as opposed to the laterally-dominated failure modes which have been the focus of the research community for the last 20 to 30 years.

In this thesis, a series of dynamic centrifuge experiments have been carried out to establish how the distribution of axial loads along the length of a pile changes during a strong earthquake. In each test, a 2×2 pile group was installed such that its tips were embedded in a dense sand layer which was overlain by liquefiable soil. The tests examine the effects arising from the hydraulic conductivity in the bearing layer, the influence of axial pile cap support and finally whether there are any differences in the behaviour of nominally jacked or bored piles under seismic loading.

The pile cap has been shown to play a substantial role in supporting axial loads during strong shaking. In cases where the pile cap was unable to support axial load, the majority of the axial loading was carried as pile end bearing, with some shaft friction being mobilised in both the liquefiable and bearing soil layers as a result of relative lateral displacements between the soil and pile. However, where the pile cap is able to support axial loads, the settlement of the pile cap into the soil led to a dramatic transfer of axial load away from the piles and onto the pile cap. These results imply that where substantial excess pore pressures may be generated at the depth of the pile tip, then the pile caps must be able to support significant axial load. The increased effective stresses below the pile cap were responsible for the mobilisation of shaft friction on the section of pile within the liquefiable layer. However, these piles were unable to mobilise shaft friction in the bearing layer due to the reduced lateral loading on the piles. The axial behaviour of the piled foundations after the end of strong shaking is affected by the recovery of pile end bearing capacity and is therefore strongly dependent on the hydraulic conductivity of the bearing layer.

The axial behaviour of nominally bored and jacked pile groups in liquefiable soil deposits are very different under seismic excitation, with the installation process of the latter substantially altering the soil conditions around the tips of the pile, such that in contrast to the bored pile groups, the jacked pile groups did not accumulate settlements until significantly after the strong shaking had commenced. These results imply that the method of installation is an important factor in the seismic response of a foundation, and may be more pronounced for real earthquakes where the number of strong shaking cycles may be more limited than those simulated in the experiments.

Acknowledgements

The Wingaroon

Baking has of course become a bit of a hobby, and certainly a much needed distraction during particularly challenging times. To all of the people who've helped my research to progress, I present the ganache which makes part of the Wingaroon!

Before beginning the ganache, prepare a batch of Macaroon shells, such as those described by Herme (2009).

Ingredients

20 g Pistachios, lightly toasted and blended till smooth with a little crème fraîche

10 Cardamom pods, lightly toasted & crushed

1 tsp Rose essence

150 g Crème fraîche

150 g White chocolate

Method

Bring the crème fraîche to a light boil & add the pistachio and cardamom

Boil for 3 minutes

Remove from heat and add the rose essence

Melt the chocolate in a bain marie & remove from heat and allow to cool slightly

Pass the cream through a sieve & add to the chocolate

Allow to cool in the refrigerator before piping into the macaroon shells. Leave the macaroon shells in the refrigerator in an air tight container overnight...

Contents

List of Figures

List of Tables

Nomenclature

Roman Symbols

A Cross-sectional area

C Concentration (%)

D, D_{10}, D_{50} Sand grain diameter, 10% finer, 50% finer

D_0 Pile outer diameter

D_r Relative density

E Young's modulus

e Voids ratio

e_c Cassagrande's critical void ratio

e_{min}, e_{max} Minimum, maximum voids ratio

f Frequency

F_{eff} Lateral load applied by soil

f_n Natural frequency

G Shear modulus

G_s Specific gravity

h Hydrostatic head

I Second moment of area

i Hydraulic gradient

J Polar moment of inertia of pile group about its center of gravity

K Earth pressure coefficient

Nomenclature

K, K_w Hydraulic conductivity, hydraulic conductivity with water

$K_{cap}, K_{shaft}, K_{base}$ Equivalent springs: cap, shaft, base

L_{eff} Separation of pile cap centre of mass and F_{eff}

$L_p, L_{p,loose}, L_{p,dense}$ Pile length, pile length in loose sand, pile length in dense sand

$m_{accelerometer}$ Mass of accelerometer

$m_{pilecap}$ Mass of pile cap

N Length scaling factor in the model

p Pressure

P, P_1, P_2 Axial pile load

Q Flow rate

q Deviatoric stress

q_b, Q_b Pile end bearing pressure, load

$Q_s, Q_{s,dense}$ Axial shaft load, axial shaft load in dense layer

R_D Relative density

$r_{footing}$ Footing radius

R_N Normalised surface roughness

r_u Pore pressure ratio

s Pile centre to centre spacing

S_r Saturation Ratio

t Time

u Pore pressure

V_{fluid} Volume of pore fluid

V_{pore} Total volume of voids in model

$\ddot{x}_{cap}$ Horizontal acceleration of pile cap

Greek Symbols

Δ Lateral displacement of pile or pile cap

δ Interface angle of friction

γ' Effective unit weight

γ_w Unit weight of water (9.8 kN/m³)

θ Angle of rotation

$\ddot{\theta}_{cap}$ Angular acceleration of pile cap about its center of gravity

μ Coefficient of friction ($= \tan \delta$)

ν Poisson's ratio

$\rho_{pilecap}$ Settlement of pile cap

σ'_r Radial effective stress

σ_v, σ'_v Vertical stress, vertical effective stress

τ, τ_{crit} Shear strength, critical state shear strength

τ_{sf} Shaft friction

$\xi_{settlement}$ Normalised settlement of free standing piles

$\bar{\tau}_d, \bar{\tau}_l$ Average shaft friction: dense layer, loose layer

$\bar{\tau_{sf}}$ Average shaft friction

ϕ_{crit} Critical state angle of friction

υ_{20} Viscosity at 20 ^{o} C

υ_w, υ_f Viscosity of water, viscosity of fluid

$\varnothing$ Diameter

Nomenclature

Acronyms

CPT Cone penetration test

CSL Critical state line

ESB Equivalent shear beam

FFT Fast fourier transform

FOS Factor of safety (against normal working loads)

$HPMC$ Hydroxy-propyl methyl cellulose

$LVDT$ Linear variable displacement transducer

$MEMS$ Micro-electro-mechanical systems

OCR Overconsolidation ratio

PE Piezoelectric

PHC Pre-stressed high strength concrete

PPT Pore pressure transducer

PTL Phase transformation line

RAM Random access memory

SAM Stored angular momentum

SPT Standard penetration test

Chapter 1

Introduction

1.1 Problem statement

Piled foundations are well established as a means for transferring axial loads applied by
a superstructure to stiff and competent soil layers in cases where the soil near the surface
is unable to provide sufficient axial resistance at a tolerable level of settlement. Piles
are particularly appropriate for supporting port structures and bridge piers, where soft or
loose soil deposits often occupy several metres of the near-surface soil profile. Additionally,
piles are useful for supporting structures on man-made fills, or on historical flood plains
or swamps, where again, relatively loose soil conditions exist near the ground surface. As
a result of the extensive use and wealth of research carried out on piled foundations, the
understanding of the axial response of piled foundations under typical working loads is
relatively well advanced. Additionally, when entering the construction phase of a new
project, piles can be load-tested to ensure that the behaviour of the piles will deliver
acceptable performance. However, a great deal of uncertainty surrounds the performance
of piled foundations during strong earthquakes, especially if liquefaction of some or all of
the soil profile occurs, due to the reduction of soil strength and stiffness.

During the 1995 Hyogoken-Nambu earthquake in Kobe, widespread liquefaction of the
man-made fills led to a series of piled foundation failures, many of which were subse-
quently carefully analysed and documented. Many of these case histories relate to the
performance of piled foundations which were subjected to significant lateral demands,
becoming the focus of a concerted research effort over the past 15 years. However, many
examples of other modes of piled foundation failure occurred (Tokimatsu *et al.*, 1996),
which have received relatively little attention. The map shown in Figure 1.1(a) indicates
that the damage to piled foundations in the 1995 Hyogoken-Nambu earthquake was very
widespread and while concentrated damage occurred near to the shore due to lateral

1. INTRODUCTION
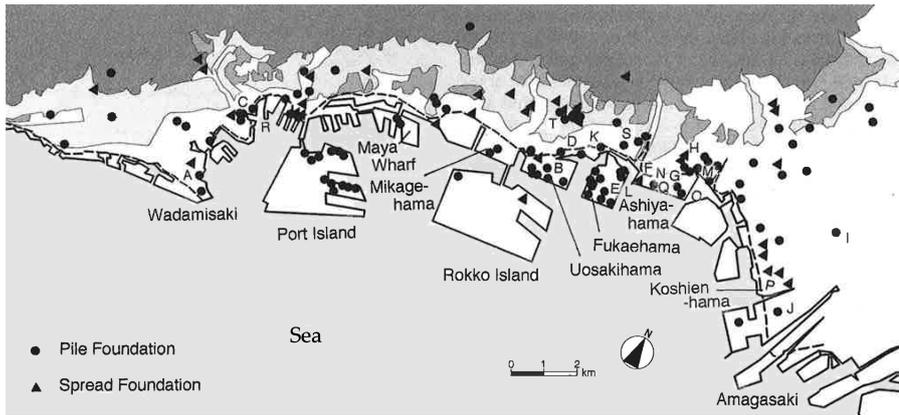
(a) Map showing location of many of the known foundation failures during 1995 Hyogoken-Nambu earthquake
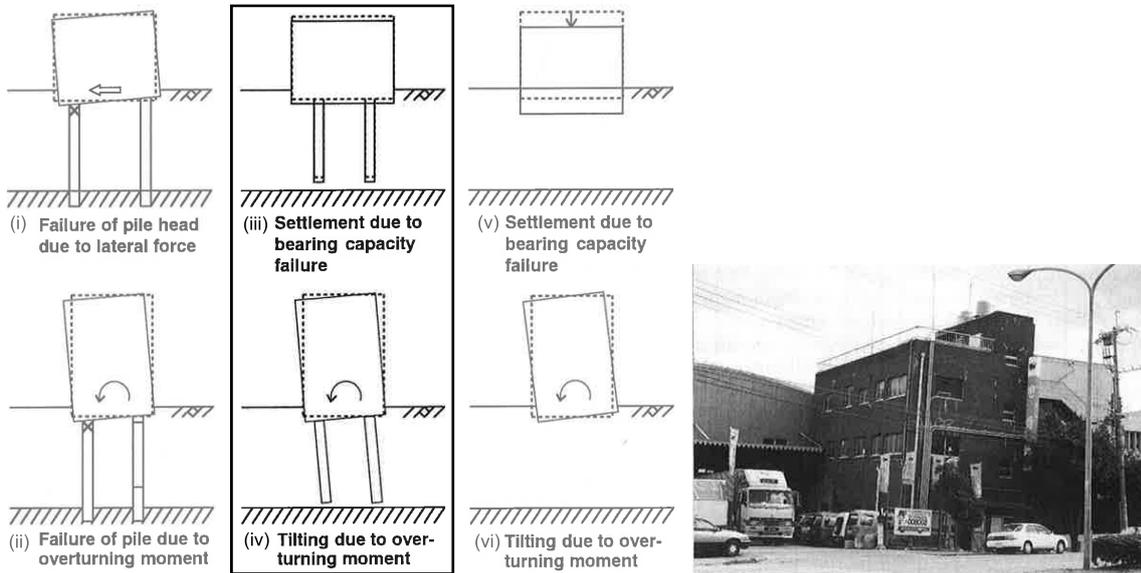
(b) Mechanisms of pile failure (modified)

(c) Tilting of building in Fukaehama

Figure 1.1: Examples and mechanisms of foundation failure during 1995 Hyogoken-Nambu earthquake, Tokimatsu *et al.* (1996)

spreading, several failures occurred further in shore where the permanent lateral ground displacements were negligible. The observed modes of pile failure in level ground were summarised by Tokimatsu *et al.* (1996) and are shown in Figure 1.1(b), with those pertaining to the pure axial failure of the foundations highlighted. In these cases, no visible distress was observed on the piled foundations, yet settlements in excess of 1 m were reported for some buildings, while many others suffered excessive tilts which rendered them unusable after the earthquake (i.e. Hamazake elementary school and the Uosaki junior high school). In cases such as these, it was concluded that due to the lack of distress on the piled foundations, the failure of these buildings was due to a loss of axial load carrying capacity.

(i) Projection of pile due to ground settlement (ii) Small horizontal gap at building base

(a) Mechanisms of gap formation

(b) Horizontal gap beneath building
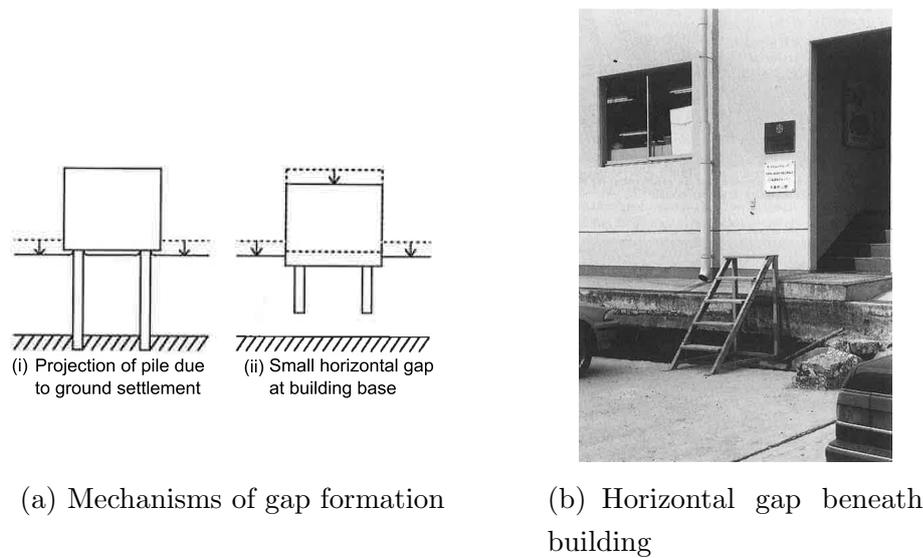
Figure 1.2: Formation of large gaps beneath pile-supported buildings during 1995 Hyogoken-Nambu earthquake, Tokimatsu *et al.* (1996)

Figure 1.3: Building supported by friction piles showing no apparent differential settlement, Japanese Geotechnical Society (1996)

While the previous examples highlight buildings which have failed by settling into the ground, there were also numerous cases where the performance of piled foundations was "good", but due to the large post-earthquake subsidence of the liquefied soil, buildings were left proud of the ground's surface, as shown in Figure 1.2(b). In such cases, substantial remedial work is required both to infill the gap beneath the building, and to restore broken services (such as water pipes etc.) which break as the soil settles away from the building.

Finally, some buildings did not suffer foundation distress despite clear indications of liquefaction damage in the immediate area (Tokimatsu *et al.*, 1996). One such example is the Ferry Terminal, shown in Figure 1.3, on the North-East section of Port Island, where the building and its friction piles settled "equally with the ground surface, maintaining a relative level between the two."

The extensive liquefaction related problem suffered by pile-supported structures are not unique to the 1995 Hyogoken-Nambu earthquake, with similar occurrences being recorded in other strong earthquakes, such as the 2001 Bhuj earthquake (Madabhushi *et al.*, 2005) and the 2010 Maule earthquake (Bray & Frost, 2010).

Despite numerous examples highlighting the importance of understanding the axial load transfer mechanisms in liquefied soil both during, and after strong shaking, this topic remains understudied and poorly understood. This lack of knowledge severely inhibits the ability to make consistent and reliable design decisions for these foundations in situations where liquefaction during a strong earthquake is an issue. This thesis therefore aims to clarify the mechanisms by which axial load is carried by piled foundations in liquefied soils during an earthquake.

1.2 Options for research methodologies

When carrying out research into geotechnical earthquake engineering, some consideration must be given towards selecting an overriding approach to the research, since this influences many aspects of the design of the research programme. A number of complementary techniques have been developed which include:

- Dynamic centrifuge modelling

- 1g modelling (small scale and large scale)

- Field testing

- Pseudo-static modelling

- Numerical modelling

Each of these techniques have particular strengths and weaknesses. For example, pseudo-static and numerical methods require a large initial effort, but once set-up, allow many thousands of scenarios to be considered, allowing the effect of small details to be considered. However, when using these methods, the response of the model is only as good as the underlying constitutive model, leaving the question of whether there are additional effects which have not been captured. In such cases, it is possible that the behaviour of the structure predicted by the numerical model might not be a good representation of reality. This is especially apparent when studying the complex interactions between a structure and the soil, where the displacements can be large and the models may be unable to correctly capture the dynamic changes in pore pressure occurring close to the

structure. On the other hand, while carrying out large scale tests on a shake table such as the E-Defense facility in Japan yields a response which is dependent on the behaviour of a real soil, these techniques are hugely expensive, both in terms of cost and human effort, meaning that research projects might only involve one or two experiments. However, it must be acknowledged that exceptionally large amounts of data can be generated in each test.

Full scale field testing allows the effects of soil stratification and non-homogeneity to be captured in the response of the prototype of interest. However, it may be difficult to generalise the results from such studies, since particular mechanisms governing behaviour cannot be easily identified. Further, since ground motions cannot be applied, researchers must either wait for a seismic event to occur, or attempt to investigate aspects of behaviour not associated with shaking (i.e. behaviour which might be observed following the end of strong shaking as excess pore pressures dissipate). Full-scale field testing therefore remains of limited use in dynamic geotechnical research.

Small scale physical modelling offers an avenue for research which overcomes many of the problems associated with other research methods. The use of small scale models with real soil allows the complex behaviours of the model to be captured, but generally without the large cost and time burdens of large scale testing. However, the non-linear stress-strain characteristics of soil mean that in order to replicate the behaviour which might be observed in the field, it is necessary to ensure that the stresses and strains are at the same level within the model. This means that in order to obtain realistic results from a small-scale model, it is necessary to use a centrifuge in order to elevate the gravity field to ensure that the appropriate stresses are present within the model.

Similar to the research techniques just described, centrifuge modelling is not perfect. When carrying out research on small scale models in a geotechnical centrifuge, it is not normally possible to exactly model a specific field scenario. Instead, the researcher must make a number of simplifications to create a "prototype," which although not an exact representation of reality, still manages to capture the important physical characteristics of the specific problem being considered. The researcher can then make a scaled version of this prototype, and use a number of scaling laws (which will be descibed in Section 3.2) to link the observed behaviours of the model to this simplified version of reality. However, as described by Haskell *et al.* (2012), the response of the structure can be fundamentally altered by the way in which the model is altered, such that careful consideration must be given to what the results coming from a centrifuge experiment actually represent. Additionally, as will be discussed in Sections 2.3.2 & 3.2, there remain some issues regarding the scaling of results between the centrifuge model and the prototype. However, if these obstacles can be overcome, then centrifuge modelling allows a series of carefully controlled

experiments to be carried out, allowing specific parameters to be altered in relative isolation without the concerns relating to the constitutive behaviour of the soil itself. This makes centrifuge modelling a useful tool for the study of a wide range of boundary value problems and has therefore been selected for use in this research programme and will be discussed further in Chapter 3.

1.3   Scope of the research

When considering the observed failures of piled foundations, a logical dividing line might well be drawn between those where significant lateral displacements of the soil occurred due to persisting shear forces (i.e. sloping ground or near quay walls) and those which have occurred in level beds. While the occurrence of axial failures may occur in the former case, it is often the lateral effects which dominate. Therefore, in this study, the research will be restricted to the consideration of piled foundations within level beds.

As hinted in the description of full-scale field testing, real soil profiles can be far from the uniform soil profiles which are typically prepared in a laboratory. However, it is normal practice to simplify a real soil profile into a limited number of different soil layers for modelling purposes. By following this approach, it becomes possible to produce more consistent models whose results can be more readily linked to specific aspects of soil behaviour and allow meaningful investigations into the effects of different parameters on the overall response of the system. In the case of a piled foundation, the simplest idealised profile may include a single layer. However, more common is the situation where the pile passes through a loose layer, with its tips embedded in a relatively dense bearing layer. As shown in Figure 1.4, it might be reasonable to model the soil profile at Kobe Port as a layer of loose sand approximately 14 m thick underlain by a layer of dense sand. In this research programme, the experiments which will be presented were designed specifically to investigate the behaviour of pile groups embedded in these dual layer soil profiles.

Finally, piles are rarely found as isolated members. The layout of a piled foundation often involves groups of between 2 and 4 piles, placed at strategic locations across a larger building footprint. In the case of a bridge foundation, it is typical to include a more even distribution of piles across the area of the foundation. While interaction between the different elements of a larger foundation will undoubtedly occur, this research programme does not intend to investigate this aspect. Rather, consideration will be given to the case of a single 2×2 pile group, which, while greatly simplified, should capture many of the important aspects of pile behaviour during an earthquake, which will be discussed further in Section 2.4
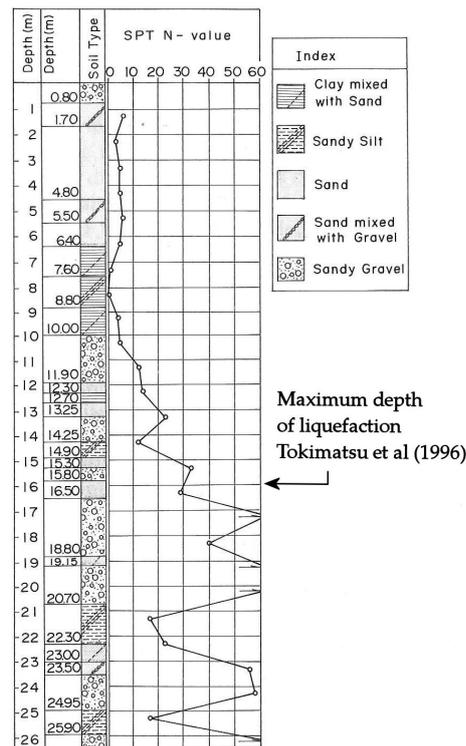
Figure 1.4: Soil profile from Kobe Port, (modified from Inagaki *et al.*, 1996)

In working towards the aim of clarifying the axial behaviour of piled foundations, this research will restrict itself to considering the situation of single 2×2 model pile groups in saturated, level ground consisting of a simplified dual layer soil profile.

1.4 The axial behaviour of piled foundations during earthquakes: a roadmap

Following a discussion of existing literature on the behaviour of soils subjected to cyclic loading, and the behaviour of piles under normal and seismic conditions in Chapter 2, a series of research questions are formulated which guide the ensuing investigations. Chapter 3 addresses some of the issues involved with dynamic centrifuge modelling, as well as introducing the actuator used to apply the model earthquakes, and the techniques used for preparing the sand profiles, including the implementation of an automatic saturation system. Chapter 3 also includes details of the pile groups used in the experiments and a discussion of the limitations of the instrumentation used in the models.

Following this background information, Chapters 4 to 6 consider the axial behaviour of the model pile group while subjected to dynamic excitation. In the first two of these chapters, the behaviour of bored piles is considered, and in Chapter 4, consideration is given to the case where a pile group is embedded such that the pile cap is not in contact

with the soil surface, allowing the load transfer mechanisms of the pile to be studied without the complication of the role of the pile cap. While the axial load transfer remains the focus of this chapter, additional work which considers the settlement response of these pile groups is presented along with a proposed normalisation technique. In Chapter 5, attention moves to the more common scenario where pile caps are in contact with the ground surface and can therefore play a role in supporting the axial loads during the earthquake. This chapter therefore focusses on how the pile cap affects the distribution of axial loads during an earthquake.

Following the discussion in Chapter 2 which highlights the importance of the installation method on the observed axial response of pile groups under normal working loads, Chapter 6 aims to investigate whether the axial behaviour of a pile group during an earthquake is significantly affected by the method of installation. Pile groups which are representative of bored piles and jacked piles are therefore tested and compared. Finally, this chapter attempts to investigate the effect of pile surface roughness on both the pile group settlement and the axial load carrying capacity of the piles during the earthquake.

Having established the behaviour of piled foundations during an earthquake, Chapter 7 considers the behaviour of the pile groups discussed in the preceding three chapters in the moments after the earthquake, when excess pore pressures begin to dissipate. The investigation focusses on the differences in behaviour arising as a result of the different loading conditions at the pile head, and the implications of differences in hydraulic conductivity on the development of axial load and subsequent settlement after an earthquake.

Finally, in Chapter 8, results from the Chapters 4 to 7 are summarised and discussed in the context of their implications for designing piled foundations in seismic areas. Based on the results of this experimental programme, avenues for further research are described.

It should be noted that in this thesis, all of the numeric quantities presented have been converted to prototype scale, using the scaling laws given by Schofield (1981) (which will be described in Section 3.2).

Sketches of the model layouts used in the experiments described in Chapters 4 to 6 are given at the beginning of the relevant chapter. In addition to these, more detailed model layouts are provided in Appendix A.

Chapter 2

Review of Literature

2.1   Introduction

In order to understand the behaviour of a piled foundation during an earthquake, it is necessary to understand some of the effects which may contribute to the observed response of the piles. In this Chapter, some of the key concepts which are relevant to the experimental programme discussed in this thesis are presented. The Chapter is broken into three main sections, beginning with a summary of the expected response of soils to both monotonic and cyclic shear loading. A brief overview of the axial resistance of a piled foundation is then presented, including a discussion concerning the influence which the mode of installation has on the axial stiffness of piled foundations. Finally, existing research pertaining to the axial behaviour of piled foundations subjected to seismic loading and subsequent dissipation of excess pore pressure is considered. Furthermore, concepts are introduced in this section which may influence the axial capacities of the pile group under seismic loading.

2.2   Behaviour of soil

In order to study a more complex geotechnical problem, it is necessary to have a basic framework which describes the behaviour of a soil as it is subjected to different loading scenarios. The *Critical State* model described by Schofield & Wroth (1968) provides an accessible way of understanding the behaviour of soil, linking the parameters of deviatoric stress (q), confining pressure (p') and voids ratio (e). In the model, soils which are subjected to shear stresses exceeding a yield surface will attempt to reach a unique line, known as the critical state line (CSL), at which point, shearing can continue without changes to the soil's state. In e-p' space, the critical state line plots at a lower voids ratio

than a normally consolidated soil at the same confining pressure. When shearing takes place slowly, soils which are at a greater voids ratio ("looser") than the CSL at the same p' will contract (reduction in voids ratio) in order to reach the CSL, while those at lower voids ratio ("denser") will dilate (increase in voids ratio). If the soil is saturated, these changes in voids ratio imply that pore fluid must be migrating within the soil skeleton to accommodate the changes in void volume. If the shearing takes place rapidly, then fluid flow cannot occur quickly enough, and instead, a change in pore pressure occurs; contractile soils tending to increase their pore pressures, while dilative soils will experience a reduction in pore pressures. This concept was discussed in the context of cyclic loading by Martin *et al.* (1975), who argued that the volumetric strain potential of a saturated and dry soil should be the same, and therefore the increase in excess pore pressure generated by cyclic loading should equal the product of the total expected volumetric strain and the bulk modulus of water. Since the grains become less loaded as a result of the pore pressure increment, the total volumetric strain was assumed to be equal to the volumetric strain occurring in a dry soil skeleton as a result of the cyclic loading minus the elastic volume recovery of the soil grains.

It must be noted that while the framework of critical state soil mechanics is generally referred to in this thesis, an alternative framework was proposed by Casagrande (1936), who initially defined a critical void ratio (e_c), which separated the contractile and dilative soils and which was independent of confining pressure. While it is now generally accepted that original definition of critical void ratio was incorrect, many US sources (e.g., Kramer, 1996) refer to Casagrande's updated model which included the effect of confining pressure on the critical voids ratio. The similarity between Casagrande's steady state model and the critical state model of Schofield & Wroth (1968) has led to the two frameworks remaining in use concurrently.

In the critical state framework, the shear strength of a soil at the critical state is proportional to the effective stresses in the soil according to a frictional strength model, as shown in Equation 2.1. While the shear strength of the soil shown in the equation is linked to the vertical effective stress, analogous forms of the equation exist for different stress spaces (i.e. q-p'). The equation implies that the generation of positive excess pore pressures leads to a reduction in the shear strength of the soil. In extremis, Equation 2.1 implies that if excess pore pressures rise sufficiently high to cause the effective stresses to fall to zero, then the shear strength of the soil is likewise reduced to zero.

$$\tau_{crit} = tan(\phi_{crit})\sigma'_v \tag{2.1}$$

2.2.1   Loose sands subjected to undrained cyclic loading

Under earthquake loading, shear waves, propagating from the bedrock are the major factor in the occurrence of ground movements (Kramer, 1996). As a result, soil behaviour relevant to earthquakes is commonly studied by applying cyclical shear loads on a soil body.

The behaviour of loose soils under cyclic loading was investigated by Seed & Lee (1966), who applied cyclic axial loading (which generates cyclic shear on a 45 ^{o} plane) in an undrained triaxial test. In these tests, the contractile nature of the soil under shear led to the gradual generation of excess pore pressures until the effective stresses had reduced close to zero (excess pore pressure ratio, $r_u = 1$). At this point, which was termed initial liquefaction, the stiffness of the soil was observed to reduce dramatically, leading to the development of large cyclic strains as shown in Figure 2.1.

The behaviour of loose soils under cyclic loading is further discussed by Ishihara *et al.* (1975), who introduces the concept of a phase transformation line (PTL), which demarcates the contractive and dilative responses of a soil under shear. A very similar concept was also put forward by Luong & Sidaner (1981), who used the term characteristic state line (equivalent to Ishihara's PTL). Figure 2.2(a) shows the characteristic state line (or PTL) at a constant stress ratio extending outwards from the origin, and below the failure line. As loose soils are sheared cyclically, the excess pore pressures increase gradually, leading to a reduction in the confining pressure. The stress path therefore gradually moves from right to left in Figure 2.2(a). Ishihara *et al.* (1975) explains that as long as the stress path does not reach the PTL, then the increases in pore pressure during the unloading of the sample is quite modest. However, if the cyclic loading continues, then there comes
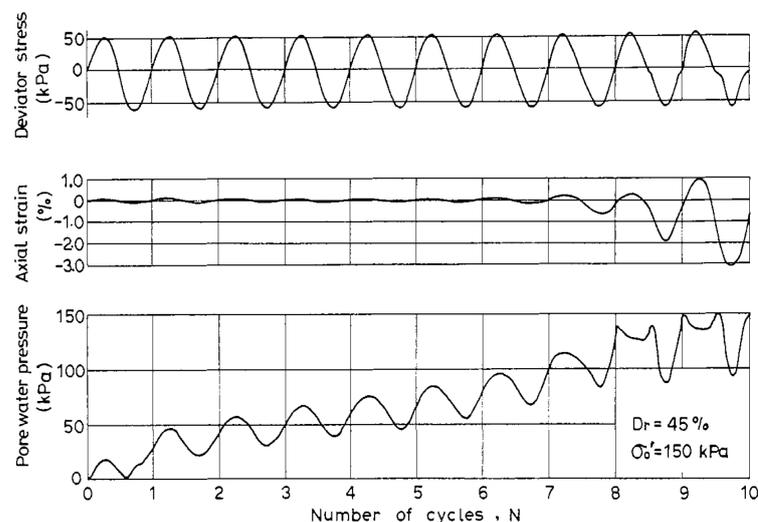
Figure 2.1: Generation of excess pore pressure under cyclic loading, Seed & Lee (1966)
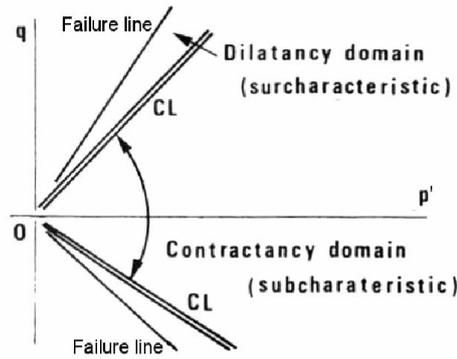
(a) Characteristic state for saturated sands, Luong & Sidaner (1981)
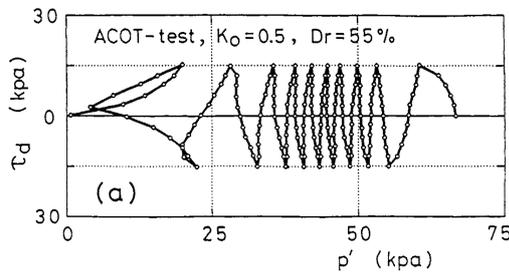
(b) Stress path for soil under cyclic shear, Ishihara (1996)
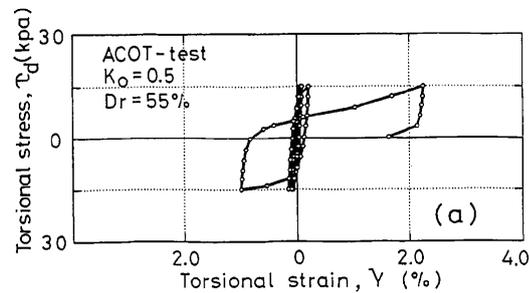
(c) Soil strain under cyclic shear, Ishihara (1996)

Figure 2.2: Behaviour of loose soils under cyclic shearing

a point where the stress path reaches the PTL, beyond which the soil's behaviour becomes dilative. In addition, the soil is described to be unstable, and very large increases in pore pressure are then observed in subsequent cycles when the soil is unloaded. This behaviour can be observed in Figure 2.2(b), where it can be seen that the PTL is crossed close to p' = 30 kPa. The large increases in pore pressure during the unloading of the soil lead to the stress path cycling very close to the origin, with the soil exhibiting both contractile and dilative behaviours (in the subcharactersitic and surcharacteristic regions of Figure 2.2(a)) each cycle, leading to experimental observations where the pore pressure cycles at twice the shearing frequency (i.e. Carnevale & Elgamal, 1993; Farrell & Kutter, 1993; Seed & Lee, 1966). Additionally, Ishihara *et al.* (1975) found that the soil strains increased dramaticaly once the PTL had been reached, which can be seen in the strains of Figure 2.2(c), which accompany the data of Figure 2.2(b), as well as the data of Seed & Lee (1966) shown in Figure 2.1.

The dramatic loss of stiffness and shear strength of these loose soils when the excess pore pressures reduce the effective stresses close to zero is generally referred to as liquefaction. In particular, Seed & Lee (1966) defines initial liquefaction to be the point at which the vertical effective stresses are first reduced to zero, while Ishihara (1993) adopts this

definition with the added constraint that double amplitude axial strain should be greater than 5 % and occur within 20 cycles. Other definitions exist; for example Sladen *et al.* (1985) discusses liquefaction in terms of an unstable reduction in the deviatoric stress which can be observed on loose soils which are sheared in an undrained triaxial test (termed the quasi-steady state by Ishihara (1993)). For the purposes of this thesis, the definition of Seed & Lee (1966) has been adopted.

2.2.2 Dense sands subjected to undrained cyclic loading

While the generation of positive excess pore pressures in a loose soil is expected from the critical state framework, the opposite is true for a soil lying below the critical state line, which would be expected to dilate under shear loads. However, it was reported by Castro (1975) that at small shear strains, dense soils also generate an increment of excess pore pressure, leading to the gradual build up of significant excess pore pressures in cyclic triaxial tests. These observations have been repeated by many researchers carrying out cyclic triaxial tests, including Hyodo *et al.* (1998); Mitchell & Dubin (1986). As shown in Figure 2.3, the stress paths of loose and dense sand both show the build up of excess pore

(a) Loose Dog's Bay sand   (b) Dense Shirasu sand

Figure 2.3: Cyclic loading of loose and dense sands, Hyodo *et al.* (1998)

pressures due to the cyclic shear loading. However, while the loose sand shown in Figure 2.3(a) shows a rapid loss of stiffness once the characteristic state line (marked PTL in the figure) has been reached, the dense sand accumulates strain much more slowly, and with a very gradual softening taking place over many cycles. This key difference led Castro (1975) to term the gradual softening of a dense sand as cyclic mobility. Since the softening of dense sands takes place over many cycles, it is apparent that under typical earthquake loading, a dense sand will maintain significant stiffness even in cases where the excess pore pressures temporarily reduce the effective stresses to zero.

While the results of Castro (1975) indicate that excess pore pressures build up very slowly in a dense sand, the build up of excess pore pressures within uniform dense deposits of sand during a dynamic centrifuge test has been found to occur rapidly from the beginning of the earthquake motion (Coelho *et al.*, 2007; Elgamal *et al.*, 2005). Similar to the undrained tests, it was found that while the generation of excess pore pressures takes place much more rapidly, these dense sands were highly dilative upon shear, resulting in rapidly mobilised shear strength.

2.2.3 Non-uniform soil deposits

While the preceding sections have discussed the pore pressure generation in sands within uniform soil deposits, this is rarely the case in the field, where many factors influence the behaviour of soil as summarised by Ishihara (1996). However, of particular relevance to this thesis is the effect of soil stratification as well as the effects of overconsolidation and non-homogeneity within a soil layer.

Typically, soils which are most at risk of seismically-induced liquefaction, such as alluvial deposits or man-made fills, have been deposited relatively recently. Hence the large overconsolidation ratios (OCR) which can be found in some soils are of little relevance to liquefaction problems involving sand-dominated soil profiles. However in certain circumstances, it is possible that overconsolidated soils exist locally. One example of particular relevance is the overconsolidation which can arise due to the installation of a piled foundation, which will exist only in a relatively small region around and below the pile tips. The effect of overconsolidation on the liquefaction resistance of sands was investigated by Ishihara & Takatsu (1979), through a series of undrained cyclic triaxial tests on Fuji river sand with an initial vertical effective stress of 100 kPa and overconsolidation ratios of up to 4. The results of these tests indicated that in order to cause liquefaction in 20 cycles, the cyclic stress ratio needed to be increased by the square root of the overconsolidation ratio. This implies that generation of excess pore pressures in soils can be expected to occur more slowly as the overconsolidation ratio increases. The effects of overconsolidation ratio were further discussed by Dobry & Abdoun (2011). In stress-controlled cyclic

triaxial tests, a threshold shear strain of approximately 0.01% exists for normally consolidated soils, below which excess pore pressures do not tend to be generated, perhaps indicating the limit of purely elastic deformation of the soil skeleton. However, while the threshold strain is relatively independent of the sand type and relative density, it is highly dependent on the overconsolidation ratio. As a result, at higher overconsolidation ratios, the build-up of excess pore pressures was similarly found to occur more gradually. Similar conclusions concerning the effect of overconsolidation ratio on the build up of excess pore pressures were reached by Sharp *et al.* (2003), based on the results of dynamic centrifuge tests where overconsolidation was achieved at all points in the model by increasing the g-level at the beginning of the test.

While uniform deposits of soil provide a good basis from which to study various aspects of soil behaviour, it is important to recognise the potential effects which local non-homogeneity can introduce to the behaviour. An investigation into the inclusion of loose pockets of sand ($R_D \approx 35$ %) within a matrix of saturated dense soil ($R_D \approx 75$ %) in a dynamic centrifuge test was described by Chakrabortty *et al.* (2011). Under the influence of seismic loading, it was found that the loose soil pockets readily liquefied. As the earthquake loading continued, the excess pore pressures in the loose sand migrated into the dense sand and resulted in a higher level of excess pore pressure in the dense sand near to the loose soil inclusion than in a similar test containing only dense sand. While earthquakes are often considered to be undrained events, these results clearly indicate that significant pore pressure migration can occur on the time scale of the earthquake event, meaning that these events cannot be considered truly undrained. In addition, local heterogeneity has affected the pore pressure response of the surrounding soil matrix. An extension of the argument put forward in the investigation of Chakrabortty *et al.* (2011) is that the converse might well be true such that regions of sand with more gradual excess pore pressure generation, such as dense or overconsolidated soils, will act to reduce the build-up of excess pore pressures in a surrounding soil matrix. It also remains to be seen the distance to which local heterogeneities affects the generation of excess pore pressures in a greater soil volume.

2.2.4 Sloping soil deposits

While the occurrence of liquefaction in level sand beds is the primary focus of this thesis, the presence of sloping ground introduces additional engineering challenges. Following the onset of seismically-induced liquefaction, lateral spreading may occur, where the liquefied soil deposit tends to exhibit very large shear strains in the downslope direction as a result of the soil's shear resistance being exceeded by the persisting shear stresses (Ishihara, 1993; Kutter *et al.*, 2004; Seed, 1967). If the soil profile contains a relatively impermeable

layer, then void redistribution can occur at the interface, leading to the formation of a
water film and as a result of the decoupling between the two layers, large relative lateral
movements can occur (Fiegel & Kutter, 1994).

2.2.5 Behaviour of sands after cyclic loading

Following an earthquake, the excess pore pressures which have been generated during an
earthquake must dissipate. Florin & Ivanov (1961) viewed the phenomenon of liquefaction
as a breakdown of structure and subsequent suspension of particles within the pore fluid.
The soil grains fall under the action of gravity to the bottom to form a new structure,
implying the upwards drainage of fluid. The upwards flow of fluid following an earthquake
can also be inferred from the limiting condition of $r_u = 1$, since this implies a hydraulic
gradient after the earthquake in the vertical direction. As a result of the dissipation of the
generated excess pore pressures, large soil settlements are often reported following major
earthquakes (i.e. Berrill $et\ al.$, 2001; Fujii $et\ al.$, 1998). Typically, earthquakes are con-
sidered undrained events, and as such, all of the settlements result from post earthquake
dissipation of excess pore pressures (Ishihara, 1993). The magnitude of these settlements
was researched by both Ishihara & Yoshimine (1992) and Tokimatsu & Seed (1987) on
the basis of undrained cyclic triaxial tests. While the former study finds that the final
post-earthquake volumetric strains are linked to increasing maximum shear strain, and
reducing relative density (shown in Figure 2.4), the latter finds the volumetric strain in-
creases with increasing cyclic stress ratio and reducing corrected SPT count of the soil.
While the two investigations provide techniques for estimating the post-earthquake volu-
metric strains based on different parameters, there is a strong link between the corrected
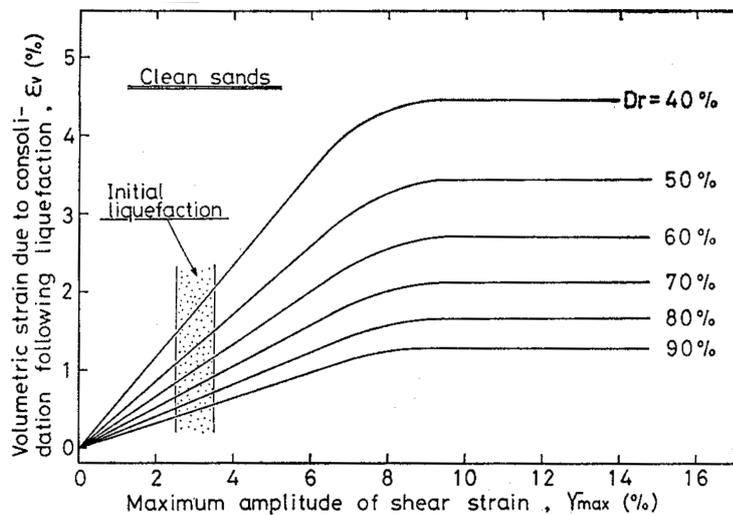
Figure 2.4: Volumetric strains occuring after an earthquake due to the dissipation of
excess pore pressures, Ishihara & Yoshimine (1992)
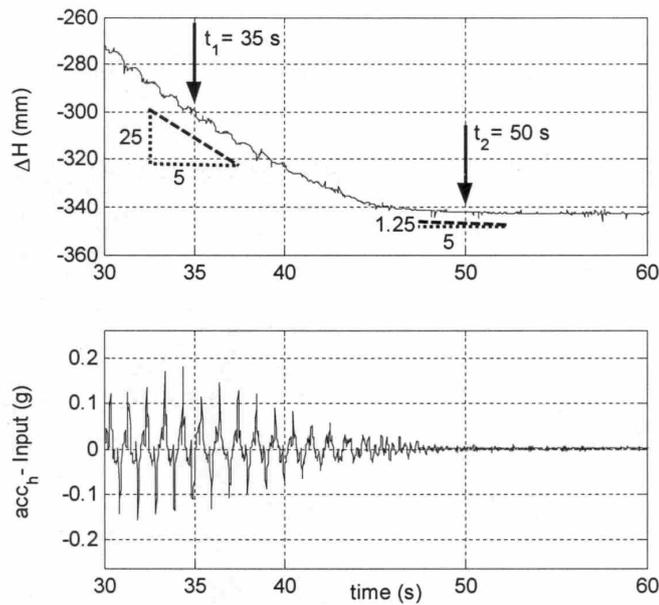
Figure 2.5: Rate of soil settlement during and after earthquake loading, Coelho (2007)

SPT blow count and the relative density (Cubrinovski & Ishihara, 1999), as well as between the cyclic stress ratio and the maximum shear strain induced in a soil. Therefore the trends reported by both investigations are in broad agreement.

While both of these investigations assumed that the actual earthquake loading of the soil is undrained, the large excess pore pressures which are generated during an earthquake inevitably lead to some drainage occurring during a real earthquake. Attempts were made by Coelho (2007) to measure the soil surface during a series of dynamic centrifuge tests, finding that the rate of settlement of the soil was approximately 20 times greater during the earthquake loading than immediately after the event, as shown in Figure 2.5. Further to the discussion in Section 2.2.3, these results indicate that earthquake events are not truly undrained events, and that some settlement must occur during the earthquake itself.

2.3   Piled foundations

The use of piled foundations in the field is governed by a large number of factors including cost, the role of the piled foundation, the loads being applied by the structure, the required response of the foundation system as well as logistics. As a result, piled foundations found in the field are of many different materials and cross-sections. Additionally, an increasing number of installation methods are available. However, in essence, piled foundations might be split into two groups: displacement and non-displacement piles. In the former, piles are installed directly into the ground, with the generalised name indicating the significant

17

(a) Axial loads on piled foundations

(b) Modelling axial response with springs
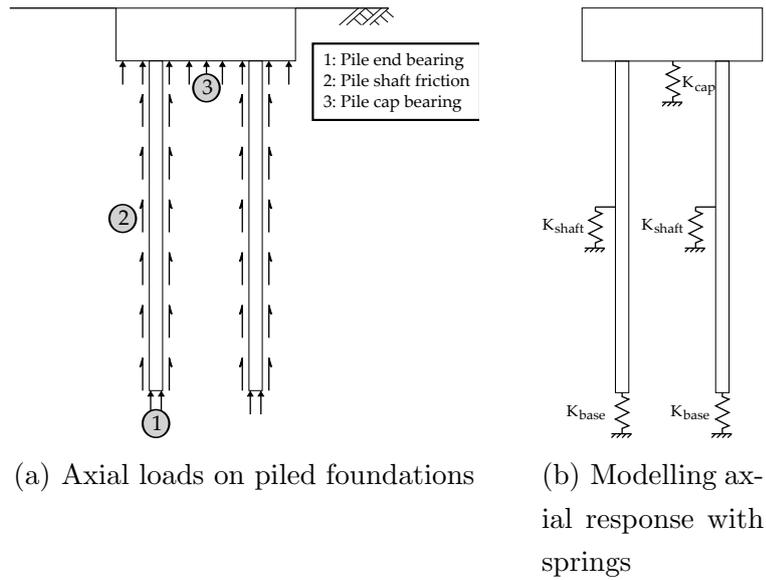
Figure 2.6: Conceptualised pile group

volume of soil which must be displaced to allow the progression of the pile into the ground (Fleming *et al.*, 2009). In the latter, a bore is created in the ground before the pile is created in-situ (typically by pouring concrete into the bore containing a reinforcement cage).

Regardless of the "class" of piled foundation selected, piled foundations can generate axial capacity in three areas as shown in Figure 2.6(a).

While a number of factors were highlighted governing the choice of pile, foundation design is still primarily concerned with the estimation of axial capacity (Randolph, 2003). In order to model the mobilisation of loads at different levels of settlement, non-linear springs are often used to represent the different components of axial load, as shown in Figure 2.6(b). While a single spring is shown for each of the different areas identified in Figure 2.6(a), models would tend to incorporate several springs to allow for differences such as relative movements at different depths along a pile and soil stiffness (for example, Yetginer *et al.*, 2006)

2.3.1 Pile end-bearing capacity

At the ultimate limit state, the bearing capacity failure of a pile will involve plunging. At this point, the large settlement implied in the plunging failure mechanism implies that the bearing capacity of both displacement and non-displacement piles would be the same.

A variety of methods exist for estimating a pile's end bearing capacity. While some historical solutions are based on deformation mechanisms (Berezantzev *et al.*, 1961; Vesic,

Strain direction transitions
——— Transition from vertical compression to extension
- - - Transition from horizontal extension to compression
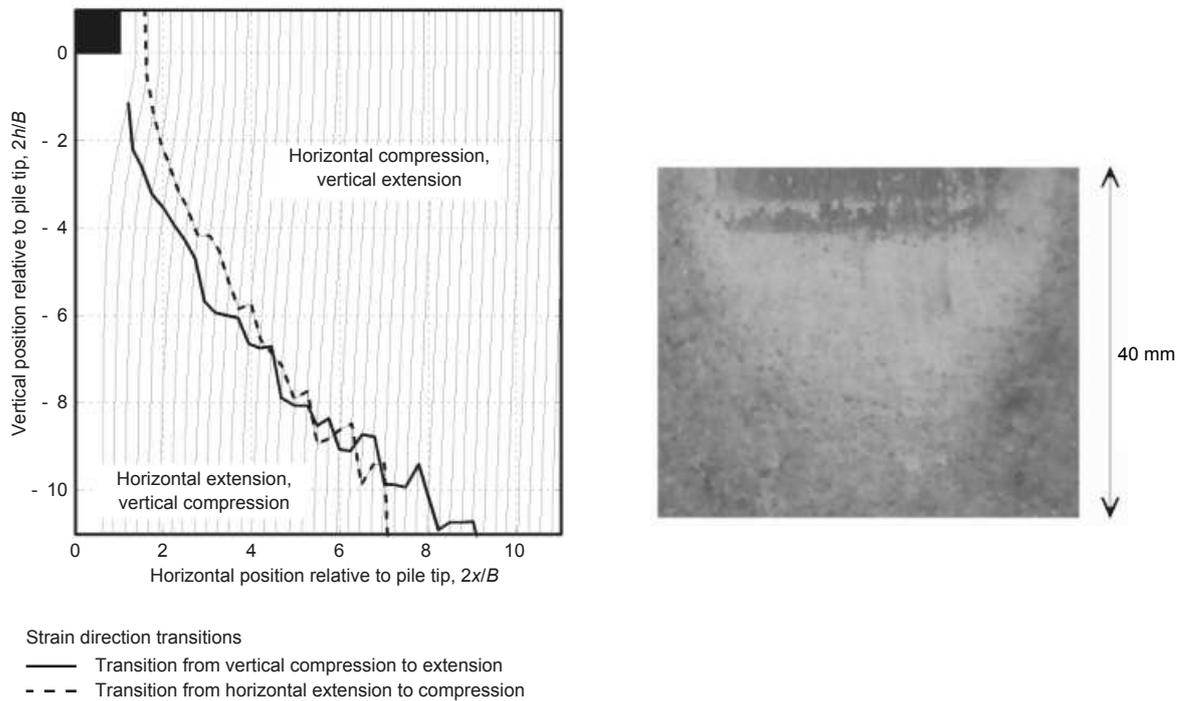
(a) Streamlines of soil flow and strain reversal points

(b) Zone of crushed soil beneath tip of jacked pile

Figure 2.7: Alteration of soil stresses resulting from installing a jacked pile (White & Bolton, 2004)

1967), the analogy between a piled foundation and a CPT have led to modern methods attempting to directly use the base resistance recorded by a CPT probe to establish the base capacity. White & Bolton (2005) argued that a pile's base resistance at the ultimate limit state should be equal to the base resistance of a CPT. While differences exist between the two in field cases, corrections which take account of the embedment within a layer of different stiffness, and possible stresses as a result of the installation process led to the normalised resistance of a pile being approximately 0.9 times that of a CPT, with the pile diameter not making an observable difference to the correlation.

Although displacement and non-displacement piles might exhibit similar ultimate resistance, examples in the literature show that the axial response of a piled foundation before plunging failure is highly dependent on the installation method chosen. Implied in the installation of displacement piles is that the soil below the piles will undergo large straining as the pile tip progresses.

An investigation into the behaviour of a jacked pile was carried out through 1-g testing by White & Bolton (2004). The use of a clear perspex window allowed direct observations of the soil deformations occurring as a pile tip advanced towards, and passed a soil horizon. Below the pile tip, soil experiences vertical compression and horizontal extension within

a well defined zone extending from the shoulders of the piles at 35 degrees from the pile's axis. Once the soil had passed outside of this zone, the strain rates reversed so that the soil experiences vertical extension and horizontal compression. As a result of the large forces required to install the pile, the soil beneath the jacked piles is left in an overconsolidated state after installation. Directly beneath the pile tips, a "cone" of highly crushed sand exists as a direct consequence of the extremely high stresses in the sand at this location (Figure 2.7(b)). By contrast, the stresses during the installation of non-displacement piles are typically very low. The differences in the stresses experienced by the soil give rise to significant differences in the axial responses. Deeks *et al.* (2005) investigated the axial responses of a bored, jacked and driven pile. As shown in Figure 2.8, the displacement piles provide a much stiffer response. The serviceability limit state of a pile is often taken to be a settlement of 10 % of the outer pile diameter ($0.1\,D_0$) (Randolph, 2003). At this point, Figure 2.8 indicates that while a bored pile might only have mobilised 15 - 20 % of its ultimate capacity, a displacement pile such as a jacked pile will have mobilised close to its ultimate capacity. It is also clear from Figure 2.8 that the stiffness of jacked piles is significantly larger than a bored pile. This result is consistent with the field investigation of Gavin & Lehane (2003) who showed that the greater stiffness of the jacked piles was linked to the greater residual stresses at the base of the jacked pile.
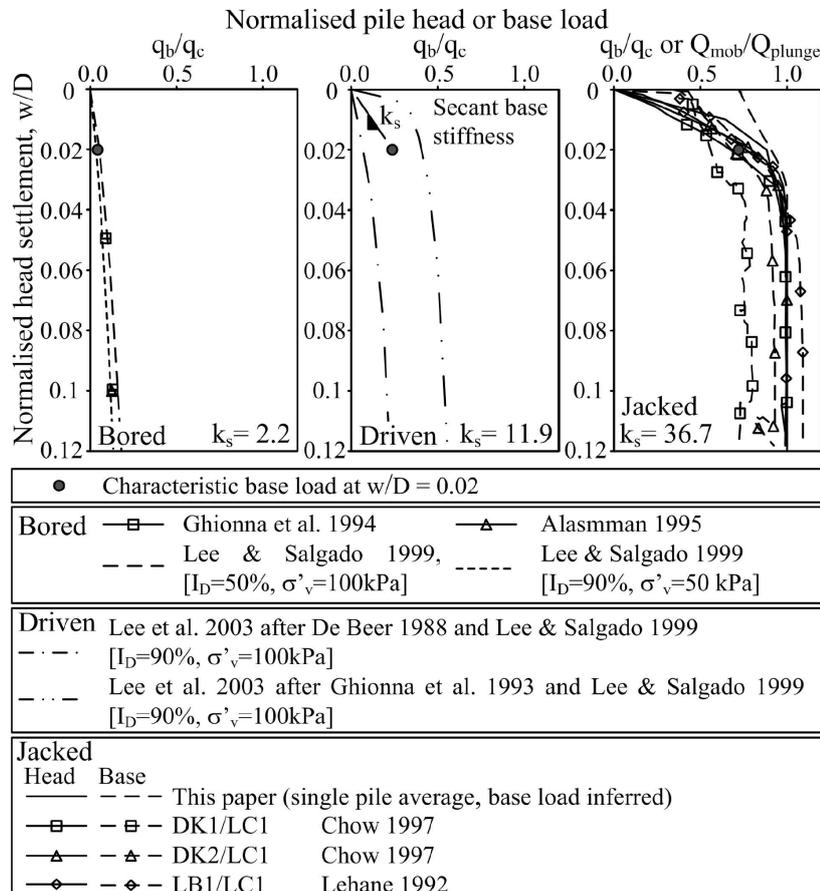
Figure 2.8: Relative stiffness of jacked, driven and bored piles, Deeks *et al.* (2005)
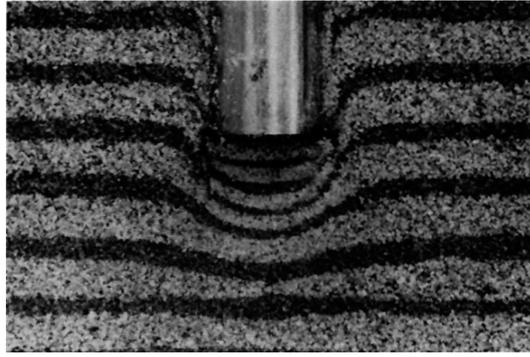
Figure 2.9: Deformation of sand layers beneath a model pile, Yasufuku & Hyde (1995)

Again, based on the similarities between a CPT probe and a pile, many methods for predicting the mobilisation of base resistance with settlement propose the use of the cone resistance from a CPT investigation. As an example, Randolph (2003) introduced a hyperbolic relationship proposed by Fleming (1992), intended for bored piles, but allowing for the possibility of residual soil stresses beneath the pile tips. However, in situations where no CPT data is available, alternative methods must be found for estimating the mobilised pile resistance at different settlement levels.

The investigation of White & Bolton (2004) into the soil deformation beneath a piled foundation highlighted some similarities between the deformations observed as a model pile is jacked, to those which would be expected from a spherical cavity expansion (shown in Figure 2.9). The observed similarities rationalises some of the methods for predicting the base capacity of a pile using a spherical cavity expansion (e.g. Randolph, 2003; Yasufuku et al., 2001). In the case of the solution proposed by Yasufuku et al. (2001), the global properties of the soil layer are used (i.e. shear modulus, effective stress at the level of the pile tips, soil friction angle) in the solution to predict the plunging resistance of the pile, from which it was recommended that 29 % of the base capacity provides a reasonable estimate of the base resistance at the serviceability limit state. It must be noted that while some similarities between the observed soil deformations and the cavity expansion solution, there are some flaws. White & Bolton (2004) in particular highlight that the cavity expansion assumes that the soil displacements depend only on the radial co-ordinate. However, while this was found to be reasonable beneath the pile, contours linking zones of equal displacement were found to converge near the pile shoulders, violating the main assumption of the spherical cavity solution. However, the solution of Yasufuku et al. (2001) was found to produce reasonable results when compared with a series of field tests. This solution has therefore been adopted as a method for obtaining a reasonable estimate of the end bearing capacity of bored piles in this research programme.

2.3.2 Shaft Friction

The axial resistance derived on the shaft of a pile in sand is typically associated with the friction which can be mobilised at the soil-pile interface, according to Equation 2.2 (Lehane *et al.*, 1993) and depends on three main items:

- Angle of friction at soil-pile interface

- Radial effective stress

- Mobilisation distance

$$\tau_{sf} = \sigma'_r tan\delta \tag{2.2}$$

It is however often impractical to measure the radial stresses acting on a pile and therefore, the form of Equation 2.2 is often modified to approximate the radial stresses on the pile to the horizontal effective earth pressures, which can in turn be represented by the product of the lateral earth pressure coefficient and vertical effective stress, as shown in Equation 2.3.

$$\tau_{sf} = K\sigma'_v tan\delta \tag{2.3}$$

The angle of friction, δ, which is mobilised at the soil-pile interface is typically related to the normalised roughness (Schneider, 2007; Uesugi & Kishida, 1986). A series of interface shearing tests carried out by Lehane & White (2005), as well as a numerical study by Loukidis & Salgado (2008), indicated that the values of interface friction angle were not affected by stress level (at moderate levels of normal stress) or by the relative density of the sand. However, this may not remain true at very large normal stresses, or in the case of a displacement pile, where grain crushing may occur, leading to a sand of significantly smaller grain size at the pile interface. In these scenarios, the normalised roughness at the pile-soil interface would be larger, and as a consequence, a larger interface friction angle would be expected (Mortara *et al.*, 2010; Yang *et al.*, 2010).

The importance of installation effect on the ultimate level of shaft friction has been recognised for many years (e.g. Meyerhof, 1976), with the shaft friction resistance of a jacked pile typically showing greater resistance than that of a driven pile which in turn exhibits greater resistance than that of bored pile. In these scenarios, the installation of the piled foundation plays a key role in determining the radial stresses acting on the pile.

In the case of bored piles, some studies have shown that the radial stresses acting on the pile can be linked to the vertical effective stresses by a constant lateral stress coefficient (Amira *et al.*, 1995; Meyerhof, 1976). However, in the case of displacement piles, the radial stresses are significantly altered from this simple distribution.

In the case of jacked piles, White & Bolton (2004) and Klotz & Coop (2001) found that the intense shearing of the soil around the pile shoulder led to zones of high dilation near the tips of the piles. The increases in radial stresses near the pile tips were found to be strongly influenced by the lateral stiffness in the soil layer, and as suggested in an earlier work by Lehane *et al.* (1993), this means that in very dense sand layers, the increase in radial stress near the pile tips may be very large. However, White & Bolton (2004) observed that the continued jacking of the piles led to stress relaxation, so that as the distance from the pile tip increases, the radial stresses become much smaller as the soil densifies away from the pile interface. This is roughly in line with the results of White & Lehane (2004), where it was observed that the cycles of axial load associated with the installation of a driven pile led to the gradual degradation of radial stress as the pile was progressively driven past a particular soil horizon. However, while small amplitude cycles of displacement lead to densification of the soil away from a pile, large amplitude displacement cycles, lead to the opposite effect (Foray *et al.*, 2011). This was similarly found by White & Bolton (2004), where the sand in the interface zone next to the pile was highly dilatant when the driven piles were monotonically loaded. Under earthquake loading, significant cyclic shearing will take place, and therefore this result might suggest that some densification of the soil will occur in the region of shearing. It is then possible that if the shearing strains become large during the earthquake, significant dilation could occur, leading to increased effective stresses near the pile interface and therefore a recovery of shaft friction. It is also the case that after the earthquake, displacement of the soil relative to the pile (either due to settlement of the soil as described in Section 2.2.5, or settlement of the pile itself) could lead to a highly dilatant response of the soil, again leading to increases in the shaft friction capacity of the pile after an earthquake.

The shaft resistance on a piled foundation is highly dependent on the relative movement between the pile and the surrounding soil. In the field, studies have shown that shaft friction is mobilised at relatively small displacements of approximately 1-10 mm (e.g. Lehane & White, 2005; Lehane *et al.*, 1993). However, studies attempting to investigate shaft friction in a centrifuge have found that the shaft friction is mobilised at similar levels of displacement at model scale (e.g. Amira *et al.*, 1995; Fioravante, 2002; Foray *et al.*, 1998). It has been proposed that the issue of scaling arises as a result of the shaft friction resistance being dominated by the behaviour of soil within a very narrow shear band. The size of the shear band around a pile is often reported to be in the range of 5-15 particle diameters (e.g. Fioravante, 2002; Foray *et al.*, 1998; Loukidis & Salgado, 2008),

regardless of whether the tests are carried out in the centrifuge or the field. This presents particular difficulties when assessing the shaft friction responses of piles in the centrifuge, particularly if the loading is cyclical and the displacements are relatively small so that the ultimate resistance might not be mobilised in any given cycle. In this respect, it must be expected then that the shaft friction measured during dynamic centrifuge tests will be lower than that which might be experienced in the field.

The shaft friction capacity of piles is known to be different in tension and compression, Randolph (2003). The ratio of the strength in tension to than in compression is thought to lie in the region of 0.7-0.8. In reality, this will be unimportant for most earthquake loading. If the pile group experiences a rocking mode during shaking, tensile loads may be applied to individual piles in the group as they attempt to pull out. However, superimposed on any tensile loads arising from such action will be reduced by the overall foundation loading which will continue to act in the compressive direction.

2.3.3 Pile cap bearing capacity

Typically, foundation design is carried out without considering resistance on the base of the pile cap. Under typical working loads, this approach is logical since the axial load stiffness of a pile is typically much greater than that of a pile cap and hence the pile cap typically plays little or no part in the transfer of axial loads from the structure to the soil. Poulos (2001) suggests that in the future, raft capacity of a foundation could be incorporated into the ultimate limit state design of a building, while ignoring this aspect at the serviceability limit state.

2.4 The effects of liquefaction on axial pile behaviour

Under earthquake loading, the most severe and catastrophic examples of damage to structures often occur as a result of laterally spreading soils. As soil layers spread past a piled foundation, passive soil pressures can develop against the foundation, leading to very large lateral loads, especially in cases where a relatively impermeable layer exists near the soil surface (i.e. Berrill *et al.* (2001)). As a result, a great deal of research has focussed on the effects of lateral spreading on piled foundations (e.g. Abdoun *et al.*, 2003 examined the bending moment distribution on piles in laterally spreading soils, finding that the maximum bending moments occurred close to interfaces between soil layers of differing stiffness; Brandenberg *et al.*, 2007 investigated the development of lateral loads from a laterally spreading clay crust, finding the response was softer than expected due to the zone of influence of the pile group extending a large distance upslope). While the scenario

of lateral spreading is of great interest to engineers, the study of Tokimatsu *et al.* (1996) was discussed in Chapter 1 and highlighted that the axial behaviour of a piled foundation remains an important, yet understudied topic.

2.4.1 Axial loading of piled foundations during an earthquake

The axial loading of piled foundations during an earthquake is complex, with the structure having to carry the vertical loads which are applied under normal operating conditions, as well as additional axial loads arising from the seismic excitations. In some earthquakes, the recorded vertical ground motions can be quite large (i.e. vertical accelerations exceeded 2g in some locations during the 2011 Christchurch earthquake, Bradley, 2011), which will consequently lead to vertical inertial loads on the structure. However, the effects of the vertical ground shaking are beyond the scope of this thesis. Instead the emphasis is placed on the effects of horizontal excitation of a soil-structure system, which experiences time-varying lateral loads and therefore dynamic moments as a result of the horizontal ground motions. In the case of a single pile, the dynamic moments must be resisted by the distribution of lateral loads acting on the pile. However, in the case of a pile group, moments can also be resisted by differences in the vertical load distribution, both on the piles, and on the pile cap. The redistribution of axial loads as a result of a laterally spreading layer was observed by Pamuk *et al.* (2003) and in dry level ground by Fukumura *et al.* (2003), the variation in axial loading due to the lateral loading can be quite large,
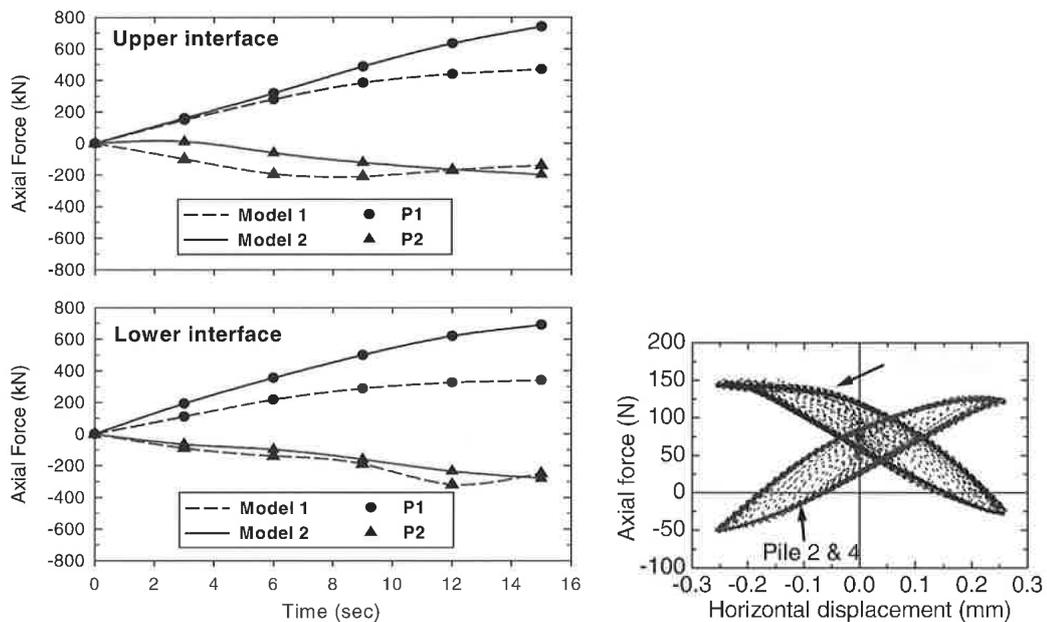
(a) Lateral spreading, Pamuk *et al.* (2003)   (b) Level beds (unsaturated), Fukumura *et al.* (2003)

Figure 2.10: Variation in axial head load due to lateral loading

as shown in Figure 2.10, hence in order to study the axial behaviour of piles during an earthquake, consideration must be given to the horizontal loading of the structure.

2.4.2 Seismic axial capacity of piled foundations

While the axial loads are known to vary at the head of piles within a pile group during an earthquake, this topic remains relatively understudied. In the Section 2.3, the three different regions in which piled foundations sustain axial loads were introduced. A key feature of the end bearing capacity and the shaft friction capacity was noted to be the effective stress level in the soil profile. Relatively little work has been carried out to establish the bearing capacity of piles under earthquake loading. Typically, analytical solutions for bearing capacities are linked in some way to the effective vertical stress in the ground. This approach has therefore been extended in some analyses when considering the base capacity of a pile during a liquefaction event (i.e. Boulanger *et al.*, 2003; Charlie *et al.*, 2009). These approaches however were not verified experimentally, leading Knappett & Madabhushi (2009a) to carry out dynamic centrifuge experiments in which the axial loads at the head and base of a pile within a 2×2 pile group were measured. In this study, it was observed that following the generation of large excess pore pressures, the axial loads at the base of the piles depended on the contact between the pile cap and the soil surface. When the pile cap was in contact with the soil surface, a reasonable estimate of the pile tip loads was obtained using the bearing capacity of Yasufuku *et al.* (2001) with the reducing soil stiffness and effective vertical stress in the free field as shown in Figure 2.11. However, by contrast, the axial loads at the pile tip within a second pile group (within the same model) were found to remain much higher throughout the entire earthquake
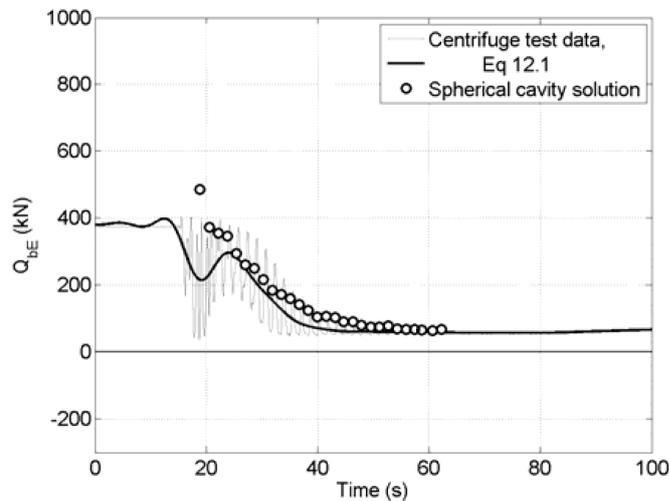
Figure 2.11: Degradation of bearing capacity during an earthquake, Knappett & Madabhushi (2009a)

(a) Lateral pressure and excess pore pressure next to pile

(b) Cone of dilation beneath pile cap
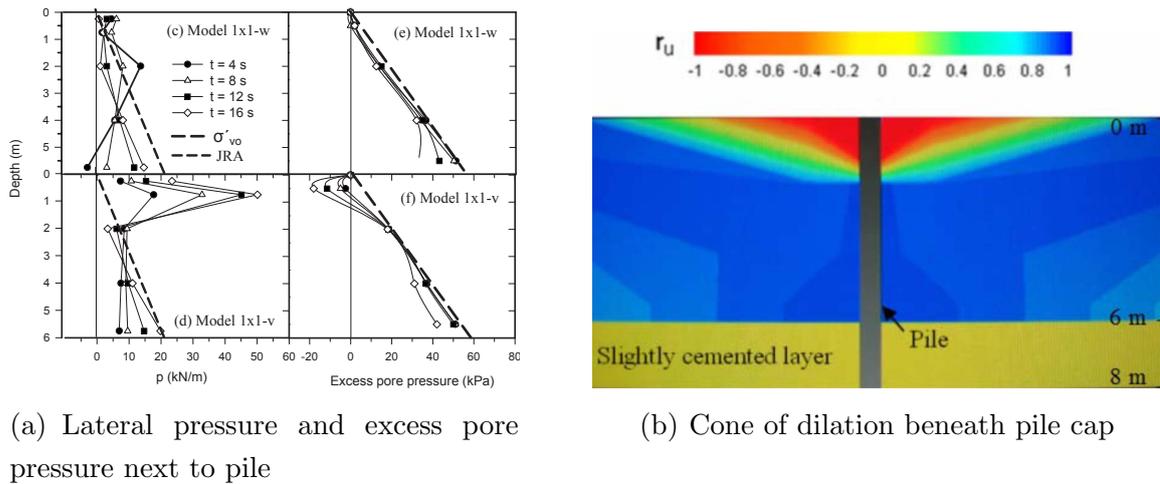
Figure 2.12: Excess pore pressures below a pile cap in laterally spreading soil, Gonzalez *et al.* (2009)

and it was suggested that this might be due to dilation-induced negative pore pressures in the soil below the pile tips. However, in this study, the soil in the bearing layer was relatively fine, meaning that large local variations in excess pore pressure were possible on the time scale of the earthquakes. For a bearing layer with larger hydraulic conductivity, fluid may be able to "flood" the region of soil below the pile tips during the earthquake, meaning that the negative pore pressures required to sustain the axial resistance can not be maintained, leading to a different response being observed. Alternatively, it may be that if the hydraulic conductivity of the base layer is increased substantially, then the generation of excess pore pressures may not occur to the same degree, leading to much larger end bearing capacity throughout the earthquake. However, the effect of the hydraulic conductivity within the bearing layer on the axial response of pile groups has not been investigated to date.

The shaft friction capacity of a pile in Equation 2.2 was shown to depend on both the effective radial stresses and the angle of friction at the interface between the pile and the soil. Since the effective stresses during liquefaction fall to zero during a liquefaction event, it is commonly perceived in practice that the shaft friction capacity of a pile falls to zero during an earthquake in liquefiable soils. However, Knappett & Madabhushi (2008b) reported that the shaft friction (in the same tests previously described) remained non-zero throughout the earthquake and Knappett (2006) suggested that this shaft friction could be being mobilised in the dense bearing layer, where, as discussed in Section 2.2.2, dense sands are known to be highly dilatant upon shearing. While the shaft friction measured on the piles remained positive throughout the earthquake, Knappett (2006) reported a cycle on cycle degradation of the shaft friction magnitude, and suggested an analogy to the reduction in radial stresses described by White & Lehane (2004).

The loss of shaft friction and pile end bearing capacities described by Knappett & Madabhushi (2008b) and Knappett & Madabhushi (2009a), leads to the natural conclusion that the pile cap must begin to support significant loading during an earthquake if the pile cap is in contact with the soil surface. Knappett & Madabhushi (2008b) observed a significant reduction in excess pore pressures below the pile cap during an investigation into the behaviour of pile groups in laterally spreading soil. It was suggested that the settlement of the pile group into the soil led to dilation in the soil below the pile cap and gave rise to this reduction in excess pore pressures. Such a scenario might then explain the ability of the pile cap to support significant axial loads as the pile end bearing and shaft friction loads reduce in level ground. However, an investigation into the effect of permeability on the behaviour of pile groups founded on a rigid base and subjected to laterally spreading soil was carried out by Gonzalez et al. (2009). In these experiments, the permeability of the liquefied soil was altered by using pore fluids of different viscosity. Where a pore fluid with a large viscosity was used in the model (a similar case to that examined by Knappett & Madabhushi (2008b)), it was found that a similar zone of reduced excess pore pressures existed below the pile cap, despite the pile groups being unable to settle), as shown in 2.12. The results of Gonzalez et al. (2009) therefore suggest that the reduced excess pore pressures observed by Knappett & Madabhushi (2008b) may be a result of the lateral spreading process rather than the settlement of the pile group. The question of the soil state beneath a pile cap in level ground during an earthquake is therefore still uncertain. If the zone of dilation is found to exist beneath the pile cap, then this has implications for the shaft friction capacity of the pile since the dilation will lead to a strengthening of the soil near the surface and therefore a possible increase in the shaft friction capacity.

2.4.3 Changes in effective stresses near piles

While the lateral loading of piles is important since it is responsible for generating the dynamic moments which lead to additional axial loads during an earthquake, the lateral loads may equally play a role in the shaft friction capacity of a pile during an earthquake since, according to Equation 2.2, the capacity is highly dependent on the lateral effective stress acting on the pile. Although at small displacements the response of a liquefied soil is very soft, once a threshold strain is reached, the behaviour becomes dilative and large lateral forces are applied as a result of the soil "locking up" and shearing at its critical state strength. While the behaviour at large strain is typical of a laterally spreading soil, where the soil's displacement continually increases, it is possible that similar effects could be observed in level sand beds.

Tokimatsu & Suzuki (2004) investigated the excess pore pressures close to a piled foundation in a series of large scale physical model tests and found large differences in the

(a) Tokimatsu & Suzuki (2004) (b) Uzuoka *et al.* (2008)
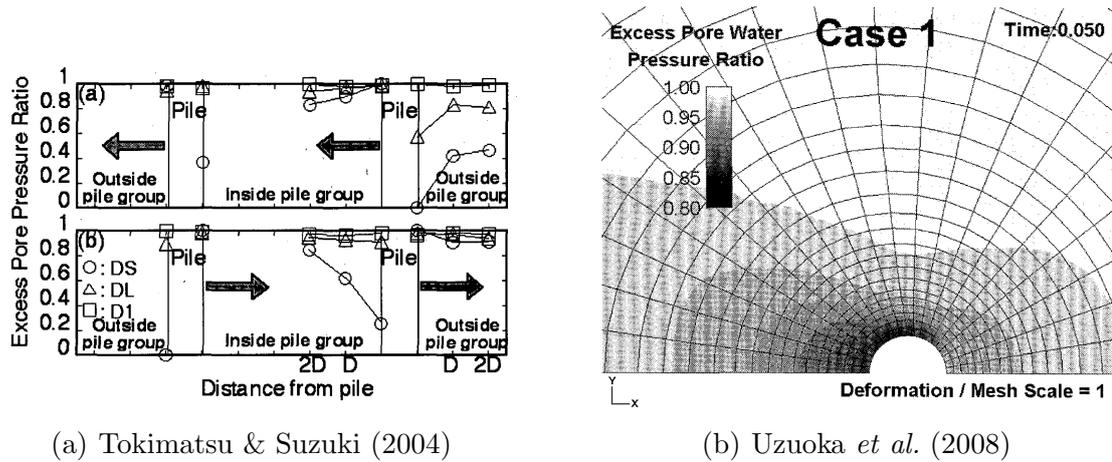
Figure 2.13: Pore pressure changes occurring close to laterally displacing pile

excess pore pressure distribution in the near and free fields. In these experiments it was observed that as a pile advanced, a reduction in excess pore pressures occurred behind the pile, while in front, the excess pore pressures were largely unchanged, as shown in Figure 2.13(a). Near-field effects on the excess pore pressures were similarly observed by Motamed *et al.* (2009) during a study of a large scale pile group behind a quay wall using the E-Defense facility. However, in this study it was found that the excess pore pressures on the front side of the piled foundation showed larger reductions than on the trailing side near the soil surface. Additionally, Uzuoka *et al.* (2008) carried out a numerical investigation into the effect of shearing rate and hydraulic conductivity, finding that the pressure distribution was highly dependent on both. At smaller hydraulic conductivities, it was found that excess pore pressures could reduce both in front of, and behind an advancing pile in liquefied soil, as shown in Figure 2.13(b).

A further consideration which affects the excess pore pressures around a pile is the magnitude of relative lateral displacement between the pile and surrounding soil. A series of tests were carried out by Dungca *et al.* (2006) where a pipe was pulled laterally through a model as the soil was subject to horizontal accelerations. Dungca *et al.* (2006) observed that at low relative displacement, the excess pore pressures reflected liquefaction, but once a threshold strain had been reached, termed the *"reference strain of resistance transformation point,"* the excess pore pressures reduced. The magnitude of the reference strain was found to be highly dependent on the rate of shearing (as shown in Figure 2.14(a)) as well as the hydraulic conductivity of the soil, which led to reducing reference strain as the hydraulic conductivity reduced. The displacement of the pipe, as well as the excess pore pressures measured on either side of the pipe are shown in Figure 2.14(b).

The results of Dungca *et al.* (2006) highlighted the importance of the magnitude of relative movement between the soil and pile. Brandenberg *et al.* (2005) carried out a series of dynamic centrifuge tests in which both pile groups and single piles with different bending

29

(a) Effect of shearing rate on reference strain

(b) Excess pore pressures and displacement of pipe (modified)
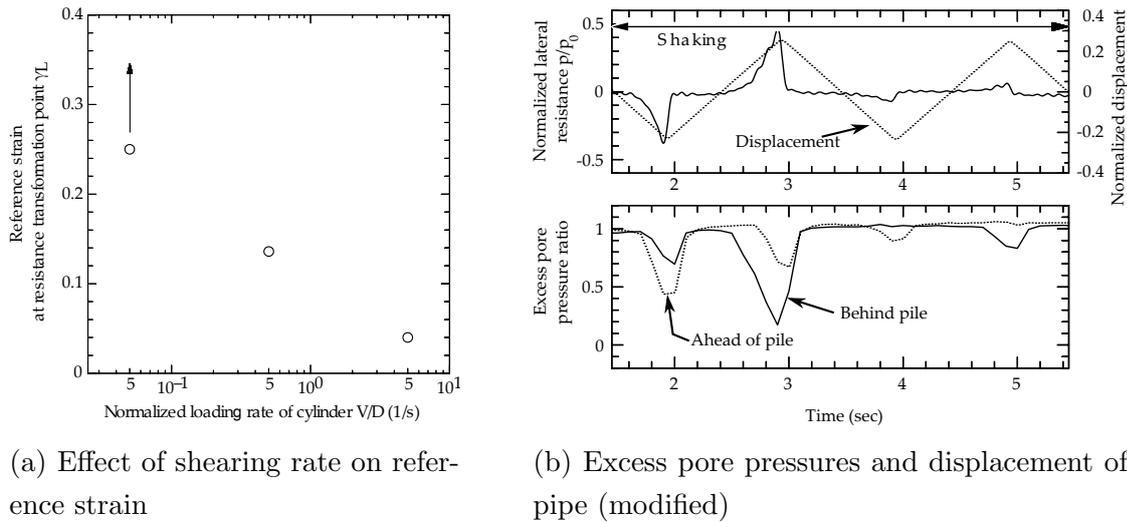
Figure 2.14: Negative excess pore pressures past a threshold strain, Dungca *et al.* (2006)

stiffness were embedded within a sloping soil deposit, highlighting the importance of the relative soil-pile stiffness. In cases where the pile was relatively stiff, as shown with line A in Figure 2.15, the pile is able to resist the lateral loads applied by the liquefied soil and clay crust, so that the soil displaces past the pile. However, when the piles are relatively compliant, as shown with curve C, the displacement of the pile was much larger than that of the soil, due to the large deflections imposed by the clay crust.

Similar results were found by Cubrinovski *et al.* (2006), where 30 cm diameter steel and pre-stressed high strength concrete (PHC) piles were subjected to laterally spreading soils. The steel piles being relatively stiff were found to attract the full passive pressure from the non-liquefied crust, yet lateral deflections of the pile itself were small. The relatively flexible PHC piles on the other hand experienced large lateral deflections without mobilising full passive pressures due to the lower relative lateral displacements between the soil and pile. In level ground scenarios without a laterally spreading crustal layer, large lateral deflections of the pile are still possible due to the inertial loads being applied by the superstructure. The relative displacements are however complicated since the displacements of the bearing layers, liquefied soil layers, pile and pile cap are all cyclical, with depth varying phase differences. The situation is therefore complex and the lateral displacement of the pile relative to the soil depends significantly on the phasing of the pile and soil at each depth. With stiffer piles, the pile cap displacements will remain more closely in phase with those in the bearing layer, while larger phase differences between the pile cap and the bearing layer are expected with a more compliant pile. This could lead to different situations where the pile displacements could lead those in the liquefied layer (i.e. stiff piles), where the pile displacements lag those of the liquefiable layer (i.e. compliant piles), or where the direction of relative displacement between the pile and the soil changes with depth, as observed by Tokimatsu & Suzuki (2004). Since the excess pore pressures
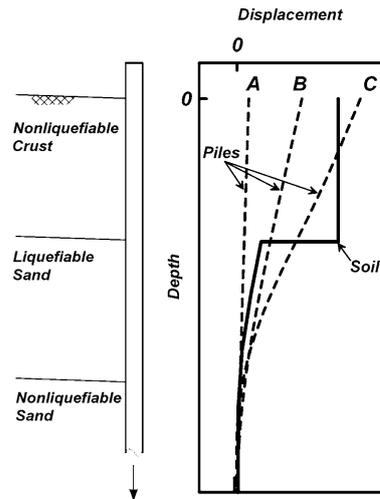
Figure 2.15: Effect of pile stiffness on relative soil-pile displacement

near the piles are greatly affected by the magnitude of relative displacement, it can be expected that the excess pore pressure distribution, and therefore radial stress distribution around a pile will vary greatly both around the pile (as shown in Figure 2.13(b)) and with depth (due to the differences in the magnitude of relative displacement).

2.4.4 Group effects

The response of individual piles within a pile group is known to be affected by the presence of neighbouring piles. Brown *et al.* (1988) carried out full-scale tests on piles in a sandy profile, finding that greater lateral loads were carried by leading rows, than those in subsequent rows as the "leading rows push soil away from the area acting to provide soil resistance." The effect was considered further by McVay *et al.* (1998), who investigated the effect of the number of rows within a pile group and finding that beyond the third row, the reductions in lateral loading on the piles was insignificant. A similar effect was observed by Rollins *et al.* (2006) in full scale tests in clay. In this study, the pile centre-centre spacing was investigated, and it was found that the difference in loading carried by the different piles reduced as the pile spacing increased until, at a pile spacing of 5.65 pile diameters, very little group effect was observed. While the effects just mentioned were observed in "static" tests, a similar effect was reported by Maheetharan (1990) based on dynamic centrifuge tests on pile groups in dry sand, finding that the group effects were minimal at a spacing of 6 pile diameters. The effect of pile spacing has similarly been observed in saturated tests, including that of Tokimatsu & Suzuki (2004), where as shown in Figure 2.13(a), the changes in excess pore pressure due to the relative displacement of the pile is smaller inside the pile group than outside. While currently unknown, it is likely that the lateral group effects just described will play a part in the axial resistance of a piled foundation when subjected to earthquake loading. On trailing piles, the reduction

in lateral loading implies lower lateral pressures, while smaller changes in excess pore pressure within the group implies that within the group, smaller effective stresses might occur. Both of these effects imply that the shaft friction capacity of the pile will be reduced according to Equation 2.2, meaning that the combined shaft friction capacity of piles within a pile group may be smaller than that which might be predicted for a single pile.

2.4.5   Settlement of piled foundations during seismic loading

While a structure and its foundation must firstly be able to carry the extreme loads which are applied during an earthquake, the settlements which occur concurrently are also important. However, similar to the axial loading of a piled foundation during strong shaking, the settlement of a structure during an earthquake remains poorly understood. De Alba (1983) carried out a series of experiments in which a section of model pile was tested with a constant head load at 1g on a shaking table with an applied surcharge to elevate the effective stresses. During these experiments, a gradual rise in excess pore pressure was observed as well as a steadily increasing pile settlement. The study showed that the development of settlement against pore pressure was relatively consistent for each level of pile group loading and soil relative density, and that when excess pore pressure ratio was plotted against the initial factor of safety, FOS, (defined to be the point where pile settlements exceeded 0.1 D_0 and calculated according to Vesic, 1967), a reasonably unique line was obtained showing the point where settlements exceeded the failure criterion of 0.1 D_0. However, in these tests, the pile head load was maintained at a constant level. It has already been discussed that under seismic excitation, the axial loads at the head of the pile will vary significantly.

Following the work of De Alba, centrifuge test data was fitted to the previously described curves by Knappett & Madabhushi (2008b) and shown in Figure 2.16(a). While the data shown appears to fit the trends very well, the centrifuge data used in this comparison was taken from pile groups which were in contact with the soil surface. As shown by Knappett & Madabhushi (2008b), the axial loads on the piles reduce immediately at the beginning of the earthquake and therefore does not represent the same condition as that tested by De Alba. Additionally, while these charts provide a convenient method of determining the required initial factor of safety to prevent settlement failure at different levels of liquefaction, they are possibly very unconservative. In these charts, the locus denotes the excess pore pressure ratio at which settlement failure at the various initial FOS first occurs. These curves do not indicate what the ultimate settlements would be. This point is particularly important in the results of the later study, since the generation of excess pore pressures occurs rapidly. It therefore remains to be seen how settlement

(a) Limiting FOS for 0.1 D_0 settlement (modified)

(b) Development of settlement with increasing excess pore pressure ratio
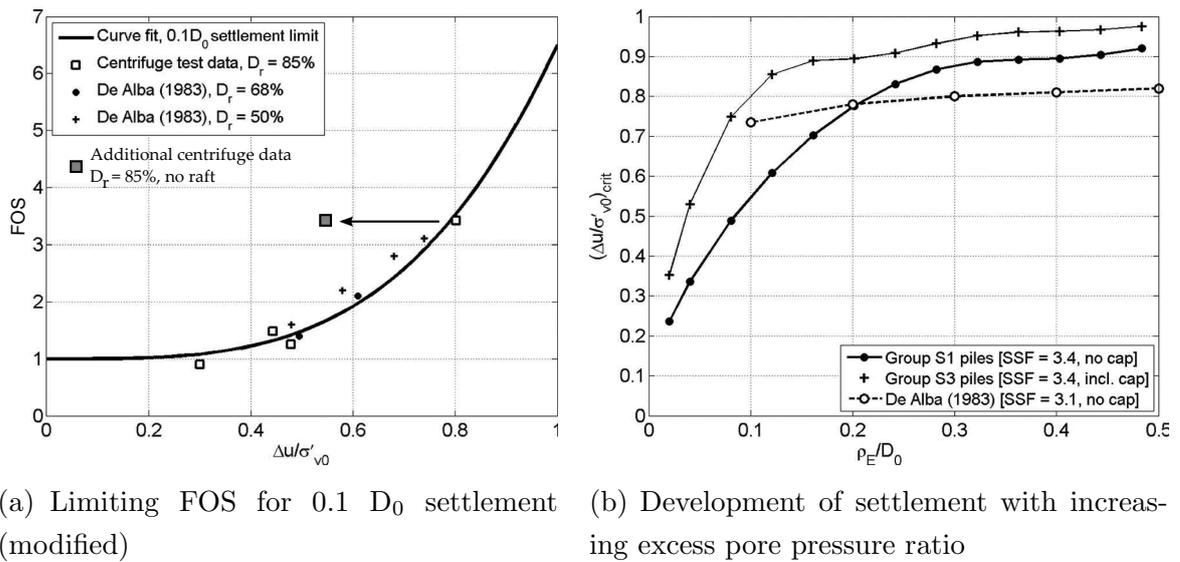
Figure 2.16: Settlement of pile groups with increasing excess pore pressure in static and dynamic tests, Knappett & Madabhushi (2008b)

would develop should the excess pore pressures not develop beyond a specified limit (for example, in a dense sand, where excess pore pressure ratios might not rise above 60 % as was the case in Coelho *et al.* (2007)). The importance of this point can be partially observed in Figure 2.16(b), where it can be seen that once pore pressures begin to stabilise, the settlement continues to increase.

As stated earlier, the comparison of centrifuge settlement data with De Alba's presented by Knappett & Madabhushi (2008b) do not reflect the same scenario since the centrifuge data shown in Figure 2.16(b) represents the case where the pile cap is in contact with the soil surface. The effect of contact between the pile cap and the soil surface was investigated in level beds of dry sand by Horikoshi *et al.* (2003), who found that the settlements of the pile group were reduced by more than 4 times when the pile cap was in contact with the soil surface. For the case of saturated soils, a similar effect can be observed in Figure 2.16(b) which shows that at all levels of excess pore pressure generation, the settlements of the pile groups with caps in contact with the soil surface was much smaller than those where the pile cap was free of the soil. The curve of S3 in Figure 2.16(b) has been used to provide an additional data point in Figure 2.16(a), and shows that the centrifuge data now lies substantially above the curve of De Alba. This suggests, for the case where the pile cap is not in contact with the ground, that while the average axial head load remains fairly constant, the additional axial loads required to resist the dynamic moments leads to greater pile group settlement.

It must also be considered that the settlements shown in Figure 2.16(b) are measured relative to a fixed datum, and therefore do not provide an indication of the settlement of the pile cap relative to the soil surface, which in practice is likely to be of greater interest

from the point of view of load transfer mechanisms. It was postulated in Section 2.4.2 that the hydraulic conductivity of the bearing layer could affect the bearing capacity of the piled foundations during the earthquake. If this turns out to be the case, then it can be expected that differences in the hydraulic conductivity of the soil would impact the settlement of the piled foundation. However, this aspect has yet to be investigated.

2.4.6 Buckling of piled foundations during an earthquake

The analogy of a piled foundation in liquefied soil to that of a long slender column has led some researchers to suggest that buckling is a viable mechanism for the failure of a pile. O'Rourke *et al.* (1994) carried out a series of analyses of a piled foundation passing through a laterally spreading layer into a rigid bearing layer, proposing that the observed failure mechanism depended on the relative stiffness of the laterally spreading soil and the axial load, as shown in Figure 2.17. The minimum axial load required to buckle the piles (point B) highlighted the dual role played by the soil in providing lateral restraint to the pile which is attempting to buckle, but also in providing lateral loads which act to increase the pile head deflection, and therefore reduce the critical buckling load in the same manner as an initial imperfection in the case of a simple strut. The concept of pile buckling was later examined by Bhattacharya *et al.* (2004), who carried out a series of dynamic centrifuge experiments on piles in level soil beds, but rigidly fixed at the base of the pile. By applying lateral restraint so that the piles heads were unable to deflect in the direction of shaking, it was shown that with axial loads close to the critical Euler buckling load, that unstable failure of the piles occurred following the onset of liquefaction.

This work was further investigated by Knappett & Madabhushi (2009b,c), who showed through numeric and dynamic centrifuge modelling that it was possible for highly loaded pile groups whose pile tips were embedded in a rigid layer (such as rock-socketed piles) to
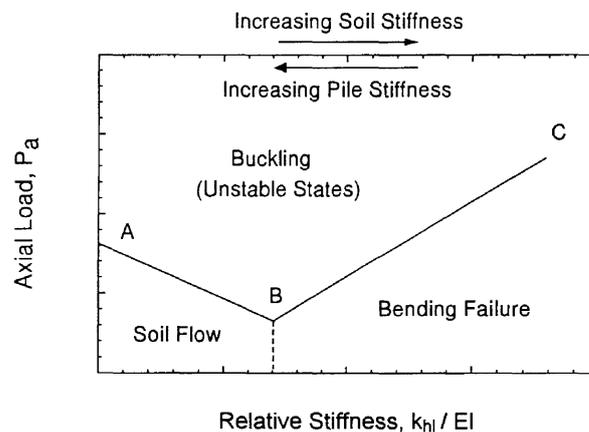
Figure 2.17: Interaction diagram showing modes of failure, O'Rourke *et al.* (1994)

suffer from an unstable collapse. An additional centrifuge test was described by Knappett (2006) where long piles passed through a 21.6 m thick liquefiable layer and had their tips embedded in dense sand. These piles were thought to be loaded close to their Euler buckling load, assuming the critical length for buckling to be 21.6 m. However, despite liquefaction throughout the liquefiable layer, the piles were not observed to buckle, but the pile group did suffer very large settlements. However, it may be that the level of pile loading was not sufficient to cause buckling of the piles since the nominal test acceleration was used for the scaling of loads, and as will be described in Section 3.2.1 the actual g-level acting at the level of the pile cap is lower and therefore would reduce the loads applied to the piles below the critical buckling load. While the dynamic moments on the pile group during an earthquake lead to cyclic variation in the pile head load which might temporarily increase the axial load on a pile sufficiently to pass the buckling load, the piles on the opposite side of the pile group experience loading sufficiently below the buckling load and it is unknown to what extent this will effect the buckling mechanism of the more heavily loaded piles. Therefore, buckling load for pile groups whose piles are not rock-socketed remains an unresolved issue, but is outside the scope of this thesis.

2.5 The axial behaviour of piled foundations after an earthquake

When a piled foundation is embedded in a soil profile undergoing consolidation settlement, axial loads additional to those from the superstructure will be applied to the pile as consolidating soil "drags" the pile downwards. Since the the mobilisation of shaft friction capacity is thought to take place at relatively small strains (Alonso *et al.*, 1984; Fellenius, 1972), the shaft friction acting along the lengths of the pile are often taken to be their ultimate values, hence the location of the neutral plane is found by equilibrium Fellenius (1972). The depth at which the shaft friction changes from negative (drag load) to positive has become known as the neutral point or plane (Alonso *et al.*, 1984; Fellenius, 1984), as shown in Figure 2.18. The discussions of Fellenius (1984); Fellenius & Siegel (2008) consider an unmoving neutral plane and hence the pile displacement is linked to the soil's displacement at this depth. However, as noted in the analysis of Wong & Teh (1995), the shaft friction capacity changes with the dissipation of excess pore pressures, leading to an evolving distribution of axial loads on the pile shafts. In order to model the pile head settlement, Wong & Teh (1995) proposed the use of a simplified model incorporating the springs shown in 2.6(b), whose stiffness' change with the dissipation of excess pore pressures.

Boulanger & Brandenberg (2004) discussed an alternative application of the neutral plane concept, accounting for the increasing shaft friction capacity with time and assuming that
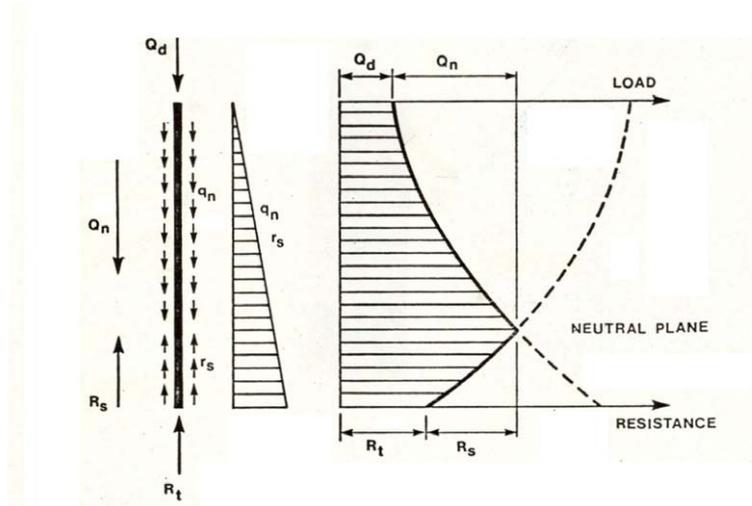
Figure 2.18: Definition and construction of the neutral plane, Fellenius (1972)

the radial stress in Equation 2.2 is directly proportional to the vertical effective stress. Under the approach of Boulanger & Brandenberg (2004), the position of the neutral plane changes as the dissipation of excess pore pressures continues due to the increasing shaft friction capacity with depth, leading to smaller estimated pile group settlements at the end of the dissipation process.

Rollins & Strand (2006) attempted to capture the effects of down drag on a single pile due to the dissipation of excess pore pressures in a liquefied soil layer through full-scale field testing as shown in Figure 2.19(a). The figure indicates that axial loads were applied through a loading frame and it was intended to keep the axial head load constant throughout the experiment. Explosive charges were used to generate large excess pore pressures, and led to liquefaction of the soil throughout the loose layer, while in the dense bearing layer, excess pore pressure ratios remained relatively low. Increasing the axial head load before the experiment resulted in the whole pile registering positive shaft friction, but following the onset of liquefaction, the shaft friction across the liquefied zone reduced close to zero. As excess pore pressures dissipated, the shaft friction in the previously liquefied layer led to increasing down drag loads on the pile within the loose layer, and as a result, increasing amounts of shaft friction in the dense layer but only a modest increase in pile base resistance. However, while the shaft friction profiles follow expected trends at depths greater than the top of the liquefied zones, some questions remain concerning the reported data above the liquefied zone. As a result of the excess pore pressures remaining very low in the bearing layer below the liquefied zone, the reported pile settlements were very low in comparison to the soil settlements, being 7 mm and 270 mm respectively. This would indicate that in the non-liquefied layer between 0 m and 5.5 m depth, large down drag forces would be expected, following Boulanger & Brandenberg (2004). However, as clearly shown in Figure 2.19(b), the shaft friction in this case remained positive. While the experimental results of Rollins & Strand (2006) are interesting and demonstrate the

(a) Soil profile and testing schematic

(b) Changes in axial load during experiment
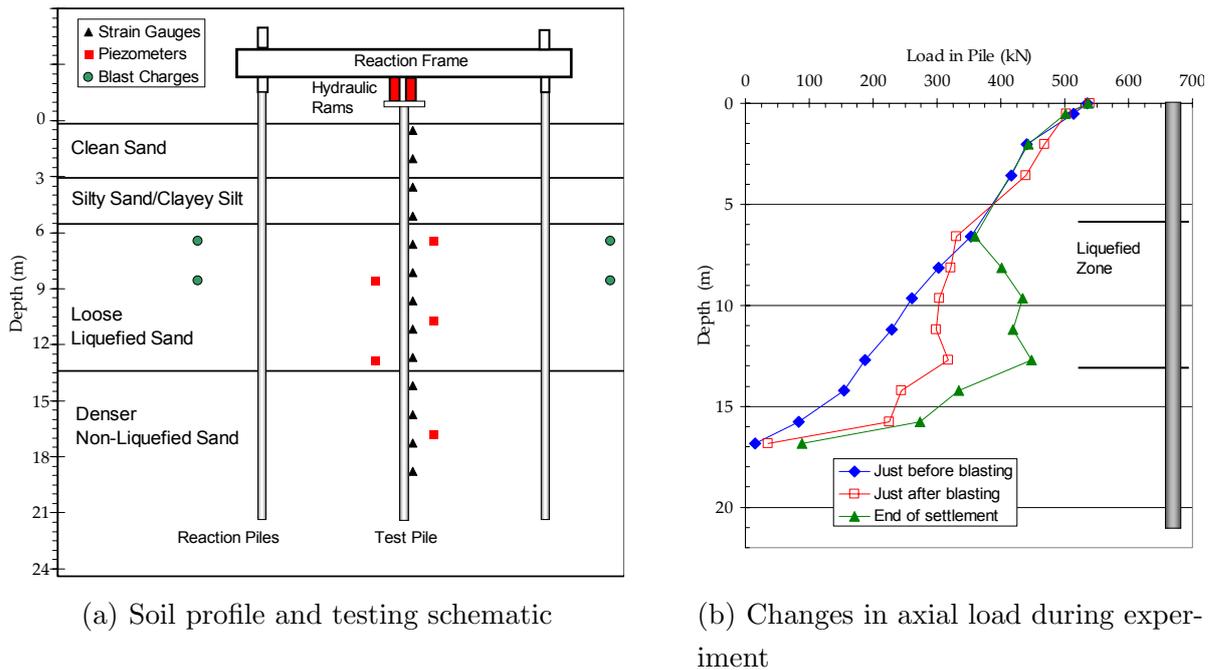
Figure 2.19: Development of downdrag forces as a result of excess pore pressure dissipation

development of down drag forces after an earthquake, there remain many open questions regarding the development of these forces. It must also be observed that in the case of Rollins & Strand (2006), the axial head loads were kept largely constant after inducing liquefaction. However, as described in Section 2.4.2, the axial pile head loads can reduce significantly in cases where the pile cap is in contact with the soil surface and where large excess pore pressures develop near the pile tips. In these scenarios, it is likely that the axial load applied at the pile head will develop with the dissipation of excess pore pressures, and potentially lead to the shaft friction forces developing differently to those reported by Rollins & Strand (2006).

It was discussed in Section 2.2.2, that even in dense sands, significant excess pore pressures can be generated, meaning that while the pile settlement following the earthquake was very small in the test of Rollins & Strand (2006), if greater excess pore pressure generation existed throughout the rest of the soil profile, larger pile settlements might occur. This was observed by Knappett (2006), who reported large pile group settlements, in excess of 0.6 D_0, in the scenario where model piles were free of the soil surface and the excess pore pressure ratio close to the pile tips was 1. Charlie *et al.* (2009) carried out a series of 1-g experiments, where explosive charges were used to generate different levels of excess pore pressure ratio across a 2.7 m deep soil profile, reporting that the settlement of model H-piles increased dramatically with excess pore pressure ratio.

2.6 Summary

In this Chapter, the existing research concerning the axial behaviour of piled foundations in liquefied soil has been presented. The experimental programme of Knappett (2006) provided many insights regarding seismic bearing capacity and shaft friction, yet many aspects remain to be investigated. In particular, in the case of the shaft friction which persists during an earthquake, the existing research was able to demonstrate that shaft friction existed in an average sense for the tests conducted. However, in order to understand the shaft friction capacity of a pile in liquefied soil, knowledge of the distribution of axial forces along a pile during an earthquake must be obtained, so that the observed shaft friction can be linked to a particular mechanism, or effect. As highlighted in Section 2.4.5, the settlement experienced by a piled foundation is still not fully understood, and as shown in Figure 2.16, settlement continues to develop during an earthquake beyond those shown in the charts of De Alba. In addition, while large differential or absolute settlements can give rise to structural failures (depending on the situation), it can also be important to consider the vertical settlements of the piles relative to the soil as this can impact services connected to the building, or the degree of remedial work which will be required following an earthquake. Finally, when attempting to investigate the transfer of axial load on a pile during an earthquake, it may be more useful to consider the settlements of the pile group relative to the soil surface. In Section 2.3, it was discussed that the axial behaviour of piled foundations under normal working conditions is greatly influenced by the method of installation, with displacement piles typically enjoying a higher axial stiffness compared with non-displacement piled foundations. However, the effect of installation method on the axial behaviour of piled foundations in a liquefiable soil during an earthquake has yet to be researched.

This thesis aims to clarify the load transfer mechanisms responsible for supporting the axial loads on piles which are embedded in dense soils overlain by liquefiable deposits. In particular this thesis will investigate:

- The distribution of axial loads along the piles in order to understand possible mechanisms which give rise to the existence of shaft friction in a liquefied soil deposit, as well as the role played by the pile cap in the axial behaviour of a pile group.

- The effect of an increased bearing layer permeability and whether the differences in localised pore pressure effects leads to significant changes in the load capacities of the foundation.

- Whether the changes in soil state induced by the installation of displacement piles leads to significant differences in the axial behaviour of these piles during an earthquake.

Chapter 3

Modelling Techniques

3.1   Introduction

This Chapter describes the techniques and equipment used in order to investigate the axial load distribution of piles in liquefied soils. Particular emphasis is placed on the model pile groups which were used during the research programme, as well as discussion about the implications and limitations of both the equipment and instrumentation which were used. Finally, the development of a computer-controlled saturation system is described at the end of the Chapter.

3.2   Centrifuge Modelling

When investigating the behaviour of a linear system (i.e. where f(A) + f(B) = f(A+B)), the response of a small model would be expected to be an exact scaled version of a larger version of the same model. However, this is not the case for geotechnical problems due to the non-linear stress-strain characteristics of a real soil. This presents a challenge for researchers interested in complex geotechnical problems, since it implies that in order to obtain a realistic response for a given scenario, the stresses in the model must be similar to those which would be observed in the intended prototype.

The use of centrifuge modelling has become an established method for investigating complex geotechnical problems using small scale models. The enhanced g-field created in the centrifuge leads to elevated stress levels in the model such that they are similar to those encountered at homologous points in the prototype. In order to interpret the results from a centrifuge experiment, a set of scaling factors must be applied. Schofield (1981, 1980)

proposed a set of scaling laws based on dimensional analysis which are reproduced in Table 3.1 for a model subjected to a centrifugal acceleration of N × g.

Table 3.1 indicates different scaling laws for time when considering dynamic events and seepage events. The discrepancy in time scaling can be solved by altering the hydraulic conductivity of the soil such that it is decreased by a factor N. For example, in a centrifuge test carried out at 50 g, the hydraulic conductivity should be reduced by a factor of 50. In order to decrease the hydraulic conductivity by such a large factor, two approaches could be taken. The first is to scale the size of soil particles being used in the model relative to the soil particles in the prototype. According to Hazen's relationship, shown in Equation 3.1, hydraulic conductivity can be reduced by altering the particle size. This approach, however, has a major disadvantage that the particles in the model may have to be reduced significantly in size. In order to change the hydraulic conductivity by a factor of 50, the D_{10} size particles need to scale by a factor of 7 in the model. As a result, in order to model fine sand particles in a prototype, silt particles may have to be used in the centrifuge model to satisfactorily reduce the hydraulic conductivity. This may result in a significant change to the soil's constitutive behaviour. A second approach is to decrease the hydraulic conductivity of the model soil by using a pore fluid with increased viscosity. For example, in a 50g centrifuge test, the pore fluid will have a viscosity of 50 cSt compared to the prototype pore fluid which normally has a viscosity of 1 cSt (water).

Table 3.1: Scaling laws linking quantities in the model to the prototype

	Parameter	**Scale Factor**	**Units**
General	Length	N^{-1}	m
	Area	N^{-2}	m^2
	Volume	N^{-3}	m^3
	Mass	N^{-3}	Nm^{-1}s^2
	Stress	1	Nm^{-2}
	Strain	1	-
	Force	N^{-2}	N
	Bending Moment	N^{-3}	Nm
	Seepage velocity	N^{-1}	ms^{-1}
	Time (Consolidation)	N^{-2}	s
Dynamic	Time (Dynamic)	N^{-1}	s
	Frequency	N^{1}	s-1
	Displacement	N^{-1}	m
	Velocity	1	ms^{-1}
	Acceleration	N^{1}	ms^{-2}

$$K \approx 0.01 D_{10}^2 \ (\ K \text{ in m/s when } D_{10} \text{ is in mm }) \tag{3.1}$$

The procedure of using highly viscous pore fluid in dynamic centrifuge models has been well established (e.g. Stewart *et al.* (1998) discusses a variety of pore fluids used by different researchers since 1981). Issues such as increased viscous damping due to the high viscosity pore fluid have been investigated. Madabhushi (1994) has shown by conducting conjugate sets of centrifuge tests with both water and high viscosity silicone oil as pore fluids that the increased viscous damping due to use of silicone oil is insignificant. Ellis *et al.* (2000) have shown by conducting resonant column tests that the viscous damping effects are only significant at small strains. In large strain problems such as those created during earthquake loading, the material damping in the soil overwhelms the viscous damping effects. It is therefore acceptable to use high viscosity pore fluids in dynamic centrifuge tests.

It may also be considered that the discrepancy in time scaling need not be corrected. Wilson (1998) carried out a pair of dynamic centrifuge experiments where the soil profiles (consisting of relatively fine Nevada sand) were similar, but where the pore fluid had different viscosities of 1cSt and 10cSt (test was carried out at an acceleration of 30g). Measurements of pore pressure indicated only small differences in the magnitude of excess pore pressures, leading to the suggestion that dynamic pore pressures were not significantly affected by the fluid viscosity. However, as noted by Wilson (1998) this is not expected to be the case in general, especially if coarser soils are used in the model. As described in Section 2.4.3, excess pore pressures can vary considerably from those observed in the free-field, resulting in large local hydraulic gradients. It is therefore likely that close to the piles, where partial drainage may occur during the earthquake, the soil behaviour may be strongly dependent on the choice of pore fluid viscosity. Additionally, it is expected that even in the free-field, some aspects of soil behaviour, such as soil settlement during the earthquake will be affected by the viscosity of the pore fluid. Excess pore pressures also dissipate much more quickly after an earthquake when lower viscosity fluids are used, and therefore the response observed in this phase of an experiment is significantly affected. In all of the experiments described in this thesis, pore fluids with high viscosities were used.

It should be noted that by carrying out experiments with small scale models, many simplifications to the intended prototype must be undertaken, and with this in mind, centrifuge models often only aim to capture the important aspects of a problem. The understanding which is obtained from the model can then be generalised and applied to provide guidance in design, or used in complementary research methods to predict the behaviour of a more complex system. The effect of the boundary conditions which are applied must also be carefully considered, since they may induce a specific soil or structural behaviour which have important implications for the wider applicability of the

results. An example of this is the pile buckling mode of failure described by Bhattacharya (2003) where the piles were rigidly fixed to the base of the container, implying a rock-socketed end condition with no rotation at the base of the pile.

While centrifuge modelling is the method of choice in this thesis, there are many alternative and complementary techniques (e.g. numerical modelling, full-scale testing etc.) which could be selected under different circumstances. Further details concerning centrifuge modelling, as well as many of the other mainstream techniques for carrying out geotechnical research are found in Muir Wood (2004).

3.2.1 Turner beam centrifuge

Experiments were carried out using the 10 m diameter Turner beam centrifuge, described by Schofield (1980) and shown in Figure 3.1. In its present form, models (and a counter-weight) are loaded on a swinging platform and can be tested with a combined package weight (including swinging platform and any supplementary actuators or equipment) of up to 920kg at accelerations of up to 150 g. A counterweight is loaded onto the opposite arm of the centrifuge to the model, with a mass which, at the test acceleration, will approximately balance the centrifugal forces from the model. This arrangement reduces significantly the lateral loading applied to the central spindle.

The design of the platforms is such that at the test acceleration level, the top surface of the swinging platform is at a radius of 4.125 m within the centrifuge. To prevent confusion during the execution of tests, a series of standard centrifuge revolution speeds are used to conduct tests at different "nominal" g-levels, which sets the desired g-level in the model to be correct at a radius of 4 m (typically one third of the model's height from the base). However, in the case of dynamic centrifuge experiments, models sit at smaller radius (as shown in Figure 3.2), resulting in the acceleration levels within the model being slightly lower. For the experiments described in this thesis, the g-level at one-third height from the base of the model is approximately 93 % of the "nominal" level, meaning that in

Figure 3.1: The Turner beam centrifuge. Photo: Steve Chandler
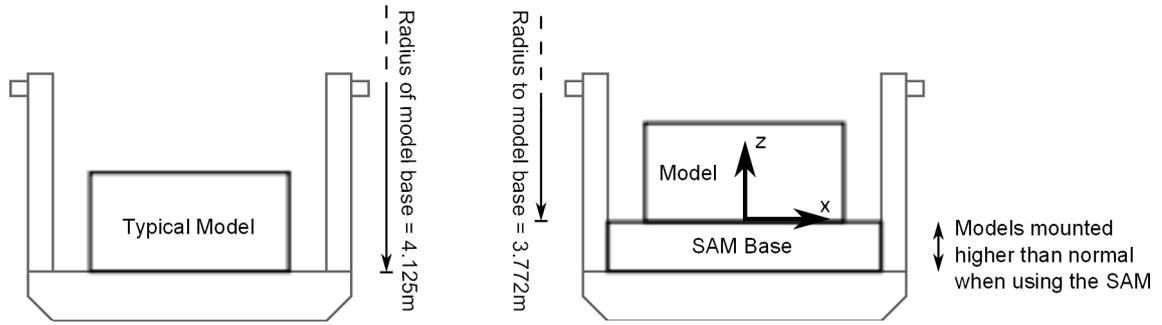
Figure 3.2: Working radii in Turner beam centrifuge
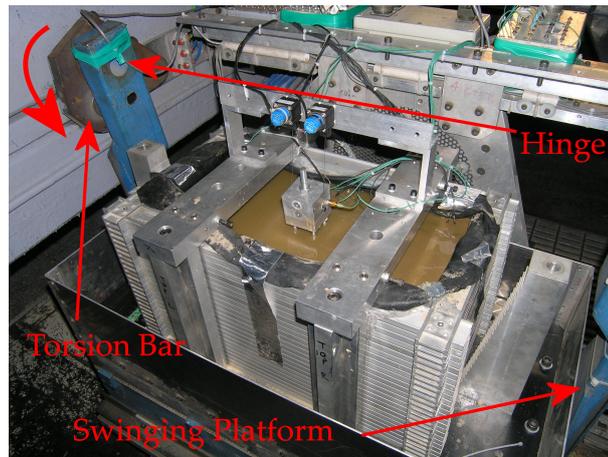
Figure 3.3: Swinging Platform and torsion bars

a "50 g" test, the acceleration level is 46.3 g. The numeric quantities presented in this thesis have been corrected so that they reflect the actual g-level. The fluid viscosity in the first test (and in subsequent tests to maintain similarity) carried out was set to the level assuming the standard nominal g-level. Hence fluid viscosities are approximately 8 % higher than water in the prototype.

Torsion bars (shown in Figure 3.3 are used to reduce the loading on the hinge mounting points for the swinging platforms. As the g-level is increased, the model gradually rotates so that its z-axis (defined in Figure 3.2) becomes aligned with the centrifuge. As the g-level increases past approximately 8 g, the torsion bars rotate, so that shortly after the package becomes aligned with the centrifuge, the bottom of the package comes into contact with the end plate of the centrifuge, meaning that the hinges do not carry further loads. However, since the swinging platform sits against a vertical end plate, the earth's gravity acts perpendicular to the model meaning that the model's vertical axis is not completely aligned with the g-field. In the tests carried out at 46.3 g, the error in alignment is $\approx$ 1.24 ^{o}.

Services (electrical power, fluid, air lines etc.) and data connections (between the control room and the model package) are transmitted through a series of slip rings mounted

on the centrifuge spindle. Generic in-flight visual monitoring of the test is carried out using small web cameras which are mounted near the spindle while additional monitoring of specific elements (e.g. driving pile groups in MS10) can be carried out by mounting additional web-cams at advantageous locations on the model.

3.3 Model Containers

When carrying out dynamic centrifuge experiments, the choice of container becomes important since the modeller is aiming to capture the behaviour of a limited soil mass within a semi-infinite soil layer. To eliminate boundary effects in the container being used, the containers walls must be able to deform with the same stiffness as the surrounding soil. Zeng & Schofield (1996) describes the use of "equivalent shear beam" (ESB) containers where rings of aluminium are separated by a rubber layer. The shear stiffness of the box can then be matched to the dynamic stiffness of a particular soil profile. However, these containers have a fixed shear stiffness and the number of rings is typically small. If the soil stiffness is not matched to the container, then some boundary effects can be expected and p-waves will be generated in the model. Additionally, the low number of rings will lead to strain discontinuity at the boundary wall, again introducing some boundary conditions.

Laminar containers overcome some of the issues of an ESB container. Laminar boxes typically comprise a number of metal rings, separated by either a low-friction material (e.g. Hushmand *et al.*, 1988), or a series of roller bearings (e.g. Brennan *et al.*, 2006). Under this arrangement the container achieves very low horizontal shear stiffness, meaning that the soil layer itself is able to determine the stiffness of the box. There are however some boundary effects introduced with these containers due to the finite mass of the rings themselves. The ability of the rings to slide through relatively large amounts means that these containers are particularly well suited to lateral spreading problems.

When studying liquefaction problems, the soil's shear stiffness rapidly reduces with the onset of liquefaction, meaning that at the beginning of an earthquake, the soil's shear stiffness might be orders of magnitude higher than at the end of the earthquake. This makes the use of a laminar box highly desirable for the experiments carried out. The laminar box used in testing, shown in Figure 3.4 comprises of a stack of 25 rings fabricated from Dural (sand blasted finish), which are separated by a series of roller bearings. The container has an inner plan area of 500 mm × 250 mm, with a height of 300 mm. A latex "bag" contains the sand and fluid within the rings of the box and fluid can be introduced to the base of the model through 4 channels in the base of the container. Further discussion concerning the performance of the container can be found in Brennan *et al.* (2006).
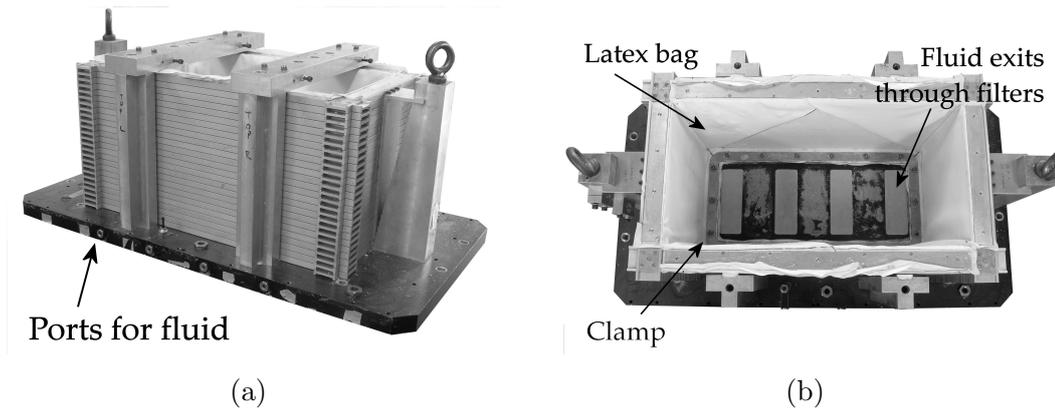
Figure 3.4: Laminar box

3.3.1 Complementary Stresses

Zeng & Schofield (1996) discuss the issue of complementary shear during dynamic centrifuge experiments. If the container is unable to provide the required complementary shear stresses, then the dynamic moments which result must be countered by a varying vertical effective stress distribution along the base of the model. In rigid-wall or ESB containers, the complementary shear stresses can be dealt with by using "shear sheets" (e.g. Madabhushi *et al.*, 1994) or "shear rods" (e.g. Wilson, 1998). When using a laminar container, the flexible boundaries make the use of shear sheets or shear rods challenging and hence they are not typically used. This may mean that p-waves arise in the models due to the lack of complementary shear, especially in the early stages of the earthquake before liquefaction has been achieved.

It is assumed that due to the soft nature of the latex rubber, sand particles at the boundary of the box will tend to "bite" into the latex bag and therefore that the critical interface for the generation of complementary shear stresses is between the latex rubber and the metal rings. A series of tests were carried out using the CAM-Shear apparatus (described by Kuo, 2011) where a 100 mm × 100 mm sample was subjected to a small pressure (between 0.5 kPa and 4 kPa) and moved steadily across a Dural surface. These tests indicated that the interface friction angle is 20 ^{o} and 24 ^{o} for untreated and sandblasted Dural respectively. The interface friction angle is clearly lower than that of the sands listed in Table 3.2. With the exception of MS02, the tests described in this thesis were conducted in a saturated state. The total horizontal stress therefore acts at the interface between the latex and metal rings, while the soil shear stresses in the soil are linked to the effective stresses. It is therefore thought that the friction between the latex and metal rings will be sufficient to ensure that the bag does not slip relative to the rings during the experiments. This suggests that the effect of pounding due to unbalanced

complementary shear stresses may not be a large issue in the laminar container when investigating liquefaction problems.

3.3.2 Model Earthquakes

Model earthquakes were fired using the stored angular momentum (SAM) actuator described by Madabhushi *et al.* (1998). The SAM actuator delivers simple quasi-sinusoidal input motions at with a shaking frequency, amplitude and duration which is selected by the user. Photographs which show the key components of the actuator along with an example input acceleration are shown in Figure 3.5.

Figure 3.5(c) shows the reasonable uniformity of the input acceleration. It can also be seen that the input accelerations do contain some harmonics of the fundamental frequency. However, the amplitude of the harmonics are very much smaller than that of the input motion, and reduce with increasing frequency.

At other research institutions, different actuators (e.g. servo-hydraulic shakers, electromagnetic shakers) are used. These actuators allow more complex input motions to be

(a) Front view

(b) Rear view

(c) Input acceleration in MS06, Earthquake 2
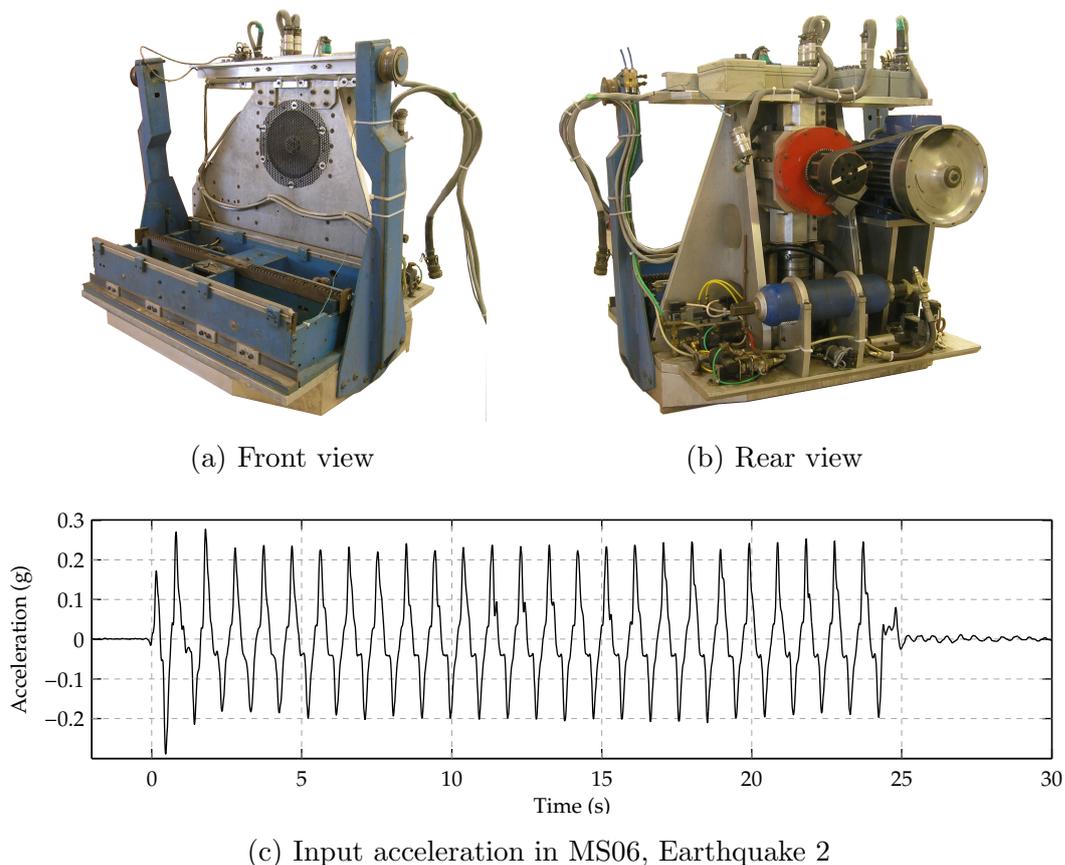
Figure 3.5: SAM Actuator

delivered to the model, allowing input motions from past earthquakes to be applied to the model. Typically, strong motion records from historic earthquakes will contain one or two large cycles of acceleration, with the remaining cycles being of much smaller peak acceleration. This suggests that the earthquake motions being applied by the SAM actuator subject the models to much harsher earthquakes than would be experienced in the field with similar acceleration levels. However, the use of "real" input motions is also questionable. Their use gives an indication how a structure might have performed during that particular earthquake. The acceleration records from past earthquakes are all completely different in terms of duration, magnitude and frequency content; even in the same earthquake event, localised site conditions lead to structures being subjected to very different motions. Therefore, although the use of real input motions may capture some of the important characteristics of an earthquake motion which might occur in the future, they do not necessarily give a better indication of structural performance than that obtained from a simple input motion. In addition, use of complex input motions mean that it is very difficult to distinguish the different mechanisms which are responsible for the behaviour of the soil-structure system.

In each of the tests carried out, earthquakes were designed to have a fundamental frequency of 1.1 Hz and a peak amplitude of 0.2 g. The duration of shaking was 23 s, with the exception of the first earthquake in MS06, where a longer earthquake lasting 46 s was used.

3.4 Soil Properties

Different sands were used in the course of this research and their properties are summarised in Table 3.2. The maximum voids ratio of the sands were found according to the "quick-tilt" test described by BS1377-4:1990. Minimum voids ratio of Fraction C sand was found by pluviation, following Cresswell *et al.* (1999). The value of e_{min} for Fraction E and
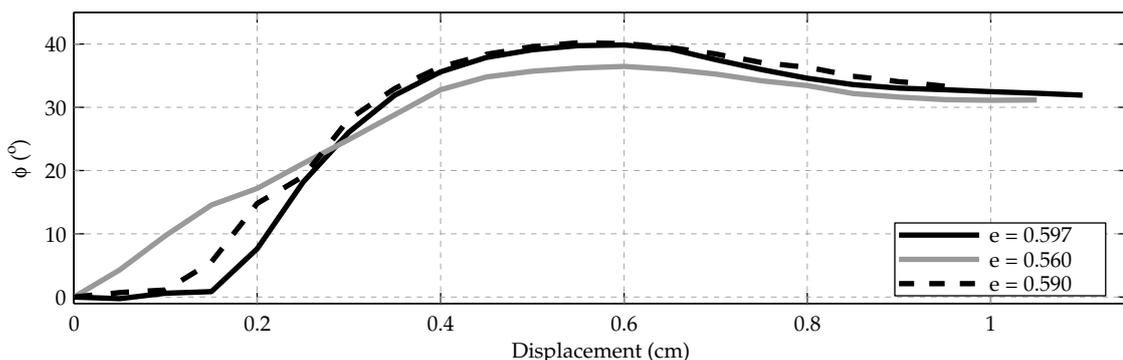
Figure 3.6: Direct shear tests on Fraction C sand at $\sigma'_v \approx 200$ kPa

Table 3.2: Properties of sands used in tests

Sand	Fraction C	Fraction E	Hostun
D_{10} (mm)	0.442	0.11	0.286
D_{50} (mm)	0.59	0.175	0.424
e_{max}	0.829	1.014 †	1.067
e_{min}	0.491	0.614 †	0.555 ‡
ϕ_{crit} (^{o})	31	33 †	33 ‡
G_s	2.65	2.65	2.65
Leighton Buzzard designation	25/52	72/100	N \A

†: Tan (1990)   ‡: Mitrani (2006)

Hostun sand, quoted in other research, was obtained by vibratory methods. The critical state friction angle of Fraction C was obtained from repeated direct shear tests at a confining pressure of 200 kPa with samples prepared by raining sand from a fixed height into a sample container of dimensions 100 mm × 100 mm. The results from the tests are shown in Figure 3.6. The properties quoted for Fraction C were found to be in reasonable agreement with those quoted by Sun (1990) and Stone (1988), the latter of which reports a series of direct shear tests, suggesting a value of ϕ_{crit} of 32 ^{o}.

The particle size distributions of the sands were found by single particle optical sizing (SPOS). The technique is known to produce size distributions which suggest particle sizes 20 - 30 % larger than those obtained by traditional sieving analysis (Abbireddy & Clayton, 2009; White, 2003). The differences in the obtained size distributions is due to the non-spherical nature of real soil particles. The particle size distributions of the sands described in Table 3.2 is shown in Figure 3.7, superimposed on the curves of Tsuchida (1970) which show the range of liquefiable soils. Fraction E sand, which was used in the models to form the liquefiable layers falls within the range of the most liquefiable soils.
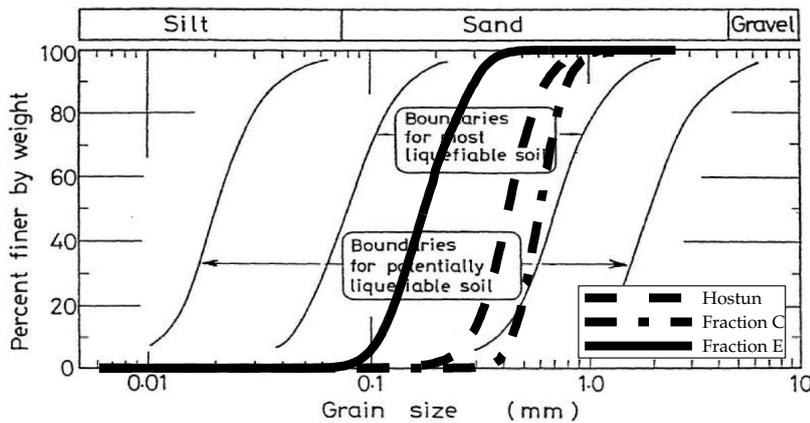
Figure 3.7: Particle size distributions for the sands used, superimposed on curves of liquefaction boundaries after Tsuchida (1970)

3.5 Instrumentation

When carrying out experiments with small-scale models, the use of instrumentation needs careful consideration. Whilst in an ideal scenario, the distributions of pressure, accelerations, stresses etc. would be known at every point throughout the model, in practice this is not possible. The addition of instrumentation can affect the model itself in a variety of ways. The instruments have a definite size and mass and therefore when the model is subjected to horizontal shear waves during an earthquake, the instruments could potentially induce shearing in the soil local to the device. The cables between the instrument and the acquisition equipment can potentially act both as local soil reinforcement and also drainage paths. In addition, the existing data acquisition system allows a total of 32 instruments to be used in each acquisition.

In order to address these concerns, robust yet miniature devices were used in the experiments described in this thesis. The different instruments which were used in the models are shown in Tables 3.3 and 3.4. These instruments have been used by many researchers, and individual descriptions of each instrument, with the exception of the strain gauges and MEMS accelerometers can be found in Knappett (2006). Additional discussion concerning the use of strain gauges on the heavily instrumented pile group can be found in Section 3.7.2, while the MEMS accelerometers are discussed in Stringer *et al.* (2010).

With the exception of piezoelectric accelerometers, the instruments used in the experiments were powered by a signal conditioning module. The modules are configured to supply either 5 V or 10 V to each instrument, while the data signal can be amplified by approximately 1, 10, 100 or 1000 times. The piezoelectric accelerometers used in the experiments are charge-based devices, and are used with a non-configurable charge amplifier.

3.5.1 Specific instrumentation limitations

It has been alluded to in Section 3.5 that the act of making a measurement can affect the measurement itself. This must be considered along with the suitability of the instrument to measure the desired quantity. In this section brief consideration will be given to some specific limitations which should be kept in mind when interpreting the data.

3.5.1.1 Pore pressure transducers

The PDCR81 PPTs used in these tests measure pressure via strain gauges mounted on a flexible diaphragm, as shown in Figure 3.8 and described by Konig *et al.* (1994). Although

Table 3.3: Instrumentation details: Manufacturers

Class	Instrument	Manufacturer	Model
Pressure	Pore Pressure Transducer (PPT)	Druck	PDCR81 PDCR810
	Total Pressure Cell	Tokyo Sokki Kenjyujo (TML)	PDB-PA
Acceleration	Piezoelectric Accelerometer	D.J. Birchill	A/23/S & A/23/TS
	MEMS Accelerometer	Analog Devices	ADXL78 ADXL193
Displacement	Linear Variable Displacement Transducer (LVDT)	RS Components	DC15
	Draw Wire Potentiometer	ASM	WS31
Load	In-line Axial Load Cell	Novatech	F259-Z3375
Strain	Strain Gauges	Tokyo Sokki Kenjyujo (TML)	FLA-2-350-23

Table 3.4: Instrumentation details: Typical settings and sensitivity (model scale)

Class	Model	Full Range	Excitation Voltage	Gain	Typical Sensitivity	Calibration Range
Pressure	PDCR81	7 bar	10	100	43 kPa/V	0 to 350 kPa
	PDCR81	1 bar	10	100	10 kPa/V	0 to 100 kPa
	PDCR810	1 bar	10	10	100 kPa/V	0 to 100 kPa
	PDB-PA	3 MPa	5	1000	1.2 MPa	0 to 1.5 MPa
Acceleration	A/23/S & A/23/TS		N/A	N/A	8 g/V	+/- 1g at 79.6 Hz
	ADXL78	35 g	5	1	18 g/V	+/- 1g at 79.6 Hz
	ADXL193	120 g	5	1	51 g/V	+/- 1g at 79.6 Hz
Displacement	DC15	30 mm	10	1	3.5 mm/V	-15 to +15 mm
	WS31	500 mm	10	1	55 mm/V	0 to 500 mm
Load (Pile Group I)	F259-Z3375	1kN	10	1000	81 N/V	0 to 90 N (Tension)
					5.2 Nm/V	0 to 0.45 Nm (Bending)
					870 N/V	0 to 11.5 N (Shear)
Load (Pile Group II)	FLA-2-350-23		5	100	1.9 kN/V	0 to 116 N
			5	1000	185 N/V	0 to 116 N (Compression)
			5		150 N/V	0 to 2.7 Nm (Bending)
			5		5 kN/V	0 to 35 N (Shear)
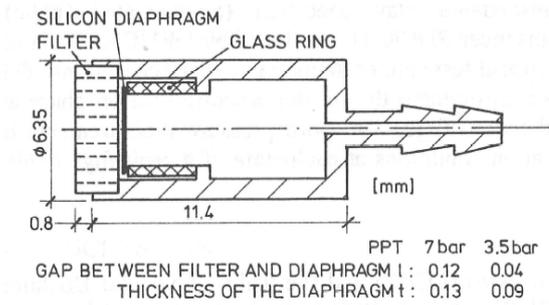
Figure 3.8: Schematic of Druck PDCR81, after Konig *et al.* (1994)

the deflection of the membrane is small, it implies that a small volume of water must pass through the filter (placed in front of the diaphragm) which protects the device from direct sand contact. Phillips & Sekiguchi (1991) found that the presence of filters made from sintered bronze, similar to those used in this research, led to a reduction in the amplitude of a time varying pressure wave at 100 Hz (model scale) by approximately 25 %. While these tests were carried out in without the presence of soil, in the tests described within this thesis, the PPTs are embedded within the model. This is likely to have a further effect on the ability of the instrument to measure sudden spikes in pore pressure, since the permeability of the soil will affect the flow of fluid into the device. It is therefore likely that dynamic components of pressure recorded in the tests carried out will both lag the actual pressure, and be of reduced magnitude.

3.5.1.2   Linear variable displacement transducers

LVDTs tend to suffer from high frequency noise (Kutter & Balakrishnan (1998), and as a result, the output signal tends to be heavily filtered. The DC15 LVDTs used in this research are internally filtered so that the -3dB frequency is 100 Hz (model scale). This implies that the instruments are not suitable for obtaining dynamic components of displacement. Therefore, only the low frequency components of frequency from these devices are considered reliable. Kutter & Balakrishnan (1998) describes a method for obtaining the dynamic displacement record of a particular object, where an LVDT is used to obtain the low frequency component of displacement, while the dynamic component is provided by double integration of an acceleration signal.

3.5.1.3   Piezoelectric accelerometers

The frequency response of the piezoelectric accelerometers is shown in Figure 3.9, where it can be seen that over the range of interest in this research (defined at model scale as the lowest fundamental frequency tested, 50 Hz, to 10 times the largest fundamental frequency, 800 Hz) the accelerometers have a reasonably flat response. It is apparent

that below 25 Hz (model scale) the frequency response becomes less satisfactory. The accelerometers are therefore unsuitable for directly obtaining estimates of displacement.

Brennan *et al.* (2005) suggests a procedure for estimating dynamic displacements, where the accelerations are double integrated, with the signal both high and low pass filtered after each step. This method is however unsuitable for cases where significant residual displacement accumulates (e.g. in cases where lateral spreading occurs). In these cases, techniques such as those described by Kutter & Balakrishnan (1998) are required.

In order for an accelerometer to faithfully record the motions of the soil, it must move with the soil, i.e. remain "coupled" with the soil. This issue was discussed briefly by Morris (1979) who carried out an analysis which examined the behaviour of a mass in two elastic half spaces. The analysis assumed that the coupling of the soil and accelerometer would be good so long as the natural frequency of the mass in the soil system remained well above the frequencies being measured. The natural frequency of the mass-soil system is reproduced in Equation 3.2.

$$f_n = \frac{1}{2\pi} \sqrt{\frac{8Gr_{footing}}{(1-\nu)m_{accelerometer}}} \tag{3.2}$$

Equation 3.2 indicates that the natural frequency is related to the square root of soil stiffness. Following the onset of liquefaction, the dramatic loss of soil stiffness means that this natural frequency will also reduce significantly. It is therefore likely that the accelerometers are unable to faithfully provide the true accelerations in liquefied soil. This was also suggested by Brennan *et al.* (2005).
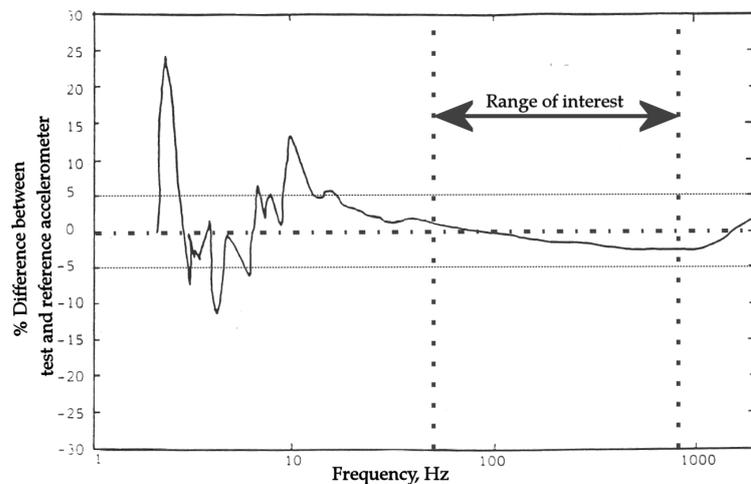
Figure 3.9: Frequency response of A/23 piezoelectric accelerometers, modified from Madabhushi (1992)

53

3.5.1.4   MEMS accelerometers

Micro-Electrical-Mechanical Systems (MEMS) accelerometers form part of a new class of instruments which have become available recently. The instruments obtained during this research were packaged sufficiently small (5 mm × 5 mm × 2mm) to allow their placement in novel positions (e.g. within a model pile). The instruments are conceptually a mass-on-spring and as such, these instruments allow measurement of the g-field acceleration as well as dynamic accelerations.

The frequency response of these instruments is thought to be good over the range of frequencies significant to this research out, as shown in Figure 3.10. Since these instruments can measure the acceleration of the g-field, it presents the opportunity to measure inclinations or rotation of either the soil or an object (such as a pile) during an earthquake. However, while the trend from the data may be reasonable, the dynamic data (high frequency) must be considered with care. Figure 3.11 shows the components of acceleration from the g-field and horizontal acceleration recorded by a rotated MEMS. If the MEMS rotates cyclically during the earthquake, then the dynamic component of acceleration recorded by the MEMS transducer will contain components of both the g-field and the horizontal acceleration which cannot be separated.
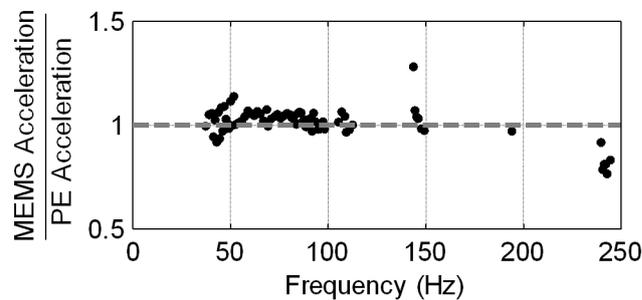
Figure 3.10: Comparison of acceleration recorded by piezoelectric and MEMS accelerometers in frequency domain (model scale)
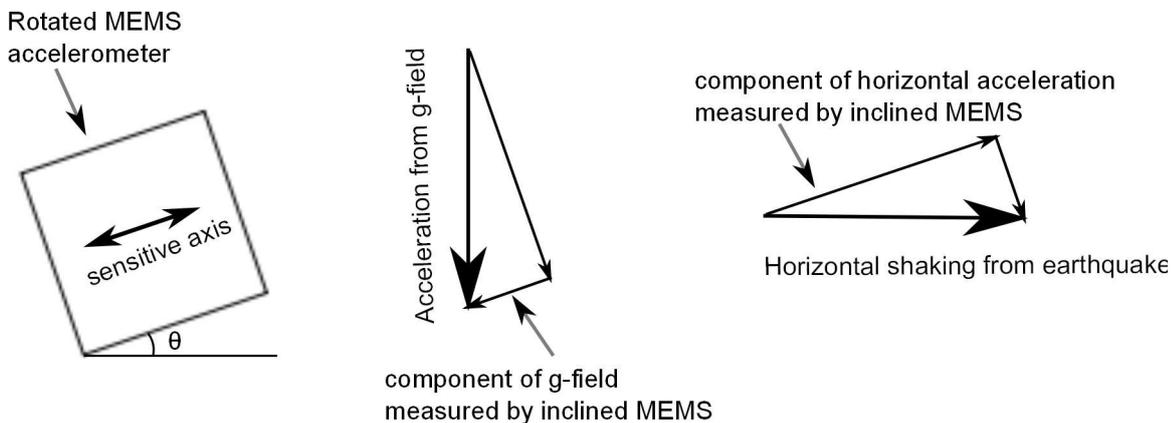
Figure 3.11: Components of acceleration recorded by MEMS accelerometer

3.5.1.5 Total stress cells

Similar to PPTs, total pressure cells measure pressure through the deflection of a flexible diaphragm. This immediately raises concerns about soil arching which might prevent accurate measurement of soil pressures. The issue was discussed by Dewoolkar *et al.* (1998), who found that under dynamic conditions, the use of total stress cells was acceptable with saturated sands. However, pressures recorded before an earthquake, as well as any change in pressure after an earthquake will be questionable due to soil arching.

3.5.1.6 In-line axial load cells

In-line axial load cells provide very linear response when the loading is purely axial. However, as shown in Table 3.4, these instruments are significantly affected by shear loads and bending moments.

3.5.1.7 Strain gauges configured for axial loading

The strain gauges bridges on the model piles described in Section 3.7.2 were optimised to measure axial loading. However, although strain gauge bridges can be optimised for a particular type of loading, they tend to be affected by loads in other directions (e.g. bending moment or shear). Larson (1977) developed a load cell consisting of multiple strain gauge bridges to allow measurement of bending, axial and shear loads in isolation. Calibration of each bridge for each type of loading was carried out (i.e. bridge for measuring axial load was calibrated for axial load, shear and bending moment). This allowed the individual loads to be isolated after the experiment. While technically possible to use a similar stress cell in the experiments carried out, the limitation on the number of channels which could be used in a dynamic centrifuge test (see Section 3.6) would have severely limited the collection of other data in the centrifuge experiments. It was therefore decided to accept the error in measurement for these experiments in favour of being able to place a greater number of strain gauges on the piles, as well as other instrumentation in the model. During the course of the experiments, some strain gauge failures were encountered. These were often due to broken wiring, or minute leak paths allowing fluid to reach the electrical terminals under high fluid pressure. This highlights the need for load measurement at multiple locations in the pile group.

The strain gauge bridges were calibrated for shear and moment loading, and the parameters shown in Table 3.4 indicate the results when the loading was applied in the direction expected during the tests due to the earthquake motions. The strain gauge bridges were

found to be relatively insensitive to shear loads. However, the gauges are affected to some degree by moment loading. As an example, maximum pile cap accelerations in the first earthquake of MS05 and MS06 were of the order of 6 g at model scale. With a pile head mass of approximately 1.5 kg, and assuming that the centroid of the lateral force from the soil acts at a depth of approximately 0.15 m, then the pile head moment would be approx 3.4 N, which would register a voltage of approximately 0.02 V.

3.6 Data Acquisition

During centrifuge experiments the purpose built *CDAQS 2/32 CD 198 Acquisition* module was used to collect data. The module enables up to 32 channels of data to be collected at a maximum sampling rate of 5 kHz (model scale). The module is controlled by a computer in the centrifuge control room. Acquired data is temporarily held in temporary memory by CDAQS until it is uploaded to the controlling computer. Two implications arise from the temporary storage of data. Firstly, the module limits the total stored data to 2 megabytes, equating to a maximum of 32,000 data points with 32 channels. In order to achieve both a sufficiently high sample rate during the earthquakes and capture data for a reasonable period after the earthquake (in excess of 2 minutes at model scale), data during a test must be acquired in multiple phases, covering, as a minimum, the earthquake and the subsequent dissipation of pore pressures. Secondly, the module is known to be suffer from occasional crashes; since acquired data is only held in temporary memory any system crash results in the total loss of any data which has not been uploaded. Therefore, to address these two issues, data was acquired in three separate phases during centrifuge tests, as shown in Table 3.5, with acquired data uploaded at the first opportunity (i.e. swing up data is uploaded before the earthquakes are fired). On occasions where CDAQS module crashes, the system can be restarted in-flight.

Alternative data acquisition systems were available for use at the time of testing, which would have allowed both additional channels to be sampled and a higher sampling frequency to be used. However the CDAQS acquisition system provides far higher quality (lower noise) data due to the digitisation of the signals close to the model container.

Table 3.5: Sampling rates during different test phases (model scale)

Phase	Duration	Sample Rate
Swing-Up	$\approx$ 25 min	4 Hz
Earthquake	1.5 s / 2 s	4 kHz
Dissipation	3 min	10 Hz
Swing-Down	$\approx$ 5 min	4 Hz

3.7   Model Pile Groups

In the course of this research programme, two different designs of pile group were used. In a series of pilot tests (MS01 to MS04), the pile group described by Knappett (2006) was used. During the execution of these tests, it was decided to create a more densely instrumented pile group such that the load distribution along the pile shaft could be determined. In the section which follows, the pile group used in the initial tests will be referred to as the "simply-instrumented pile group," and that used in the later tests "heavily-instrumented pile group."

3.7.1   Simply-instrumented pile group, JK-PG

When using the simply-instrumented pile group (shown in Figure 3.12(a), measurements of axial load were made possible on one of the legs of the pile group, using an in-line axial load cell at the head of the pile, while a total pressure cell was inserted into the base of the pile. Wiring to the total pressure cell was protected from mechanical damage by routing the wires within the pile, exiting near the head of the pile through a small hole (above the soil surface in the tests carried out). Accelerometers were mounted onto the pile cap to measure accelerations aligned with direction of applied shaking. Additionally, measurements of pile cap settlement were made using draw-wire potentiometers attached to the two sides of the pile cap normal to the direction of shaking (i.e. on the same face as the accelerometers).

Key parameters of this pile group are reproduced in Table 3.6, while more detailed description of the design and manufacture of this pile group are found in Knappett (2006).

Table 3.6: Characteristics of the prototype pile groups and comparison with two possible field piles

	Field pile groups		Model Pile Groups	
	RC Concrete	Steel	JKPG	MSPG
Pile outer diameter, D_0 (mm)	496 †	500	460	500
Pile length, L_p (mm)			14.1	9.25
EI (MNm^2)	15 - 30 †	92.5	121	90
EA (GN)	6	3.1	9	4.6
Pile centre-centre spacing, s (m)			2.6 (5.6 D_0)	2.9 (5.8 D_0)
Pile cap dimensions (m)			4.1 × 4.1	4.75 × 4.75

†: Knappett (2006)

(a) Simply-instrumented pile group

(b) Heavily-instrumented pile group
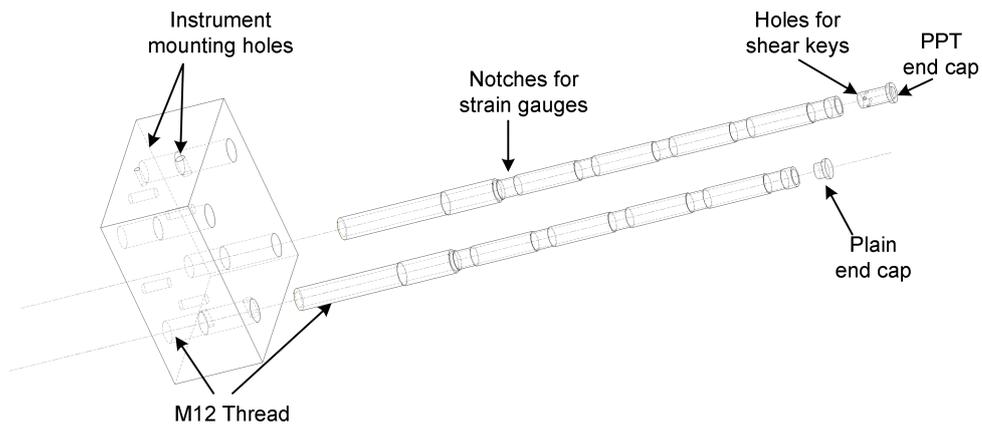
(c) Exploded view of new pile group
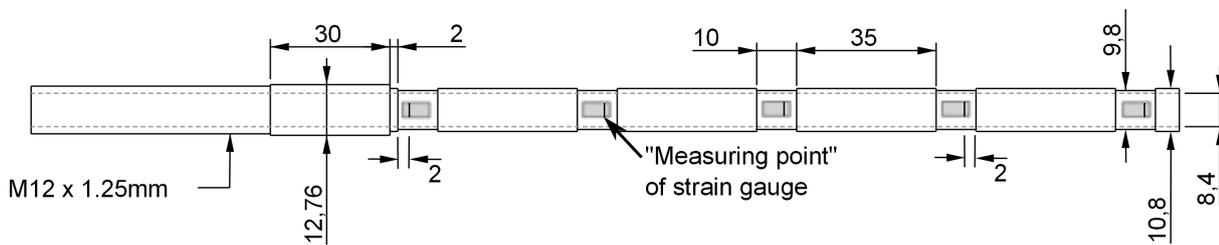
(d) Pile leg dimensions at model scale (mm)

Figure 3.12: Pile groups used during research programme

In the tests carried out with this pile group, the pile tips were embedded in a dense layer of Fraction C. From Tables 3.2 and 3.6, this means that the pile diameter to particle size (using the D_{50} size) ratio is 14. Gui *et al.* (1998) suggests a minimum ratio of 20 when carrying out tests with a CPT. Where the ratio is lower than 20, particle freedom is restricted, leading to an increase in resistance. The pile tips in the experiments with this pile group were at approximately 30 pile diameters depth. The results of Gui *et al.* (1998) suggest that at this depth and with a pile diameter to particle size ratio of 16, the base resistance would be approximately 10 % greater. Taylor (1995) suggests that for circular footings, the ratio of footing diameter to particle size should be a minimum of 15. It is therefore recognized that the combination of the sand used in the dense layer and the diameter of the piles will result in a slightly increased base resistance. However, it will be shown in Section 4 that the settlement of the pile group does not appear to have been greatly affected. Additionally, the initial tests were conducted to investigate whether a coarser sand in the dense layer would lead to drastically reduced settlements which might change the mechanism of pile group failure from settlement to buckling. The increased base resistance would be expected to encourage the change of mechanism, and therefore it is deemed that the small error arising from the particle size affects were acceptable.

3.7.2 Heavily-instrumented pile group, MS-PG

Strain gauges were selected for use in measuring the axial load distribution on the piles. In order to easily attach the strain gauges to the pile, it was decided to increase the model pile diameter. The MS-PG pile group was therefore designed for tests which would be carried out at a g-level of approximately 50 g. The piles and pile cap were machined by the central engineering workshops, using Dural for both the piles and the pile cap. Dural tubing with an outer diameter of 12.8 mm, and wall thickness of 2.2 mm was used to create the piles. The outer diameter was reduced to 10.8 mm (wall thickness = 1.2 mm) for the main body of the piles. To increase the axial strains at the point of axial load measurement, a 10 mm long notch was machined in the piles, reducing the wall thickness at these points to 0.7 mm. The key dimensions of these piles are shown in 3.12(d).

The pile groups were designed to allow the pile groups to be tested with an air gap between the pile cap and the soil surface (free-standing) and also with the pile cap in contact with the soil surface (cap-supported). The piles were therefore designed so that the length below the pile cap could be extended. The heavily-instrumented pile group is shown both in its assembled form, and as an exploded sketch in Figure 3.12(b) & 3.12(c) respectively. At the top of each pile, a threaded section screws into the top of the pile cap, while the smooth and slightly larger diameter section immediately below slides within a similarly sized hole in the bottom half of the pile cap. The diameter of the pile and the hole in the

3. MODELLING TECHNIQUES

(a) Strain gauge bridge wiring

(b) Location of gauges on pile section
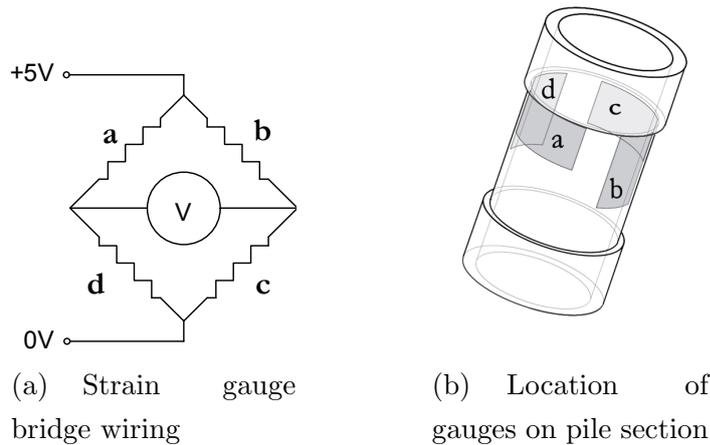
Figure 3.13: Strain gauge configuration

pile cap were machined to be nominally the same so that the pile cap would effectively restrain the head of the piles. A nut is tightened on the threaded end of the pile against the pile cap to secure the piles in place. To avoid reducing the wall thickness excessively in the threaded section on the pile, an M12 x 1.25 mm thread was used.

Similar to the simply-instrumented pile group, accelerometers are mounted to the pile cap in the direction of shaking. Draw-wire potentiometers are used to measure the settlement of the pile cap relative to a fixed datum and are similarly mounted to the pile cap.

It was decided to measure the axial loading at 5 separate locations along the pile length. The strain gauges, manufactured by Tokyo Sokki Kenkyujo Co., which were used in the bridges were temperature compensated for aluminium and had a resistance of 350Ω and a gauge factor of 2.15. The bridge circuit and the orientation of the gauges which was used is shown in 3.13(a) - (b) and is designed to maximise the sensitivity to axial strains, while minimising that of bending and shear strain. Strain gauges were bonded to the pile at the notch locations using cyanoacrylate as supplied by the strain gauge manufacturer. The bonded strain gauges were coated in a thin layer of silicon dispersant to ensure that the exposed surface of the gauge did not affect the strain measurement. A Ø1.5mm hole was drilled through each slot, allowing the strain gauge wiring to be routed through the pile. The remaining space in the slots was filled with Araldite, which provided both waterproofing and physical protection to the strain gauges. The piles which were not instrumented with strain gauges had similar slots machined so that the behaviour of the piles would be consistent.

Two designs of end cap were used on the piles. The piles which had been strain gauged were fitted with a solid end cap, as shown in 3.14(a). In later tests, an attempt was made to measure the acceleration experienced by the pile tips and also the inclination of the piles using MEMS accelerometers. A single MEMS was glued to the top of the solid

(a) Simple end cap   (b) PPT end cap
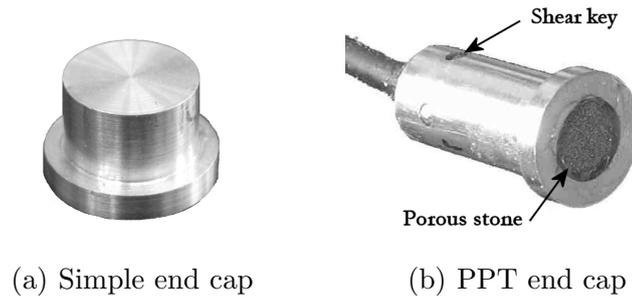
Figure 3.14: Pile end caps

end caps using cyanoacrylate (superglue), with one aligned with the direction of shaking (MEMS model ADXL78) and one aligned with the pile axis (MEMS model ADXL193). The two piles which were not strain gauged were fitted with pore pressure transducers which measured pore pressures at the tip of the piles. The PPTs were installed in the end cap shown in 3.14(b). Silicon dispersant was placed in the annular space between the pile and the PPT as well as behind the instrument to prevent fluid passing the instrument. The silicon barrier meant that the PPTs would be subject to water pressure on one side only. Shear keys were therefore inserted behind the PPT to resist any movement during the test. A porous bronze disc was placed in front of the PPT to act as a barrier to the sand and was held in place using Araldite. In the first three tests where these PPTs were used (MS05 to MS07), no attempt was made to saturate the air pocket between the PPT and the bronze filter, leading to poor dynamic response. From tests MS08 to MS12, an attempt was made to saturate the pile tips prior to installation in the model by placing the pile group under vacuum with the tips submerged in the pore fluid. This improved the dynamic response of the instrument. However, since the volume between the filter and the PPT diaphragm in the pile tips is larger than normal, it is to be expected that the dynamic response will be somewhat reduced, and there will be a greater phase lag with respect to the actual pressures.

Calibration of the piles for axial loading was carried out before each test. In each case, the piles were placed so that they were oriented vertically. Axial loads were applied using a load "hanger," placing the piles in compression as shown in Figure 3.15(a). Calibrations for shear and bending moments were carried out by placing the pile group so that the piles were horizontal as shown in Figure 3.15(b). Loads were then applied vertically to the end of the pile group, and also (for bending moment calibration) at a distance 45 mm beyond the tip of the pile using a rod extension which slotted over the end of the pile tip. When carrying out the calibration for shear loading, the global value of bending stiffness (EI) was obtained for the pile group by measuring the vertical tip deflection of the pile using an LVDT. The vertical loads applied to cause the tip deflection also caused a small rigid body rotation of the pile group (due to stiffness of the clamp holding the pile group

(a) Axial load   (b) Bending and shear
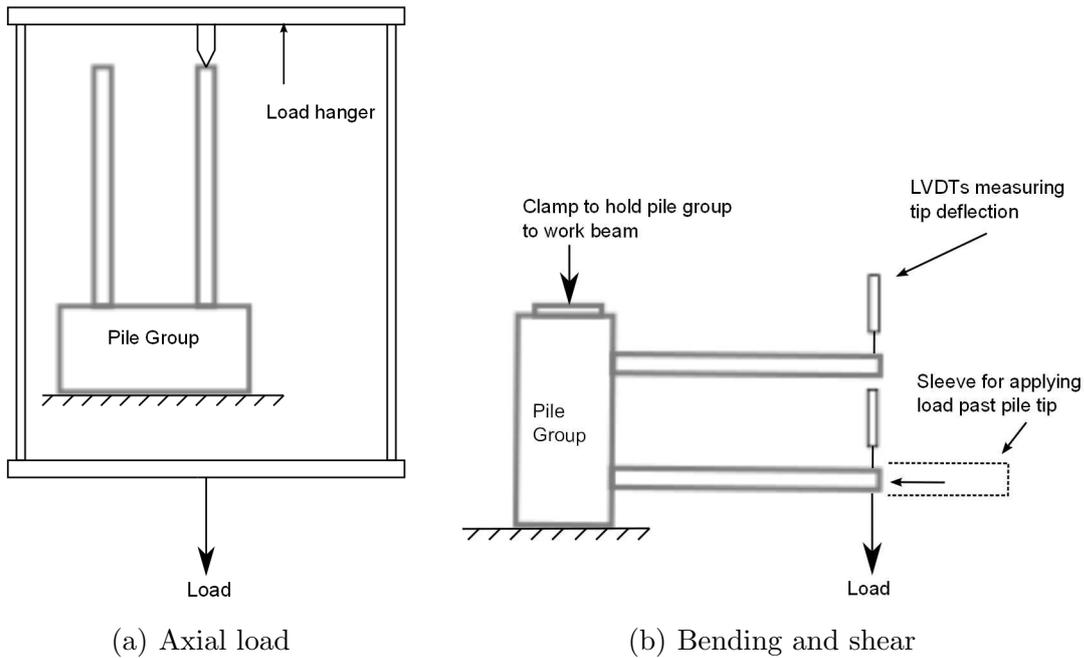
Figure 3.15: Set-up for calibration

to the work beam). The deflection of an unloaded pile was therefore also measured so that this error could be removed.

3.7.2.1 Axial load offsets with MS-PG pile group

When interpreting data from the instruments in the model, it is necessary (with the exception of accelerometers) to obtain a "zero" reading and reference the voltages obtained during the test to this point. Scaling the difference in voltage between the reference point and any subsequent or preceding time allows the variation in the quantity of interest to be obtained. When carrying out centrifuge modelling, the values at 1g immediately prior to the experiment (i.e. before the centrifuge begins to spin) are a convenient reference point.

However, interpreting the voltage offset for the axial strain gauges proved challenging. When carrying out the experiments, it was assumed that due to the low stresses in the model at 1g, the shaft friction before the experiment would be negligible, and the values immediately prior to swing up of the centrifuge therefore offer a convenient "zero" point. Ideally the same argument would hold after the experiment once the model has returned to 1g so that negligible shaft friction should also be observed and therefore the values after stopping the centrifuge should also offer a reasonable "reference" for selecting the offset voltages.

However, over the course of the experiments, it was found that some differences would be recorded between the pre-test and post-test strain gauge offsets. These can arise from a variety of causes such as:

- Residual axial load on the pile from the experiment

- Effect of bending moments or shear on the output voltage

- Permanent deformation of the pile as a result of the axial loading

- Residual strains arising from imperfect bonding between the strain gauge and the pile

- Thermal effects arising from external temperature differences or due to the current through the gauges

When calibrating the piles for axial load towards the end of the experiment series, it was observed that on some occasions, a voltage offset could develop if the pile was left unloaded for a period of time. This suggests some thermal effects on the piles. Additionally, offsets were sometimes encountered as a result of the loading of the pile, suggesting some residual strains arising from imperfect bonding of the gauges could account for some of the voltage offsets observed during the experiments. Both of these effects would suggest that using the offsets taken at the end of the experiment might be preferable. In the case of the former, it would be expected that any thermal effect would tend to stabilise, so that after the period following the initial powering up of the instruments before the test and the 30-40 minutes taken to swing-up the centrifuge, it might be reasonable to assume the thermal affects no longer influence the readings. Typically, the largest loads are seen at the very start of the experiment. Therefore if any accumulated strains are occurring, it may be that the greatest accumulation occurs near the beginning of the experiment, during swing up, and potentially the first cycle of earthquake loading. The offset voltages have therefore been taken from the post-test readings.

In the cap-supported experiments of MS07 - MS09, which will be discussed in Chapter 5, the axial loads were found to drop significantly following the start of the earthquake, reaching a "plateau." In some cases, it was found that after subtracting the voltage offsets some strain gauges recorded voltages which suggested tension throughout several cycles, despite the pile accumulating settlement. In these cases, an additional offset was applied to the gauges so that the average of the axial load on these "plateaus" was zero. An example from MS09 is shown in Figure 3.16, with units in model scale.
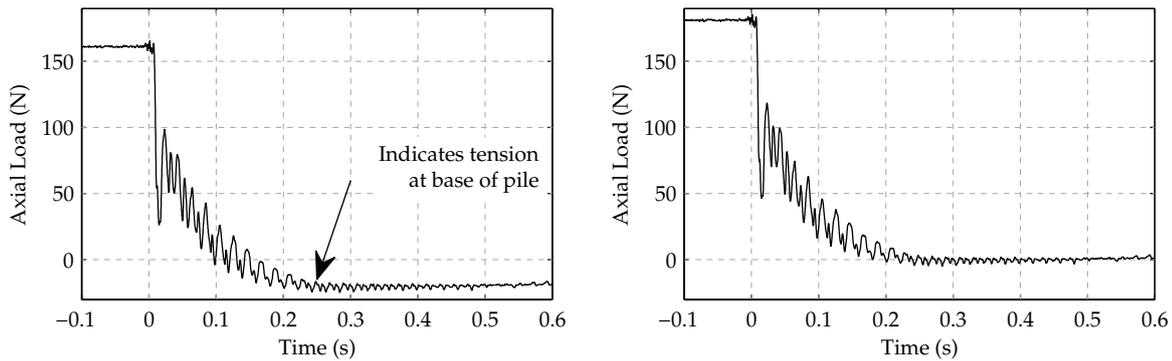
(a) Data corrected using offset at end of flight

(b) Data corrected so that plateau is set to be "zero"

Figure 3.16: Axial loads recorded by SG A during MS09

3.7.3 Interface angles of friction

In tests MS01 to MS11, the piles were installed into the model with no surface treatment following the initial machining. The surface roughness of the piles was measured using a Surfcom profilometer. It was found that the normalised surface roughness is 0.5×10^{-3} and 2×10^{-3} for Fraction C and Fraction E sand respectively. Following Uesugi & Kishida (1986), this suggests an interface friction angle of approximately 17 ^{o}, as shown in Figure 3.17. The surface roughness was increased in MS12 by bonding grains of Fraction E sand to the surface of the piles using the gel form of cyanoacrylate (superglue). Assuming that the surface roughness is close to the particle size of the Fraction E, this implies normalised roughness of 0.25 and 1 for Fraction C and Fraction E sands respectively. From Figure 3.17, it is assumed that the interface angle of friction becomes close to the critical state angle of friction.
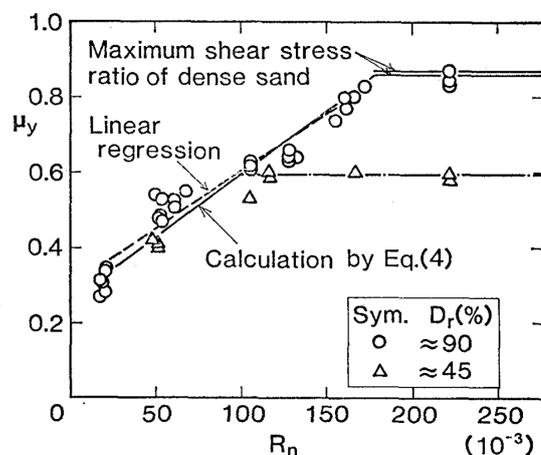
Figure 3.17: Interface angle of friction between Toyoura sand and mild steel

3.7.4 Realistic field piles

The design of the JK-PG pile groups by Knappett (2006) was carried out with a realistic steel pile of outer diameter 496 mm and wall thickness 19mm in mind. These pile sections were thought to be representative of piles used in the field according to Fleming *et al.* (2009). However, following the discussion of the actual g-level in the centrifuge in Section 3.2.1, the prototype quantities of the model piles do not reflect the original prototype. Instead, the prototypes are now compared against a steel pile with outer diameter 500 mm and wall thickness 9.5 mm in Table 3.6. This still appears to be within the normal range of wall thicknesses for steel piles used in the field (Fleming *et al.*, 2009). The prototype reinforced concrete pile discussed in Knappett (2006) is also included for comparison. While the example reinforced concrete piles are much less stiff axially than the model piles used in the tests, in some cases, steel casings are inserted into boreholes to stabilise the hole when concrete piles are cast (steel jacketed piles). In these cases, the bending and axial stiffness of the pile would be increased substantially, to the point that they may by represented by the model piles used in this research. It should also be noted that the model piles were tested with closed-ends. This condition is seldom encountered in the field. However, when tubular piles are jacked or driven into the ground, a soil plug tends to form. This represents to some degree the closed-end nature of the model piles. In the course of this research, it is assumed that soil plugs remain unaffected by the earthquake.

3.7.5 Installation of pile groups at 1g - "Bored piles"

In tests MS01 to MS09 the pile groups were manually installed at 1g. In the initial tests (i.e. MS01 to MS04) the pile group's position in plan view was set manually, using rulers as a guide. In tests MS05 to MS09, a template was fabricated, which allowed consistent placement of the pile group, as shown in Figure 3.18. In all cases, a small spirit level was

Figure 3.18: Installation of heavily instrumented pile group at 1g

used to ensure that the pile group was installed vertically into the model. Since the pile group was installed under low stress conditions, it is thought that the results obtained from pile groups installed in this manner are most representative of bored piles in the field. Throughout this thesis, piles which have been installed at 1g will therefore be referred to as bored piles.

3.7.6 Installation of pile groups at 50g - Jacked piles
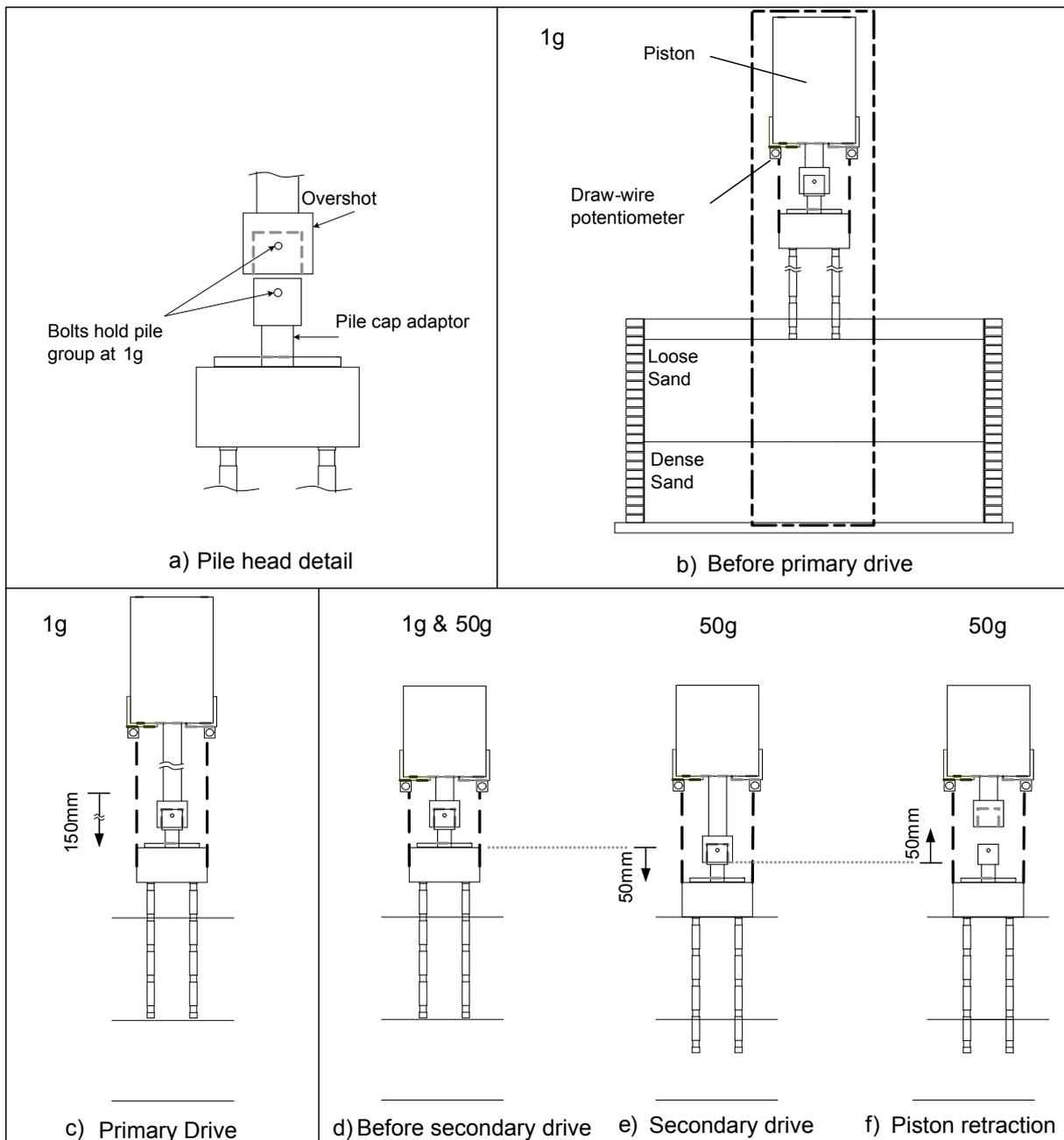
Figure 3.19: Process followed to jack the heavily instrumented pile group

Tests MS10 to MS12 were designed to investigate the effect of the installation method on the observed response of the pile group to dynamic loading. In these tests, the piles were installed in a two part process, using pistons to "jack" the piles into the model. Additional height above the model is required to install the pile groups in this method which as a bare minimum would equate to the total length of the pile group and the piston. It was therefore decided that the process would be carried out in two stages to reduce the overall height of the package. The procedure followed is shown in Figure 3.19.

In order to ensure the piston and pile group were aligned, a cylindrical adaptor was attached to the top of the pile group, and an adaptor, which fitted over the top of this cylinder, was attached to the piston. Under 1 g conditions, a piston with a 150 mm stroke length was used. The piles were driven 150 mm (model scale) by slowly increasing the pressure applied to the piston. After the initial drive was completed, the piston was replaced with a 50 mm stroke piston. Back-pressure was applied to the piston to ensure that loads were not applied to the pile group during the swing up of the centrifuge. Once the test g-level of 50 g had been achieved, the back pressure was released from the piston, and pressure increased slowly to drive the pile group. After the driving was complete, the piston was retracted by applying back pressure to the piston to ensure that it did not interfere with the pile group during the earthquake. During each phase where the pile group was being driven, data was logged at 100 Hz. The data collected during the jacking process will be discussed in further detail in Chapter 6. Gui & Bolton (1998) carried out tests with a model CPT in the centrifuge which indicated that approximately 5 CPT diameters were required for a probe to fully develop the resistance of a new sand layer. Since the final phase of pile installation takes place at g over a distance of approximately 4.6 diameters, it is thought that this final installation phase is sufficient to fully mobilise the soil's resistance. As a result, it is believed that the piles in these tests behave in a manner similar to jacked piles in the field and will therefore be referred to as such in this thesis.

3.8 Model Preparation

3.8.1 Sand Pouring

The dense sand layers in all of the models were poured using the automatic sand pourer described by Madabhushi *et al.* (2006); Zhao *et al.* (2006). The same work found that while the relative density achieved was primarily a function of the mass flow rate of sand being poured (relative density increases with reducing flow rate) and the sand being used, but that the distance through which the sand falls also has an effect. Using the original

configuration of the sand pourer, Fraction E sand could only be poured to relative densities greater than 50 %. This was greater than the target relative density of approximately 35 %, meaning that a manual sand pourer (shown in Figure 3.20) had to be used to create the loose sand layers in MS01 to MS04.

When using the manual sand hopper, the sand's mass flow rate is controlled by a variable-size orifice, whose position can be set using a extendible bolt. Sand falls through a fixed tube to the model container. However, sand arching across the variable orifice is a common problem when using the manual sand hopper, meaning that the flow rate tended to be highly variable and often much lower than intended. The would be expected to cause large variations in relative density in sand layers poured using the manual sand pourer, in particular, creating pockets of sand which are much more dense than the majority of the sand layer.
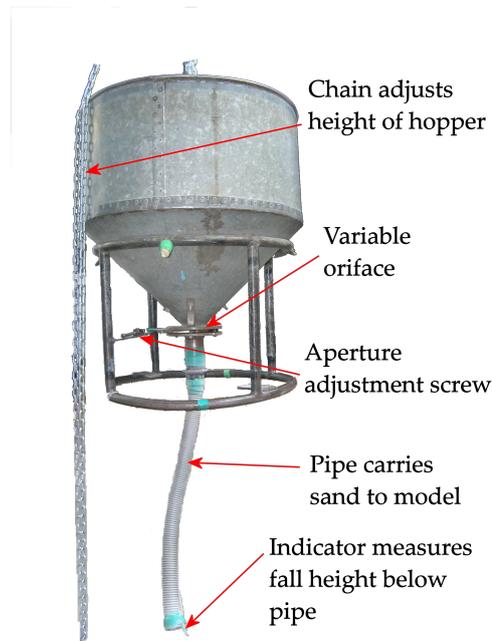
Figure 3.20: Manual sand hopper used in MS01 to MS04 to pour loose sand layers
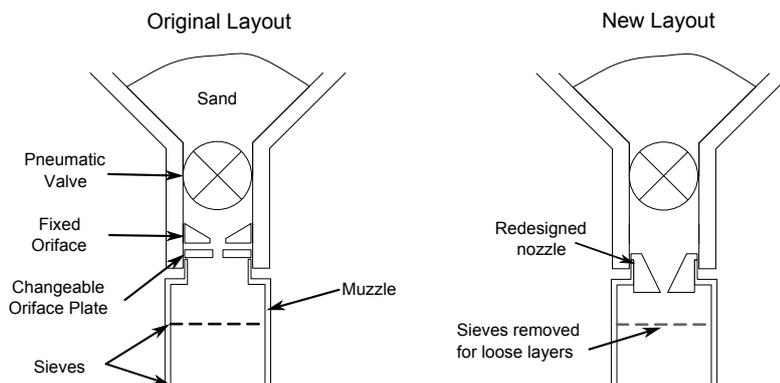
Figure 3.21: Alterations made to the delivery system of the automatic sand pourer

Table 3.7: Sand pouring settings

Layer	Loose	Dense	Dense
Sand	Fraction E	Fraction E	Fraction C
Nozzle diameter (mm)	7	5	5
Number of sieves	0	2	2
Sieve mesh size (mm)	N \A	0.85	1.7
Fall Height (mm)	500	750	500
Relative density (%)	35	90	100

Examination of the automatic sand pourer revealed that it was fitted with a fixed orifice plate of 9 mm diameter, below which a replaceable orifice allowed the flow rate of sand to be altered. Additionally, sieves held in a muzzle below the orifice plates spread out the falling sand so that a more even sand surface is obtained. A schematic of the original set-up is shown in Figure 3.21. As found by Zhao *et al.* (2006), the mass flux of a given sand is the controlling factor in the achieved relative density. Further than this, it is logical that it would actually the mass flux per unit area of model covered by the falling sand which determines the relative density. Hence both the sieves below the orifice, and the fixed orifice plate act to limit the smallest achievable relative density. By removing both of these items, it was found that a relative density of 23 % could be achieved with Fraction E sand, which was beyond the range anticipated in this research. It must be noted however that when the sieves are removed from the muzzle, the sand tends to fall as a concentrated jet. This means that as the sand is poured, the surface is no longer uniform, but forms a series of ridges. Despite this, it was felt that the greater consistency with which models could be poured using the automatic sand pourer remained preferable to continued use of the manual sand hopper. Therefore, the automatic sand pourer was used for both the loose and dense sand layers in models MS05 to MS12, using the settings which are shown in Table 3.7. The relative densities quoted in the tables were found by carrying out several calibration runs during the course of the test series, with the results confirming that the relative density remained reasonably constant. Additional calibration of the new layout was carried out and described by Chian *et al.* (2010).

The sand pouring process was periodically halted to allow both PPTs and accelerometers to be placed within the models. Prior to placement, the intended location of the instrument was lightly marked in the sand, and the actual "as-placed" location was measured after the instrumentation had been placed. The wires from the instruments were taped to the internal latex bag so that the instruments would remain in position as the sand pouring continued. Once the sand level had passed above the required height, the surface was levelled by running a flat edge along a pair of reference bars at the required height.

3.8.2 Saturation

The development of the CAM-Sat saturation system will be described in the following sections. Further details concerning the system and the range of testing carried out during it's development can be found in Stringer & Madabhushi (2009, 2010a).

In order to correct the discrepancy in time scaling highlighted in Section 3.2, models (with the exception of that in MS02) were saturated with a viscous fluid. In the past, researchers at the University of Cambridge have used silicone oil as a pore fluid (e.g. Haigh, 2002), however more recently, solutions of Hydroxy-Propyl Methyl Cellulose (HPMC) have been used both at Cambridge (e.g. Knappett, 2006) and elsewhere (e.g. Kulasingham, 2003). Aside from cost and logistical advantages, HPMC has a unit weight very close to water, while silicone oil's unit weight is approximately 80 % of water's.

Solutions of HPMC were prepared using deaired water and dry powdered HPMC following Stewart *et al.* (1998), who found that the solution's concentration, C (percent by mass), could be calculated for a required viscosity using the following equation:

$$v_{20} = 6.92C^{2.54} \tag{3.3}$$

3.8.2.1 Existing method of saturation

At the commencement of the research programme, models at the University of Cambridge were saturated using a manually controlled system, recently upgraded by Knappett (2006). In this system (shown schematically in Figure 3.22) both the model and the reservoir (large motorised mixing tank) of pore fluid are placed under a vacuum of approximately -90 kPa. The vacuum acting on the fluid reservoir is then reduced, creating a pressure difference which drives the pore fluid into the base of the model. The research worker estimated the rate of fluid flow from a crude mass measurement (scales with 0.5 kg resolution) over a set period of time. This system had a few notable drawbacks:

- The researcher had to continually monitor the flow rate.

- The resolution of the mass flux was too low, meaning that the models were vulnerable to excessive disturbance.

- Changes to the pressure were made manually, so could only occur when the researcher was checking the flow rate.
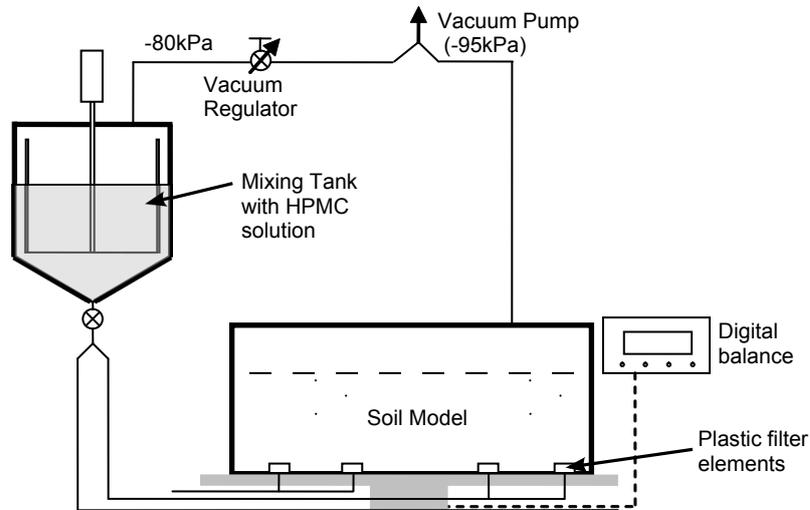
Figure 3.22: Existing saturation system, modified from Knappett (2006)

3.8.2.2 Model disturbance during saturation

Introducing fluid to the base of the model helps to improve saturation, since any air remaining in the model can escape through the top of the model. However, care must be taken to avoid excessive model disturbance. As a first order approximation, the rate at which fluid flows through the model will be governed by Darcy's law, and as shown by Equation 3.4, increasing flow rates leads to increasing hydraulic gradients.

$$Q = KiA \tag{3.4}$$

By introducing the fluid at the base of the model, the hydraulic gradients which drive the flow also act to reduce the vertical effective stresses in the model. If the gradients become too high, the model could fluidise, leading to excessive disturbance. The fluid pressure at
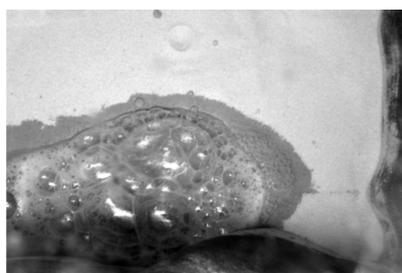
(a) Piping (after Knappett, 2006)
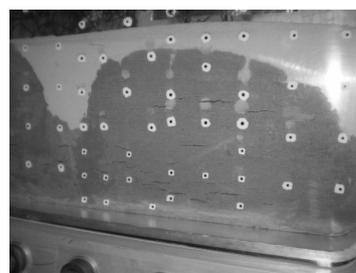
(b) Cracking and lifting of soil plugs (Stringer *et al.*, 2009)

Figure 3.23: Examples of model disturbance

any point in the model must also be controlled since additional disturbance can occur if the pressure relative to the atmosphere rises too high. Figure 3.23 (a) shows the scenario where the fluid finds a preferential path to the surface, leading to "piping". In Figure 3.23 (b), the fluid pressure has risen to a level which is high enough to balance the combined weight of sand and fluid above (plus any friction on the sides of the container), leading to plug-type failures.

3.8.2.3   Selecting an appropriate rate of saturation

In order to select an appropriate rate of saturation, the following process could be followed to calculate the mass flux at which severe model disturbance will occur:

If effective stresses in the model are reduced to zero due to the upward hydraulic gradients, then fluidisation will occur. The most critical point for this during saturation happens as the fluid breaks through the surface. At this point, the effective stresses without the hydraulic gradient are simply the buoyant unit weight of the soil, which is given in Equation 3.5. Before this point, effective stresses in the saturated soil are higher due to the dry unit weight of soil acting above the saturation front.

$$\gamma' = \left(\frac{G_s + S_r e}{1 + e} - 1 \right) \gamma_w \tag{3.5}$$

At the most critical point, the pressure gradient due to the hydraulic gradient must be less than or equal to the buoyant unit weight, as shown in Equation 3.6.

$$\frac{dp}{dz} = \gamma_w \frac{dh}{dz} = \gamma_w i < \left(\frac{G_s + S_r e}{1 + e} - 1 \right) \gamma_w \tag{3.6}$$

The maximum allowable flow rate is obtained from Darcy's law

$$Q_{max} = AKi_{max} < AK_w \left(\frac{v_w}{v_f} \right) \left(\frac{G_s + S_r e}{1 + e} - 1 \right) \tag{3.7}$$

The described approach assumes that one-dimensional flow upwards is occurring during saturation, which is encouraged by placing a thin layer of coarse sand across the base of the model. For a test where a fluid with a viscosity of 80 cSt is to be used Equation 3.7, shows that the maximum allowable mass flux for a fine sand such as Fraction E sand is 0.6 kg/hr, whereas coarser sands such as Hostun sand could tolerate 2-3 kg/hr. It is recognised that there will be a zone of capillary rise above the hydrostatic water table. In this zone, there will be a pressure drop owing to capillary suction which contributes to

drawing the pore fluid into the model. However, this pressure drop is beneficial in pre-venting model disturbance because the pore pressures in this zone will be negative, and therefore increase the effective stresses. The CAM-Sat system operates by controlling the mass flux with time and therefore will automatically account for the initial tendency for fluid to be drawn into the model due to the capillary suctions. It should also be noted that where unsaturated void spaces become discontinuous, then the presence of a "trapped" air bubble may locally alter the hydraulic conductivity. However, the final degree of sat-uration measured during testing of the CAM-sat system, and the good dynamic response of PPTs in dynamic centrifuge tests saturated with the system suggests that this is not adversely affecting the model preparation.

3.8.2.4 Computer-controlled saturation: CAM-Sat

In order to improve the quality of saturation as well as reduce the monitoring burden on the researcher, computer-control was implemented on the saturation system. A schematic of the final saturation system is shown in Figure 3.24. The system was upgraded in two phases (taking place after test MS07), which are indicated in Figure 3.24. While much of the original system layout remains, three key differences were introduced.

- measuring scales have greater resolution

- a small fluid reservoir is used

- models flushed with CO_2 prior to saturation
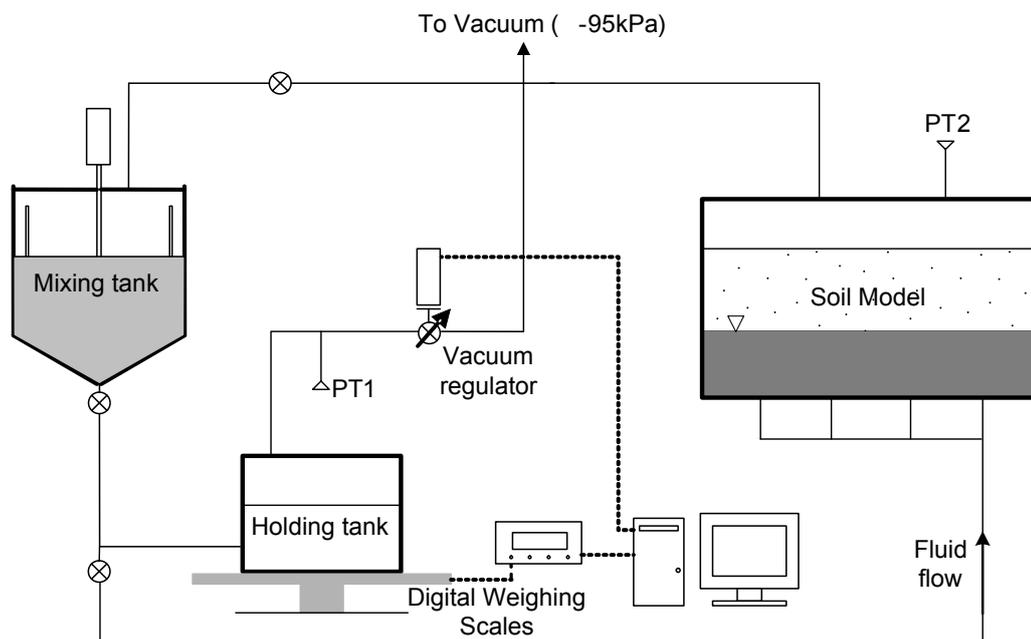
Figure 3.24: CAM-Sat system configuration

3. MODELLING TECHNIQUES

In the CAM-Sat software, the researcher sets upper and lower mass flux thresholds which should be maintained during the saturation. During saturation, the mass flux is continually calculated and compared with the user-defined thresholds. If necessary, the vacuum acting on the fluid reservoir is altered to keep the mass flux within the acceptable limits. The mass flux was calculated as the difference in mass of the model over a period of ten minutes (mass of the mixing tank was significantly greater). The time base of ten minutes was selected to balance the need to obtain resolution in the calculated mass flux (longer measuring period gives greater mass flux resolution) and the need to respond to required changes relatively quickly. Since the mass of the model was still quite large, the resolution of the measuring scales was limited to 50 g, meaning that mass flux resolution was 0.3 kg/hr. During the saturation, the researcher is able to view the mass flux, while additional details are also kept in a log file. The system was tested prior to use on models prepared for the centrifuge. While the details of the testing programme are found in Stringer & Madabhushi (2009), Figure 3.25 shows the data from the saturation of a model which comprised of a single layer of loose Hostun sand ($R_D \approx 35$ %) with a pore fluid which had a viscosity of 10 cSt. During the saturation, the mass flux thresholds (shown as black dashed lines) were altered twice to check the ability of the system to react to the user altering the required mass-flux. Since the required hydraulic gradient for a given flow rate increases proportionally with the viscosity of the fluid, the success of this test implied that the CAM-Sat system would be able to maintain control of the saturation when the fluid viscosity is a minimum of 50 cSt. The tests carried out in Stringer & Madabhushi (2009) indicated that the CAM-Sat system achieved a saturation ratios, S_r of 98 to 99 %, where saturation ratio is defined by Equation 3.8.

$$S_r = \frac{V_{fluid}}{V_{pore}} \tag{3.8}$$
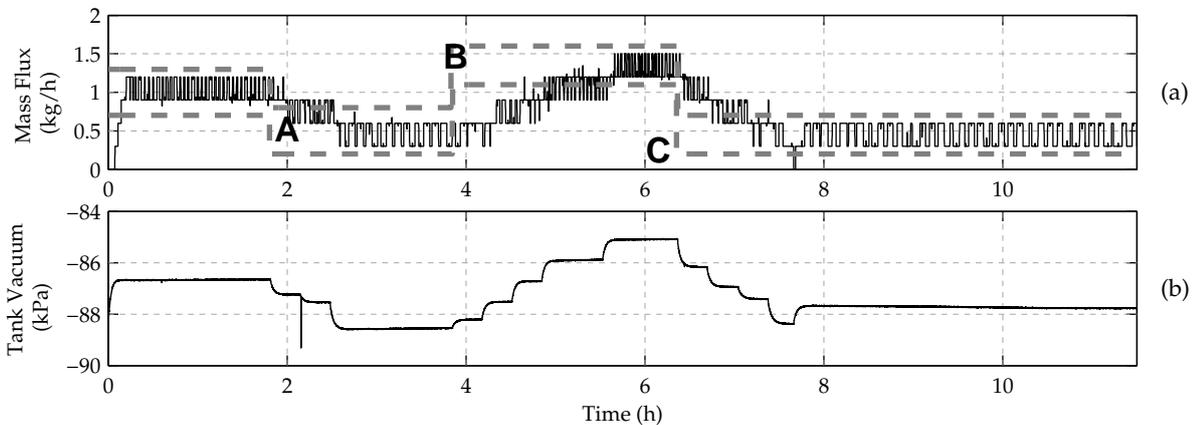
Figure 3.25: Saturation log for model H

(a) Saturation log   (b) Saturation front
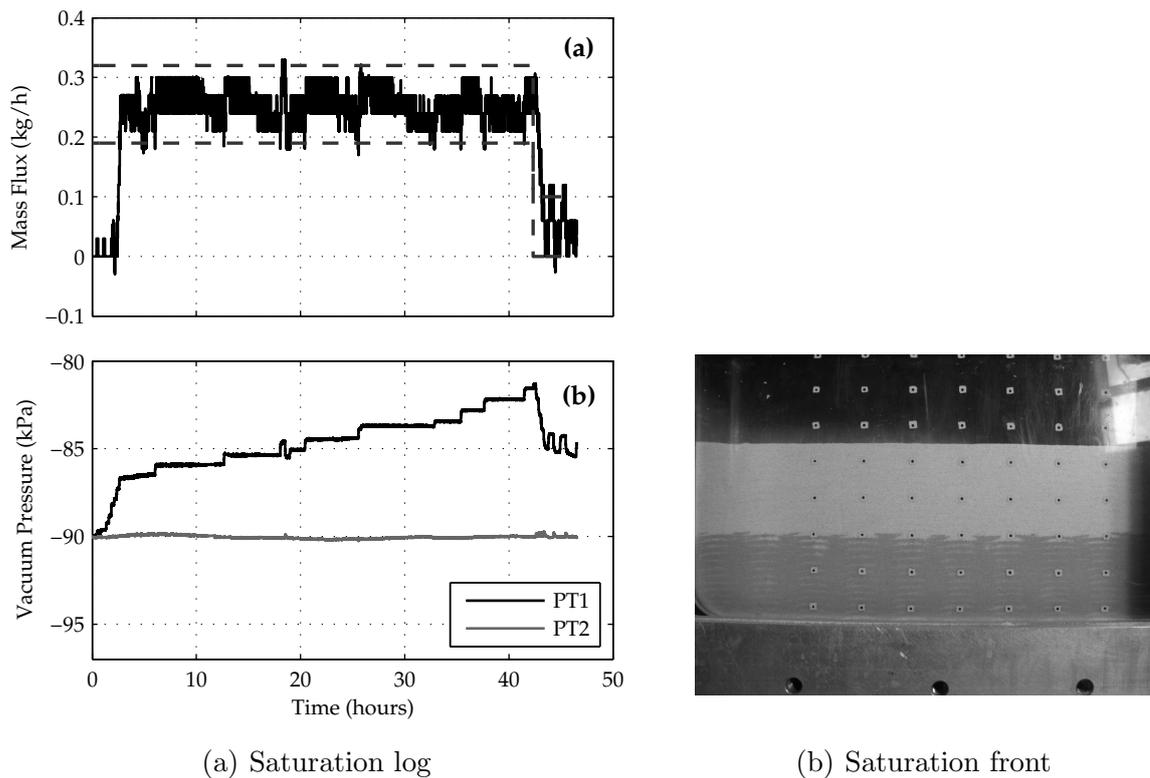
Figure 3.26: Saturation log and the observed horizontal saturation front during testing of the updated Cam-Sat system

The critical mass flux for saturating loose Fraction E sand with 80 cSt fluid calculated in Section 3.8.2.3 is approximately 0.6 kg/hr. This implies that the mass flux resolution in the initial implementation of the saturation system was only marginally sufficient for this type of test. Adding a small reservoir greatly improved this aspect. The reservoir was designed to have a capacity of approximately 30 l - sufficient for the model containers currently in use at the centre. If greater capacity is required, the user can refill the reservoir during saturation using the connection to the large mixing tank. By reducing the mass being measured to that of the small reservoir and the fluid, scales with a smaller capacity but greater resolution (5 g) could be used. This improved the mass-flux resolution to 0.03 kg/hr using the same time base for the calculation. The improved mass-flux resolution enabled a "soft-stop" feature to be incorporated to the updated system; at the beginning of the saturation process, the researcher defines a target mass which indicates the model is completely saturated. Once the mass of fluid reaches the target, the "soft-stop" is initiated, and the system reduces the flow to a trickle. While this doesn't achieve a complete halt to the process, the flow rate is reduced sufficiently that the process can continue to run until the researcher can conveniently stop the saturation. Since the researcher no longer needs to physically check the saturation, it is desirable to have an indication that the saturation is progressing normally. This is achieved by the software sending basic monitoring parameters (system pressures, total mass and mass flux) to the

researcher by email on an hourly basis if selected.

Takahashi *et al.* (2006) found that the saturation ratio achieved in a similar system to that shown in Figure 3.22 was improved by flushing the model with CO_2 prior to introducing the pore fluid, due to the greater solubility of CO_2 compared with air. Therefore, an additional step was carried out on models MS08 to MS12 prior to saturation. These models were firstly evacuated to a high degree of vacuum ($\approx$ -90 kPa) and then brought back to atmospheric pressure by the addition of CO_2 at the top of the model. The model was left under approximately 5 kPa for an hour before beginning the saturation process.

An example saturation log from the upgraded system is shown in Figure 3.26(a), which shows the much tighter control over the mass flux which could be maintained with the upgraded system. Figure 3.26(b) shows a near-horizontal saturation front during this test.

3.9 Effect of level sand surfaces

It was described in Section 3.8.1 that the dry sand models were finished using a flat edge to level the models. However, the radial g-field in the centrifuges means that the model doesn't quite represent the level ground prototype which was intended. Rather, the actual prototype is slightly curved, with maximum height at the centre. It was decided not to attempt to correct for this error due to the current procedures of loading the model. Since the Turner centrifuge is located below ground level, completed models must be lowered onto the centrifuge using a crane. This induces some disturbance to the model and any curved surface would therefore be destroyed as the model was loaded.

(a) Earthquake 1   (b) Earthquake 2
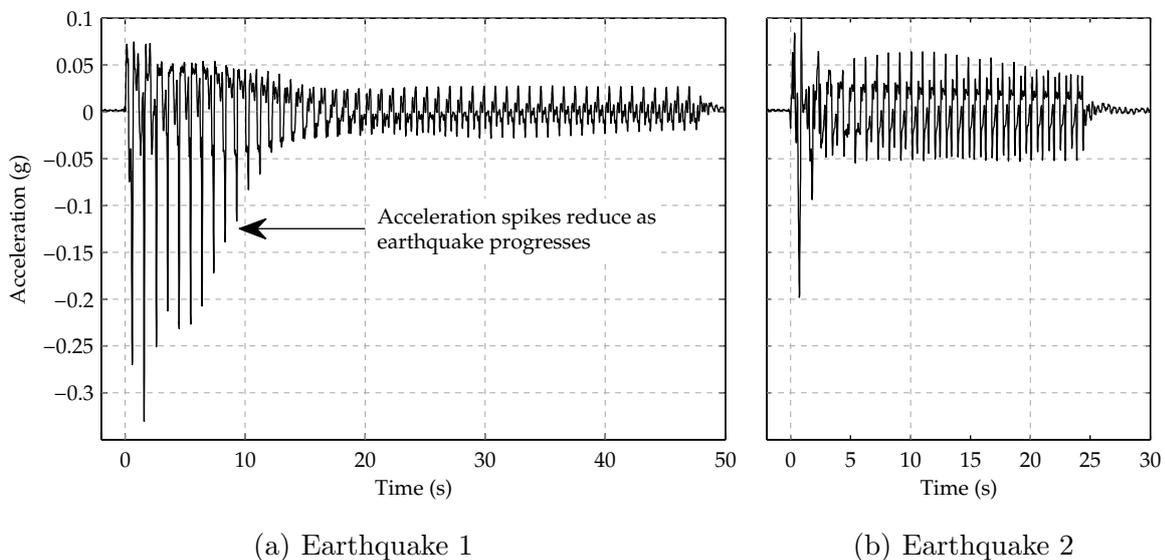
Figure 3.27: Acceleration records at 1 m depth in MS06
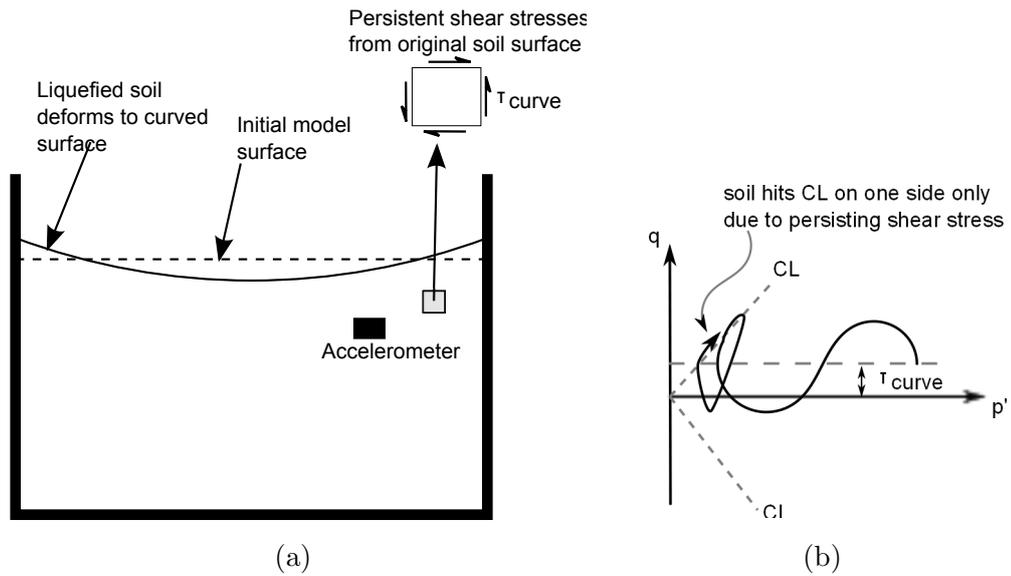
Figure 3.28: Effect of radial g-field on flat surfaces

Under test conditions, the flat (relative to a parallel g-field) surface of the model will induce additional shear stresses in the model. During the earthquakes, the onset of liquefaction leads the soil to redistribute in order to adopt a curved (relative to a parallel g-field) surface. This effect was observed in the acceleration records near the beginning of earthquakes. As an example, the accelerations for an accelerometer buried approximately 1 m below the soil surface in MS06 is shown in Figure 3.27. In this test, two earthquakes were fired in a single flight. In the first earthquake, large dilation spikes are seen in one direction only at the beginning of the earthquake. These spikes are then seen to reduce in amplitude, and the accelerations then become more symmetrical. In the second earthquake, these large dilation spikes were not observed. The shear stresses due to the soil attempting to alter its surface profile, along with the shear stresses acting at the time of the dilation spike are shown in Figure 3.28 (a), while (b) shows the concept in q - p' space. It should be noted that as the soil adopts the curved profile, the value of τ_{curve} reduces.

3.10   Summary

In this Chapter, the modelling techniques which have been used in the research programme have been described. In the experiments carried out, models were constructed within a laminar box container using Leighton Buzzard sands which was poured using either a manual sand hopper, or a computer controlled sand pourer. The process of sand pouring was periodically stopped to allow the placement of miniaturised instrumentation within the models. In all but one test, models were subsequently saturated with a viscous fluid using a computer-controlled saturation system.

In each test, a single model pile group was installed in the models. Initial tests were carried out with a pile group which allowed axial load measurement at the head and base of a single pile, while later tests utilised a pile group in which up to two piles were instrumented to measure axial load at 5 locations using strain gauges. The pile groups were installed either under 1 g conditions, where they are thought to best represent bored piles, or in a two-phase jacking process which aimed to replicate the soil stress conditions around jacked piles in the field.

Each test was carried out using the Turner beam centrifuge, and earthquakes were fired using the SAM actuator.

Chapter 4

Settlement and Load Transfer of Free-Standing Pile Groups

4.1 Introduction

The tests of Knappett & Madabhushi (2008b), discussed in Section 2.4.2, indicated that contrary to general perception, piles situated in liquefiable soils were able to generate shaft friction during an earthquake. In these tests, the shaft friction was calculated as the difference between the pile head and pile tip axial loads. It was therefore not possible to distinguish the different sections of pile which were responsible for generating positive shaft friction, and Knappett (2006) suggested that the shaft friction was generated in the dense layer of the model. However, the actual distribution of axial load along a pile during an earthquake remains unresolved. As discussed in Section 2.4.3, significantly different excess pore pressures to those in the free field can exist near to a pile which is undergoing lateral displacement. Therefore, while the soil in the free field may be fully liquefied, this is not necessarily the case near the soil-pile boundary. This raises interesting questions concerning the axial load distribution along a pile during the earthquake since it is possible that some contribution to the shaft friction observed by Knappett & Madabhushi (2009a) may come from the "liquefiable" sand.

The work of Knappett & Madabhushi (2008b) indicated that free standing pile groups can suffer intolerably large co-seismic settlements even when their pile tips have been embedded in relatively dense soils due to the existence of excess pore pressures within the dense sand during the earthquake. The sand used in the bearing layer of these tests was Fraction E silica sand, which as shown in Table 3.2 is relatively fine and therefore fluid movement on the time scale of an earthquake is relatively limited. If a much coarser soil exists in the bearing layer, then the excess pore pressures during an earthquake could

be significantly altered. If large excess pore pressures can no longer be sustained in the bearing layer as a result of the higher hydraulic conductivity, then the soil in the bearing layer of the model would be expected to deliver a very stiff axial response to the pile which may result in the pile behaviour being quite different to that observed in the tests of Knappett & Madabhushi (2008b).

This chapter aims to investigate the behaviour of free standing pile groups in the context of the two issues described above. An initial pilot test, MS01, was carried out using the simply instrumented pile group described in Section 3.7. The tests aim to investigate whether the use of a coarse sand in the bearing layer of the model leads to significantly different settlement response of the foundation. By using the highly instrumented pile group (also described in Section 3.7), additional tests were carried out to investigate the axial loading at different points along the length of the pile and hence gain an understanding into the areas of the pile which contribute to the observed shaft friction during an earthquake and the underlying mechanisms. The post-earthquake behaviour of the piles, both in terms of the axial load distribution and also the settlements, will not be discussed in this chapter. Rather, this aspect will be considered in Chapter 7.

4.2   Centrifuge models

A total of 4 tests were carried out with pile groups in a "free-standing" configuration. Testing pile groups in this configuration allows the axial load distribution of the pile groups to be studied without the complication of pile cap interaction. In cases where an exceptionally weak clay layer is present at the surface, then it is possible that the field scenario may reduce to that of a free standing pile group. Although the presence of the clay layer will alter the top boundary condition slightly in terms of pore pressure dissipation, if the clay is both very weak and thin, then even small pore pressure build up below the clay layer could lead to channels or cracks in the clay. This would allow excess pore pressures to dissipate rapidly, making it similar to the case where the clay is non-existent. If piping channels are unable to form and the fluid is unable to escape, then the excess pore pressures will be unable to dissipate beyond that equal to the vertical stress applied by the clay layer. If the clay layer is of limited extent, then the excess pore pressures will only be a few kPa larger than normal compared with when the clay layer is not present. It is however of great importance that in these possible field scenarios that the clay layer neither applies significant lateral loading to the pile cap or provides anything other than minimal vertical resistance during the earthquake (i.e. very low undrained strength). If either of these conditions are not met, then the behaviour of the pile group will be heavily influenced by the presence of the clay layer and the results discussed in this chapter will not apply.

(a) MS01

(b) MS02
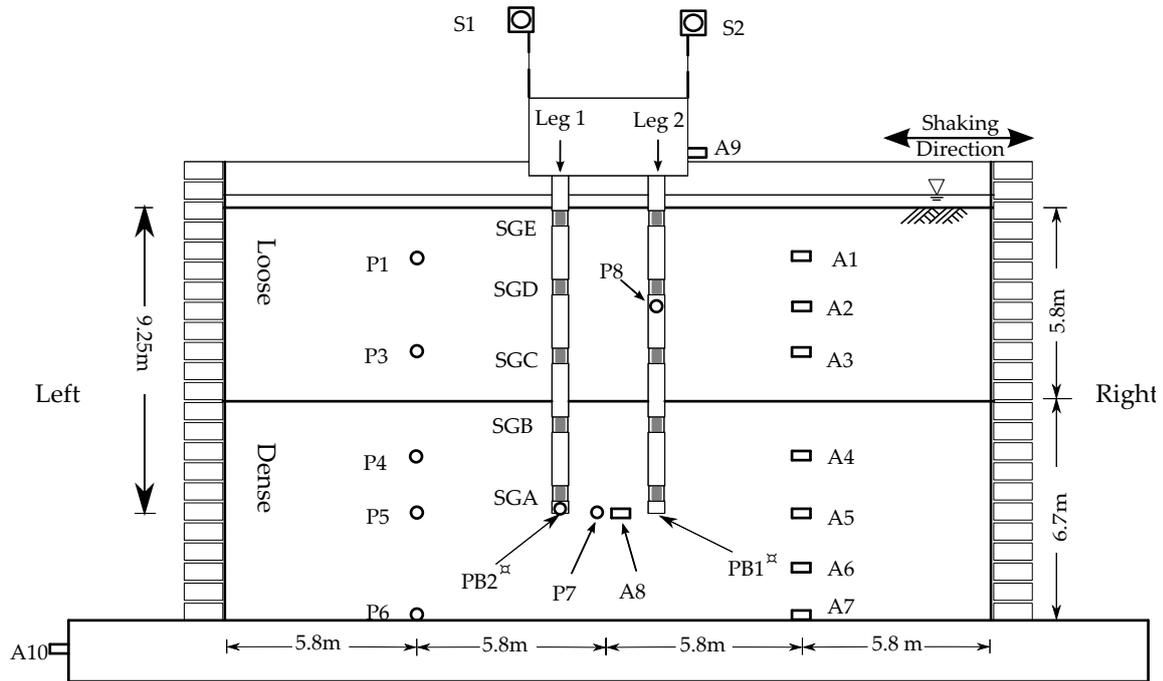
Figure 4.1: Section view through the centreline of the model layouts

(c) MS05
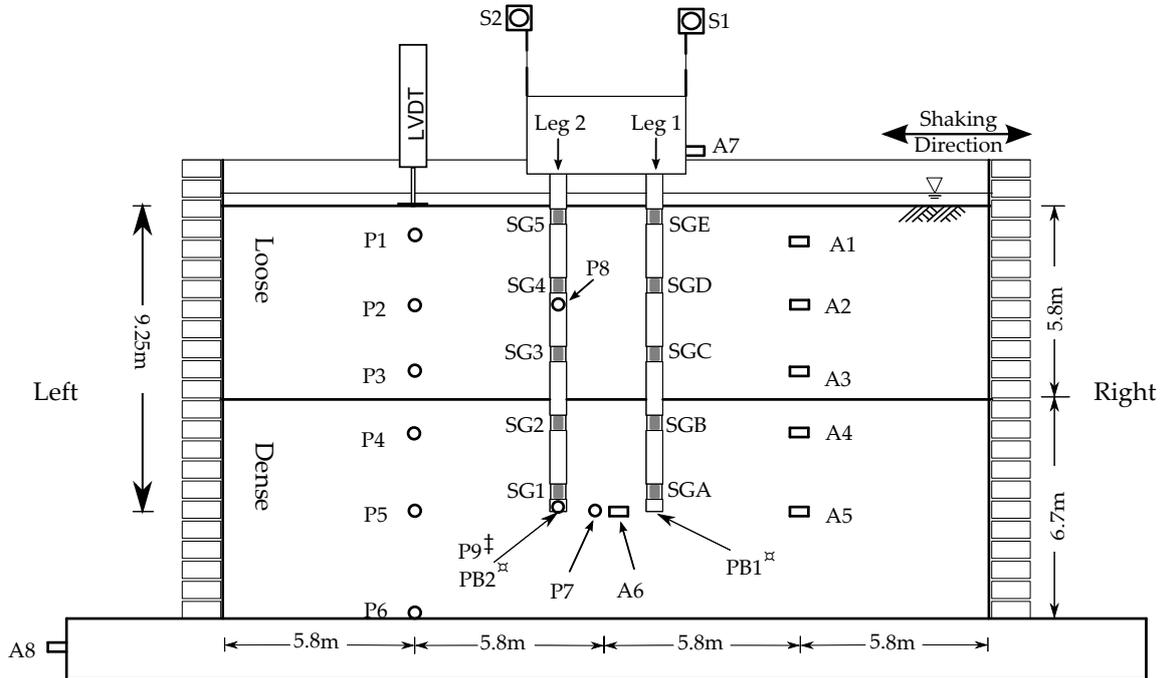
(d) MS06

Figure 4.1: Section view through the centreline of the model layouts

(e) JK-06

(f) JK-12

Figure 4.1: Section view through centreline of the model layouts, reproduced from Knappett (2006)

Table 4.1: Soil profiles used in free standing pile tests

		MS01	MS02	MS05	MS06	MS11	JK-06	JK-12
Loose	Sand	Fraction E	Fraction E	Fraction E	Fraction E	Fraction E	Fraction E	Fraction E
	Relative Density (%)	35	35	35	35	35	35	35
	Thickness (m)	9.6	9.6	5.8	5.8	6.9	20.0	9.6
Dense	Sand	Fraction C	Fraction C	Fraction C	Fraction C	Fraction C	Fraction E	Fraction E
	Relative Density (%)	100	100	100	100	100	90	90
	Thickness (m)	11.1	11.1	6.7	6.7	5.5	7.4	11.1

Table 4.2: Test parameters for free standing piles

Flight	G-level (g)	Pile Group	L_p Loose (m)	L_p Dense (m)	P/Pile (kN)	Static FOS $0.1D_0$	Static FOS Ult	Earthquake Number	Earthquake Frequency (Hz)	Earthquake Duration (s)	Earthquake Peak acc (g)
MS01											
1	74.1	JK-PG	9.6	4.4	331	2.5	6.5	1	0.67	44.5	0.13
2	74.1	JK-PG	9.6	5.0	469	1.8	4.8	1	0.67	44.5	0.13
MS02											
1	74.1	JK-PG	9.6	4.4	331	3.7	9.5	1	0.4	29.6	0.04
			9.6	4.4	331	3.7	9.5	2	0.54	29.6	0.07
			9.6	4.4	331	3.7	9.5	3	0.67	29.6	0.11
			9.6	4.4	331	3.7	9.5	4	0.67	44.5	0.18
2	74.1	JK-PG	9.6	4.4	469	2.6	6.7	1	0.4	29.6	0.04
			9.6	4.4	469	2.6	6.7	2	0.54	29.6	0.07
			9.6	4.4	469	2.6	6.7	3	0.67	296	0.1
			9.6	4.4	469	2.6	6.7	4	0.67	44.5	0.17
MS05											
1	46.4	MS-PG	5.8	3.5	337	1.8	5.4	1	1.08	23.2	0.23
	46.4	MS-PG	5.8	4.2	337	2.0	5.8	2	1.08	23.2	0.23
MS06											
1	46.4	MS-PG	5.8	3.5	337	1.8	5.4	1	1.08	46.4	0.22
	46.4	MS-PG	5.8	4.5	337	2.1	5.9	2	1.08	23.2	0.22
JK-06 S5	1	73.2	JK-PG †	19.8	4.4	1317	1.1	2.3	1	0.68	38.4	0.17
JK-06 S6	1	73.2	JK-PG †	19.8	4.4	2417	0.6	1.3				
JK-12 S1											
1	74.1	JK-PG	9.6	4.4	331	2.4	6.3	1	0.67	45.4	0.3
2	74.1		9.6	5.8	469	1.9	4.8	1	0.67	44.9	0.34

†: Same geometry as pile groups used in MS01 and JK-12, refer to Knappett (2006) for further details concerning the properties of the piles in this group.
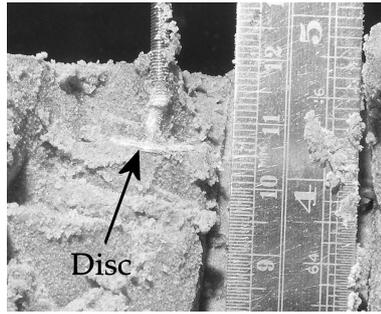
Figure 4.2: Excavated position of the disc attached to the LVDT in MS06

The instrumentation layout of the different models tested are shown in Figure 4.1. Additionally, key parameters of the soil profiles are shown in Table 4.1, while parameters pertinent to the pile group and the earthquake loading are given in Table 4.2. As shown in Figure 4.1(d), an LVDT was placed in MS06 to measure settlement of the soil surface during the earthquake. A small disc was attached to the central measuring rod of the LVDT in order to reduce the bearing pressure applied to the soil by the LVDT. However, it was found during excavation that this disc had settled considerably once the soil had liquefied, as shown in Figure 4.2. The data from this instrument is therefore only considered valid in the initial swing-up of the centrifuge.

Table 4.2 indicates that two flights were carried out in tests MS01 and MS02, allowing the pile cap mass to be altered. Where multiple earthquakes were carried out in the same flight, a sufficiently long time gap between earthquakes was left to ensure that pore pressures had fully dissipated before the next earthquake was fired.

The static factors of safety shown in Table 4.2 were calculated as the sum of estimated shaft and end bearing capacities of the pile groups. The shaft friction capacity of the piles is calculated according to Equation 2.3, with $K \approx 1 - sin(\phi_{crit})$ and $\delta = 17^o$ (as described in Section 3.7.3). End bearing capacities of the piles have been estimated following Yasufuku *et al.* (2001). It should be noted that the axial capacities of the piles tend to increase after each earthquake due to the settlement of the pile group in the preceding earthquake. The settlement results in a greater embedded length of the pile and greater vertical effective stress at the pile tip level, leading to increased shaft friction and pile end bearing capacities.

In addition to the 4 tests carried out in this research programme on free-standing pile groups, two additional tests are discussed in relation to pile group settlement during an earthquake. These tests were conducted in an earlier research programme, and full details can be found in Knappett (2006). The model layouts for these two tests are shown in Figure 4.1(e) & 4.1(f), while the test parameters are included in Table 4.2.

It is important to note that there are some differences in the prototype values which will be discussed in this research programme and those in the original work of Knappett

(2006). The differences are due to the operational g-level which has been used in the interpretation of the data, as discussed in Section 3.2.1. In this Chapter, the data has been scaled by the values shown in Table 4.2, whilst in the work of Knappett (2006), the nominal g-level of 80g was used. The numeric quantities shown in the model layouts of JK-06 and JK-12 have been altered to reflect the g-level used in this Chapter, while the number in brackets indicates the dimension at model scale in mm.

4.3 Free field soil behaviour during the earthquakes

4.3.1 Pore pressures

As shown in Figure 4.1, a vertical array of PPTs was placed in the free field in each test. Measurements of excess pore pressures in the first earthquake of MS01 and MS06 are shown in Figures 4.3 & 4.4. In each of the graphs, the dashed lines indicate the pore pressure required to cause full liquefaction in the free field.

It can be seen that in both of the tests shown, the pore pressures rise rapidly at the beginning of the earthquake, with full liquefaction being reached throughout the loose layer within a few cycles. In the experiments carried out, the instruments in the loose layer were found after the test to have settled significantly. This is particularly visible in the measurements at P2 in Figure 4.4, where the pore pressures rose to the level required for full liquefaction (determined from its initial position), and then steadily increased further
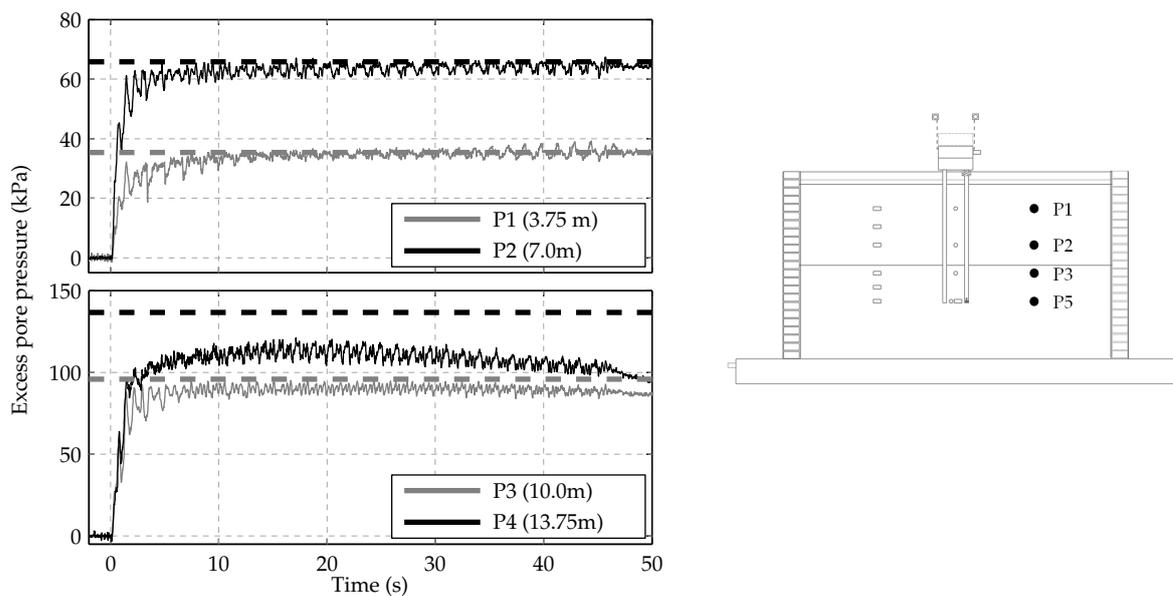
Figure 4.3: Excess pore pressures in MS01
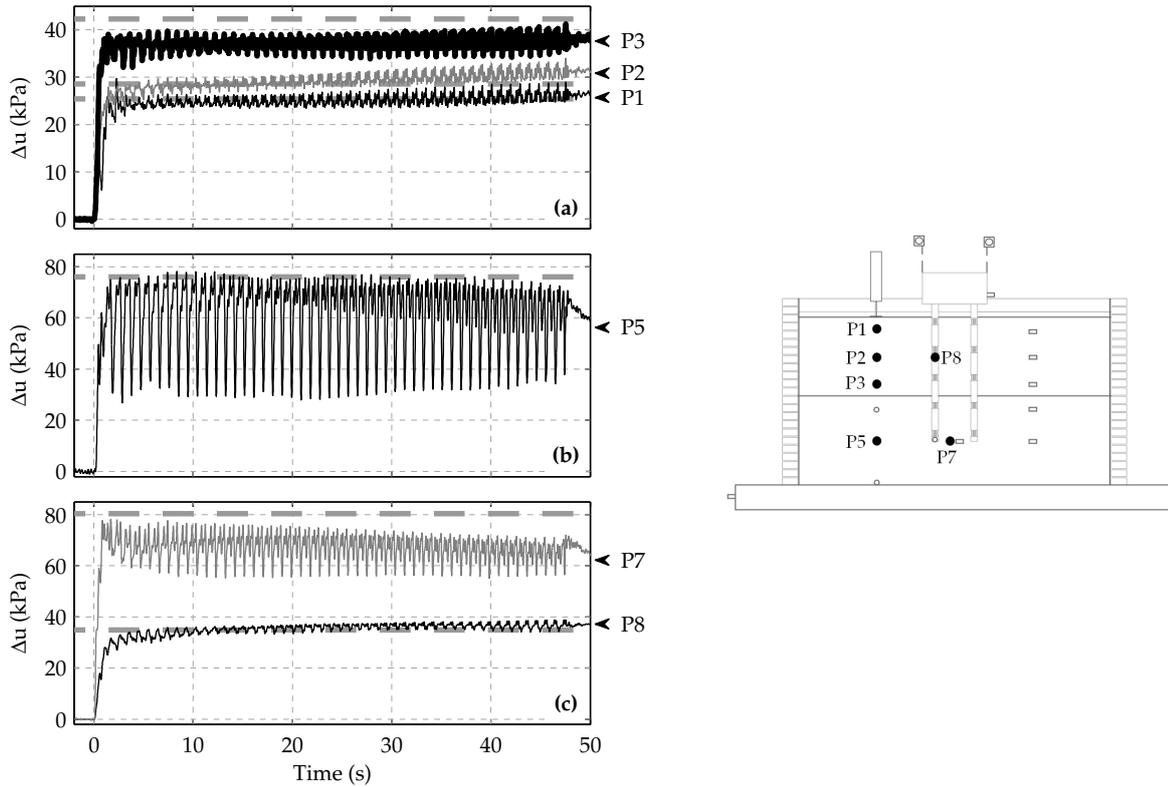
Figure 4.4: Excess pore pressures in MS06

till as the instrument sunk. The pore pressures recorded immediately after the end of the earthquake indicate that full liquefaction was maintained throughout the earthquake.

Figure 4.4 indicates that in the dense layer full liquefaction was reached in the free field twice per cycle (at P5) in MS06. In each cycle, the pore pressures at P5 indicate two downward suction spikes in excess pore pressure, with one spike much more dominant than the other. The pore pressures recorded at P7 at the same level, but within the group indicate that the pore pressures again reached values close to liquefaction twice per cycle, and again recorded two spikes in pore pressure. However, the two spikes recorded at P7 are much closer in magnitude to each other.

Pore pressure spikes are often observed to occur at points of maximum soil acceleration (e.g. Kutter & Wilson, 1999), as the soil dilates to resist large shear stresses associated with the high acceleration. Figure 4.5 shows the pore pressure at P5, as well as the accelerations and displacement (following Brennan *et al.*, 2005) at A6 and A7 (acceleration direction shown with double arrows). The suction spikes occur later than the peak acceleration in the soil (A6) as well as being quite broad in the time domain. Figure 4.5 (c) shows the double-integrated accelerations at A6 and A7. The spikes at P5 occur in the half cycle where the dense soil is moving from left to right (as defined in Figure 4.1). At the same time, the pile cap is moving from right to left. This means that at the time of the suction
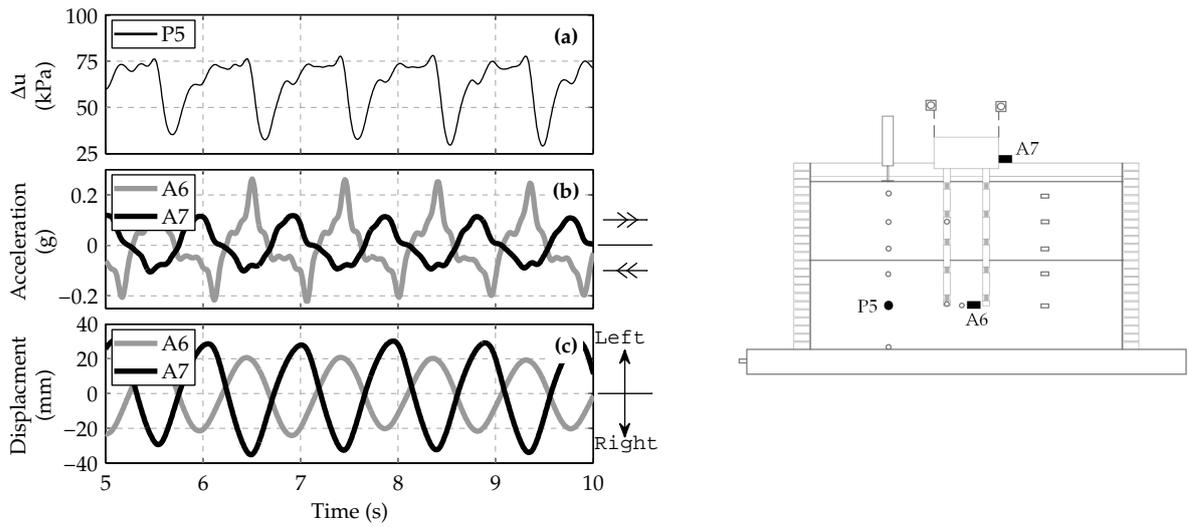
Figure 4.5: Dilation spikes in dense soil layer with acceleration and displacement in dense layer and at pile cap

spike, the pile group is applying additional shear forces to the dense soil on the side of the model with the PPTs leading to the larger dilation spikes which were observed, as shown in Figure 4.6(a). In the opposite half cycle, these shearing stresses from the pile group act on the opposite half of the model, so a large spike is not observed at P5.

Within the pile group, the suction spikes are much smaller, indicating that smaller shear stresses are placed on the soil within the pile group. Within the pile group, the shearing stresses applied to the soil are applied equally in both directions, leading to the suction

(a) Soil Element 1

(b) Soil Element 2

(c) Location of pile cap and soil element 1 at time of main spike
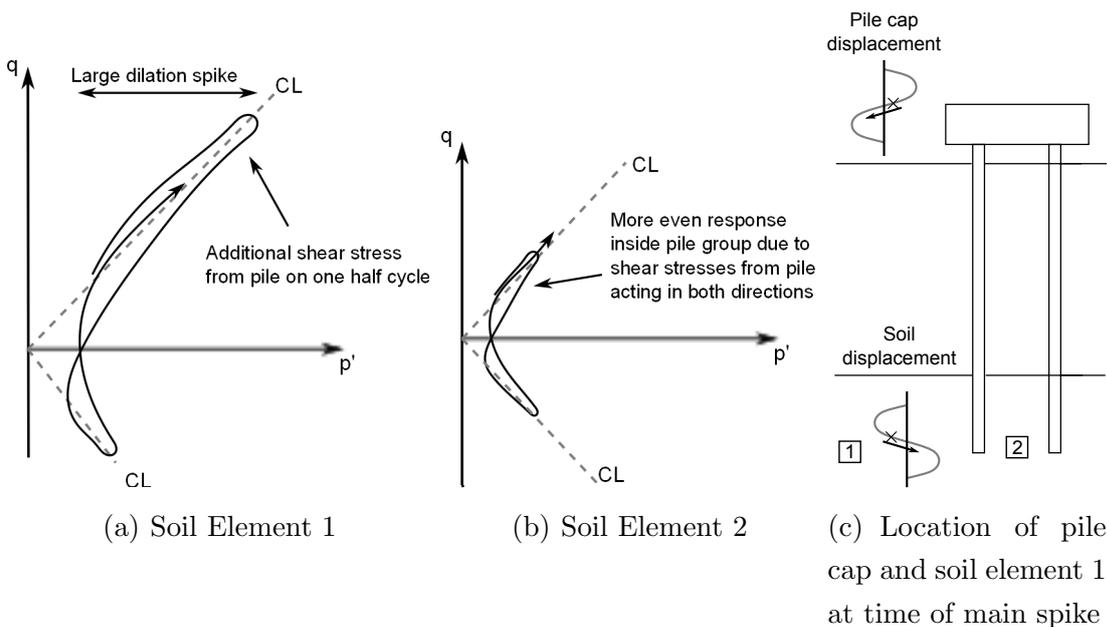
Figure 4.6: Interpretation of pore pressure spikes in the dense layer of MS06 at P5 and P7

spikes being of similar magnitude, as shown in Figure 4.6(b). Similar observations regarding the magnitude of pore pressures within pile groups were made by Tokimatsu & Suzuki (2004). It is thought that these smaller shear stresses within the pile group arise due to a confining, or shielding, effect of the piles.

The extra depth of the model in MS01 led to the pore pressures not rising high enough to cause full liquefaction at the pile tip level during the earthquake, as shown in Figure 4.3. Additionally, the pore pressures appear to indicate smaller dilation than that observed in MS06. It is thought that this reflects the increased distance between the piles and the free-field instruments in this test compared with that of MS06.

4.3.2   Accelerations

The accelerations observed at selected points in test MS05 are shown in Figure 4.7 (Note that while MS06 is generally used as the "reference test", accelerometers A4 and A5 in MS06 failed. Therefore the accelerations from MS05 are displayed here). It can be seen in Figure 4.7 (a) that the accelerations in the loose sand are highly attenuated, and reduce to almost zero after only 1-2 cycles.
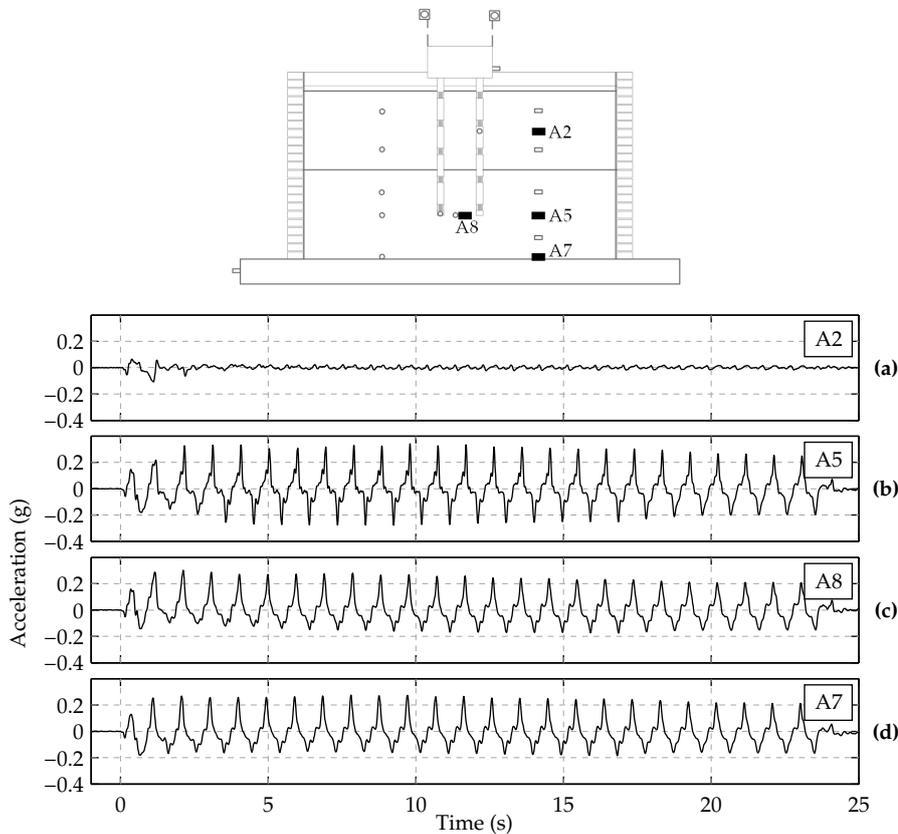
Figure 4.7: Accelerations in MS05
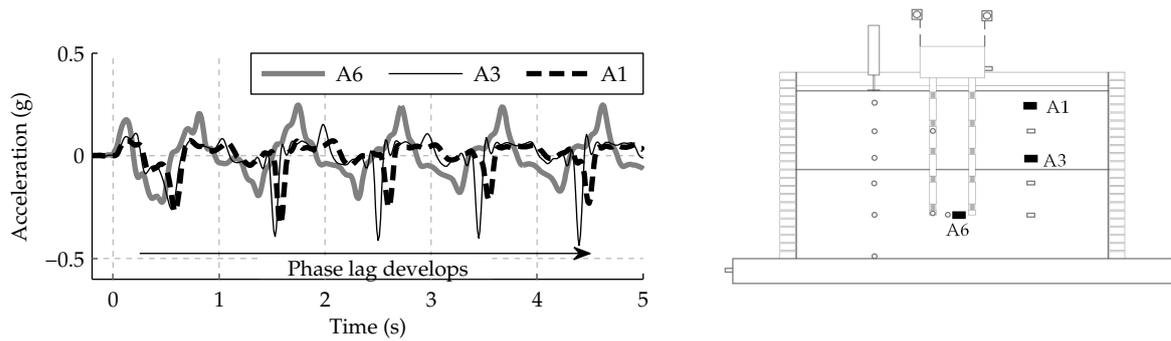
Figure 4.8: MS06 free field acceleration

As explained in Section 3.5.1.3, it is questionable whether the piezoelectric accelerometers used in the models are able to faithfully reproduce the soil acceleration in the loose layer. However, it is assumed that the results are indicative of a general trend that the accelerations in this layer become relatively small due to a significant loss of shear stiffness as the loose soil liquefies. Additionally, near the beginning of the first earthquakes in MS01 and MS06, large acceleration spikes in one direction developed in the loose soil, showing increasing phase lags developing with vertical distance above the loose/dense interface as shown in Figure 4.8. These acceleration spikes do however attenuate strongly as the earthquake progresses, with the accelerations later becoming both more symmetrical and of smaller amplitude. It is thought that the acceleration spikes are a result of the liquefied soil attempting to adopt a curved surface as discussed in Section 3.9. It is assumed that the phase lag information remains valid since the acceleration spikes reflect when the cyclic shear stresses are applied to the soil, causing it to reach the failure line. These large phase lags are further indicators of the low shear stiffness of the liquefied loose soil. When the model was excavated, it was found that the accelerometers in the loose layer had rotated and sunk significantly. It is therefore assumed that the accelerometers are in their nominal positions only at the start of the tests.

By contrast to the very low accelerations in the loose sand, strong accelerations were recorded in the dense layer throughout the earthquake. Figure 4.7 (b) and (d) indicate the accelerations at the pile tip level and the base of the container respectively. It was found that within the dense layer, the accelerations displayed some limited amplification, and some small increases in phase lag with reducing depth to the soil surface. The large differences in the stress-strain behaviour of the sands is typical of loose and dense sands subjected to dynamic shear loading, as discussed in Section 2.2.

Detailed comparison of the accelerations at A5 and A8 revealed that the accelerations recorded between the pile tips led the accelerations of those in the free field at the same depth. The magnitude of the accelerations at A8 were quite similar to those recorded at A7 (base of the container). This observation suggests that the shear stiffness below the

pile group is larger than that in the free field. It is thought that this effect is realised as a result of the higher confining stresses which must exist to resist the pile tip loading. The observation that there is a disparity between the phase lag in the free field and between the pile tips acts to reinforce the ideas explained in Figure 4.6. In MS01, the confining stresses within the model are higher at the level of the pile tips (due to the pore pressures not rising high enough to cause full liquefaction at the greater depth of the pile tips in this model). Under the higher stress levels which exist in MS01 at the pile tips (both as a result of the length of the piles and also as a result of lower excess pore pressures), the phase lags in the free field and between the pile tips are operationally very similar in terms of acceleration magnitude and phase.

4.4 Normalised settlements of free standing pile groups

During all of the tests with saturated soil, the pile groups suffered large settlements which began to develop immediately. Pile group settlements during the tests were calculated as the average of the two potentiometers, S1 and S2. The soil surface itself will also settle during the tests, both during and after the actual earthquake. As a result, the "pile group settlements" presented in this Chapter are relative to a fixed datum. Additionally, since the soil in the dense layer is at 100% relative density, it is assumed that there is no significant settlement in this layer as a result of the earthquake loading. Under this assumption, the pile group settlement is also a measure of the settlement of the pile tips relative to the dense layer. Figure 4.9(a) shows the settlements from the tests of MS01 and MS05. From this figure, it can be observed that the settlements in MS05 are smaller than those recorded in MS01, and also that in both tests, the settlements in the second of the earthquakes developed at a lower rate than in the first earthquake. This is particularly interesting in the case of MS01, where the pile cap mass was increased after the first earthquake, and therefore would be expected to suffer a larger settlement. The latter was similarly observed by Knappett (2006) in tests where the pile groups were embedded in a bearing layer of dense Fraction E sand.

While the magnitudes of the settlements of the pile groups during the various earthquakes appears quite disparate, there appears to be some similarity in the form of the settlement curves during the earthquakes. Additionally, the mechanism of pile group settlement proposed by Knappett & Madabhushi (2008a) suggests a very strong link between pile group settlement and the number of cycles, due to the stomping which takes place once per cycle on each leg. It was therefore decided to attempt an empirical normalisation of the pile group settlements. By considering the results shown in Figure 4.9(a), it was decided to attempt the normalisation of pile group settlements according to Equation 4.1. The settlements normalised in this manner are shown in Figure 4.9(b), plotted against
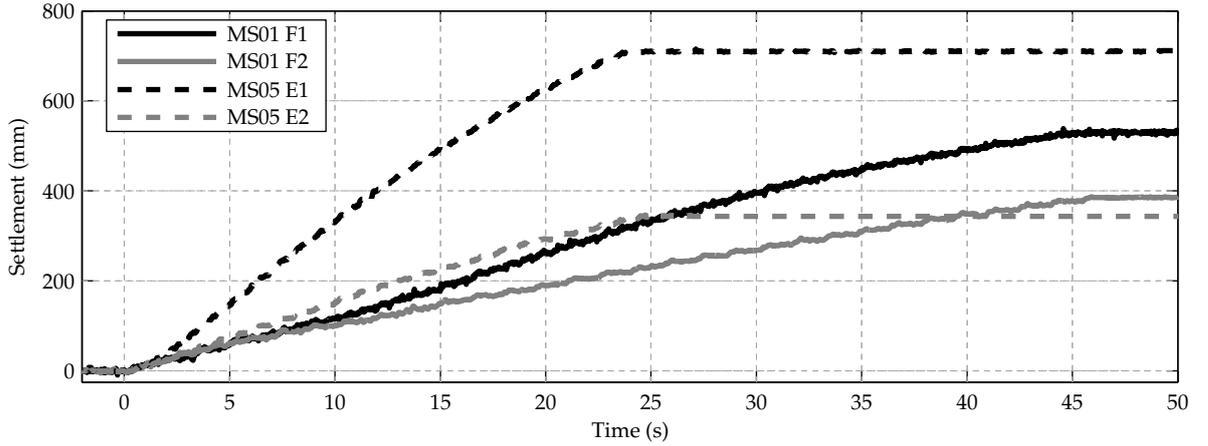
(a) MS01 and MS05
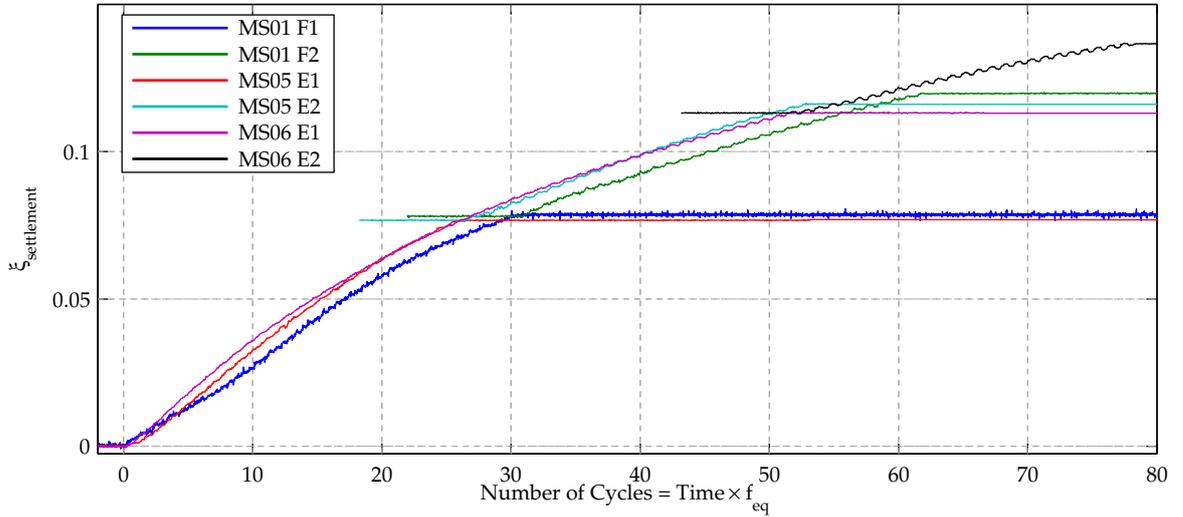
(b) Normalised settlements of pile groups with tips embedded in Fraction C sand

Figure 4.9: Settlement of the free standing pile groups

the total number of cycles which the pile group has been subjected to. In other words, the portion of normalised earthquake settlement in the second earthquake is set to begin at the end of the normalised settlement from the first earthquake.

$$\xi_{settlement} = \int \left(\frac{\frac{d\rho_{pilecap}}{dt}}{D_0} \right) \left(\frac{\sigma'_{v0}(t)\pi D_0^2}{4P_{pile,av}} \right) dt \qquad (4.1)$$

As can be seen, when normalised in the manner described, the test data from the three tests collapse very well onto a single curve. It is interesting to note that the chosen normalisation parameter, $\xi_{settlement}$, can be thought of comprising two independent groups (shown in the two sets of brackets). The first group is the conventional normalisation of settlement by pile diameter, differentiated with respect to time. The second group expresses the ratio of vertical effective stress before the earthquake at the pile tip level (in

the free field), to the stress applied by the pile tips for the case where all of the pile cap axial load is carried in end bearing. It should be noted that the initial vertical effective stress used in the parameter $\xi_{settlement}$ changes to reflect the current position of the pile tips (i.e. it increases slightly through the earthquake as the piles settle).

The reasons why this normalisation appears to work are not clear. However, a potential reason lies in the bearing capacity equation of Yasufuku *et al.* (2001), which directly links the bearing capacity to the effective stress in the soil at the level of the pile tips. During the experiments, it was observed that the pore pressures rose rapidly in the free field, as shown in Figure 4.3 & 4.4. In the free field, this results in the effective stresses dropping significantly. However as shown later in Figure 4.14, the tips of the piles in these pile groups continue to apply large loads to the soil directly beneath the pile tips and therefore the effective stresses below the pile tips cannot reduce in the same manner as those in the free field. This may partially explain why the normalisation of settlements appears to produce a unique curve.

In experiments which will be described later, pore pressure transducers were placed inside the pile tips to measure the excess pore pressures directly below the pile tips. If this data was available for these tests, then a modified version of $\xi_{settlement}$ could be used, where the second normalised group directly linked the pile loads to the effective soil stresses in the soil directly below it. This would allow the effects of transient pore pressures at the pile tips to be captured and provide an improved approach to estimating the settlements which could be useful for design. It should also be noted that the number of model configurations represented by this chart remain small, and therefore additional tests may be required to validate this result. However, with the data obtained, some interesting implications can be drawn from Figure 4.9(b).

4.4.1 Effect of number of cycles

In Figure 4.9(b) the normalised settlements indicate that the settlement of the pile group continues to increase under earthquake loading even after 75 cycles. Similar to the raw settlements shown in Figure 4.9(a), the rate of pile group settlement reduces significantly, implying that the pile group would eventually reach a limiting settlement. An interesting feature of the normalised settlements is that in the second earthquake of each test, the settlement continues to develop with the same trend as that in the first earthquake. This effect is clearly visible in the data from the first earthquake of MS06 and the data from the two earthquakes in MS05, where it can be seen that the settlement data in MS05 continues to follow the same trend as MS06 whose initial earthquake had the same duration as the combined duration of earthquakes in MS05. This observation is similarly visible in the other tests, including MS01, where the centrifuge was stopped between earthquakes to

allow the axial pile group loading to be increased. This implies that the amount of settlement which has occurred up to a given point is important in determining the future settlement which will occur. Since the settlements were still observed to be increasing after 75 cycles, this means that in real earthquakes, buildings which manage to survive an initial earthquake can be expected to suffer additional settlements if another earthquake occurs in the same region. The results also indicate that for two identical buildings which are built before and after a large earthquake, very different settlement responses can be expected during a future strong earthquake.

The observation that pile group settlements were still increasing after 75 cycles has interesting implications for the curves of De Alba (1983). These curves, which were found to provide a good fit for the data of Knappett & Madabhushi (2008b), link excess pore pressure ratios in the free field to the initial static factor of safety at the serviceability limit state (settlement of $0.1\ D_0$). However, in these tests, the pore pressures were increasing throughout the experiment, until liquefaction was reached. The curves therefore indicate the point at which the settlement first exceeds the settlement criterion. Although full liquefaction was reached within a few cycles in the tests described in this thesis, the observation that settlement continues to increase with number of cycles may also apply to other values of pore pressure ratio. It is therefore likely that if the pore pressure ratio was held at lower values for a sustained period of time, then additional settlements would occur beyond those suggested in the curves of De Alba (1983).

4.4.2 Effect of increased axial pile cap loading

It was shown in Figure 4.9(a) that the settlements recorded in the second earthquake of MS01 were smaller than those in the first earthquake. This was surprising since the pile cap axial loading was increased between the first and second earthquakes of MS01. However, the normalised settlements shown in Figure 4.9(b) indicate that the settlements recorded in the second earthquake with the greater axial pile loading do follow the general trend of the data, implying that the settlements are actually larger than those which would have been obtained in the second earthquake had the pile cap axial load not been increased. The normalisation which was shown in Equation 4.1 therefore suggests that the settlements are proportional to axial load.

4.4.3 Implications for modelling

From Table 3.6 and the model layouts shown in Figure 4.1, it is found that the the piles tested in MS01 and MS05/MS06 were initially $14.5\ D_0$ and $6.9\ D_0$ above the base of the container. Throughout the course of shaking, these reduced to $\approx 12.5\ D_0$ in the case of

MS01 and ≈ 4.0 D_0 in the case of MS06. Despite this, it can be seen in Figure 4.9(b) that the normalised settlements follow very similar curves. This implies that the rigid base of the container does not affect the settlement of pile groups in sands at low effective stress (due to high pore pressures) while at least 4 pile diameters of soil remain between the pile tips and the base of the container. Additionally, in Section 3.7.1, it was discussed that the piles used in the JK-PG pile group had a pile diameter to soil grain size ratio of 14 and that additional base resistance might have been mobilised in MS01. As can be seen in Figure 4.9(b), the normalised settlements in MS01 lie slightly below the curves in MS05 and MS06 (which had much larger values of pile diameter to soil grain size). While this may be due to the particle size effect, it is clear that it has not significantly affected the results.

4.4.4 Effect of bearing layer hydraulic conductivity

The model layout of MS01 is very similar to that of test "JK-12," described by Knappett (2006). Preparation techniques in both cases were very similar, and the pile groups used in the two tests were identical. However, the experiment of JK-12 was carried out in an equivalent shear beam container (briefly described in Section 3.3. Additionally, the model layouts shown in Figure 4.1(e) & 4.1(f) indicate that two pile groups were tested in the same experiment, resulting in the pile group's centre being located at approximately one quarter of the length of the container. The results of Teymur (2002) suggest that the boundaries of the container are insignificant within the central third of the container. While slightly outside this zone, it is thought that the settlement of the pile group will not have been significantly affected by the container's boundaries. It can be seen in Figures 4.1(a) & 4.1(f) that the loose layers in these tests were nominally identical, while different sands and relative densities exist in the bearing layer. However, due to the differences in the properties of the sand, the initial static factor of safety for axial loads are very similar. Hence, the results from MS01 and JK-12 should be directly comparable, and the uncorrected settlements are plotted against time in Figure 4.10(a).

Figure 4.10(a) indicates quite clearly that the reduced hydraulic conductivity of the Fraction E sand in the bearing layer of JK-12 has led to a significant increase in pile group settlement. The similarity of the test parameters also indicates that this test would plot significantly above the normalised settlement curve shown in Figure 4.9(b). The cause of the increase in pile group settlement is not fully understood, but the large difference in the soil's hydraulic conductivity in these tests provides a possible explanation. Whereas the total axial load applied to the pile cap is not changing during these tests, there is significant variation in axial load on the piles each cycle to counter the dynamic moments, as will be explained in Section 4.5.3. As the loads increase on the pile, the pore pressure
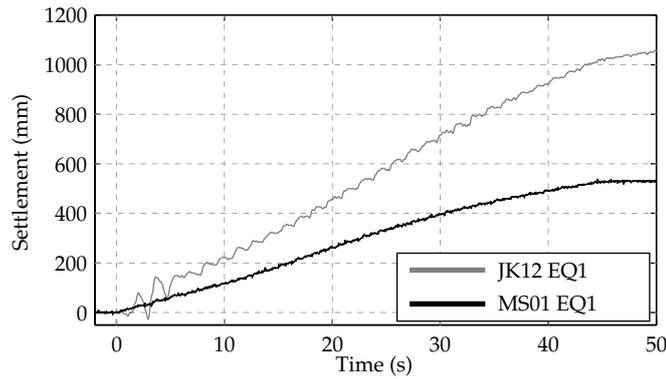
(a) Pile group settlement in MS01 and JK-12
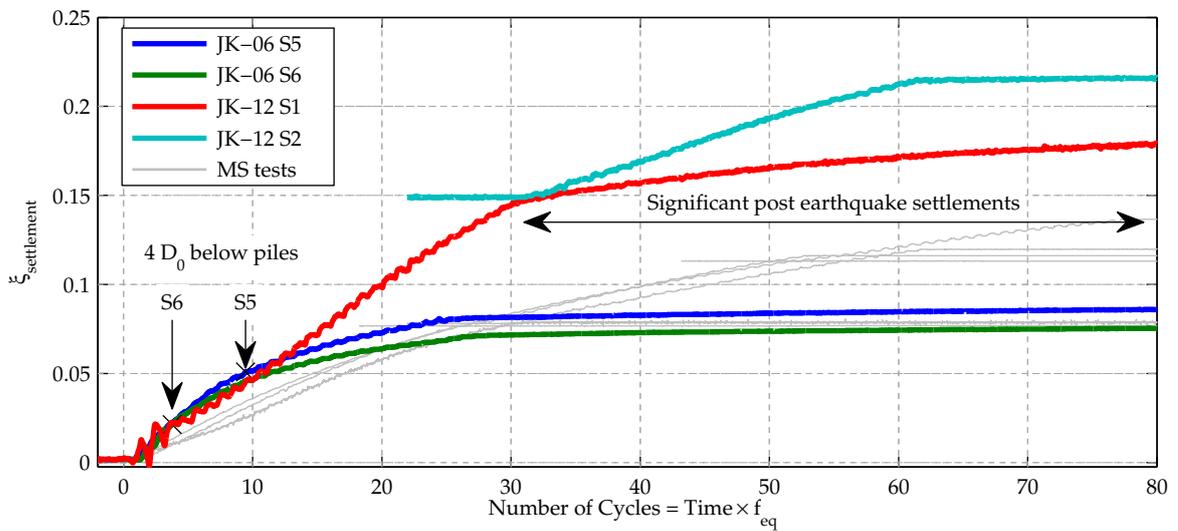
(b) Normalised pile group settlements with JK-06 and JK-12

Figure 4.10: Pile group settlement with free standing pile groups described by Knappett (2006)

would be expected to show a localised, and temporary, increase in excess pore pressure. This localised increase in pore pressure would then be expected to dissipate, leading to some increase in effective stress and therefore soil stiffness beneath the piles. If the hydraulic conductivity is reduced significantly, as is the case in JK-12, then the time for the excess pore pressure increase to dissipate would be longer, meaning that the soil is in its weakened state for longer and therefore additional settlement is possible.

While the test data from JK-12 clearly did not fit the normalised settlement curve of Figure 4.9(b), it was decided to attempt normalisation of the other free standing pile group tests described by Knappett (2006) to see if these data sets would form another curve which could then be used to predict the settlement of free standing pile groups with their pile tips bearing in a layer of dense Fraction E sand. The results of this attempt are shown in Figure 4.10(b). In the figure, the curves from Figure 4.9(b) and described in Section 4.4 are shown in light grey.

It is clear that the overall normalisation of the data is far less satisfactory with this new data set, apart from the very initial portion of the curves, where the normalised settlements up to 10 cycles seem to again collapse to a similar curve. Beyond this point, the curves diverge, even in the case of JK-06, where the pile groups were tested in the same container. However, some points must be borne in mind which may have affected the data presented. Firstly, in JK-06 the pile groups started with approximately 6.5 D_0 of soil between the pile tips and the base of the container. These pile groups were highly loaded and suffered very large settlements as a result. This means that the gap between the pile tips and the bottom of the box became very small after a limited number of cycles; the settlements of pile group S6 were large enough that the pile tips would come into contact with the base of the container towards the end of the period where the excess pore pressures were dissipating. As shown in the figure, the gap became smaller than 4 pile diameters after $\approx$ 10 and 4 cycles for pile groups S5 and S6 respectively in JK-06. It is thought that the small separation to the base of the box is responsible for reducing the settlements significantly in these tests. It was discussed in Section 4.4.1 that in earthquakes following the initial event, the curves continued smoothly from the end point of the first. While this is exhibited to some degree in Figure 4.10(b) (curves JK-12 S1 and S2), there is a definite change in gradient between the two curves. However, as shown in Figure 4.10(b), there was significant settlement of pile group S1 after the earthquake in JK-12; this is a feature which was not present in any of the other tests plotted where a second earthquake was conducted. It is suggested that this has led to the apparent change in gradient between these two curves.

While the results in Figure 4.10(b) are by no means satisfactory, it is proposed that they are sufficiently encouraging to warrant further investigation of the extent to which the normalised settlement proposed is able to predict the pile group settlement in a wider range of circumstances.

4.4.5 Effect of pore fluid

In all of the foregoing plots of settlement, the effect of pore pressures has not been included. In each of the saturated tests carried out, the majority of the increase in excess pore pressure (in the free field) takes place in the first few cycles of the earthquake. As a result of this, the issue of pore pressures in the free field may become much less important since almost all of the soil behaviour during the earthquake is reflecting the state where pore pressures have fully developed. As shown in Table 4.2, the increased load in the second flight of MS02 leads to an initial static safety factor which is close to that of those tested in the first earthquake of MS01, MS05, MS06 and JK-12. Additionally, the final earthquake in MS02 was set to be similar to that fired in MS01, and hence the results from this

Table 4.3: Settlements during MS02

Flight	Earthquake	Total settlement (mm)
	1	1
	2	7
1	3	8
	4	11
	1	0
	2	7
2	3	7
	4	19

data set should give a reasonable comparison of the effect of pore pressure on the pile group settlement. However, during all of the earthquakes in MS02, very little settlement occurred, as summarized in Table 4.3. This indicates that although the normalised plots of pile settlement shown in Figure 4.9(b) do not appear to show a large dependence on the generation of excess pore pressures (lower excess pore pressures were observed at the pile tip level in MS01 than in MS05/MS06), their presence does in fact affect the results to a large degree. In situations where pore pressures develop more gradually than has been observed in these experiments, it is likely that the settlement of the pile group will similarly increase more slowly.

4.5 Pile load transfer

While interesting insights regarding pile group settlement was possible using the JK-PG pile group, its use in determining the axial load distribution along the piles is limited by only having measuring points at the head and tip of the pile. In this section, the axial load distribution along a pile during an earthquake is examined using the results in MS05 and MS06, where the heavily instrumented pile group was available. Further, similar results were obtained in MS05 and MS06 (for example, the initial pile loading will be shown in Section 4.5.1 to be quite similar). Therefore, the results from MS06 will be used as the basis for discussion due to the greater number of working strain gauges available in this test.

Much of the work in the sections following is also found in Stringer & Madabhushi (2012).

4.5.1 Initial Pile Loading

During the swing-up of the centrifuge, the axial loads were observed to increase with increasing g-level and Figure 4.11 shows the initial axial loading along the pile length prior to the earthquake, with a sketch showing the nominal locations of each of the strain gauges. The figure shows negative shaft friction in the upper regions of the pile, while towards the bottom of the piles, positive shaft friction is recorded. When the centrifuge was swung up, some settlement of both the soil and the pile occurred. In MS06, the soil settled 1.4 mm (model scale), while the pile cap's settlement was 0.36 mm (model scale). The elastic compression of the piles under the applied loads is approximately 0.01mm (model scale), indicating that downward movement occurred along the entire length of the pile. It is assumed that compression in the dense soil was limited in comparison with the loose layer. Under this assumption, the initial load distributions observed are due to the compression in the loose layer causing down drag on the piles. The downward movement of the pile relative to the dense layer leads to positive shaft friction being mobilised. It must be noted that this distribution of shaft friction would not normally be expected for a bored pile, since the soil would not normally be expected to move downward relative to the pile. Rather, as the working loads are applied to the pile, then positive shaft friction would be expected to be mobilised along the pile. However, due to the settlements which occur during the earthquake, it is not thought that this initial distribution of shaft friction significantly affects the observed behaviour of the pile group during the earthquake.
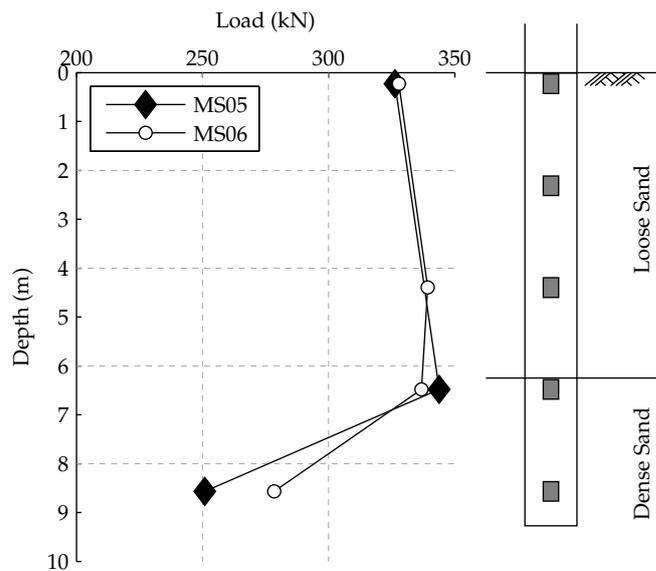
Figure 4.11: Axial load distribution before earthquake
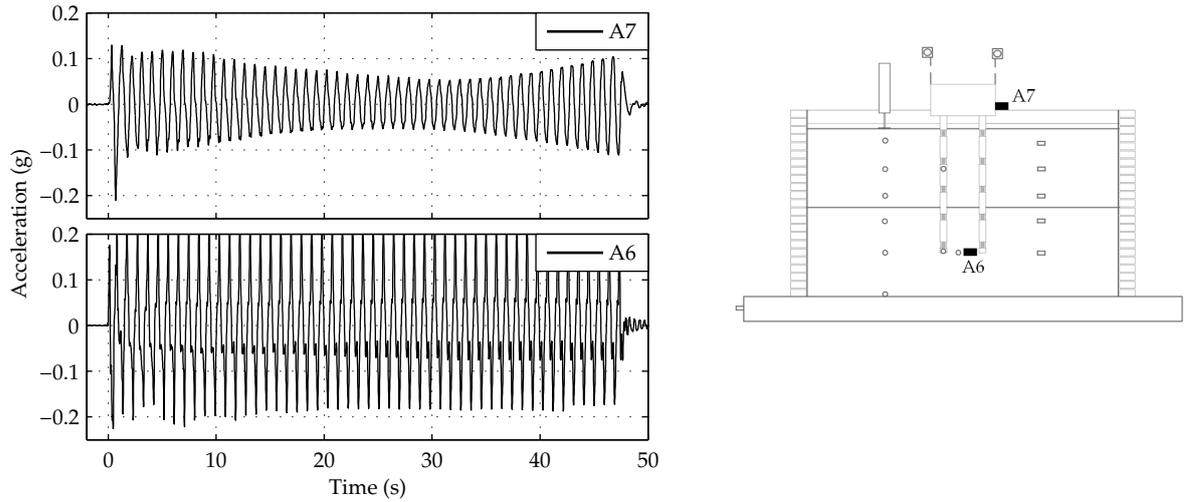
Figure 4.12: Acceleration of pile cap (A7) and at A6 in MS06, EQ1

4.5.2 Pile cap acceleration

The pile cap acceleration (A7) during MS06 is shown in Figure 4.12 where it can be seen that in the first cycle, the pile cap accelerations are nearly as strong as that in the dense soil between the pile tips (A6). After this, the pile cap accelerations attenuate strongly compared with those in the dense layer until near the end of the earthquake, when the accelerations begin to increase again. The pile cap shows large phase lags compared with the acceleration in the dense sand, with the pile cap becoming nearly 180 ^{o} out of phase with the dense layer after a few cycles. The increase in pile cap acceleration in the second half of the experiment, requires further investigation, but it is likely that a combination of factors combine to alter the dynamics of the soil-pile system. These could include, amongst others, some densification of the loose soil during the earthquake and changes in the length of the pile within the dense layer as the pile settles, which counteract the initial loss of stiffness in the model due to the rise in pore pressures.

4.5.3 Dynamic loading

Under the influence of shear waves, the soil is forced to oscillate, creating additional lateral and vertical pile loads, which are shown in Figure 4.13. In the figure, the mass of the pile cap has been omitted, as have the vertical loads which would be carried by all 4 piles to support the static vertical loads. As the soil displaces horizontally, it applies depth varying lateral loads to the pile group, which are combined to a single load, F_{eff}. The centroid of F_{eff} acts at a depth L_{eff} below the pile group's centre of mass. The lateral loads arising from the kinematic interaction between the piles and the soil must then act on the pile group, whose mass is concentrated (in this case) in the pile cap. This leads

to a horizontal pile cap acceleration, $\ddot{x}_{cap}$. Equations 4.2 and 4.3 show the equations of motion for the pile group, the second of which dictates that the vertical pile loads must increase/decrease in order to resist the moments arising from the lateral loading applied by the soil.

$$F_{eff} = m_{pilecap}\ddot{x}_{cap} \tag{4.2}$$

$$F_{eff}L_{eff} - P_1s - P_2s = J\ddot{\theta}_{cap} \tag{4.3}$$

The axial loading and shaft friction along the pile during MS06 are shown in Figure 4.14 along with the pile cap acceleration. In Figure 4.14(b), the shaft friction has been calculated as the difference in the axial load divided by the pile shaft area between two adjacent gauges. The labelling for these graphs is firstly "SF" to denote shaft friction, followed by two further letters which indicate the gauges used in the calculation (i.e. SF EC means that shaft friction was calculated between gauges SG E and SG C). As expected from Equation 4.3 it is seen in Figure 4.14(a) that the axial load at the head of the pile (SG E) displays a strong cyclic component, which has a peak-peak range of 250-300 kN for most of the earthquake. Towards the end of the earthquake, it is observed that the range of peak-peak axial loading increases due to the increasing pile cap acceleration.

In MS06, the average pile head load immediately after the earthquake is slightly lower than the initial load. Since the piles are free standing, the forces from the superstructure must always be carried in their entirety by the piles. The pile cap settlement showed a slight tilting of the pile group away from pile 1 both in the plane of shaking (from the measurements made at S1 and S2), and that perpendicular to it (from post-test observations). Therefore, the drop in load registered at the head of the pile indicates some redistribution of load to other piles in the group.
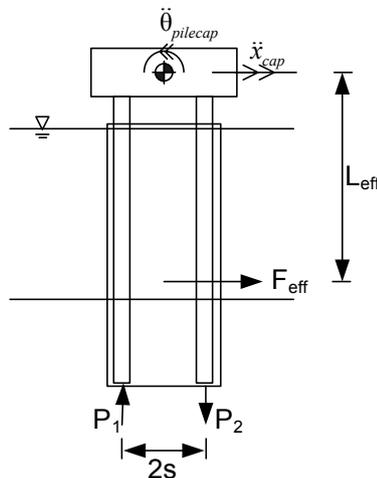
Figure 4.13: Generalised Loading

4.5.4 Initial behaviour

While Knappett & Madabhushi (2009a) showed that shaft friction could exist during an earthquake, the perception in general practice remains that shaft friction reduces to zero during an earthquake in liquefied soil. The data in Figure 4.14(b) shows clearly that positive shaft friction was maintained in the loose layer for much of the earthquake, with an unexpectedly high peak observed near the beginning. While gauges SGC to SGA in Figure 4.14(a) show a temporary reduction in axial load averaged over a cycle at around 5 s, this was not observed in the applied head load (strain gauge E) which continues to cycle close to its original value.

(a) Axial loads   (b) Shaft friction and pile cap acceleration
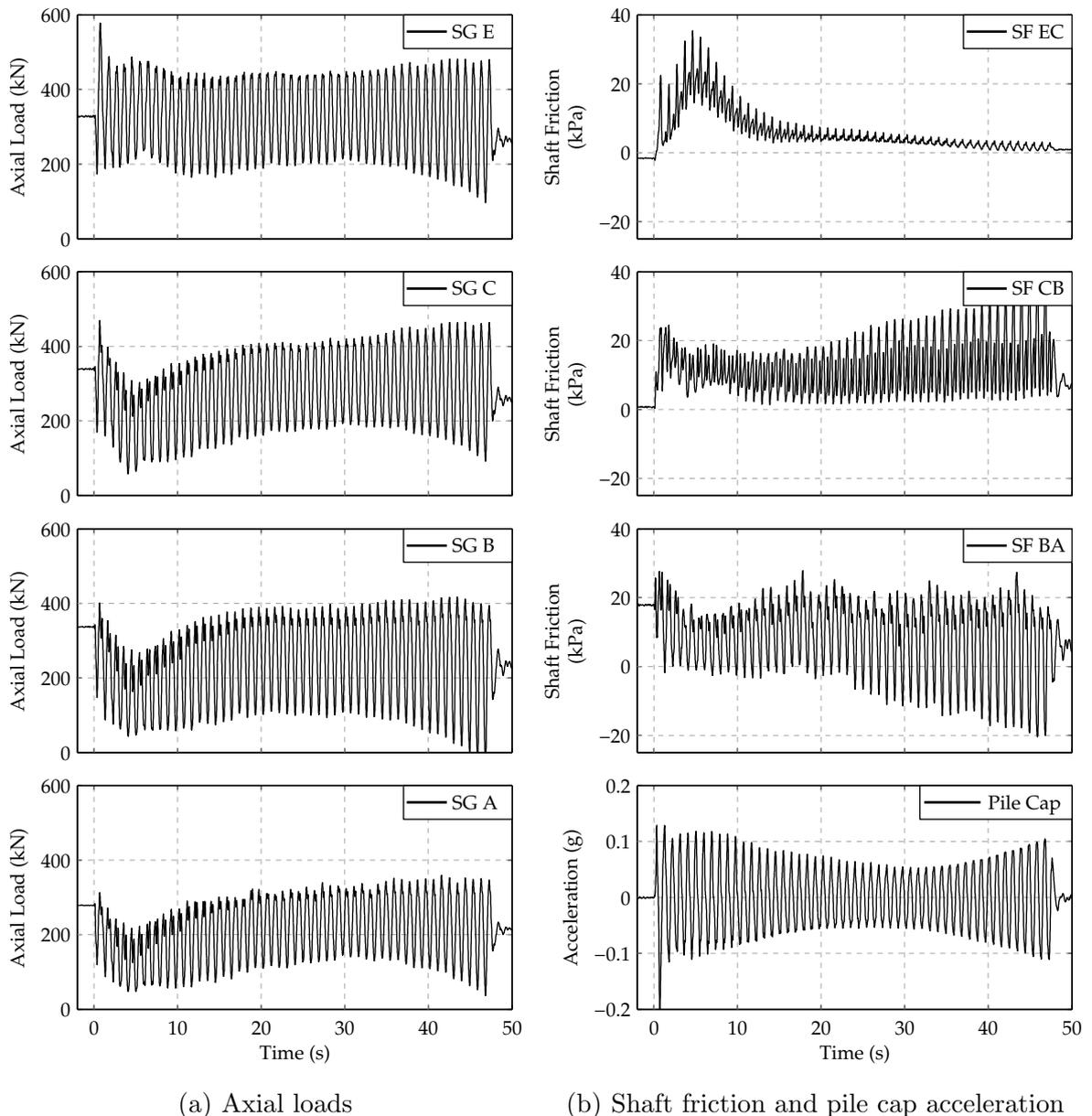
Figure 4.14: Axial loads and shaft friction measured on Pile 1 in MS06 during the earthquake
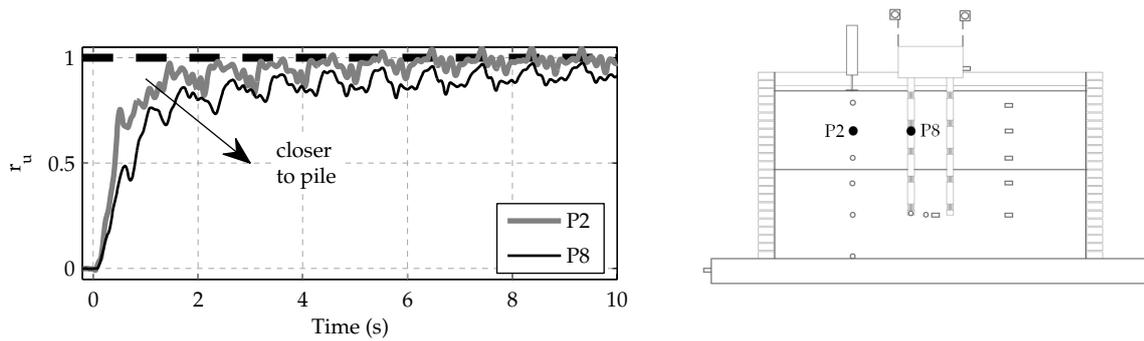
Figure 4.15: Excess pore pressure ratios at P2 and P8

The pore pressures recorded near the pile tips by P9 showed the pore pressure rising rapidly at the start of the earthquake. The associated loss of stiffness leads to a reduction in the base capacity and leads to the pile settling in order to mobilise additional capacity. By contrast, in the loose layer the pore pressures near the pile are observed to rise more slowly than those in the free field and show additional suctions due to shearing at the soil-pile interface. This effect is shown more clearly in Figure 4.15, which shows the excess pore pressure ratios for P2 and P8 near the start of the earthquake. Tokimatsu & Suzuki (2004) found that the suctions generated by the soil-pile interactions were strongly dependent on the lateral distance from the pile, meaning that close to the pile, the effects observed at P8 would be greatly exaggerated. It is therefore proposed that the reduced pore pressures near the pile in the loose layer coupled with the large pile group settlement (so that the piles move downward relative to the soil) lead to significant shaft friction being carried by the pile in the early phase of the earthquake, compensating for the loss in base capacity.

4.5.5 Effect of load phasing

Close examination of the axial loads showed that each in half cycle there are two peaks close to maximum load on each of the gauges. Figure 4.16 shows the detail of the axial loading on the pile, with points of interest within the cycle defined on the trace of SG A.

It is expected that the maximum lateral loading on the pile group from the dense layer would occur when the relative horizontal displacement between the two is greatest. However, integration of the acceleration records suggests that the greatest relative horizontal displacement between the pile cap and the tips occurs close to point II, when the acceleration of the pile cap was not at its maximum. This suggests that lateral loading must be applied by the loose layer in the opposite direction to the dense layer. The effect of resistance in the loose layer will both reduce F_{eff} and L_{eff} in Equations 4.2 and 4.3, leading to a reduction in the required moment effect from the axial loading in the piles and therefore smaller values of P_1 and P_2.
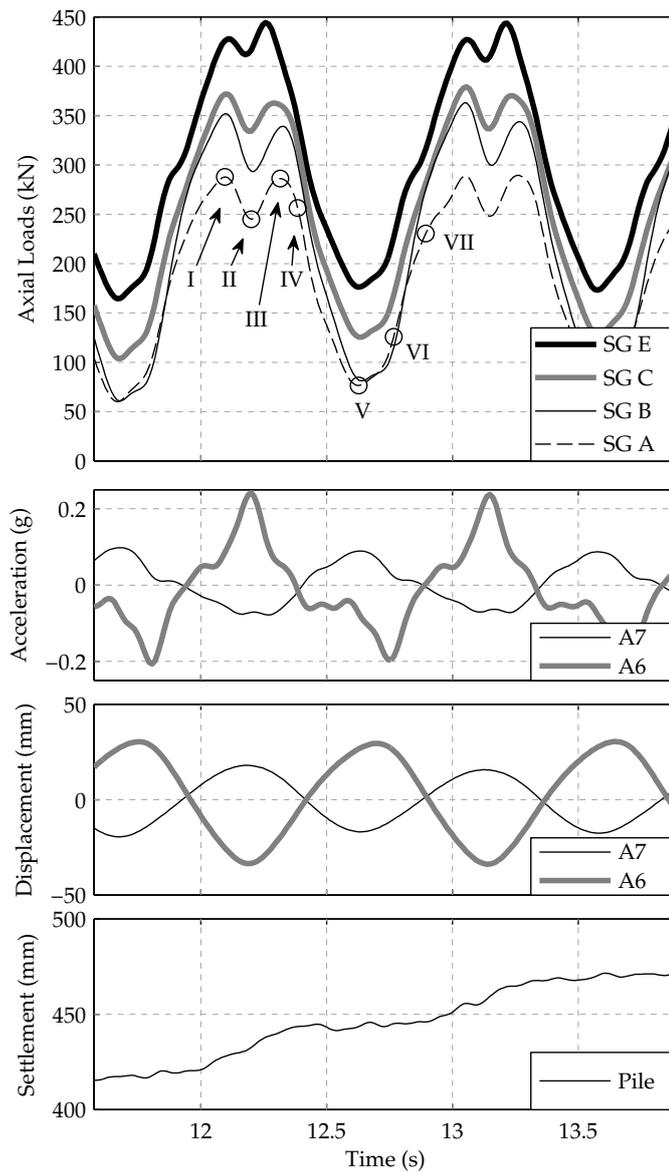
Figure 4.16: Zoomed view of axial loading along pile during a load cycle, with pile cap and dense soil accelerations, displacements and pile group settlement

As shown in Figure 4.14, the shaft friction showed interesting response and exhibited clear differences between the loose and dense layers. In the loose layer, shaft friction remained positive throughout the entire earthquake, with the shaft friction displaying two peaks per cycle. The first of the two peaks occurred very slightly after point II marked in Figure 4.16 and the second peak occurred at the point marked VI. Although point V would be expected to be a point of minimum shaft friction, it was found that this was not the case and that the minimums occurred at points IV and VII. When reporting the free field accelerations, the large phase lag compared with the dense layer was noted. Assuming no slip between the soil layers, the difference in shear stiffness between the soil and the pile will lead to complex interactions, with differing amounts of relative horizontal soil pile movement and direction.
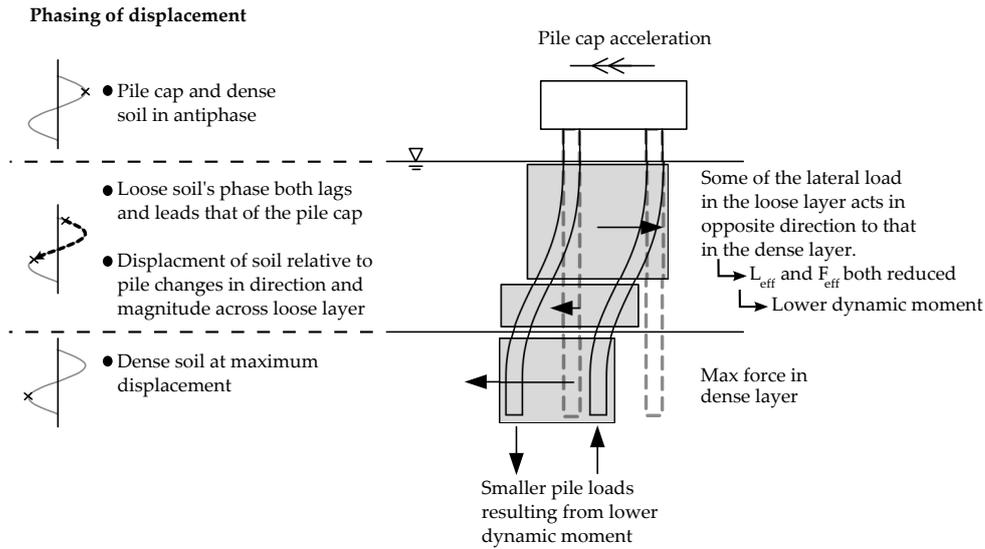
Figure 4.17: Lateral loading due to soil-pile displacement at "Point II"

An example of this is sketched in Figure 4.17, which shows the different lateral loading which acts on the pile at point II from Figure 4.16. The sine wave sketches indicates possible displacements of the pile cap, and each of the soil layers. It was observed in Section 4.3.2 that while accelerations, and therefore displacement in the base layer was largely in phase, a large variation in phase angle was observed across the loose layer. In this example, the displacements in the loose layer therefore are similarly imagined to vary significantly. As a result, the soil in the dense layer and a small zone near the interface in the loose layer apply lateral loads towards the left. In the remainder of the loose layer it is imagined that the piles are advancing into the loose soil, and therefore the lateral loads act in the opposite sense to those in the dense layer, and therefore reduce the unbalanced force acting on the pile cap.

The pore pressures at P8 seem to support this idea, with reductions being observed in the half of the cycle where loads on SG E were lowest (corresponding to greatest axial load on the pile nearest the PPT). Figure 4.18 shows a zoomed view of the shaft friction in the loose layer along with the anticipated excess pore pressures at the same level as P8, but next to the pile with the strain gauges. The "anticipated" pore pressures were calculated using the model's symmetry by maintaining the monotonic component of the pore pressures and reversing the cyclic component (obtained by passing the data through a high pass filter). It can now be seen that the peaks in shaft friction approximately align themselves with a reduction in the anticipated pore pressure. It is proposed that the increased lateral load (and therefore horizontal effective stress), and temporary reduction in excess pore pressure (as a result of the soil-pile shearing) is responsible for the observed shaft friction in the loose layer. Since the pile settles throughout the period of enhanced axial loading, high values of shaft friction are mobilised at point II. It is proposed that the
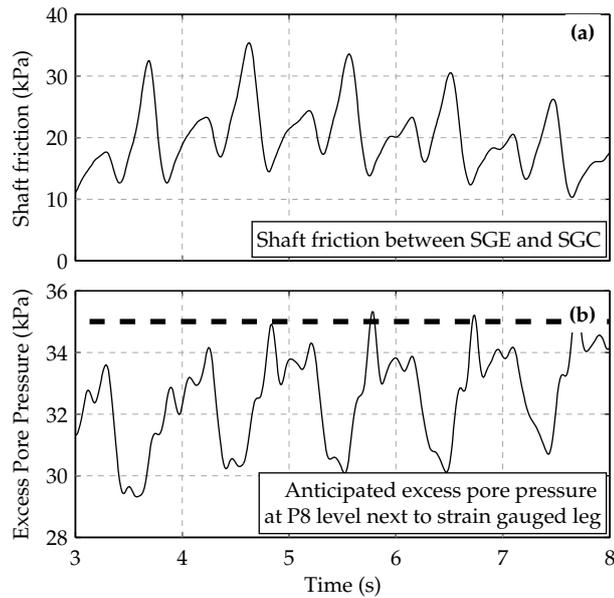
Figure 4.18: a) Shaft friction between gauges E and C; b) Anticipated pore pressures next to pile

reason why high shaft friction is not mobilised in the loose layer at the points of highest axial load (points I and III) is that the relative horizontal soil-pile displacement is low.

Three further points should be noted relating to the mobilisation of shaft friction in the loose sand layer. The first point to note is that in cases where the loose layer is relatively thin (see Figure 4.19 (a)), it is possible that the relative horizontal soil-pile movements will not be large enough to generate the suctions and increased earth pressures which gave rise to the shaft friction in these tests. Secondly, the flexibility of the pile has a large effect, since it affects the lateral displacement. Hence, stiffer piles will undergo smaller lateral displacements, leading to large relative horizontal displacements and therefore shaft friction can be mobilised. However, similar to the previous point, if the piles are

(a) Layer thickness

(b) Lateral restraint
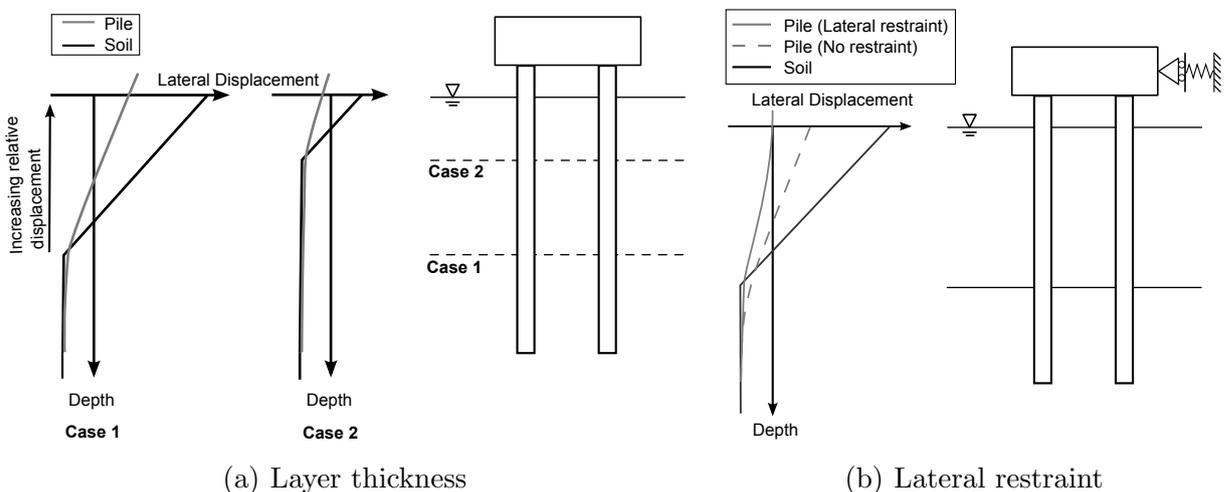
Figure 4.19: Factors affecting shaft friction in loose layer

107

less stiff, then the relative horizontal displacement between the soil and pile may not be large enough to enable shaft friction to be mobilised. Finally, if the pile head's motion is significantly restrained (for example by a bridge deck, or as part of a large foundation system) as shown in Figure 4.19 (b), then it is possible that the relative horizontal soil-pile shearing in the loose layer will be greater, leading to additional shaft friction capacity. However, further testing will be required to investigate these aspects.

4.6 Summary

In this chapter, the results from a series of tests involving a "free-standing" pile group have been considered. The tests included both the simply instrumented and heavily instrumented pile groups which were discussed in Section 3.7. It was shown that in each of the experiments, full liquefaction was achieved in the loose soil layer within the first few cycles. In the dense sand layer, full liquefaction was observed at a depth of ≈ 10 m and although excess pore pressures did rise further with increasing depth, full liquefaction was not observed at the deepest instruments within the model.

The discussion within this chapter focussed on two particular areas. Firstly the settlement which free-standing pile groups undergo during an earthquake, and secondly, the axial loads carried at different points along the pile. While positive shaft friction, considered over the entire length of a pile, was observed during an earthquake by Knappett & Madabhushi (2009a), the tests in this chapter have allowed distribution of shaft friction acting on different sections of the pile to be assessed. Specific points made regarding these two areas are summarised below:

- Settlements from the experiments of MS01, MS05 and MS06, totalling 6 sets of earthquake data (2 earthquakes per test) were found to plot on a unique curve of total number of earthquake cycles against accumulated normalised settlement. The accumulated normalised settlement is found by integrating the product of two groups with respect to time: firstly the rate of settlement normalised by the pile diameter, and secondly the ratio of initial vertical effective stress in the free field at the current depth of the pile tips to the average stress applied by the pile tips.

- The settlements were found to continue accumulating over a very large number of cycles. However, the reduction in the rate of settlement with time, apparent in the settlement curves indicates that the piles may eventually reach a limiting settlement.

- It was found that the settlement data of Knappett (2006) did not collapse onto the same curve of normalised settlement. It is suggested that the difference in settlement response is due to the large differences in hydraulic conductivity in the bearing layer, with reduced hydraulic conductivity leading to increased pile group settlements.

- The similarity in the normalised settlements of MS01 and MS06 suggests that a particle size ratio (number of soil grains per pile diameter) of 14 is acceptable for dynamic centrifuge modelling of piles in liquefied soils. Additionally, it appeared that 4 pile diameters depth below the tips of the piles was sufficient to prevent the results being adversely affected by the rigid base of the container.

- The load carrying characteristics of piled foundations without pile cap support is complex, and is argued to be strongly dependent on the interaction between soil and pile arising from their lateral motion.

- Positive shaft friction was recorded in the loose sand layer despite full liquefaction being observed in the loose soil layer away from the pile group. Pore pressure data near the pile suggests reductions in pore pressure at the moments when a peak in shaft friction was recorded. The apparent shaft friction capacity in the loose sand during the earthquake was proposed to be due to reductions in pore pressure near the pile arising from the shearing taking place between the pile and soil.

- The maximum positive shaft friction occurred near the beginning of the earthquake. As the earthquake progressed, the magnitude of the shaft friction in the loose layer reduced substantially due to increasing pore pressures near the pile.

- It was found that despite the piles being driven 7 D_0 into the dense layer, the dense layer did not restrain rotation of the pile group. This led to additional axial loading being applied at the pile base as a component of the pile tip's area became aligned with the direction of shaking.

- Shaft friction was measured in the dense layer throughout the earthquake; the capacity remained sufficiently high to resist the additional axial loads which were applied to the pile tip as the pile group rotated slightly.

Chapter 5

Settlement and Load Transfer of Cap-Supported Pile Groups

5.1 Introduction

In the previous chapter, the behaviour of pile groups with the pile cap clear of the soil surface was investigated. However, it is more often the case that pile caps are embedded within the ground. Therefore, in this chapter, an investigation into the behaviour of piled foundations with their pile caps in contact with the ground surface is carried out.

In the field, it is expected that site conditions will vary dramatically from location to location, with differences in soil type, layer thickness, and hydraulic conductivity to name a few. All of these factors potentially lead to differences in the behaviour of the pile group being considered; in Chapter 4, it was observed that the difference in hydraulic conductivity of the soil influenced the observed settlement of the pile group.

In this chapter, a series of 3 additional centrifuge tests are described in which changes are made to the hydraulic conductivity of the bearing layer, and also to the thickness of the liquefiable layer. Through the analysis of these results, and comparison with the results of MS06, this chapter aims to investigate the settlement response of cap-supported pile groups, and also the manner in which axial loads are carried during the earthquake as a combination of pile end bearing pressure, shaft friction and finally pile cap bearing pressure.

Similar to Chapter 4, this Chapter considers only the behaviour of the pile groups during the earthquake. The behaviour after the earthquake, while excess pore pressures are dissipating is discussed in Chapter 7. Much of the work presented in this chapter also appears in Stringer & Madabhushi (2011b).
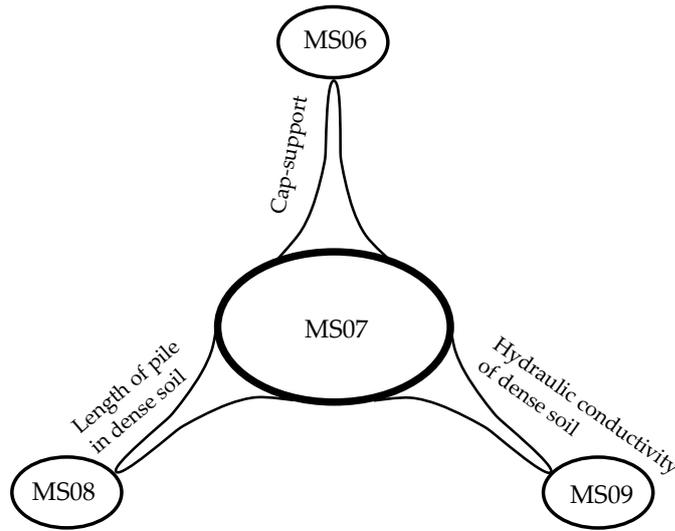
Figure 5.1: Tests carried out to investigate the behaviour of cap-supported piles

5.2 Centrifuge Models

In order to investigate the behaviour of cap-supported pile groups, a series of three centrifuge experiments were carried out. These tests will be discussed in this section, along with that of MS06 (which provides a comparison with free-standing piles). The models which will be described in this section were designed to test a number of different prototype scenarios and are summarised in Figure 5.1. The experiments in this series were all carried out at an acceleration level of 46.3 g and the heavily instrumented pile group (described in Section 3.7.2) was used in all tests. While the model layout from MS06 was shown in Figure 4.1(d), the instrumentation layouts for the tests MS07, MS08 and MS09 are shown in Figure 5.2. In addition, the key test parameters and soil profiles are displayed in Table 5.1 and 5.2 respectively.

Table 5.1: Test parameters for cap-supported piles

	Flight	**L_p**		**P / Pile**	**Static FOS**		**Earthquake**		
		Loose	Dense		$0.1D_0$	Ult	Freq.	Duration	Pk. acc
		(m)	(m)	(kN)			(Hz)	(s)	(g)
MS06	1 EQ1	5.8	3.5	337	1.8	5.4	1.08	46.4	0.22
	1 EQ2	5.8	4.5	337	2.1	5.9	1.08	23.2	0.22
MS07	1 EQ1	5.8	3.5	339	1.8	5.4	1.08	23.4	0.22
MS08	1 EQ1	5.8	3.5	339	1.8	5.2	1.08	23.7	0.22
	2 EQ1	5.3	4.0	466	1.3	3.8	1.08	23.8	0.21
MS09	1 EQ1	6.9	2.3	339	1.8	5.2	1.08	22.7	0.19
	2 EQ1	6.5	2.7	466	1.3	3.8	1.08	22.3	0.19
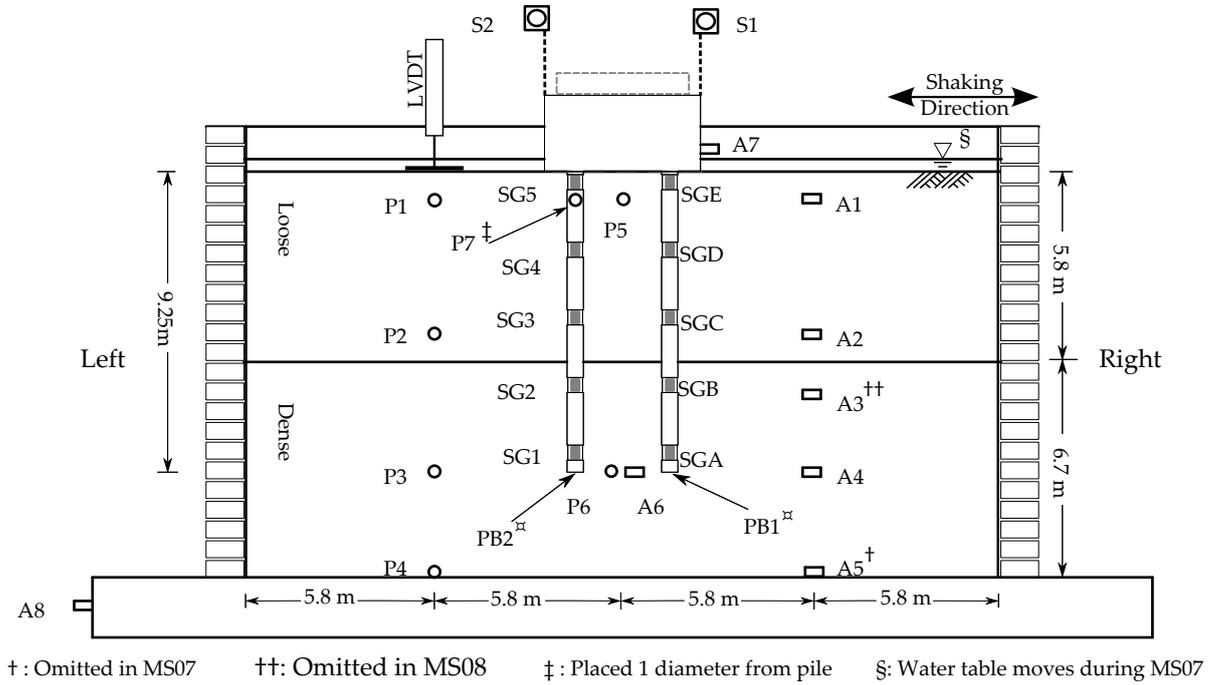
† : Omitted in MS07   †† : Omitted in MS08   ‡ : Placed 1 diameter from pile   § : Water table moves during MS07

(a) MS07 and MS08
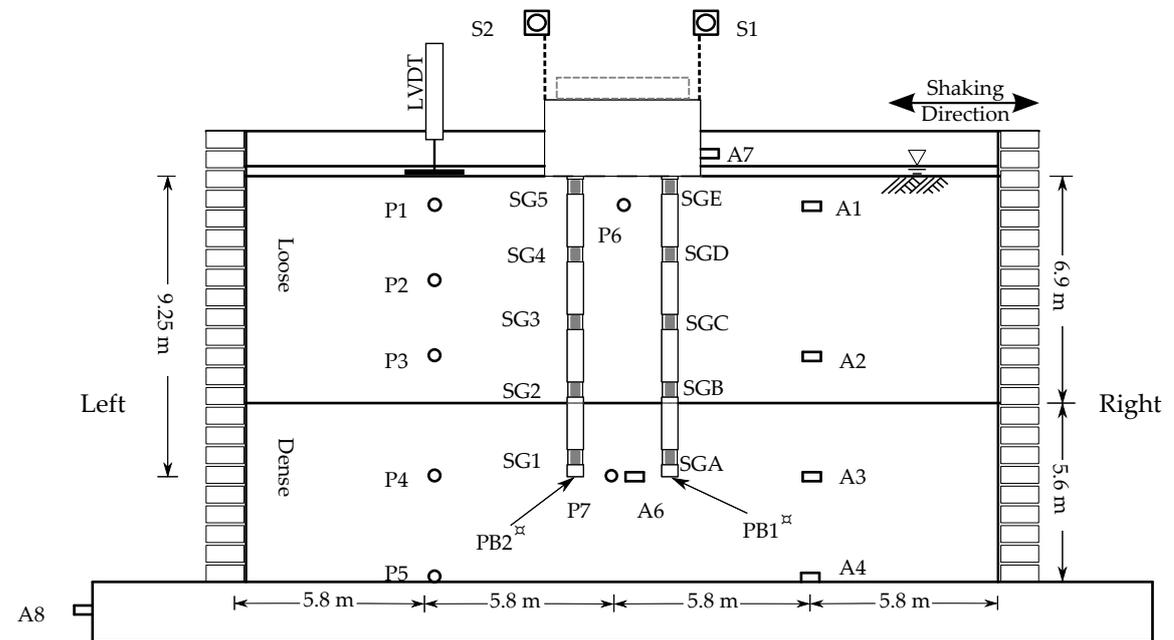
(b) MS09

Figure 5.2: Section view through the centreline of the model layouts of MS07, MS08 & MS09

113

Table 5.2: Soil profiles used in the cap-supported pile tests

			MS06	MS07	MS08	MS09
Loose	Sand		Fraction E	Fraction E	Fraction E	Fraction E
	Relative Density	(%)	35	35	35	35
	Thickness	(m)	5.8	5.8	5.8	6.9
Dense	Sand		Fraction C	Fraction C	Fraction E	Fraction C
	Relative Density	(%)	100	100	90	100
	Thickness	(m)	6.7	6.7	6.7	5.6

During the test of MS07, some problems were encountered with a new latex bag which had been installed in the laminar box container. This new bag was found to be responsible for a small leak which began during the swing up phase of the experiment. However, the pore pressures appear to stabilise before the earthquake was fired. In addition, photos of the soil surface taken before and after the earthquake (using web cameras mounted near the centre of the centrifuge) are shown in Figure 5.3. The photos indicate that in the central portions of the model, the fluid level dropped below the soil surface. However, fluid can be observed towards the sides of the model before the earthquake; after the earthquake, consolidation of the soil leads to a greater amount of the soil surface being covered. Considering that fluid will form a curved surface in the centrifuge, the pre-earthquake observation of fluid above the soil surface suggests that in the central portion of the model, the free water table will not be greater than ≈ 230 mm (5 mm at model scale) below the soil surface. The behaviour of the soil above the free water table during the experiments is unknown since no instruments were placed shallow enough in the model. However, it is thought that since the soil remains within the zone of capillary rise in this region, it is still likely to liquefy rapidly as the soil is sheared.

(a) Before EQ

(b) After EQ
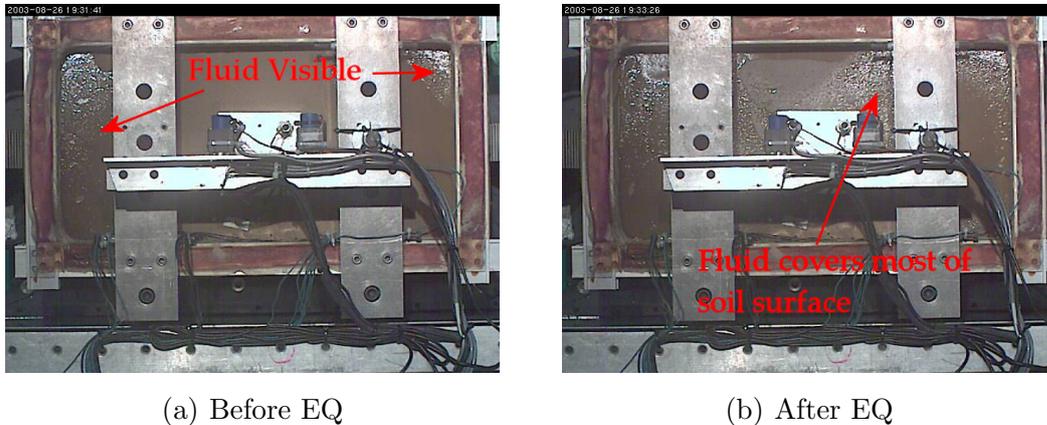
Figure 5.3: Fluid surface before and after the earthquake (plan view)

5.2.1 Soil surface settlement

The attempt to measure soil surface settlements in MS06 was discussed in Section 4.2. In tests MS07 to MS09, a larger disc of outer diameter 62.5 mm (model scale) was attached to the spindle of the LVDT and then placed on the soil surface. At the test acceleration level (46.3 g), the new disc arrangement applied a bearing pressure of 1.9 kPa. In the post-test excavations, it was nonetheless noticed that the disc attached to the LVDT still suffered some settlement. However, unlike the smaller disc which was used in MS06, the larger disc remained above the soil surface. It is thought that the settlements of the disc during the earthquake are therefore likely to be larger than the actual settlements, but that the measured change in soil surface elevation after the earthquake is reasonable. Measurements of the soil surface before and after the tests were therefore used to gain an estimate of the overall soil settlement that occurred, while subtraction of the settlements recorded post-earthquake by the LVDT enables an estimate of the total co-seismic soil settlements to be obtained.

5.3 Accelerations applied to the models

Similar model earthquakes were programmed into the SAM actuator for each earthquake performed in the tests described within this chapter. However, while the earthquakes
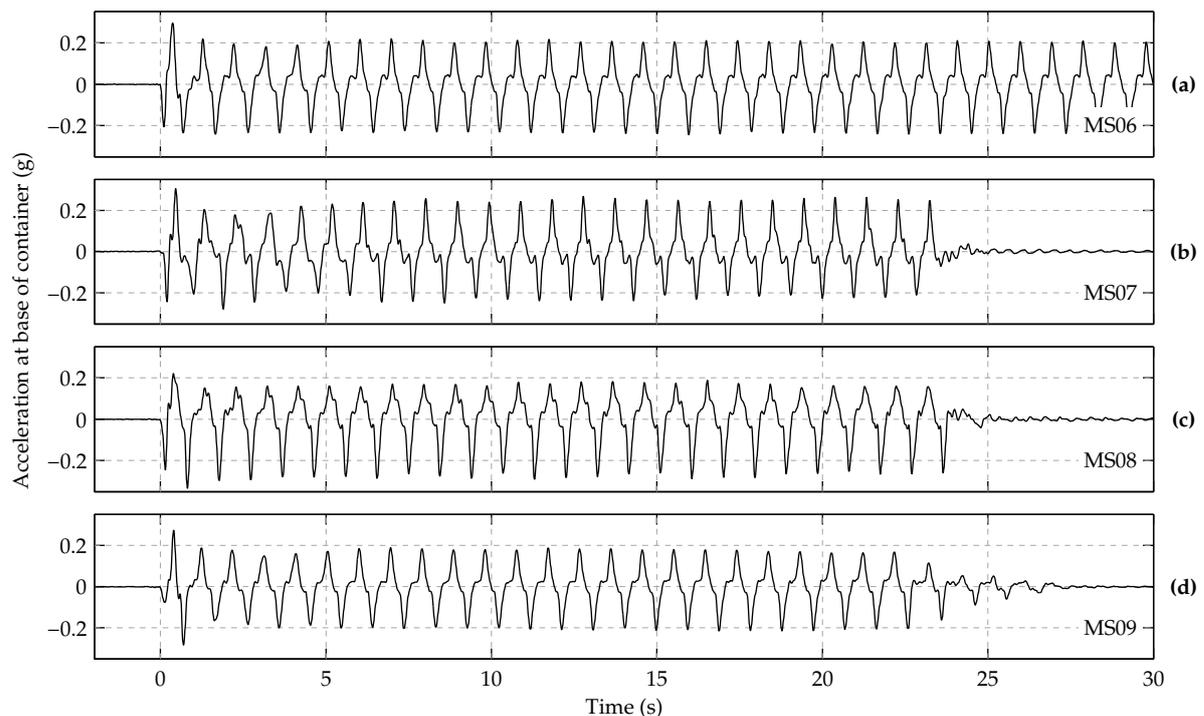
Figure 5.4: Accelerations at base of model container: a) MS06; b) MS07; c) MS08; d) MS09

were similar within the same test (i.e. EQ 1 and EQ 2 in MS08), some differences in the earthquakes delivered by the SAM actuator are visible in the motion records between tests. The acceleration recorded by the accelerometer mounted onto the rigid baseplate of the laminar box container are shown in Figure 5.4. It is possible to see that the input motions in MS06 and MS07 are quite similar and share similar magnitudes in both directions. However, in MS08 it can be seen that the peak acceleration in the direction towards the left is much larger than that towards the right. In MS09, it can be observed that although the main input motion is quite similar to that in MS07, the earthquake motion does not end cleanly, resulting in a few cycles of decaying acceleration amplitude rather than the "clean" cut-off at the end of the other earthquakes. This issue was caused by a poor release of the "fast-acting" clutch of the SAM actuator.

5.4 Free field soil behaviour during the earthquakes

5.4.1 Pore pressures

As shown in Figure 5.2, a vertical array of PPTs was placed at the same lateral location in the models as those described in Chapter 4. The pore pressures during the first earthquake recorded by the PPTs at the deepest point in the loose layer and those at the same initial depth as the pile tips are shown in Figure 5.5. The grey dashed lines in the figure indicate
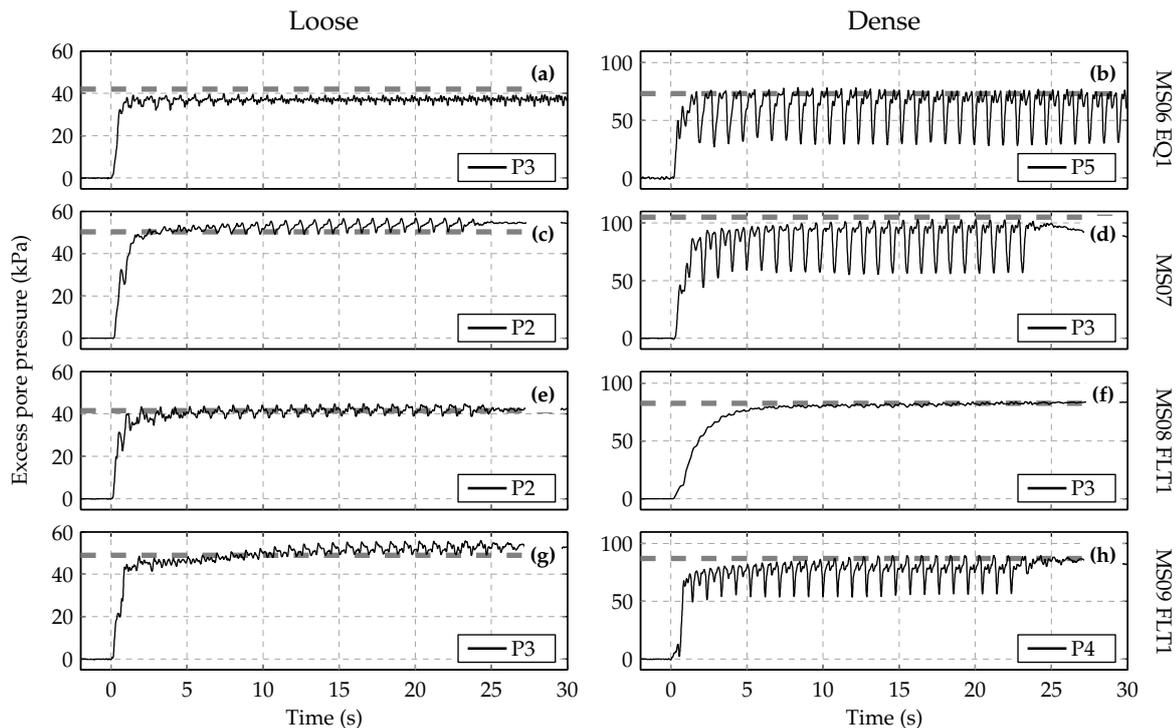
Figure 5.5: Excess pore pressures in the free field during the first earthquake of each test
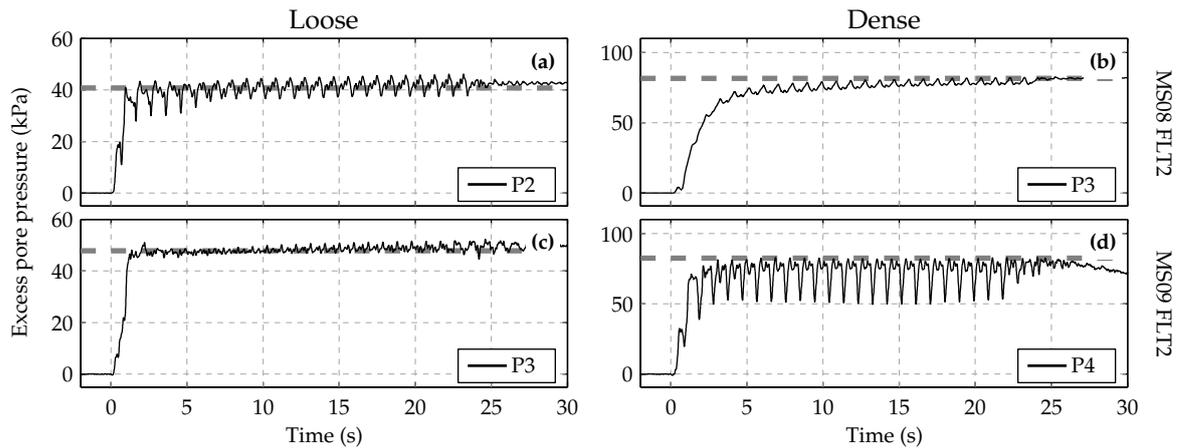
Figure 5.6: Excess pore pressures in the free field during the second flight of MS08 and MS09

the pore pressure required for full liquefaction in the free field ($\sigma'_v \approx 0$). Similar to the models in the previous chapter, the pore pressures rose rapidly in the first 2-3 cycles of shaking, and full liquefaction was reached each cycle thereafter. With the exception of MS08, large negative spikes were observed in the dense layer and are thought to be due to the same effect discussed in Section 4.3.1. It was described in Section 5.2 that the latex bag of the laminar box suffered from a small leak in MS07. This led to the water table falling slightly below the soil surface. As a result, the excess pore pressures required to cause full liquefaction are slightly larger in MS07.

As shown in Table 5.1, additional flights were undertaken in MS08 and MS09. The pore pressures recorded during this test are shown in Figure 5.6 and indicate that the pore pressure response in the second earthquake was similar to that recorded in the first.

5.5 Pile group behaviour

5.5.1 Initial pile loading

The load distribution on the piles before the earthquakes is shown in Figure 5.7, with the loads from the two legs shown in the different subplots. At the head of the pile, the loads are quite close to those expected from Table 5.1, indicating that the pile cap is not supporting significant axial load in the period before the earthquake. The loads indicate some negative shaft friction in the loose layer due to compression of the sand during the swing up of the centrifuge and before the earthquake. Figure 5.7 also shows some positive shaft friction being mobilised in the dense layer, though the majority of the axial pile load is supported in end-bearing by the pile tips.
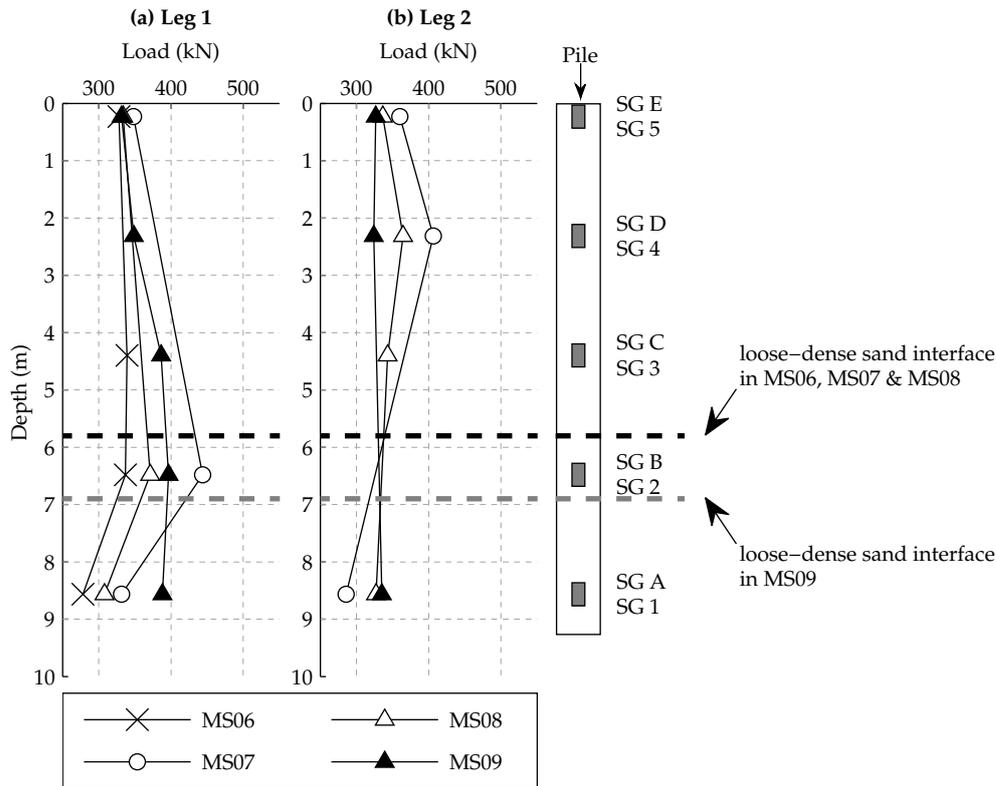
Figure 5.7: Initial axial loads on piles before first earthquake

5.5.2 Pile cap accelerations

Figure 5.8 shows the accelerations recorded on the pile cap (A7) and in the dense layer between the pile tips (A6). In each test, the pile cap accelerations lagged those in the soil near the pile tips; the phase lag increasing greatly over the first few cycles so that the accelerations became 180 ^{o} out of phase. Despite similar input motions at the container base (A8), the pile cap accelerations (A7) of the free-standing and cap-supported pile groups were very different. Figure 5.8 (a) shows that the free-standing pile group maintains large pile cap acceleration, while accelerations between the pile tips remains fairly constant. Figure 5.8 (b) shows the contrasting case of a cap-supported pile group, where pile cap accelerations attenuate progressively at the start of the earthquake as the excess pore pressures are generated. Similar pile cap acceleration responses were observed in the other experiments having cap-supported pile groups, as shown in Figure 5.8 (c-f). It was noted in Section 5.2 that a small leak in MS07 resulted in the free water table being slightly lower than the soil surface. The similarity of the pile cap accelerations in each of the cap-supported experiments suggests that this fault in the experiment has not significantly affected the behaviour of the pile group in MS07.

Comparing the accelerations between the first and second earthquake in a test (i.e. MS08, shown in Figure 5.8 (c) & (e)), it was found that the pile cap accelerations in both earth-
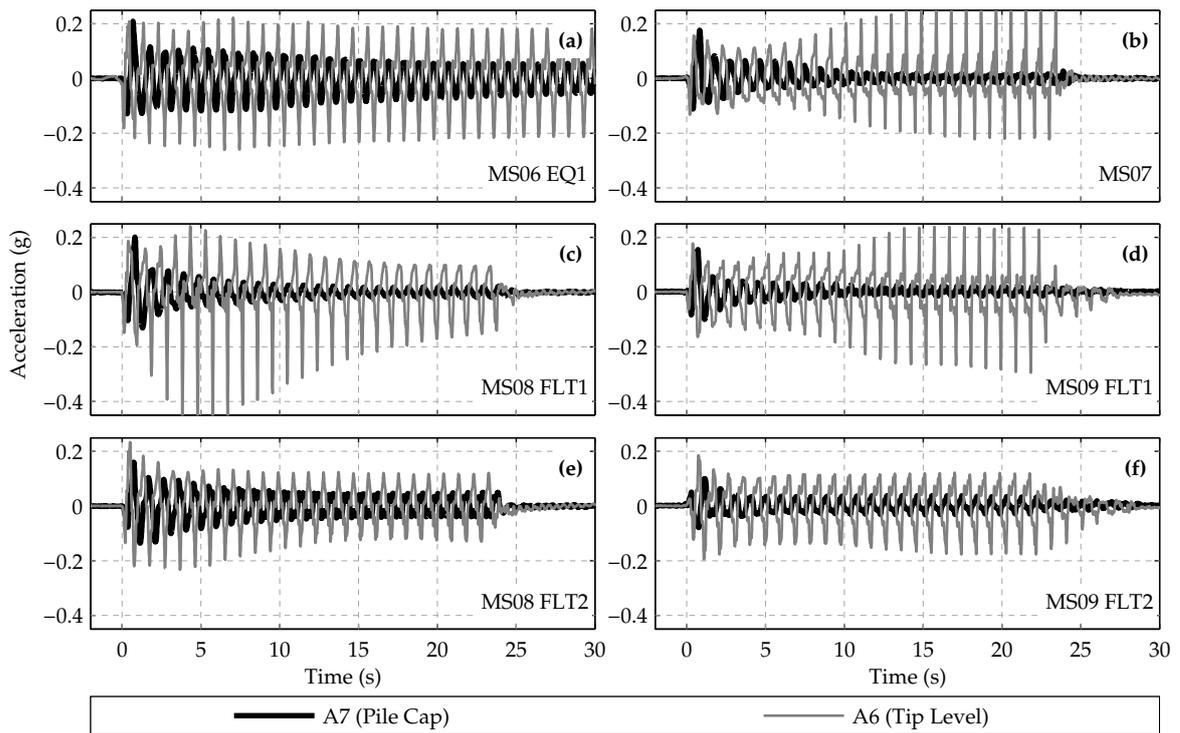
Figure 5.8: Accelerations of the pile cap and soil at the pile tips

quakes displayed the attenuation of peak amplitude following the onset of liquefaction. However, in the second earthquake, the pile cap accelerations were slightly higher than those in the in the first earthquake.

5.5.3   Pore pressures beneath the pile cap

Figure 5.9 (a) shows the pore pressure recorded below the pile cap in MS07. On the same graph, the dashed black line indicates the full liquefaction pressure at the same level in the free field. At this location, excess pore pressures initially rise to the level required for liquefaction in the free field. However, the pressures then continue to rise initially, before the trend reverses for the remainder of the earthquake. Similar observations were made in the other cap-supported pile group experiments. In MS08, the pore pressures rise was more limited, instead reducing slightly after about 5.5 s. In MS09, the pore pressure rise and subsequent fall took place at similar times to that in MS07, but the rise in pore pressures was greater, rising to approximately 18 kPa above the free field liquefaction value. In each of the three tests, the pore pressures rose for a period after the earthquake had ended, before dissipating along with those in the free field, indicating a migration of pore fluid towards the zone of dilation in the moments after the end of the strong shaking.
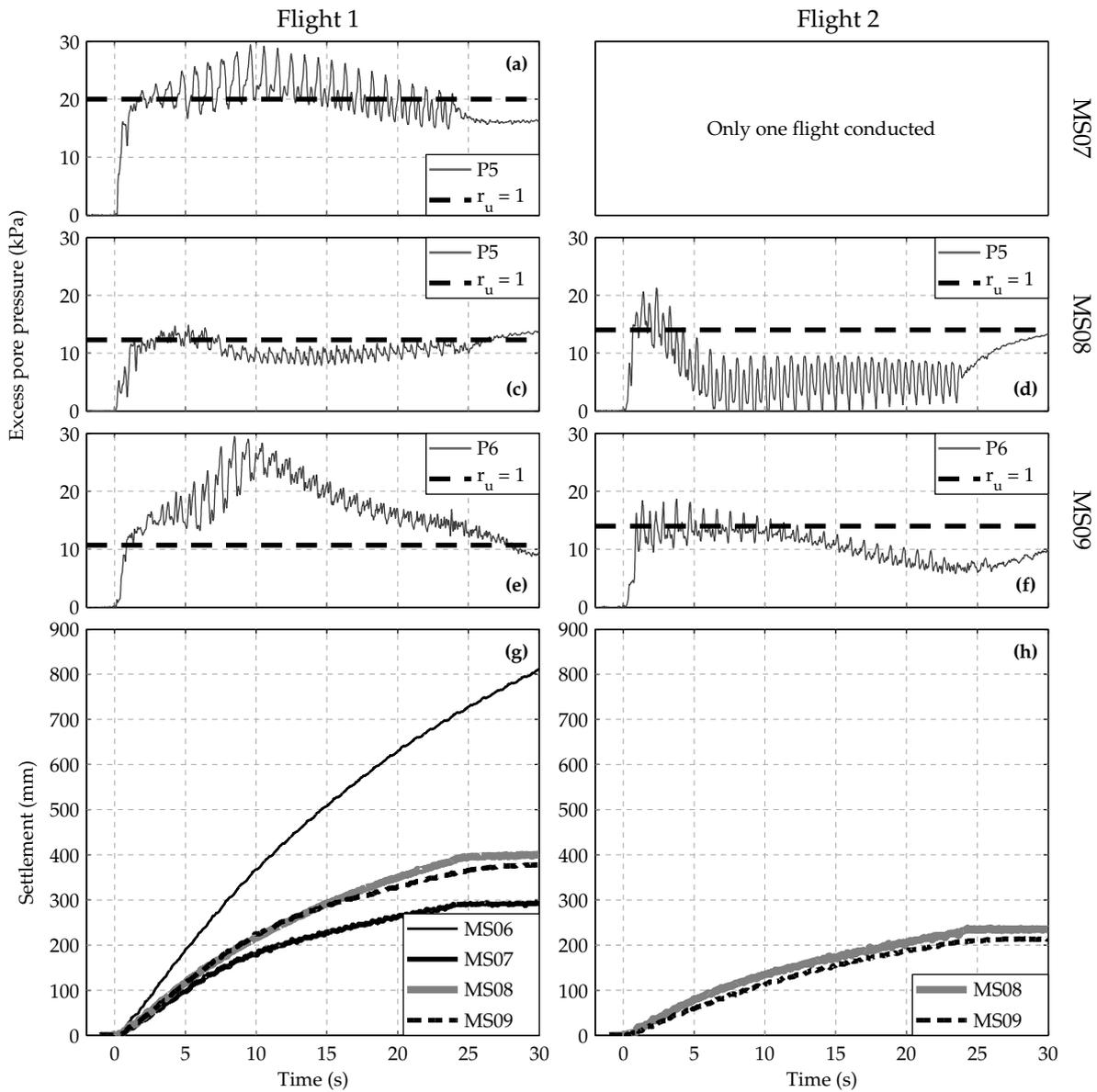
Figure 5.9: Pore pressures beneath the pile cap and absolute pile cap settlement in cap-supported tests

5.5.4 Pile group settlement

When subjected to earthquake loading, the pile groups experienced large downward settlements, as shown in Figure 5.9 (g & h), where pile cap settlement (calculated as the average of the two potentiometer readings and smoothed for clarity) is plotted. In this figure it can be seen that settlement accumulates throughout the entire earthquake motion. It is clear that cap-supported pile groups suffered much smaller settlements compared with those of free-standing pile groups. Similarly, Knappett & Madabhushi (2008a) found that the presence of the pile cap reduced settlements by a factor of approximately 2.

It must be noted that the settlements plotted in Figure 5.9 (g & h) are relative to a fixed

datum. While in some situations, these absolute settlements are of high importance (i.e. a pile group supporting a bridge pier, where large absolute settlements of a pier relative to the embankements or other piers may render the bridge unusable), it is often of greater interest to consider the pile cap settlements relative to the soil surface. If for example a building was supported on piled foundations and large absolute pile cap settlements of 1 m were recorded, it would be of little practical importance if the soil surrounding the building were to settle by a similar amount. Relative settlements of the pile cap during the earthquake were therefore estimated using the soil surface measurements as described in Section 5.2.1. Since the soil profiles were similar in MS06 and MS07, the same amount of settlement in the dissipation phase of the test was assumed to occur in MS06. These estimated relative settlements, along with the absolute pile and soil settlements are summarised in Table 5.3. When relative settlements are considered, it is clear that the effect of the pile cap is even greater than noted by Knappett (2006); during the earthquake, when the pile group is settling rapidly, the effect of contact between the pile cap and soil surface was to reduce the settlements by a factor of 3.

The relative settlements in Table 5.3 reveal some interesting points concerning the settlement of cap-supported pile groups. It can be seen that the absolute settlements of the pile caps during experiments MS07, MS08 and MS09 are quite disparate, reflecting the differences in the soil profiles. However, once the soil surface settlements are taken into account, it can be seen that the settlements of the pile cap relative to the soil surface are quite similar. This observation will be discussed further in Section 5.7.

5.5.5 Axial load transfer

The pile loading during the earthquakes for the free-standing and cap-supported pile groups was dramatically different. The differences in behaviour can be seen in Figure 5.10, which shows the axial load distributions with depth at various time instants. In the case of the free-standing pile group, the head load remains fairly similar throughout the earthquake, with any changes indicating load transferring to other piles within the group. Lower down the pile, the loads initially drop (minimum was found to be at t = 4.7 s), but then recover for the remainder of the earthquake. It is apparent from the strain gauge measurements that shaft friction was mobilised during the earthquake on sections of the pile located in the loose layer, as well as those in the dense layer. This behaviour was discussed in detail in Chapter 4. Following the end of the earthquake, the axial forces in the piles below the soil surface increase due to downdrag arising from consolidation of the surrounding soil.

In the case of cap-supported pile groups and specifically MS07, the ability to shed load to the pile cap has led to significantly different behaviour. It is shown in Figure 5.10 (b)

Table 5.3: Estimated relative pile cap - soil settlement

Test	Flight	Pile Settlement (mm)		Soil Settlement (mm)			Relative Settlement (mm)		
		Co-Seismic	Post-Seismic	Co-Seismic	Post-Seismic	Overall	Co-Seismic	Post-Seismic	Final
MS06	1 EQ1	708	0	162	115.75 †	278	593	-116	477
MS07	1 EQ1	289	11	93	116	208	196	-105	92
MS08	1 EQ1	384	70	171	106	278	213	-36	177
	2 EQ1	235	20	19	74	93	216	-54	162
MS09	1 EQ1	333	61	153	171	324	181	-110	70
	2 EQ1	213	1	30	79	109	182	-78	105

† : settlement in MS06 during dissipation assumed to be the same as MS07
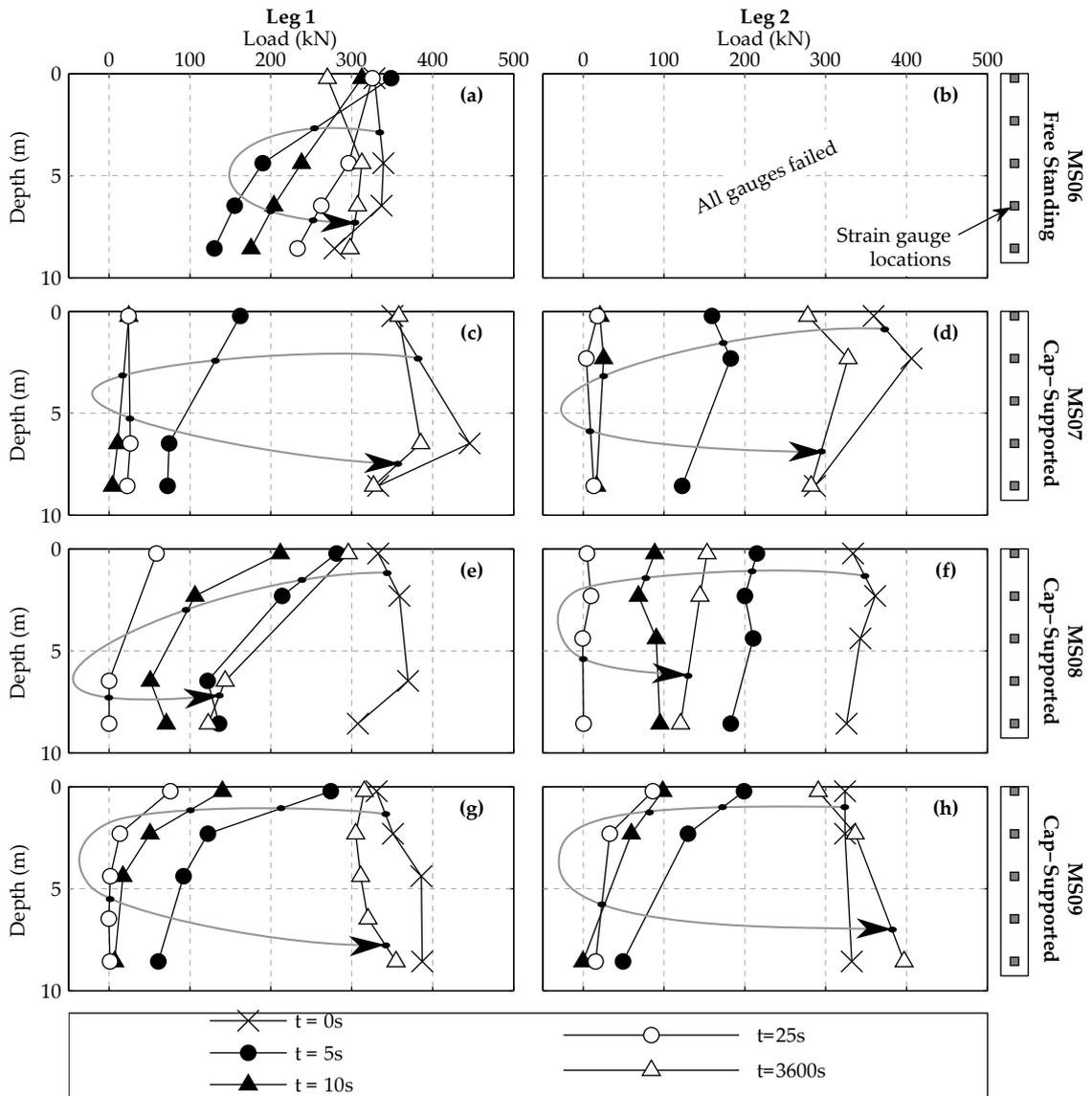
Figure 5.10: Axial loads at different time instants during the first earthquake of each test

that the axial load drops rapidly as the earthquake begins. After only 5 s of shaking, the pile head load has reduced to approximately half its initial value, whereas at the pile tips, the load is nearly a quarter of the initial value. As the shaking continues, the loads continue to reduce, until they have reached values close to zero along most of the pile after approximately 10 s of shaking. The loads remain very low for the remainder of the earthquake, but as soon as the shaking ends, the loads immediately begin increasing strongly, eventually returning to values close to those before the earthquake.

5.5.6 Shaft friction during the earthquake

The shaft friction which was recorded in the loose layer near the head of the piles, and in the dense layer near the pile tips at various time instants are shown in Figure 5.11.

Legend

◇   Value of shaft friction before the earthquake

▬   Shallowest (part a) /Deepest (part b) two gauges used to calculate shaft friction

▭   Shallowest / Deepest two gauges not available (table indicates the gauges used)

Gauges	MS06	MS07	MS08	MS09
Leg 1	E – C	E – B	E – D	E – D
Leg 2	None	5 – 4	5 – 4	5 – 4

(a) Loose layer

Gauges	MS06	MS07	MS08	MS09
Leg 1	B – A	B – A	B – A	C – A
Leg 2	None	4 – 1	3 – 1	4 – 1

(b) Dense layer
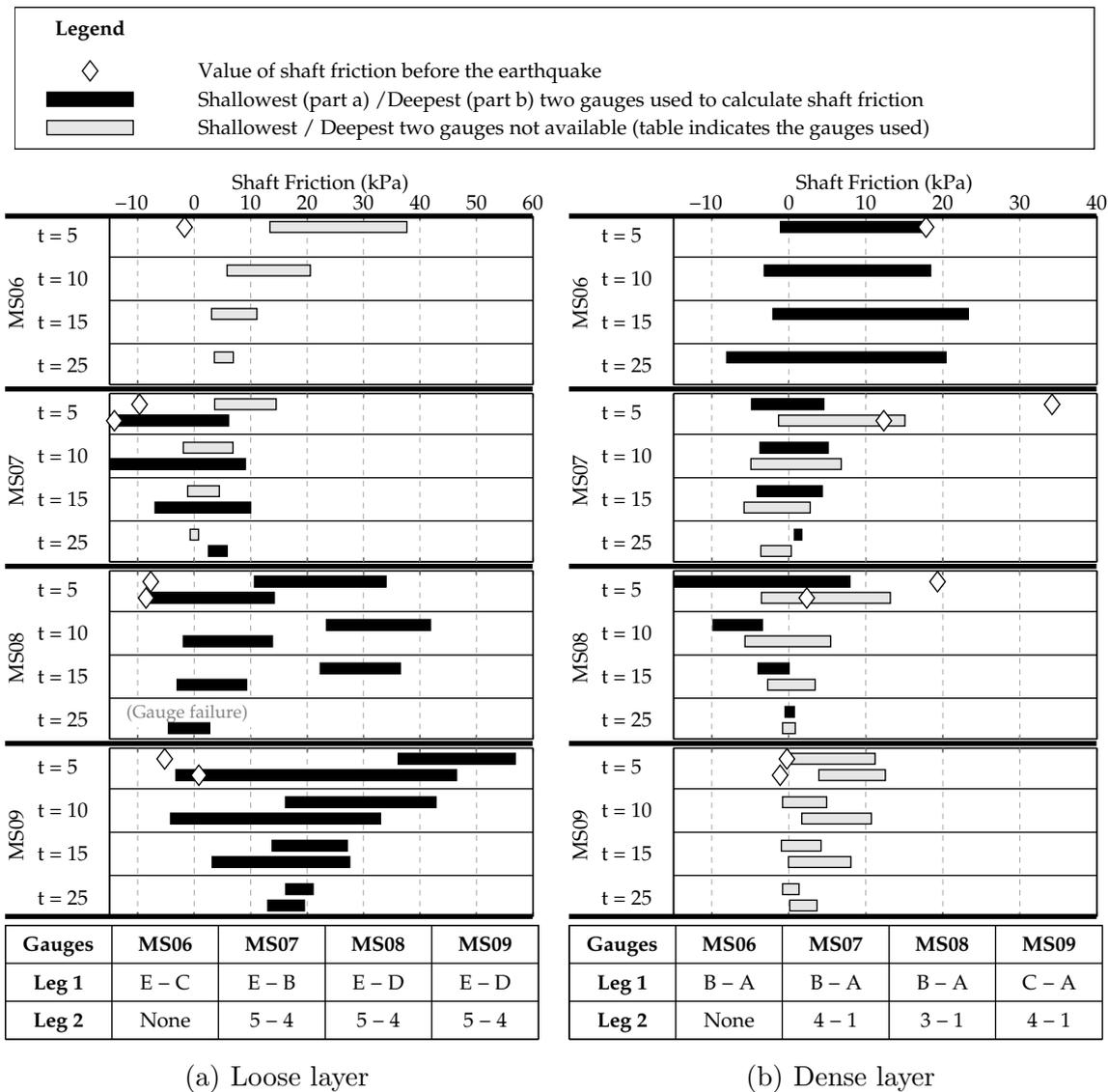
Figure 5.11: Range in measured shaft friction

The bars show the range in shaft friction recorded one full cycle either side of the time of interest, while the white diamonds plotted on the first time interval of each test show the shaft friction before the earthquake. As shown in Figure 5.2, two piles were strain gauged in each test. However, strain gauge failures meant that in some cases, shaft friction could not be calculated between the bottom pair of gauges. The gauges used to calculate the shaft friction in each case are indicated at the bottom of the figure and the bars are coloured either black to indicate that the bottom pair of gauges were used in the calculation, or light grey if different gauges were used.

5.5.6.1   Shaft friction at pile tips

In each test, the cyclic nature of the axial loading led to the shaft friction constantly changing throughout the earthquake. It can be seen in Figure 5.11(b) that for the free

standing pile group, the peak positive shaft friction remained around 20 kPa throughout the earthquake. The negative shaft friction is much lower, but became progressively more negative with time, ultimately reaching a peak value of -20 kPa in the latter stages of MS06 (shown previously in Figure 4.14).

This behaviour strongly contrasts with that observed in the cap supported tests, also shown in Figure 5.11(b). In these cases, both the average value and cyclic range of shaft friction near the pile tips decrease strongly as the earthquake progresses. It is recognised that there is a large variation in the initial shaft friction which was recorded on the piles across the tests, but the observed settlements shown in Figure 5.9 (d) would be expected to be sufficient to mobilise full shaft friction by the end of the earthquake. Of greater importance is that the axial loads in the dense layer were observed to reduce to zero (as shown in Figure 5.10) in each of the cap-supported tests after which they showed almost no cyclic variation, indicating that no load is carried at the base of the piles in these tests.

5.5.6.2 Shaft friction at pile head

The shaft friction in the loose layer at the head of the instrumented piles is shown in Figure 5.11(a), plotted in the same fashion as that in the dense layer, though in this figure, black indicates that the two shallowest gauges (ie. SG E and SG D or SG 5 and SG 4) were used to calculate the shaft friction.

In each test, the shaft friction at the head of the pile initially acts downward, however the average shaft friction becomes positive soon after the start of the earthquake. Figure 5.11(a) shows that this peak level is not sustained, and as the earthquake continues, the average shaft friction reduces. It should be noted that in the case of cap-supported pile groups, the shaft friction near the head of the pile is generally larger than that around the pile tips after the initial phase of the earthquake has passed.

5.6 Soil behaviour around pile group during the earthquakes

5.6.1 Cap-induced dilation

In Section 5.5.5, the role of the piles and the pile cap in carrying loads during an earthquake was highlighted. In Chapter 4, it was discussed that for the case of free-standing piles, there was no opportunity for the piles to transfer their loads anywhere except amongst the other piles within the group following liquefaction. This meant that the
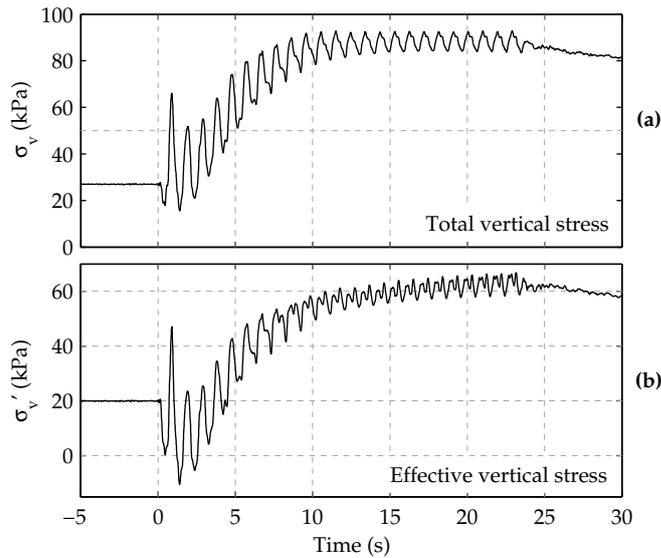
Figure 5.12: Calculated total and effective stresses beneath the pile cap in MS07

piles remained highly loaded throughout the earthquake. In addition, the kinematic lateral loads applied at the base of the piles as a result of the earthquake loading set up large dynamic moments which must be countered by the additional axial loading on the piles. Therefore, the piles within free-standing pile groups remain important as axial load carriers as well as playing a role in resisting the lateral loads and dynamic moments during the earthquake.

For cap-supported pile groups, it was shown in Figure 5.10 that immediately following the onset of liquefaction, the vertical loads (which were initially carried by the piles) transfer rapidly to the pile cap in the form of bearing pressure on the underside of the pile cap. This suggests dramatic changes to the vertical stiffness of the soil below the pile tips, and around the pile cap. In these tests, the pore pressures below the pile cap increased above the level of the free field in the early phases of the earthquake. Comparing the increase in pore pressures with the axial load carried at the head of the pile reveals that in both MS07 and MS09, the increase in pore pressure takes place while the pile head load is reducing. The pore pressures then begin reducing at the same time that the axial loads reach the plateau described in Section 5.5.5. This pore pressure response after the pile loads have stopped decreasing clearly indicates that significant drainage away from the soil beneath the pile cap is occurring during the earthquake. This is likely to be the reason why the same increase and subsequent reduction of pore pressures below the pile cap was not observed in MS08 (Figure 5.9 c), where the pile loads dropped slightly more slowly than in MS07; in this case, the additional pore pressures arising from the load transfer were able to dissipate quickly enough to keep the pore pressures beneath the pile cap low.

Before the earthquake, almost all of the vertical load is carried by the piles and therefore

126
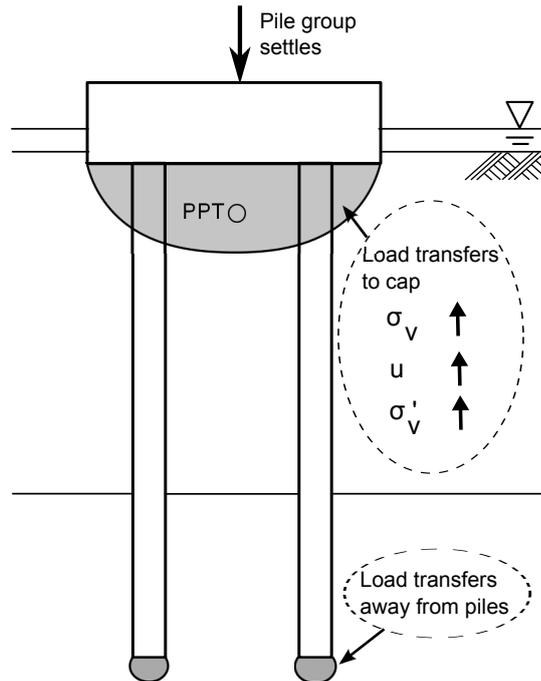
Figure 5.13: Changes to pore pressure and effective stress below the pile cap.

the vertical total stresses below the pile cap are similar to those in the free field. However, as the load transfers away from the pile following the onset of liquefaction, the vertical total stress in the soil below the pile cap must rise to maintain vertical equilibrium. This is captured in Figure 5.12 (a), which shows the vertical total stresses in MS07, calculated according to Equation 5.1.

$$\sigma_v = \sigma_{v0} - \frac{2(\Delta P_1 + \Delta P_2)}{A_{pilecap}} - \Delta\rho_{pilecap}\gamma_w \tag{5.1}$$

The pore pressures shown in Figure 5.9 indicate that this rise in vertical total stress is partly reflected by a rise in pore pressure. However the magnitude of pore pressure increase is too small to account for all of the change in total stress, hence the vertical effective stress beneath the foundation must also increase, as shown in the sketch of Figure 5.13. Figure 5.12 (b) shows this development of vertical effective stress beneath the pile cap in MS07. Below the pile cap, effective stresses briefly reduce to zero at the beginning of the earthquake when the piles still carry all the vertical loading, but as the axial loads on the piles reduce, the effective stresses increase strongly. The effective stresses underneath the pile cap continue to increase late in the earthquake as a result of drainage, which causes the excess pore pressures below the pile cap to reduce.

The dramatic transfer of axial load away from the piles during the earthquake suggests that in earthquake-prone regions, the design should take into account the possibility that the pile caps and ground beams will attract significant pressures if the structure begins to settle.

5.6.2   Excess pore pressures at the pile tip

It was described that in the design of the MS-PG pile group, PPTs were placed in the tips of the pile in an attempt to capture the pore pressure response directly beneath the piles. As described in Section 3.7.2, an attempt was made in MS08 and MS09 to saturate the cavity between the porous filter and PPT with pore fluid in order to improve the dynamic response of the instrument. The pore pressures recorded by PB1 during these two tests are shown in Figure 5.14 (c) and (d), where it can be seen that some dynamic response is evident. While the dynamic response may still be somewhat damped, the data is thought to give reasonable information concerning the average level of the pore pressures below the pile tips, and also an indication of when pore pressure spikes are occurring. In addition to the recorded pore pressure at the pile tips, the free field liquefaction pressure is shown with the dashed grey lines, taking into account the increasing depth of the pile tips during the earthquake. The pile end bearing pressure is shown the upper half of the figure, calculated as the load recorded at SG A divided by the pile tip area.

In Figure 5.14, it is observed that the pore pressures initially rise rapidly, but fall short of that required for full liquefaction in the free field for full liquefaction. The cyclic variation
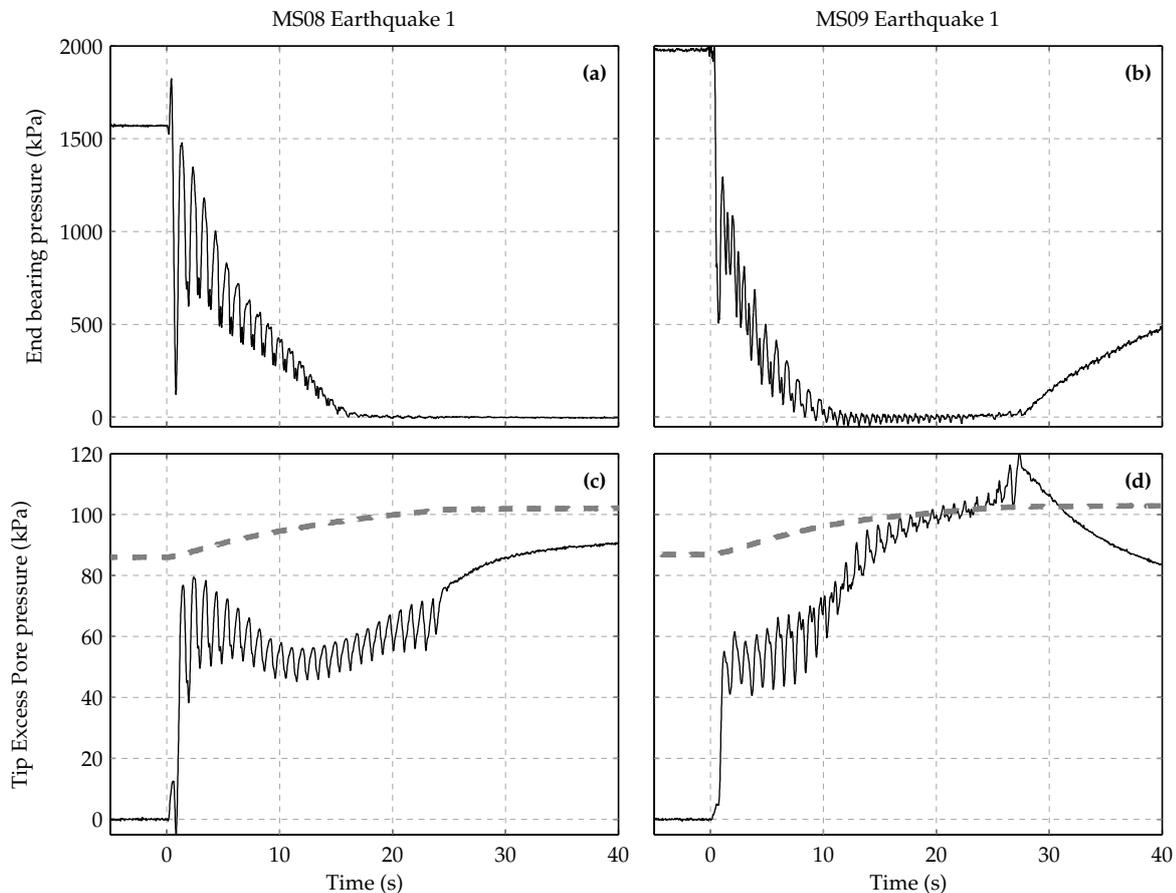
Figure 5.14: Bearing pressure at tip of Leg 1 and excess pore pressure recorded at PB1

in pore pressure which is evident is found to be in phase with that of the pile end bearing pressure. In the same way that increasing the overburden on a clay will result in a rise in pore pressure, the increasing axial loads on the pile are initially resisted by an increase in excess pore water pressure. If the axial loads were sustained for a period of time, then the excess pore water pressures below the pile tip would be expected to dissipate. However, in this case, the axial loads are continually increasing and decreasing, so that the pore pressure below the pile tip follows the changing end bearing pressure.

Following the rise in excess pore pressures below the pile tips near the beginning of the earthquake, the average pore pressure (over the current cycle) either reduces slightly (in the case of MS08), or remains fairly constant (MS09) until the axial loads on the piles have reduced close to zero. After this point, a distinct increase in the cycle averaged excess pore pressures occurs, particularly in MS09. The clear difference in the average excess pore pressures beneath the pile tips and the free field at the start of the strong shaking indicates that in this phase of the earthquake, the soil beneath the piles dilates in order to generate the required bearing capacity. Once the axial loads have transferred to the pile cap, the deviatoric stresses being applied to the soil reduce significantly and as a result, fluid from the region away from the piles flows towards the tips of the piles, enabling the excess pore pressures to increase. The rate at which the pore pressures can rise in the soil beneath the pile tips is controlled by the hydraulic conductivity of the soil. This effect is evident in Figure 5.14, where the increase in cycle-averaged pore pressure occurs rapidly in the case of MS09, whereas in MS08, the increase in cycle-averaged pore pressure is more gradual. The flow of pore fluid into the region of soil below the pile tips has interesting implications for the behaviour of the soil, which will be discussed further in Chapter 7

5.6.3 Conceptualised load transfer behaviour

The axial stiffness of the pile group is dependent of the load-settlement curves of the mechanisms which control the settlement at different points on the pile group. While many different mechanisms have been proposed for the settlement of foundations, two possible mechanisms which control the settlement of the pile group are shown in Figure 5.15. In the absence of the piles, the pile cap will behave like a shallow foundation, hence a Prandtl-type mechanism might be assumed. At the tips of the piles however, the confinement of the surrounding soil restricts the mechanism and cavity expansion solutions (i.e. Yasufuku *et al.* (2001)) may be more appropriate.

Before the earthquake, the confining pressures below the pile tips are very large and as a result, the axial response of the piles is very stiff. By contrast, the soil below the pile cap is at very low confining pressure, and hence is very soft by comparison. This leads to

(a) Mechanisms governing settlement

(b) Effective stress of soil and "stiffness" of load-settlement mechanism
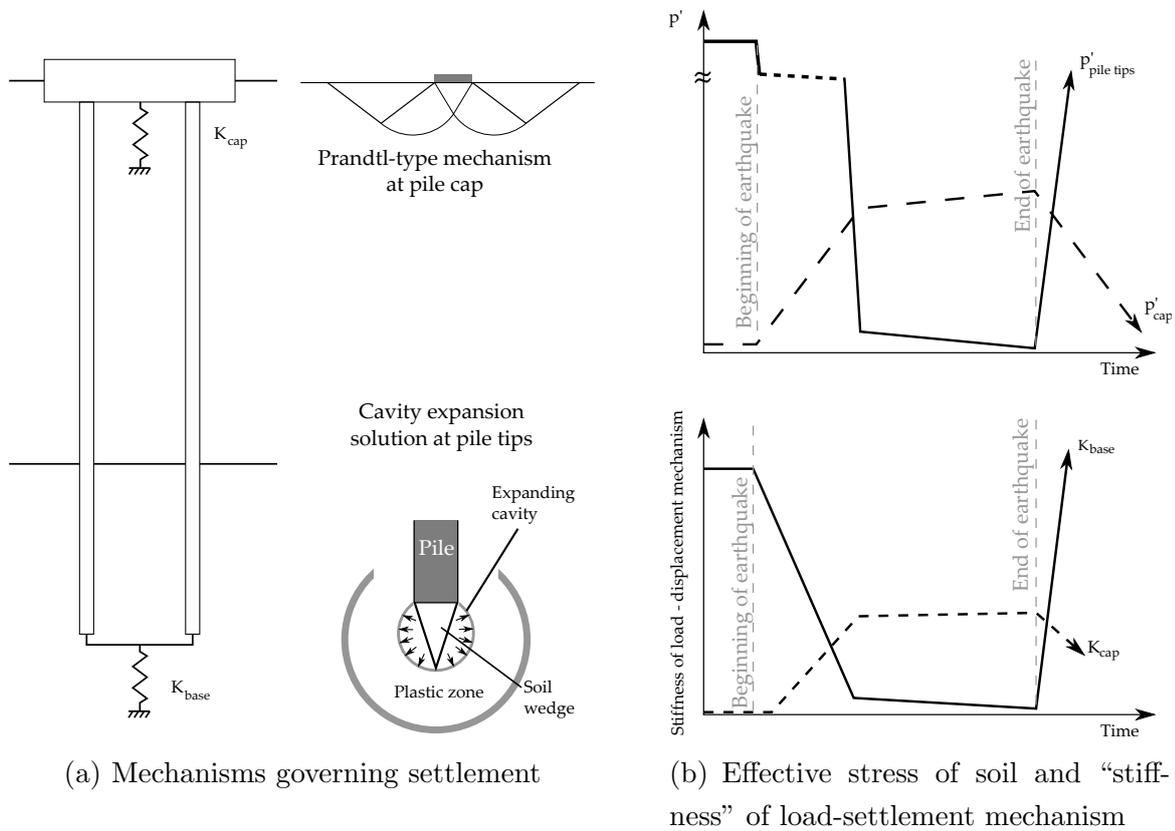
Figure 5.15: Interplay between settlement mechanisms

the loads initially being carried almost exclusively by the piles. However, pore pressures rapidly develop throughout the model following the beginning of the earthquake, and the pile group begins to settle. As a result of the soil deformation as the pile cap settles downward into the soil, some shear induced dilation occurs, leading to some resistance to the pile cap being mobilised. The mobilisation of resistance on the base of the pile cap leads to a reduction in the load carried by the piles. The ratio of the pile cap area to the pile tip area is approximately 28:1 for the MS-PG pile group. This means that a small mobilisation in resistance below the pile cap leads to a disproportionally large reduction in the load carried by the piles. Since the load being carried by the piles has reduced, the confining pressure below the pile tips must also reduce. As a result of the change in effective stresses below the pile cap and pile tips, the stiffness of the mechanisms governing the load-displacement response also change; that governing the pile cap's load displacement becomes more stiff, while that governing the pile tip's becomes less stiff. This induces further changes in where the load is carried, until it reaches its ultimate conclusion where almost all of the axial loads are carried by the pile cap.

The transfer of axial loads away from the piles and on to the pile cap has important repercussions for the moment capacity of concrete piles in seismic regions. Under normal working conditions, the axial loading on the concrete piles means that significant bending moments can be applied to the piles before any of the pile's cross-section becomes

subject to tensile longitudinal stresses. However, if the axial loads transfer away from the pile, then it follows that the bending stresses which can be tolerated by the section reduce substantially. Therefore in seismically active regions, the moment capacity of piles passing through liquefiable deposits should be calculated without the beneficial effect of superstructural loads.

5.7 Importance of the pile cap in controlling settlement and pile cap acceleration

The pile cap position not only affects the axial loading of the piles, but as shown in Figures 5.8 & 5.9, it affects the settlement and acceleration of the pile cap itself. In Section 5.5.4, it was observed that the pile cap settlement relative to the soil surface was similar in each test when the pile groups were cap-supported. This observation is made clearer in light of the transfer of axial load to the pile cap. Since the pile caps carry all of the axial loads, it implies that the settlement response must be controlled by the soil beneath the pile cap, and not the soil below the pile tips. While the soil profiles in each of the tests were different, the same sand was used in all of the loose layers, and began with the same nominal relative density. It therefore follows that if the settlement of pile group relative to the soil surface is being controlled by the soil below the pile cap, then similar settlements would be expected in the first earthquake of each test, where the pile caps shared the same axial loading. The similarity in the relative settlements between the first and second earthquakes of MS08 and MS09 (column 8 in Table 5.3) is however unexpected. This aspect requires further testing to be carried out, to quantify whether the axial loading affects the relative settlement in a similar way to that found in Chapter 4.

The dramatic improvement in the settlement response of the pile groups which are in contact with the soil surface again has implications for design. Whereas in normal situations, piles act as effective settlement reducers, in cases where significant pore pressure might occur at the pile tips during an earthquake, it is likely to be the pile cap which becomes the major settlement reducer. In these scenarios, large and robust pile caps (or ground beams) might help improve the settlement performance of the building during an earthquake.

It was shown in Figure 5.8 that pile cap accelerations of the cap-supported pile groups were very similar, whereas those of the free-standing pile group were much higher. This effect is again due to the zone of dilation beneath the pile cap and the subsequent transfer of load to the pile cap in the case of cap-supported pile groups. In the case of the free standing pile group, the lateral loads arising in the dense layer are transferred almost completely to

the pile cap, since only a limited amount of lateral resistance can be generated by the soil acting on the pile frontal area in the loose layer. However, in the case of the cap-supported pile group, the enhanced coupling with the soil in the loose layer as a result of the load transfer to the pile cap means that the pile cap's acceleration is now resisted by the large body of loose soil which, as a result of being liquefied at deeper elevations, is isolated from the large accelerations in the dense layers of the model, and therefore acts to reduce the pile cap acceleration. This in turn may be inferred to affect the lateral loads applied to the pile group when it is cap-supported. Since the pile cap accelerations are out of phase with those in the dense layer, their displacements will similarly be out of phase, meaning that the relative displacement between the cap and the dense layer is increased if the pile cap accelerations are large assuming that the base accelerations remain equal. Hence the reduction in the pile cap accelerations observed on cap-supported pile groups leads to a reduction in the relative displacement between the pile cap and the dense layer compared with a free-standing pile group. Assuming that the pile tips are forced to move with the dense layer, then the lateral loads applied to the piles will also be lower.

5.8   Shaft friction on cap-supported piles

The results shown in Figures 5.11(b) and 5.11(a) indicate the existence of shaft friction during the earthquake loading, which agrees with the experimental study described by Knappett & Madabhushi (2009a). While the expectation that any shaft friction would be mainly mobilised in the dense layer appears valid for free-standing piles, it appears that when the pile cap is in contact with the soil surface, this no longer holds.

A characteristic of all of the tests was the development of peak shaft friction in the upper regions of the pile shortly after the beginning of the earthquake and its reduction thereafter with continued shaking. Discussion of this behaviour within the context of free-standing pile groups is given in Chapter 4, and was proposed to be due to reduction in pore pressures very near to the piles as they are driven laterally by the surrounding soil. In the case of the free-standing pile groups, the pile cap accelerations remained high throughout the earthquake, and therefore the relative displacement between the soil in the loose layer and the piles remained of similar order throughout the earthquake. It was proposed that this was responsible for the continued, albeit diminished, shaft friction in the loose layer.

In the case of the cap-supported pile groups however, the accelerations of the pile cap reduce dramatically as the axial loads transfer from the piles to the pile cap. This leads to smaller pile cap displacements and therefore it becomes unlikely that the same mechanism operates in both scenarios. Rather, the dramatic transfer of axial load away from the pile

group becomes important in the mobilisation of pile shaft friction. It was shown in Figure 5.12 that the pore pressure increases below the pile cap were not sufficient to match the increasing load being supported by the pile cap, and therefore the effective stresses in the soil must be increasing strongly below the pile cap. Once axial load transfer is complete, the effective stresses directly beneath the pile cap would be close to 60 kPa. Haigh & Madabhushi (2011) found that the horizontal stresses in the soil close to piles in laterally spreading soils varied between the active and passive conditions during earthquake loading. Assuming that this result applies equally to level ground and that the effective stresses do not diminish greatly in the region of the first two strain gauges, then the shaft friction capacity calculated according to Equation 2.2 would lie between 6 kPa and 54 kPa, depending whether the horizontal stresses reflect an active or a passive condition. As shown in Figure 5.11(a), the values of shaft friction recorded near to the end of the earthquake tend to be slightly above the limit for active conditions.

The lack of shaft friction in the dense layer for cap-supported pile groups shown in Figure 5.11(b) remains quite surprising since it was shown that in these tests, the pile cap settles a great deal relative to a fixed datum throughout the earthquake. Since the dense layer of each test is not expected to suffer any significant volumetric strain during the earthquake, the raw cap settlements indicate large downward movements of the pile relative to the soil in the dense layer. It was proposed in Chapter 4 that for free-standing pile groups, the shaft friction in the dense layer was mobilised as a result of large lateral forces which led to the strong pile cap accelerations. It has been discussed that, in the cap-supported pile group tests, the kinematic lateral loads applied to the region of pile within the dense layer were much lower. It is proposed that this leads to low horizontal effective stresses around the piles in the dense layer and therefore shaft friction could not be mobilised in these "cap-supported tests".

It should be noted that in these tests, the pore pressures in the dense layer rose high enough to match the initial vertical effective stresses at the pile tip level, and as such, in the case of cap-supported piles, the axial loads were able to reduce very close to zero. In scenarios where the pore pressures close to the pile tips do not rise so high, the results of Knappett & Madabhushi (2009a) suggest that slightly smaller load transfer would be observed. As a result of the slightly higher effective stresses in the dense layer, it may then be possible that shaft friction is mobilised in parts of the dense layer. Typically, piled foundations are designed considering only the shaft and end bearing capacity of the piles. While the loading of the piled foundations under normal circumstances certainly does lend itself to this albeit conservative approach, the dramatic transfer of load away from the piles following liquefaction demonstrates that much greater consideration must be given to the performance of the pile caps, since these will become the major load carriers and the elements which determine the ultimate settlement suffered by the structure.

5.9 Summary

In this chapter, the response of pile groups which are "cap-supported" has been considered with reference to a "free-standing" pile group (which was discussed in Chapter 4). The discussion of the results focusses on both the settlement of these pile groups, in particular attempting to determine settlements of the pile group relative to the soil surface, as well as the transfer of axial load during the earthquake.

- The initial pile head loads indicate that despite placing the pile cap in contact with the soil surface, the piles in cap-supported pile groups carry almost all of the axial loads before the earthquake, due to the very stiff load-displacement response of the piles.

- Following the application of strong shaking and consequent onset of liquefaction, the pile cap accelerations were visibly reduced by the contact between the pile cap and the soil. Despite the differences in the bearing layer in which the pile tips were embedded, the pile cap acceleration of the cap-supported pile groups remained quite similar. Both effects arise as a result of the very soft nature of loose, liquefied soil.

- The absolute settlements of the pile groups were found to be quite disparate in the different configurations of cap-supported pile groups. However, estimates of the soil settlement during the earthquake indicates that the settlements of the cap-supported pile groups were quite similar, since the settlement of these pile groups is largely being controlled by the loose layer.

- The relative settlement of the pile group did not appear to be increased when the pile cap axial loading was increased. However, it is unknown if this is a similar effect to the reduction of settlement with cumulative numbers of cycles seen in Chapter 4.

- As a result of the pile group settlement, pile cap bearing pressure was mobilised, resulting in the axial loads transferring from the piles and on to the pile cap. It was found that the pile cap bearing pressure was mobilised as the result of increasing effective stresses in the soil below the pile cap.

- Pore pressures at the pile tips were observed to cycle in phase with the axial load, reflecting the sudden increase in pore pressures which are expected when the loading on a soil is suddenly changed. The average of pore pressures over an individual cycle however indicates that the soil beneath the pile tips dilates strongly while the piles remain loaded during the earthquake. Once the piles became unloaded, fluid from the soil away from the piles begins to flow into the zone below the pile tip causing the cycle-averaged pore pressure to rise.

- The dramatic transfer of axial load during the earthquake from the piles to the pile cap indicates that the performance of a building during an earthquake is highly dependent on the ability of the pile caps to support large bearing pressures. Strong and large pile caps as well as ground beams are therefore likely to improve building settlement performance during an earthquake.

- Similar to Chapter 4, it was found that the shaft friction during the earthquake did not reduce to zero during the earthquakes. Contrary to the suggestion by Knappett (2006), it was found that shaft friction in the dense layer was low for cap-supported pile groups, due to lower lateral kinematic loading being applied to the pile caps.

- Shaft friction on cap-supported pile groups was found to be largest near the pile head during an earthquake. This result is thought to be a result of the zone of increased effective stress which develops as a result of the transfer of axial load from the piles to the pile cap and the recorded peak values of shaft friction correspond to the capacity which might be expected under active soil pressures.

- In the tests carried out with cap-supported pile groups, the pore pressures were observed to reduce the effective stresses in the free field of the bearing layer to near-zero values each cycle. In the case of longer piles, the effective stresses at the pile tip level may not reduce to the same extent, meaning that the transfer of axial load to the pile cap might not be so complete. In this case, the effective stresses near the pile cap will not be so large, hence lower shaft friction may be expected. Additionally, if the load is not transferring completely, the kinematic loading of the pile group may change dramatically. If this is associated with larger effective stresses in the bearing layer, then it becomes possible that this layer may have a larger contribution to the observed shaft friction.

Chapter 6

Effect of installation method

6.1 Introduction

In Chapters 4 & 5, the behaviour of model piles which had been installed into a model under 1g conditions was investigated. As a result of the low stresses within a model at 1g, it was explained that the results from these tests relate best to the behaviour of bored piles. However, as discussed in the literature review, piles in the field are installed using a variety of methods, each with its own load-settlement characteristics. In particular, it was found by Deeks *et al.* (2005), that piles which have been installed using a jacking process have a very stiff axial response as long as the loads remain below the bearing capacity for the particular soil.

A relatively large number of dynamic centrifuge experiments on piled foundations have been carried out by various institutions around the world. In the literature, there appears to be a variety of techniques by which the model piles were installed into the soil models. These techniques can however be divided into three main categories, which are shown below, with some example studies given in Table 6.1 which show the class of experiment these installation techniques have been used for.

1. Piles are attached directly to the base of the container before sand is poured (with or without rotational constraint)

2. Piles are embedded in a "cemented" sand layer and sand poured around the piles

3. Piles are installed in a completed sand profile, either at 1g or in flight

Of the different installation methods, implicit in the first two is that the installation is carried out under 1 g conditions. While possible to install piled foundations in a completed

Table 6.1: Installation methods used in dynamic centrifuge tests

Reference	Installation method	Investigation type
Abdoun *et al.* (2003)	2,3	Lateral spreading
Bhattacharya *et al.* (2004)	1	Pile buckling
Brandenberg *et al.* (2005)	3	Lateral spreading
Gonzalez *et al.* (2009)	2	Permeability, lateral spreading
Imamura *et al.* (2004)	1	Lateral spreading
Knappett & Madabhushi (2009b)	1	Pile buckling
Knappett & Madabhushi (2008b)	3	Axial response
Li (2010)	3	Cyclic lateral loading
Stringer & Madabhushi (2010b)	3	Axial response

soil profile during a test (i.e. method 3), it is thought that only in the tests described by Li (2010) on the lateral response of pile groups in dry sand, was this actually carried out. While it might be considered that due to the large changes in effective stress and soil stiffness which occur during liquefaction that the installation method would have only a secondary effect on the pile's response, this remains completely unknown.

In this Chapter, a further two centrifuge tests, MS10 and MS12 are introduced, which were designed to investigate the behaviour of a jacked pile group. Throughout this Chapter, the axial behaviour of these pile groups will be compared with the results from MS09, which represented a bored pile group and was discussed in Chapter 5.

An earlier and shortened form of this chapter appears in Stringer & Madabhushi (2011a).

6.2 Centrifuge modelling

The experiments to investigate the response of jacked piles were carried out with a similar nominal layout to MS09 (shown previously in Figure 5.2(b)), as shown in Figure 6.1. The test parameters, including those of MS09 for reference, are shown in Table 6.2. All of these experiments were carried out at a centrifugal acceleration of 46.3 g, using the heavily instrumented pile group, MS-PG. As shown in Table 6.2, the pile loading was slightly larger in MS10 and MS12 than that used in the first earthquake of MS09. The extra loading arises from the additional adaptor (described in Section 3.7.6 which is attached to the pile cap in order to drive the pile group into the sand under g. In order to test the effect of the pile-soil interface friction angle, Fraction E silica sand was bonded to the piles for the test of MS12, as described in Section 3.7.3. It was confirmed after the test that the sand had remained fully bonded to the piles during the experiments.
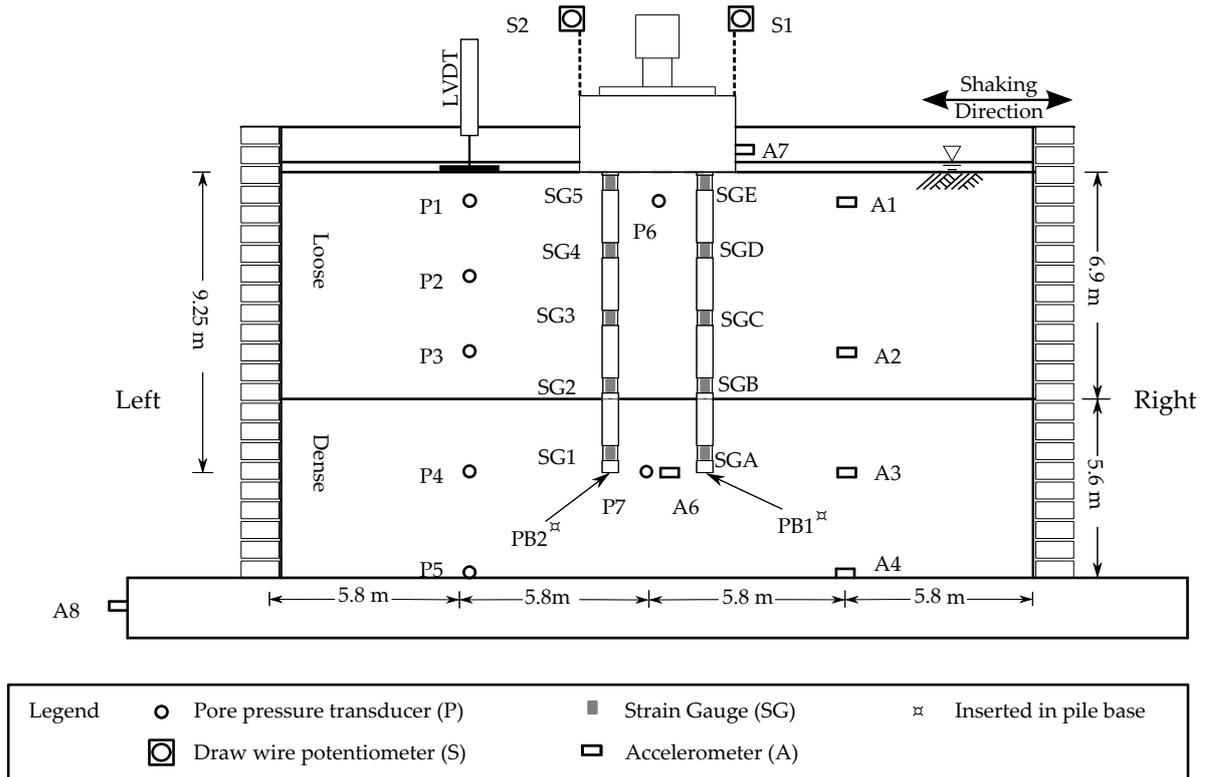
Figure 6.1: Section view through the centreline of the model layout in MS10 and MS12

The factors of safety shown in Table 6.2 were calculated in a similar manner to the previous chapters, using Equation 2.2 for the shaft friction capacity, and following Yasufuku *et al.* (2001) to estimate base capacity. It should be noted that the solution of Yasufuku *et al.* (2001) was developed for bored piles. At the ultimate limit state, it is assumed that the bearing capacity for bored and jacked piles would be the same. However, the proportion of base capacity mobilised at the serviceability limit state (0.1 D_0 settlement) will be significantly different. The investigation of Deeks *et al.* (2005) suggests that at this settlement limit, the full end bearing capacity of a jacked pile will have been mobilised. Hence the serviceability and ultimate limit state safety factors of MS10 and MS12 are the same in Table 6.2.

6.3 Jacking of pilegroup

The pile groups in MS10 and MS12 were "jacked" in two phases as described in Section 3.7.6. In both phases of the driving process, it was intended to "jack" the piles into the model slowly and steadily in order to achieve a "drained" installation of the pile group. However, the crude manual control on the pressure driving the piston which installed the pile group meant that this was difficult to achieve in practice.

Table 6.2: Test parameters for tests investigating installation effects

Flight		L_p		P / Pile	Static FOS		Earthquake		
		Loose	Dense		$0.1D_0$	Ult	Freq.	Duration	Pk. acc
		(m)	(m)	(kN)			(Hz)	(s)	(g)
MS09	1 EQ1	6.9	2.3	339	1.8	5.2	1.08	22.7	0.19
	2 EQ1	6.5	2.7	466	1.3	3.8	1.08	22.3	0.19
MS10	1 EQ1	6.9	2.3	367	4.8	4.8	1.08	23.4	0.21
	1 EQ2	6.6	2.6	367	5.0	5.0	1.08	24.4	0.19
MS12	1 EQ1	6.9	2.3	367	5.2	5.2	1.08	21.4	0.26
	1 EQ2	6.6	2.6	367	5.3	5.3	1.08	23.3	0.23

6.3.1 Initial jacking phase at 1g

As described in 3.7.6, the initial 150 mm (model scale) of jacking was carried out at 1g. In MS10, the initial jacking was completed at approximately 20 mms^{-1} (model scale), leading to maximum suctions at P6 and P7 of -17 kPa and -12 kPa. As would be expected, the suction at P6 occurred early in the jacking process, and that at P7 occurred late in the process, reflecting the times when the pile tips were approaching the instrument. In the free field, excess pore pressures of approximately 1 kPa were observed throughout the model for the majority of the drive, with temporary suctions of -2 kPa being recorded in the dense layer at the same time that they occurred at P7. In MS12, the process was carried out more slowly, at an average rate of 4.4 mms^{-1} (model scale), leading to lower excess pore pressures.

6.3.2 Final jacking phase at 50g in MS10

Figure 6.2(a) shows the distance through which the pile group was jacked (in the second phase), along with measurements of pore pressure in the near and free fields, at depths near the soil surface and also at the intended final pile tip level. It can be seen in Figure 6.2(a) that the jacking takes place in a series of steps as a result of the manual control of the piston pressure. Typically, during these "steps" in jacking distance, the pile moved downwards at a rate of 3 - 6 mms^{-1}, with one temporary spike where the speed reached 9 mms^{-1}. It can be seen in the pore pressure data that the initial jacking step (t = 7 s to t = 10 s) creates an increase in the excess pore pressures both in the free field and in the near field. However, as the jacking step continues, the excess pore pressures near the pile group reduce due to the soil shearing and ensuing monotonic dilation taking place. It can then be seen that in the remainder of the jacking process, the free-field excess

pore pressures remain relatively low. Near the pile group, a temporary reduction in pore pressure occurs at each additional jacking step, which was greater in magnitude in the dense soil layer, and increased slightly to a maximum magnitude of -5 kPa as the pile tips reached increasing depths. However, at the end of each jacking step, the excess pore pressures dissipate before the next jacking step begins. At the very end of the jacking process, at approximately t = 70 minutes, the excess pore pressure at P6 is observed to record a spike of +4 kPa, indicating that the pile cap makes contact with the soil. Although the installation of the jacked pile group has clearly generated some excess pore pressures, the magnitudes are relatively small. At the fully jacked depth of the piles,
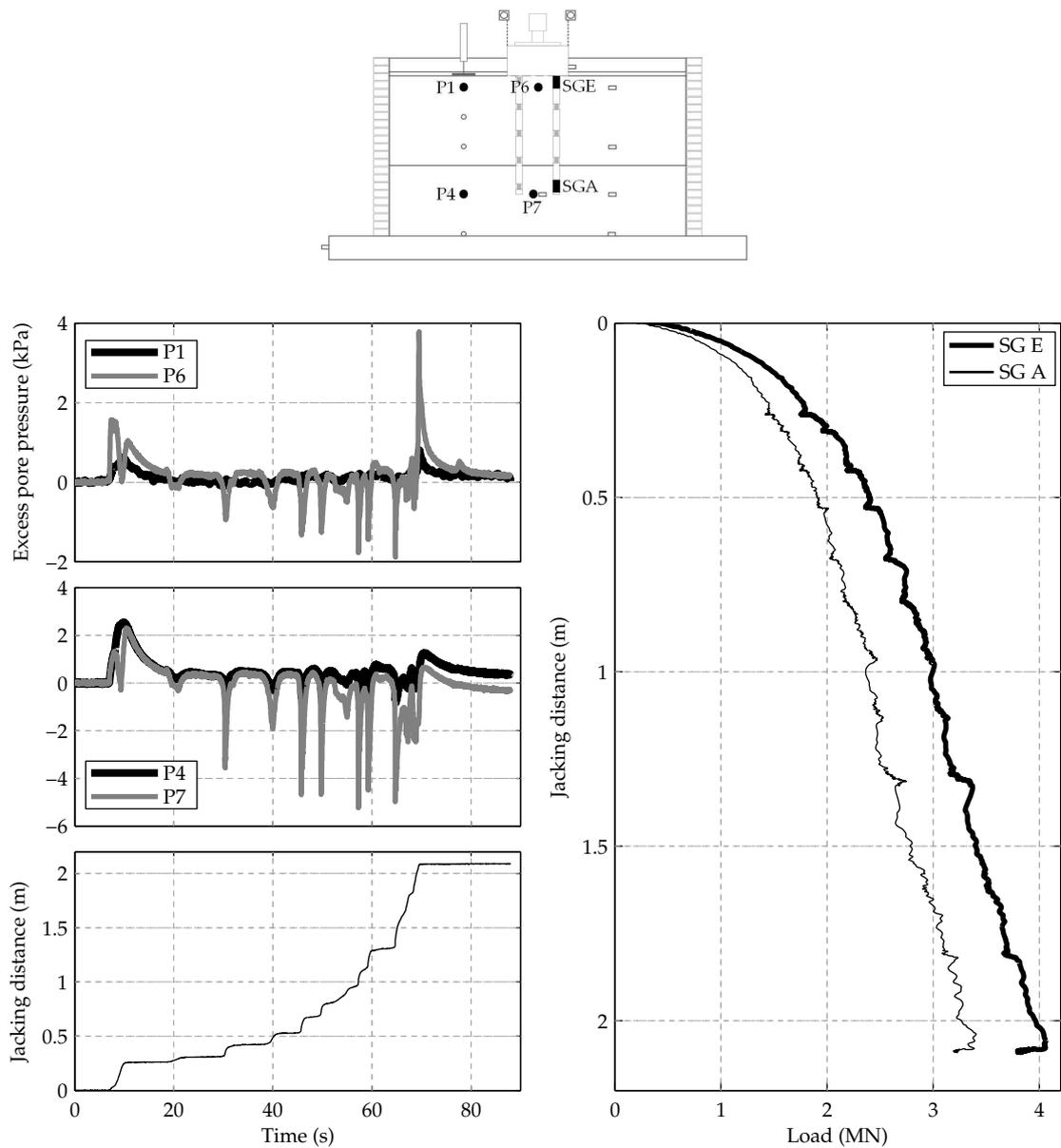
(a) Jacking distance and excess pore pres- (b) Load-settlement curve of jacking process
sures

Figure 6.2: Jacking of pile group during MS10

141

the increase in effective stresses as a result of a reduction in excess pore pressure of -5 kPa would lead to an increase in the pile end bearing capacity calculated according to Yasufuku *et al.* (2001) of approximately 3.5 %.

In Figure 6.2(b), the loads recorded at the head and tip of leg 1 in MS10 is plotted against the jacking distance. It can be seen that once the tip load reaches approximately 1.65 MN, the load settlement curve at the pile tip becomes quite linear with further jacking distance, with the end bearing resistance reaching a maximum of approximately 3.4 MN at the end of the jacking process. At the point, the pile tips were located approximately 5 D_0 below the loose-dense soil layer interface. According to Robertson & Campanella (1983), a CPT will need to penetrate a stiff layer by 5 - 10 D_0 before the full resistance of the layer is mobilised, while Gui & Bolton (1998) suggests that in centrifuge tests, the resistance was fully mobilised after only 5 diameters. White & Bolton (2005) use linear interpolation to obtain an estimate of the base resistance in a transition zone which extends 2 pile diameters before the interface layer, and 8 diameters ahead of it. These studies imply that some or all of the increase in end resistance observed with jacking distance in MS10 could be due to the piles gradually developing the resistance of the much stiffer bearing layer of the model. Since the piles have only penetrated approximately 5 diameters, it would be expected that the end bearing capacity calculated using the solution of Yasufuku *et al.* (2001) would be an overestimate of the pile capacity as this solution does not take into account the effect of the softer layer lying above the bearing layer. However, the estimate of bearing capacities estimated using this solution were found to be lower than those recorded at the pile tips during jacking by a factor of 2.1. In the study of Klotz & Coop (2001), values of unit base resistance for a displacement pile in Leighton Buzzard sand was found to increase approximately linearly with penetration depth. Assuming that at similar levels of effective vertical stress, the same relations hold, the increase in unit base resistance is approximately $125 \times \sigma'_v$. This suggests that at the final depth of the jacked piles, the base resistance would be approximately 2.2 MN, which is again much lower than those recorded in these tests. The trends of end bearing resistance were found to be strongly dependent on the relative density of the soil, and therefore some of the discrepancy will be due to the greater density of the bearing layer in MS10.

It is observed in Figure 6.2(b), that significant shaft friction was mobilised during the jacking process, reaching a maximum of 0.7 MN at the end of the drive, of which 358 kN was mobilised between gauges A and B in the dense layer, while 342 kN was mobilised between gauges B and E in the loose layer. From Equation 2.3, this provides back-calculated values of K of 5.0 and 2.8 in the dense and loose layers respectively. The magnitude of the mobilised shaft friction was checked against the average values reported by Klotz & Coop (2001). Assuming that the shaft friction is mainly dependent on the effective vertical stress, the shaft friction in a loose-medium density soil layer increases
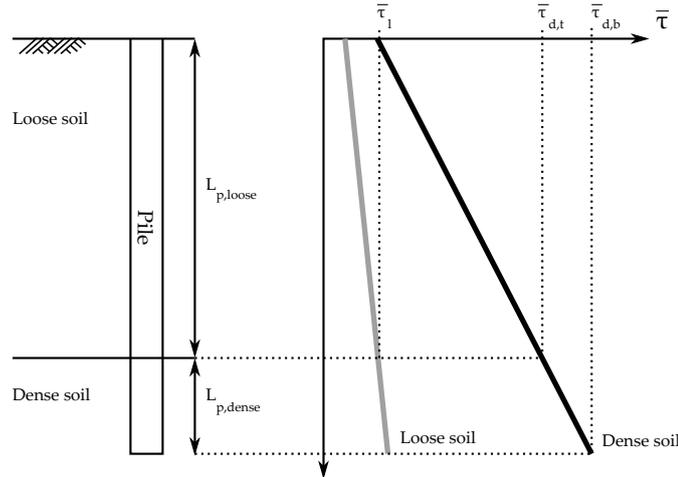
Figure 6.3: Definition of symbols in Equation 6.1

from 10 kPa to 25 kPa over the range in vertical effective stress of 0 to 150 kPa. In a dense soil ($D_R \approx 90\%$), the average shaft friction increased from 40 kPa to 80 kPa over the same range in vertical effective stress. These distributions gave average shaft frictions of 16.5 kPa in the loose layer, while in the dense layer, the shaft friction is 57 kPa and 64 kPa at embedded depths of 6.95 m and 9.25 m respectively. The estimated total shaft friction load in the dense layer was estimated using Equation 6.1, with the definitions from Figure 6.3. The shaft friction load calculated in this manner was 180 kN and 305 kN in the loose and dense layers respectively. Additionally, Li (2010) recorded the head and base loads on a pile which was monotonically jacked during a centrifuge experiment. While the distribution of shaft friction along the pile's length was unavailable, the quoted values of shaft friction recorded over the total length of the pile agree reasonably with those recorded in this study after being corrected for stress level.

$$Q_{s,dense} = \pi D_0((L_{p,loose} + L_{p,dense})\bar{\tau}_{d,b} - L_{loose}\bar{\tau}_{d,t}) \tag{6.1}$$

In MS12, the data acquisition system crashed during the in-flight jacking phase, resulting in no data being available for this test phase, however, the jacking was carried out with a process similar to that in MS10, and efforts were made to make the pressure increase on the piston both more continuous and gradual.

Following the retraction of the piston, the pile loads dropped dramatically; before the earthquake on the same pile (leg 1), the tip load had dropped to 320 kN while the head load was 410 kN, implying shaft friction of 90 kN across the pile. The axial load distribution, shown later in Figure 6.9, shows that in MS10, the shaft friction is negative near the surface, but becomes positive in the dense layer, as might be expected from the piles "rebounding" after the pile jacking. However, it can be seen that in MS12, that the axial loads recorded on leg 1 are much larger than expected from Table 6.2 and that

the distribution of axial loads suggests that the shaft friction is positive near the head of the pile, but is negative deep in the liquefiable layer. The reasons for this are unclear, however it is possible that bending moments are significantly affecting the axial loads being recorded by the strain gauges in these experiments.

The stress distribution in the soil around the jacked piles is highly complex, as discussed by White & Bolton (2004). As a result of the jacking process, the soil beneath the pile tips is highly overconsolidated, with an OCR ratio of approximately 10.6 immediately below the piles. Additionally, the shaft friction distribution recorded during jacking suggests that near the pile tips, very large radial stresses are in existence, which reduce with increasing distance from the pile tips.

6.4 Free field soil behaviour during the earthquakes

6.4.1 Accelerations

The accelerations of the soil in the free field in the loose layer (at A1) and in the dense layer at the pile tip level (at A3), are plotted in Figure 6.4. It can be seen in Figure 6.4(a) that in the loose soil, the accelerations become dramatically attenuated after only 1 - 2 cycles of shaking. However, the accelerations do not attenuate with time in the dense soil. In the first earthquake of MS12, it can be seen that in the dense layer, the peak acceleration increases slightly after 5 s of shaking. In the second earthquake of both tests, it can be seen that the accelerations are of similar magnitude to those in the first earthquake. These traces of acceleration in the "free field" of the models show that the soil accelerations in the loose and dense soil layers are similar to those which were observed in the tests with the bored piles.

6.4.2 Pore pressures

The pore pressures recorded deep in the loose layer (P3) and the dense layer (P4) from each earthquake of MS10 and MS12 are shown in Figure 6.5 along with the pressure for full liquefaction (shown with dashed grey line). The pore pressures from test MS09 were shown in Figure 5.5 & 5.6.

It can be seen in Figure 6.5(a) that similar to MS09, in each of the earthquakes of MS10 and MS12, full liquefaction was achieved in the loose layer within the first 1 - 2 cycles of the earthquake. However, the pore pressure response in the dense layer is noticeably different. In MS09, the pore pressures in the dense layer rapidly rose such that after
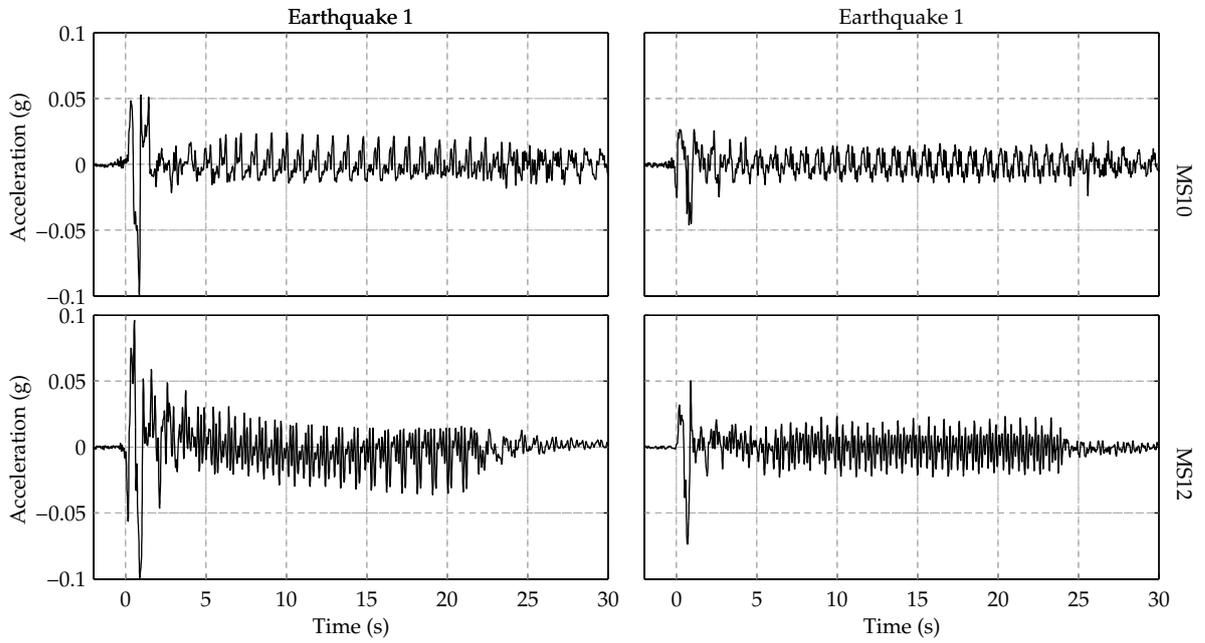
(a) Loose layer (A1)
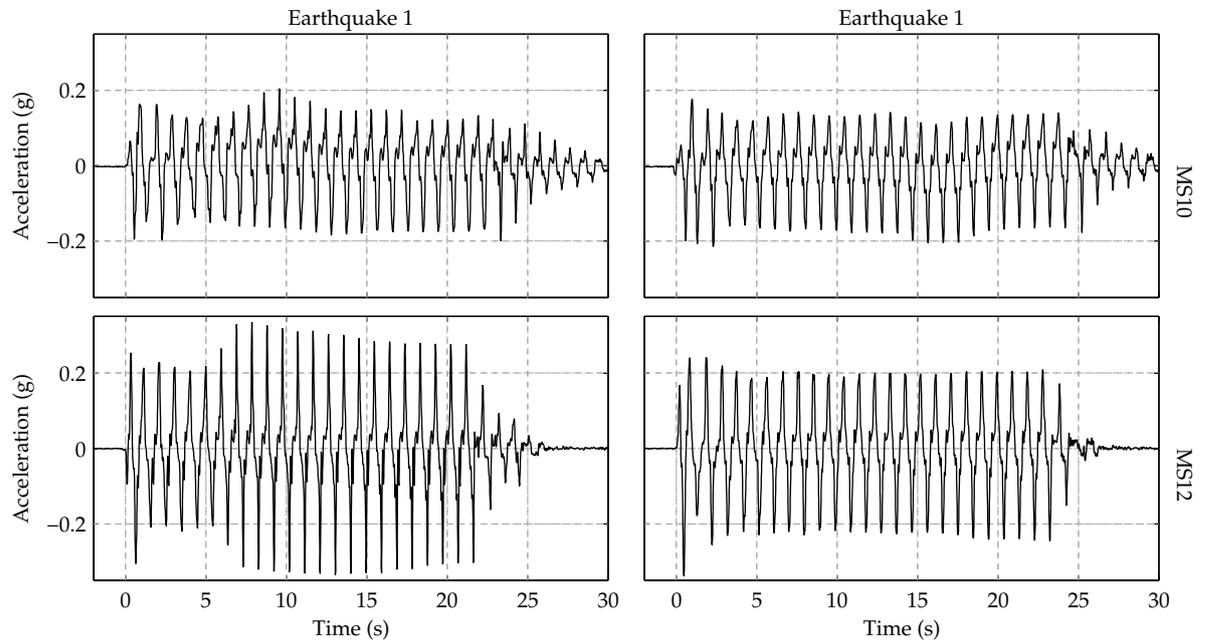
(b) Dense layer (A3)

Figure 6.4: Accelerations recorded in the free field during MS10 and MS12

(a) Loose layer (P3)　　　　　　(b) Dense layer (P4)
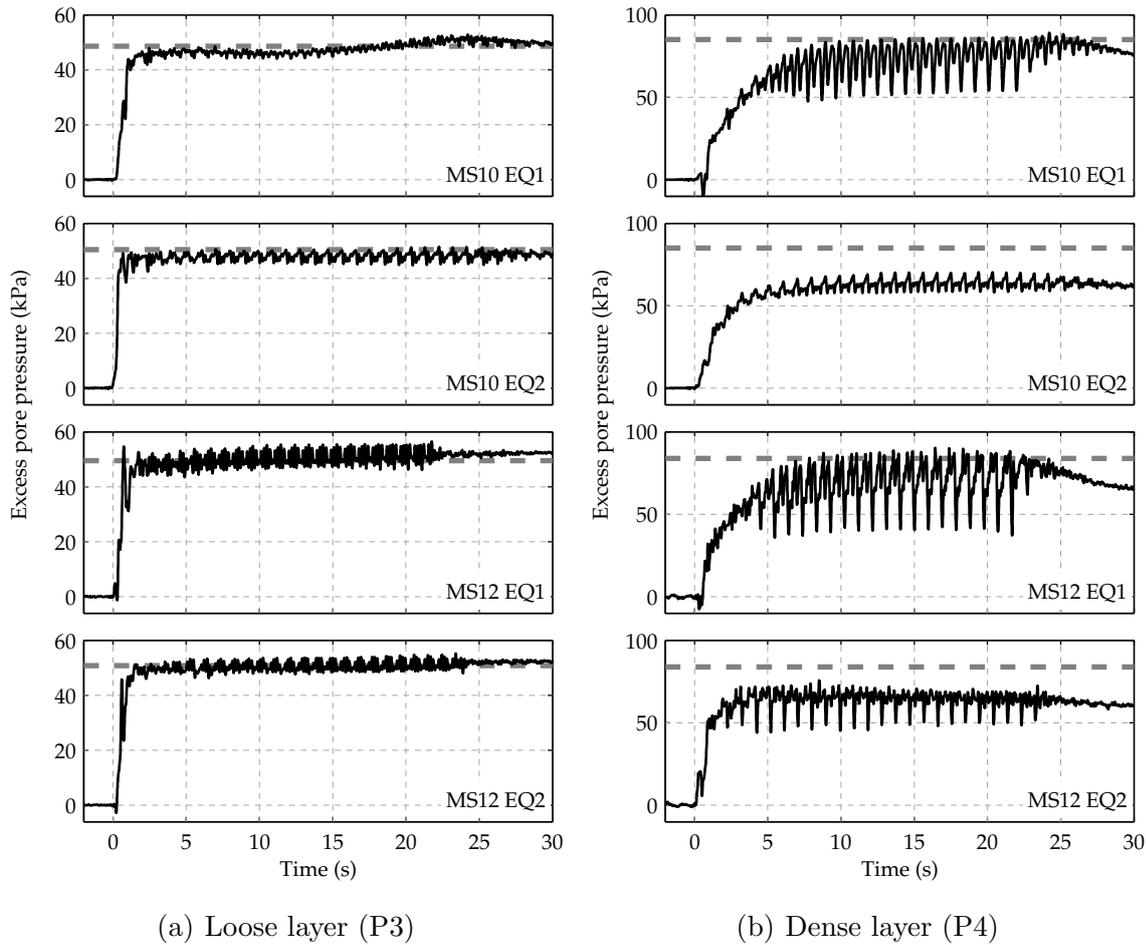
Figure 6.5: Excess pore pressures recorded during earthquakes in MS10 and MS12

a couple of cycles, the excess pore pressures reduced the effective stresses to zero twice per cycle. However, as shown in Figure 6.5(b), the pore pressures in MS10 and MS12 rise much more slowly, particularly in the first earthquake of both tests, where the pore pressures did not reach full liquefaction until approximately 8 - 9 cycles of shaking had occurred. This result is particularly interesting since it is not only different to the pore pressure build up in the dense layer of MS09, but indeed to that observed in all of the tests with bored piles at this depth. It is also interesting to note that in the first earthquake of these tests the dilation spikes in both MS09 and MS10 reduce the excess pore pressures to a minimum of approximately 50 kPa once per cycle, indicating that in these tests, the shear demands on the soil are similar. In MS12, the excess pore pressures are reduced to approximately 40 kPa each cycle, indicating that greater shear demands are being placed on the soil in the dense layer of the model, reflecting the larger input accelerations in this test (shown in Table 6.2). It was shown in Figure 5.6 that the pore pressure response in both earthquakes of MS09 were quite similar in the dense soil layer. However, it can be seen that in the case of MS10 and MS12, the excess pore pressures in the second earthquake are significantly lower than that of the first earthquake.

6.5 Behaviour of pile groups

6.5.1 Pile cap acceleration

The pile cap amplification factors at the different harmonics are shown in Figure 6.6, considered over the first six cycles of shaking and over the remainder of the earthquake. The amplification factors for the pile group are calculated as the ratio of the acceleration amplitude at the pile's base (measured at A6) and that at the pile cap (measured at A7) for each frequency, obtained using FFT. The acceleration signals used in the FFTs were of equal length and for the early part of shaking, were considered over the same time period. For the amplification factors in the later part of the earthquake, the signals were cross-correlated before taking the FFT. It should be noted that although the amplification factors are shown over a range up to 6 Hz, the FFT of the signals are dominated by the component at the nominal input frequency, with FFT peaks generally decreasing in magnitude as the frequency increases. As an example, the FFT of the acceleration
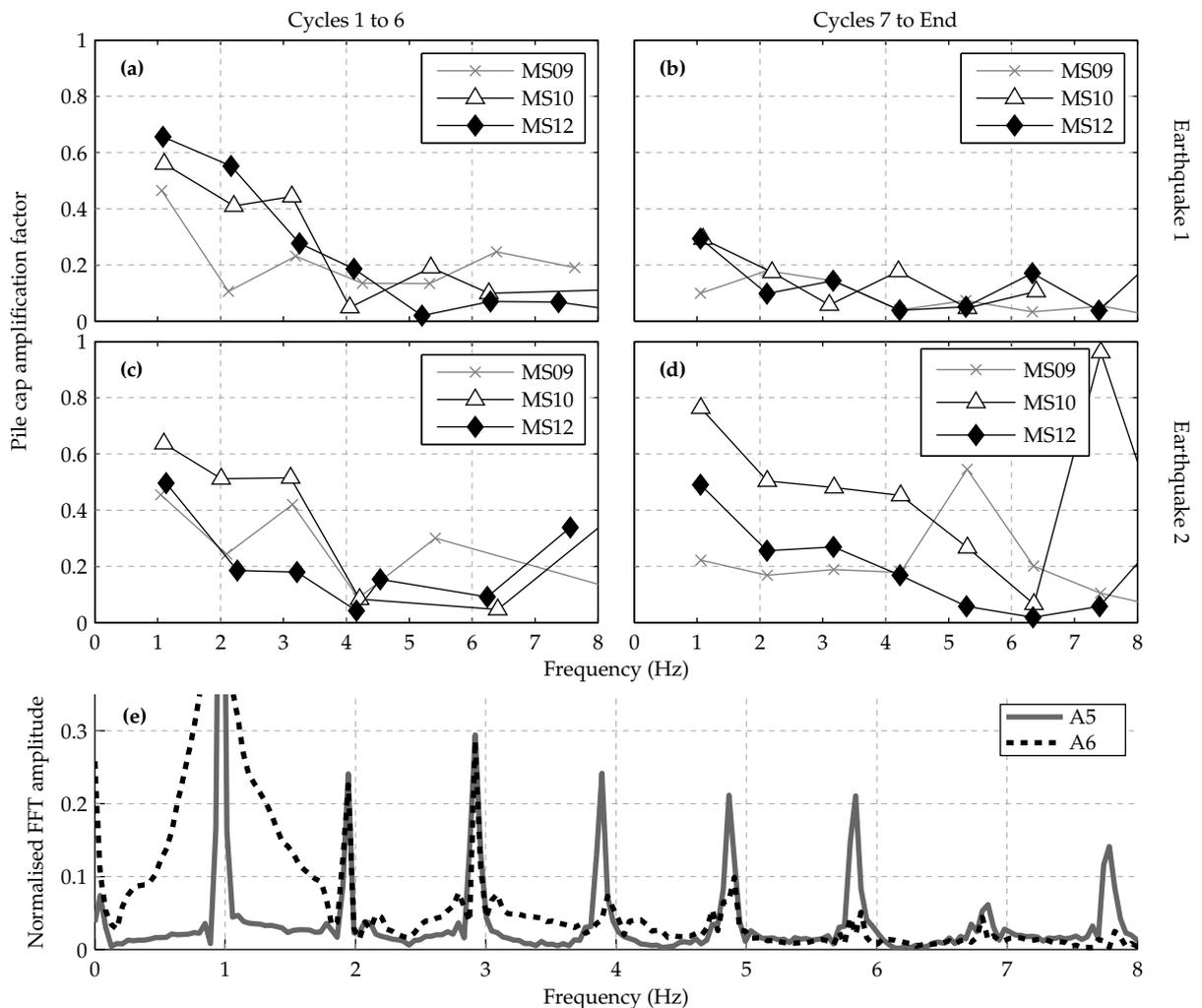
Figure 6.6: Pile cap amplification factors

recorded between the pile tips in the first earthquake of MS09 is plotted in Figure 6.6 (e). The figure shows that the input motions were dominated by the fundamental frequency, with the peak at the second harmonic typically only 20-25% of that at the fundamental frequency.

The pile cap accelerations in the first earthquake of each test showed the same general trend: large accelerations in the first cycle which rapidly attenuated while moving out of phase to the input acceleration. The results show that the attenuation of the pile cap accelerations described is most significant at the fundamental driving frequency, which due to the relative magnitudes of frequency components tends to dominate the observed response. It is further observed that the amplification factors during the first earthquake are greater for MS10 and MS12 than MS09, especially after the initial attenuation of accelerations has occurred. There also appears in the first earthquake to be a small effect due to the surface roughness of the piles during the initial few cycles of the earthquake, where the pile group in MS12 has slightly larger pile cap acceleration relative to that in MS10.

The pile cap response during the second earthquake shows some interesting features. In MS09, the pile cap again shows significantly stronger acceleration at the beginning of the earthquake, which attenuates quickly as the earthquake progresses. This feature is however not repeated in the cases of MS10 and MS12, whose pile cap response does not appear to change significantly over the course of the earthquake. In each of the three tests, the pile cap amplification factors from the steady response (after cycle 6) are observed to be larger in the second earthquake.

6.5.2 Pile group settlement

The average absolute settlement of the pile cap during the each of the earthquakes has been plotted in Figure 6.7, after being passed through a smoothing function for clarity. It is clear from Figure 6.7(a) that the jacking process has had a significant influence on the settlement behaviour in the first earthquake. The input accelerations in the first earthquake were noted to be larger for MS10 and MS12 in Table 6.2, and this also translated into slightly higher pile cap accelerations. Despite the larger pile cap accelerations, the pile groups in MS10 or MS12 did not settle more than that in MS09. Instead, Figure 6.7(a) shows that the settlements are smaller when the pile groups were jacked in flight.

The jacking process appears not only to have affected the overall settlements experienced by the pile group, but the development of settlement is fundamentally different. As soon as the first earthquake begins in MS09 (and indeed all of the tests with bored piles), the pile group immediately settles rapidly. The pile group continues to settle throughout the

(a) Earthquake 1
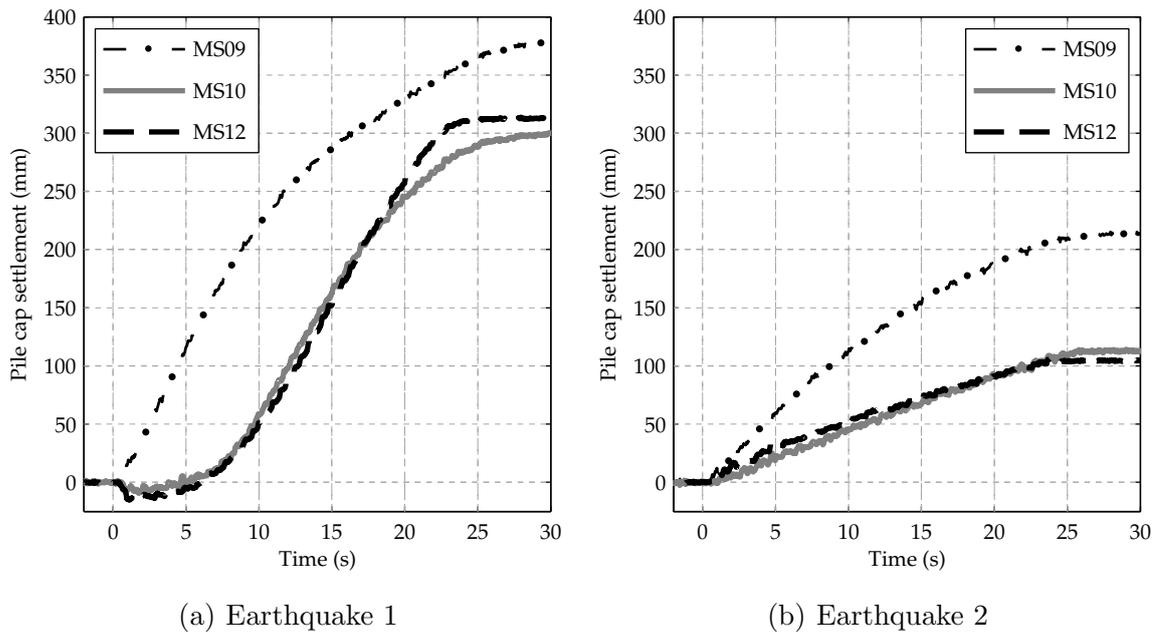
(b) Earthquake 2

Figure 6.7: Absolute settlement of pile cap during the earthquakes

earthquake, though the rate of settlement decreases with time. By contrast, in both MS10 and MS12, an initial heave is followed by several cycles of shaking where the pile group hardly settles. The rate of settlement then increases so that it is similar to that seen at the start of MS09. Similar to MS09, the pile group's rate of settlement decreases towards the end of the earthquake. The increased surface roughness of the piles in MS12 does not appear to have had a large effect on the pile group's settlement response.

The settlement response during the second earthquake is shown in Figure 6.7(b). The development of settlement for the pile group in MS09 has retained a similar form to that which occurred in the first earthquake, but, as noted in Chapter 5, despite the increased axial load on the pile group, the overall settlement is much lower in the second earthquake. It can be seen that the settlement in the second earthquake of MS10 and MS12 develops in a completely different manner to that which occurs in the first; in the second earthquake, the settlements develop simultaneously with the onset of shaking and take a form which is similar to that in MS09. However, the pile cap settlements in both MS10 and MS12 remain significantly lower than those recorded in MS09. If it were assumed that the absolute settlements of the pile cap are proportional to the axial pile load (as they were for the free-standing pile groups discussed in Chapter 4), then the absolute settlement of the pile cap at the end of the earthquake of MS09 might be corrected to 169 mm to give the estimated absolute settlement using the same loads as those applied in MS10 and MS12. However, this still remains much higher than those of the jacked pile groups.

6.5.3 Axial pile loading

The axial loads carried at the tips of the piles during the earthquake are shown in Figure 6.8, while the distribution of the axial loads (averaged over a cycle) over the length of the pile, captured at various time points is shown in Figure 6.9. It should be noted that due to the rigours of jacking the piles in flight, many strain gauges failed during the earthquakes, meaning that in Figure 6.8, a different pile tip gauge is shown in MS12 than for MS09 and MS10.

It can be seen in both figures that there were large differences between the axial loading pattern in MS09 and those in MS10 and MS12. At the pile tips (and indeed all of the other strain gauges), each test shows strong cyclical load variation, but in MS09, the axial loads undergo a large and immediate reduction in axial load when the earthquake begins. The loads continue to reduce for approximately half of the earthquake duration, after which the loads reach a near-zero "plateau" after which almost no variation in axial load was observed (on pile leg 1) for the remainder of the earthquake, as well as a period
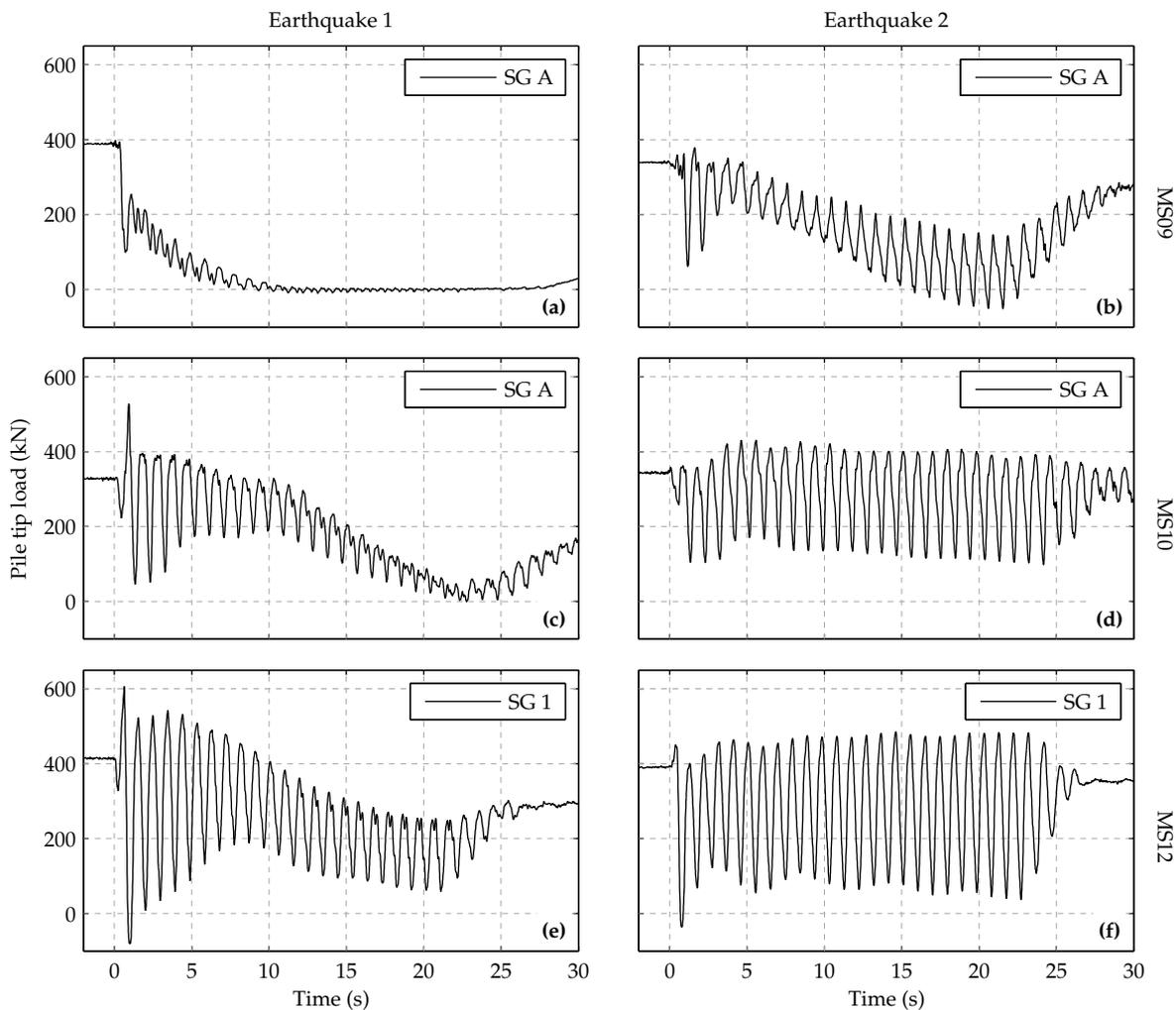
Figure 6.8: Loads recorded at the pile tips
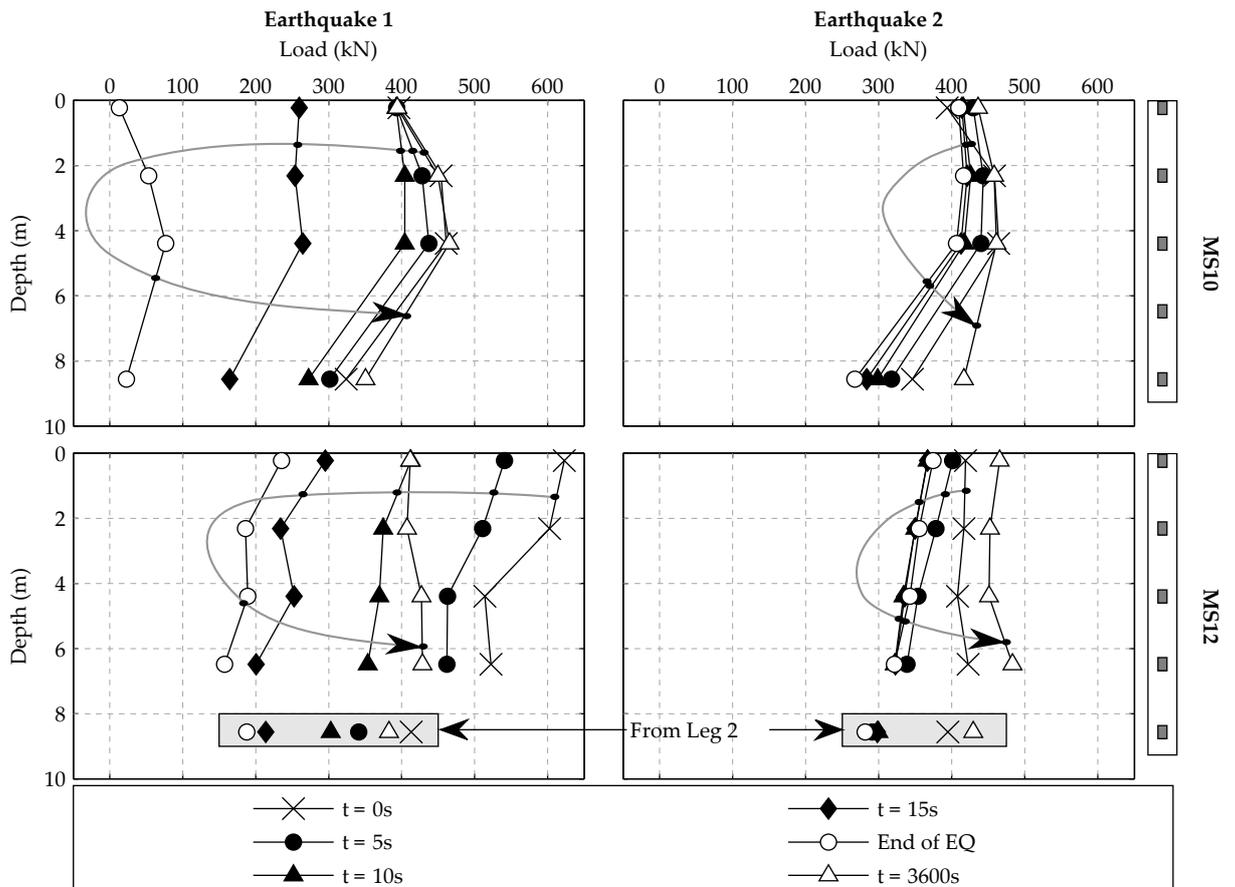
Figure 6.9: Axial loads on Leg 1 of jacked pile groups during earthquakes

of time afterwards. By contrast, the axial loads on the jacked piles in the tests of MS10 and MS12 initially cycle about a mean value which is close to that at the start of the earthquake. Following this initial period, the loads at the pile tips then reduce for the remainder of the strong shaking. In each test, the axial loads are observed to increase strongly following the end of the earthquake as the pore pressures dissipated.

The pile loads during the second earthquake again showed differences in the behaviour of the bored and jacked piles. In MS09 similar to the first earthquake, the loads began to reduce immediately, but this time the reduction in load was much more gradual, and continued until the end of the earthquake, after which the loads began to increase immediately. However, a completely different response was observed in MS10 and MS12, where the loads cycled about the same load for the duration of the earthquake. Similar to the first earthquake, the loads on the jacked piles increased following the end of the earthquake as the pore pressures dissipated.

6.6 Effect of jacking on excess pore pressure buildup

It was shown in Section 6.4.2 that the excess pore pressures rose much more slowly in the "free-field" of tests where the pile group had been jacked in-flight (MS10 and MS12). The differences in the excess pore pressure generation at the start of the earthquakes are compared directly in Figure 6.10, where the pore pressures in the dense layer of MS09 (bored pile) are plotted with those from MS10 (jacked pile) both in the nominal free-field and between the pile tips. While referred to as the "free-field," the apparent differences in excess pore pressure generation at P4 indicates that the pile group's influence extends past this point and as such the vertical arrays of pore pressure transducers and accelerometers (on the opposite side of the model) must therefore not truly in the free-field, where similar measurements would be expected in both tests. It should be noted that at both locations, the excess pore pressure generation in MS12 was very similar to that in MS10, both in terms of the rate of generation and the magnitude at any given time; for this reason the data from MS12 has been omitted from Figure 6.10 for clarity. It is thought that a possible explanation for this behaviour is found in the stress changes occurring in the soil which were induced by the jacking process. It was discussed in Section 2.3 that the process of jacking piles led to very large stress and strain changes in the soil near to the pile. It is expected that since the soil in the bearing layer of tests MS10 and MS12 was of very high relative density, that the zone of dilation around the pile shaft, which arises from the large shearing as the soil passes the pile shoulder, will be exaggerated. It is therefore anticipated that similar to the observation of White & Bolton (2004), the jacking process will have created a zone of looser soil around the pile shaft. White & Bolton (2004) further discuss highly stressed bulbs of soil which are created beneath the pile tips during the jacking process. It was shown in Figure 6.2(b) that very large axial loads were recorded during the driving process of MS10 and MS12, indicating that similar stress bulbs will be present in these tests. As shown in Figure 6.8, the pile tip loads reduced dramatically

(a) "Free field" (P4) (b) Near field (P7)
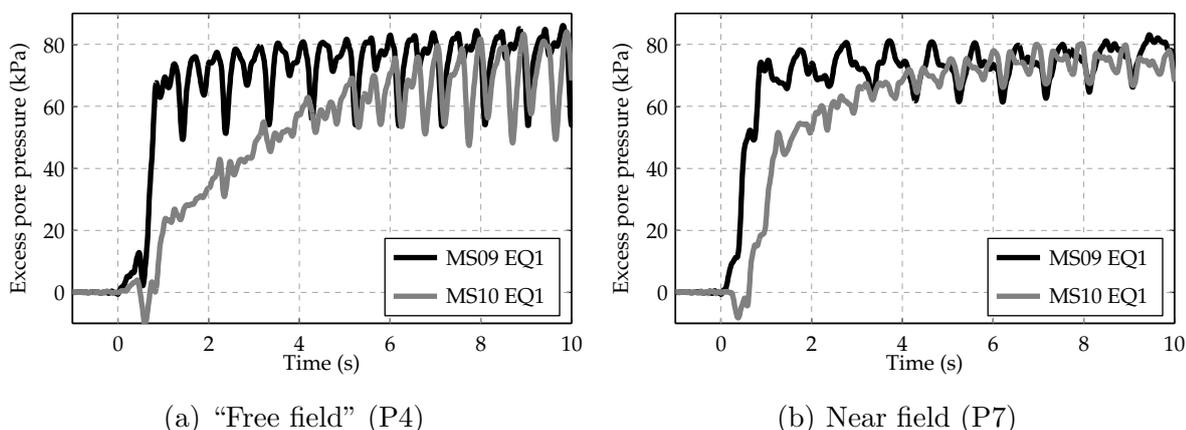
Figure 6.10: Comparison of excess pore pressure generation in dense layer with jacked and bored piles

when the jacking process was ended. This means that these bulbs of soil will have become highly overconsolidated and as described in Section 2.3.1, these soils have been found to exhibit an increased resistance to liquefaction. The various "zones" of soil around the pile during the jacking process are summarised in Figure 6.11(a), based on the discussion of White & Bolton (2004).

When the earthquake begins it is proposed that the pore pressure generation in the bulbs of overconsolidated soil takes place much more slowly than in the free field. As a result, when the free field pore pressures are generated, a hydraulic gradient is set up between the free field and the bulbs of overconsolidated soil, resulting in fluid migrating towards the bulbs as shown in Figure 6.11(b). The situation is then the reverse of that described by Chakrabortty *et al.* (2011) where the pore pressures in dense sand were elevated by the presence of pockets of much looser soil. In the scenario of the jacked piles, the presence of the overconsolidated soil is acting as a sink for excess pore pressures in the dense sand. A similar situation also exists in the soil between the piles at P7. However, comparison of the pore pressures at the two locations reveals that the pore pressures at P7 (between the piles) are actually larger than those at P4 (in the "free-field") which on the basis of the two instruments would suggest the flow of fluid away from the pile group. However, it is not thought that this is the case. Rather, as a result of the looser zones of soil around the pile shafts, it is possible that greater excess pore pressure generation takes place at this location and that as a result, the pore pressures are slightly higher than the free field, despite being closer to the bulbs of overconsolidated soil. The fluid between
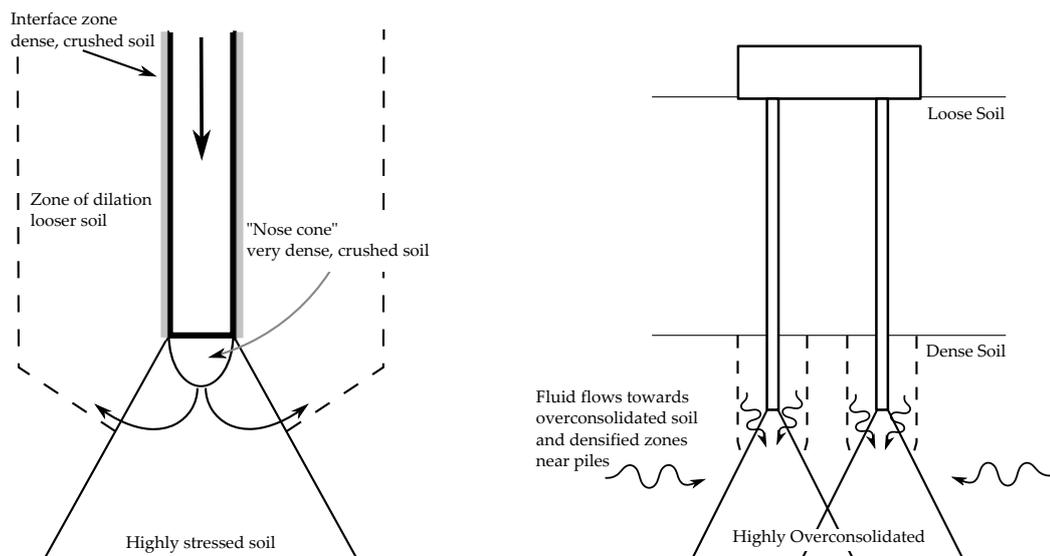
(a) Development of highly overconsolidated and densified regions during jacking, modified from White & Bolton (2004)

(b) Effect of highly overconsolidated soil on pore pressure response

Figure 6.11: Effect of jacking on excess pore pressure generation in dense layer

the piles then also migrates towards the bulbs of overconsolidated soil. As a result of this fluid migration, the excess pore pressures in the tests where the piles were jacked in flight are initially lower than those where the piles were installed entirely at 1g. However, it can be seen that after the approximately 6 to 8 seconds of shaking, the excess pore pressures in the dense layers of MS09 and MS10 become quite similar. This suggests that the pore pressures in the overconsolidated zones are no longer significantly lower than those elsewhere in the dense layer.

6.7 Development of pile group settlement

6.7.0.1 First Earthquake

The results which were presented in Figure 6.7 indicate clear differences between the behaviour of pile groups which are supported with bored piles and those which have been jacked in flight. The settlement response of the pile groups at the start of the first earthquake indicates that jacking the piles in flight led to much greater axial load capacity being available at the beginning of the earthquake, due to the much slower build up of pore pressures in the dense layer of the model. Figure 6.12 shows the settlements on both sides of the pile cap at the very beginning of the earthquake.

The immediate and large settlement of the pile group in the tests with bored piles indicates that the bearing and shaft friction capacities of the pile group are exceeded as the pile group rocks from side to side, shown in Figure 6.12(a) & 6.12(c). In this mechanism, described by Knappett & Madabhushi (2008a), the pile rotates about its trailing pile, while the leading pile punches downwards.

When the pile group was jacked in flight, the settlements seem to indicate that a different mechanism was in operation at the beginning of the earthquake, as shown in Figure 6.12(b) & 6.12(d). In these tests, the pile end bearing and shaft friction capacities remain high enough at the start of the earthquake that the leading pile does not punch downwards. Instead, the pile group rotates about the leading pile, meaning that the trailing pile lifts upwards slightly, leading to an average heave of the pile cap. In the next half cycle however, the settlement shows that the now leading pile settles close to its original position, and the new trailing leg lifts slightly, maintaining the average heave. This mechanism is not sustained for the whole earthquake; the settlements show that later in the earthquake, the mechanism described by Knappett & Madabhushi (2008a) begins to operate, and rates of settlement similar to those initially experienced by the pre-jacked pile group are reached. This suggests that as the earthquake proceeds, the settlement reducing effect of the initial stress bulb is lost.

(a) Rocking with bored piles

(b) Rocking with jacked piles

(c) Settlement in MS09

(d) Settlement in MS10
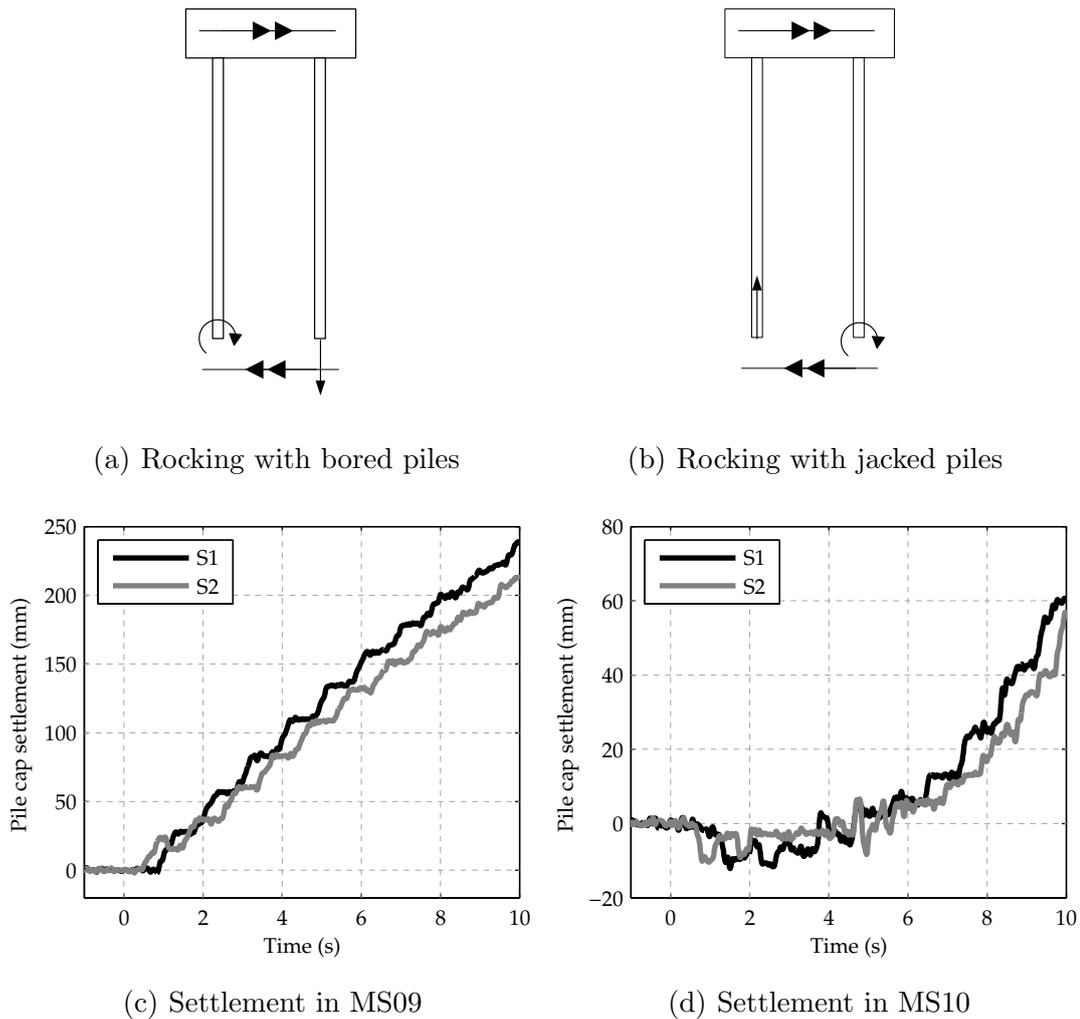
Figure 6.12: Rocking mechanisms and settlement at start of earthquakes for bored and jacked piles

6.7.0.2 Second Earthquake

It was observed in Section 6.5.2 that the settlement response of the jacked pile groups was markedly different in the second earthquake. While settlement develops with a similar profile to that observed in MS09, the magnitude of settlement is very much lower. It will be discussed in Section 6.8, that in the second earthquake of each test with jacked piles, it is possible that the pile cap never makes strong contact with the soil surface. In this scenario, the settlements might be expected to show a similar pattern to that discussed in Section 4.4, where settlements in a second earthquake continue to develop along the same curve that is observed at the end of the previous earthquake. However, it is found that this is not the case in MS10 or MS12, where the settlements develop much more slowly in the second earthquake to that observed at the end of the first. It is likely however that this is a result of the much lower pore pressures and therefore higher effective stresses which are observed throughout the dense layer in the second earthquake of both MS10 and MS12.

155

6.7.0.3 Changes in pile group settlement profile

The implication of the observed settlement responses is firstly that the jacking process has a definite effect. However, as the earthquake develops, the beneficial effects are lost and the pile group begins to exhibit a settlement response which is closer to that of a bored pile. The reasons for this are not fully understood. However, it is proposed that the settlement of the pile group late in the first earthquake begins to resemble that of the installation of a bored pile as follows.

In the tests of "bored" piles, the model pile groups were inserted into the model under 1 g conditions. While the stresses directly beneath the pile tips during the installation might become moderate during the 1 g installation, the stresses in sand away from the immediate zone around the pile tips will be at low stress. When the pile group was jacked into the model, the stresses involved are much higher, which was thought to have been responsible for the differences in settlement behaviour.

However, as the pore pressures gradually rise in the bearing layer during the earthquake, the stresses in the bearing layer (except in the region below the piles) reduces significantly. At the point where the pore pressures have fully developed, the pore pressures reduce the effective stresses in the bearing layer to zero each cycle.

While different effective stresses may be operating in the zone beneath the piles, outside of this zone, the remainder of the soil is perhaps behaving in a similar manner to dense soil at low stress; i.e. similar to the stresses observed at 1g. In this phase of the earthquake, the pile group is developing large absolute settlements.

As discussed in Chapter 5, absolute pile settlements can be interpreted as the downwards movement of the pile tips relative to the dense soil. Therefore, it might be considered that the large absolute settlement of the pile group is creating a situation which is similar to the installation of the model piles under 1 g conditions. Therefore, the very high excess pore pressures recorded in the dense layer at the pile tip level may be responsible for the pile group acting similar to a bored pile in subsequent earthquakes.

The similarities between the development of settlement of the jacked pile groups in the second earthquake compared to that of a bored pile suggests that installation effects which so affected the settlement response in the first earthquake have been destroyed by the migration of pore pressures to the region of overconsolidated soil beneath the pile tips. This was apparent in the first earthquake when, after the initially very stiff response, the jacked pile groups began to develop settlements at a rate which matched the bored pile group.

6.8   Axial load transfer of jacked piles

It has already been seen that significant differences have been observed in the response of pile groups which are supported by jacked piles. These differences, particularly the delay before the pile group begins to accumulate settlement, have significant implications for the axial load transfer of jacked piles. It was observed in Chapter 5 that cap-supported bored piles immediately began to transfer loads to the pile cap when the earthquake began and the pile cap settled more quickly than the soil surface. However, in the case of jacked piles, the pile group does not settle initially, and therefore the piles must continue to support the full vertical loads from the structure, as was shown in Figure 6.9. As a result of the initial period where the pile group does not settle, a gap opens up between the pile cap and the soil surface, such that in MS10, load does not begin to transfer away from the piles and onto the pile cap until the absolute settlement of the pile group had reached 70 mm.

In Section 5.6.1, the excess pore pressures below the pile cap of cap-supported bored pile groups were observed to be significantly affected by the advance of the pile cap into the liquefied soil. The excess pore pressures recorded below the pile cap at P6, are shown in Figure 6.13.
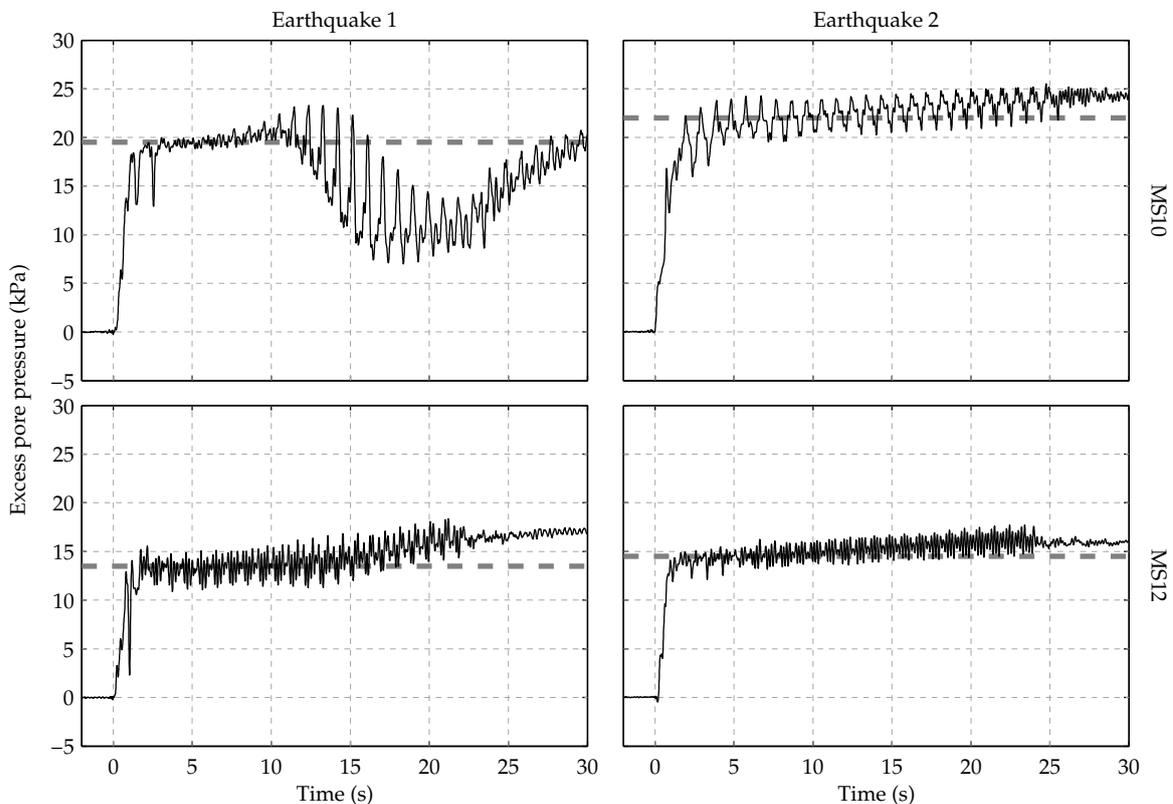
Figure 6.13: Excess pore pressures below the pile cap at P6, in MS10 and MS12

157

6. EFFECT OF INSTALLATION METHOD

It can be seen that in the first earthquake of MS10, the pore pressures initially achieve full liquefaction. However, a distinct change in the behaviour of the excess pore pressures can be observed to start approximately 10 s after the start of the earthquake. After this point, the excess pore pressures can be seen to reduce substantially, and show large spikes each cycle, indicating large shear stresses in the soil. This behaviour suggests that the pile cap in MS10 begins to advance into the liquefied soil after 10 s of shaking and is consistent with the point at which the axial loads were found to begin reducing significantly. At this point, the soil beneath the pile cap begins to mobilise resistance and the axial loads transfer to the pile cap in a manner similar to that observed with the cap-supported bored pile group in MS09.

The axial loads in MS12 shown in Figure 6.9 indicate that before the earthquake, pile leg 1 carries a greater proportion of the load than expected per pile and therefore the remaining piles in the group must be carrying smaller loads. While the axial loads were observed to reduce in MS12, it can be seen in Figure 6.13 that the continued settlement of the pile cap did not induce significant changes in the excess pore pressures recorded below the pile cap. Additionally, the reduction in axial loads in MS12 take place much more gradually than in MS10 such that at the end of the earthquake, the piles remained significantly loaded. These observations suggest that rather than indicate the transfer of axial load from pile to pile cap, the reduction in axial load may well be due to a gradual redistribution of axial load amongst the different piles within the pile group, perhaps due to softening which occurs in the overconsolidated soil. Since the settlement rates in the middle section of the earthquakes are similar in MS10 and MS12, it is thought that if the earthquake had been of longer duration, then the pile cap would have made definite contact with the soil surface, after which point the axial loads would be expected to reduce in a similar manner to MS10.

The pore pressures beneath the pile cap in the second earthquake of MS10 and MS12 again suggest that positive contact between the pile cap and the soil surface is not made. This observation is backed up by the relative settlement between the pile cap and the soil surface recorded after the end of the first earthquake, which showed that, assuming the soil profile settles equally across the model, a gap forms beneath the pile cap of 118 mm and 79 mm in MS10 and MS12 respectively (estimated as the difference between the soil surface settlement after the earthquake and the pile group absolute settlement). These are comparable with the absolute settlements of the pile groups during the second earthquake of 113 mm and 104 mm. The soil surface will also settle during the second earthquake, and therefore even in MS12, where the gap between the pile cap and soil surface is smaller than the absolute settlements of the pile cap during the second earthquake, it remains most likely that the pile cap never reached the soil surface during the second earthquake. . The pile groups are therefore free-standing for the duration of the second earthquake,

leading to the axial loads shown in Figure 6.9 remaining within a relatively small band. However, while the cycle-averaged axial loads remained within the tight band, the axial loads show a large cyclic variation, as is expected of a free-standing pile from the discussion in Chapter 4.

6.9 Effect of enhanced surface roughness

It was shown in Figure 6.9 that the strain gauges indicated an axial load distribution which was difficult to interpret. It is thought that this reflects some bending moments which were set up during the installation effect, and as a result the discussion to this point has focussed on the trends which were observed in the axial load data. If the data has been significantly affected by the presence of bending moments in these tests, then it is difficult to assess the contribution of the increased roughness of the piles in MS12 to the load carrying behaviour of the piles. However, while "splaying" of the piles during the jacking process may have led to significant bending moments, the fact that the axial loads on the two instrumented piles are observed to oscillate nearly out of phase with each other suggests that the variation in axial load is dominating the dynamic component of the recorded load. It might then be possible that some qualitative conclusions be drawn by considering the range of shaft friction rather than the absolute values. Additionally, it was found after the tests of MS10 and MS12 that the very high stress levels near the tips of the piles caused visible signs of distress to the protective epoxy, and an example from the tip of Leg 2 of MS10 is shown in Figure 6.14. It is possible that these very high stress levels near the tips of the piles could be responsible for some additional errors, especially given the reduced wall thicknesses at these points.

Keeping in mind the difficulties which have been encountered in these tests with the overall level of the axial loads, the shaft friction between the shallowest two gauges on

Damage to the protective epoxy coating leading to some strain gauges becoming exposed
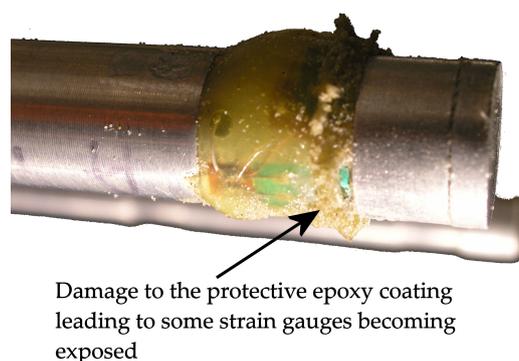
Figure 6.14: Distress evident on the protective epoxy layer as a result of jacking
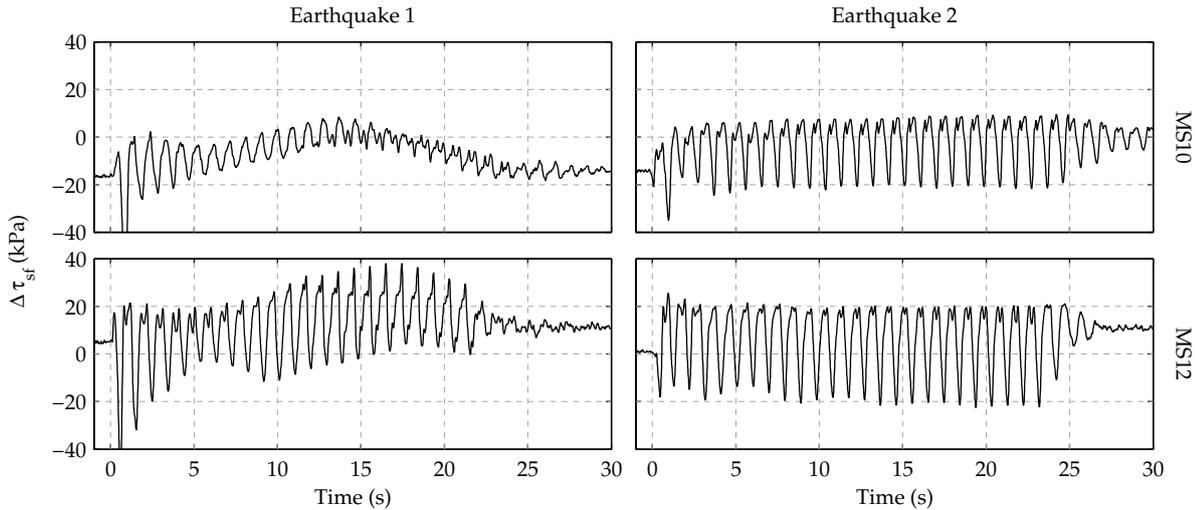
Figure 6.15: Shaft friction between gauges E and D in MS10 and MS12

Leg 1 have been shown in Figure 6.15. Even at these locations, the challenges with the shaft friction are evident, with the maxima actually tending to correspond to minima in the axial loading at the time. Assuming however that this is an offset issue and that the range of shaft friction recorded is reasonable, then it can be seen that in both earthquakes, the range in shaft friction over each cycle in MS12 is larger than that recorded in MS10. In the first earthquake, the range in shaft friction on the "smooth" piles is approximately 10 kPa at this location, while it is approximately 30 kPa with the roughened piles. In the second earthquake, when the piles were free standing throughout the earthquake, the range in shaft friction was increased relative to the first earthquake, with the range in MS10 being approximately 25 - 30 kPa, while in MS12 the range is approximately 40 kPa.

From these observations, it is possible to deduce that the roughened piles has increased the shaft friction. In the "smooth" case, the interface angle of friction is approximately 17 ^{o}, while in the roughened case, the interface angle of friction is assumed to take the critical state angle of friction, which for the position of gauges E and D will be 33 ^{o}. All else being equal, the shaft friction capacities of the piles will vary according to $tan(\delta)$ under static conditions. This would imply that the shaft friction capacity of the roughened pile would be expected to be 2.1 times larger than that of the smooth piles. The differences in range of shaft friction is observed to lie between 3 in the first earthquake and 1.3 in the second earthquake, which seems reasonable as a comparison. The observed increase in shaft friction in the second earthquake is interesting, and perhaps is a reflection of a slight increase in relative density in the loose sand between the first and second earthquakes implied by the soil's settlement after each earthquake.

The discussion of shaft friction in these tests is obviously far from satisfactory to make definite conclusions, however, it appears from these preliminary tests on the behaviour of jacked tests that there may be an effect on the load carrying characteristics of the piles due

to the interface angle of friction. Further tests, with more refined axial load measurement would be required to investigate this more thoroughly. The axial load measurement in these tests would have been significantly improved if the bending moments had been measured concurrently, and if greater protection of the gauges had been available. The latter could have been solved if the gauges had been mounted on the internal surface of the pile, although this introduces several practical considerations (i.e. how to accurately place, secure and attach wires to the strain gauges).

The test of MS12 was carried out with sand grains bonded to the pile surface to simulate a fully rough pile interface. It was expected that as a result of increasing the roughness on the sides of the piles, there would be increased axial capacity during the earthquake and therefore a reduction in the pile group settlement. However, in the first earthquake with the jacked pile groups, the absolute settlements of the pile group in MS12 were larger. It was discussed in the previous section that the pile group in MS10 became cap-supported mid-way through the first earthquake, while in MS12, the pile group did not appear to come into contact with the soil surface during the first earthquake. As a result, from the point where the pile cap starts to carry axial loads in MS10, it can be expected that the settlements in MS10 would be reduced compared with a free-standing pile. This was found to be consistent with the point where the settlements in MS10 became smaller than those in MS12.

In the second earthquake of both MS10 and MS12, it was discussed in Section 6.8 that the pile groups did not come into contact with the soil surface. Under these conditions, it was observed in Figure 6.7(b) that the absolute settlements in both tests were very similar.

The similarity of the settlements of the pile groups in Earthquake 1 before contact was made in MS10, and throughout the second of the Earthquakes strongly suggests that the interface friction angle is not a key variable to the settlement of a jacked pile group during an earthquake. This seems contradictory to the point made that the shaft friction which is developed on the pile under the seismic loading may be increased by a larger interface friction angle. It was however shown in Figure 6.9 that at the start of the first earthquake, and throughout the second earthquake, the pile tips were highly loaded, carrying approximately 75 % of the total axial loads (again not withstanding the difficulties encountered in measuring the axial loads in these tests). It therefore seems reasonable that for these closed ended piles, that the settlement response is being largely controlled by the soil around the pile tips. Since the changes in soil stresses which have affected the behaviour of the jacked pile groups compared with the bored pile groups, came about through the displacement of soil under high confining stress (i.e. installation during the test), it is expected that similar conditions exist beneath the piles in both MS10 and MS12. It may be expected that the increased roughness of the piles may affect the interface zone next

to the pile. However, this does not affect the soil beneath the piles. Therefore it is reasonable that the interface angle of friction has not affected the overall settlement of these pile groups.

It must at this point be pointed out that if the piles carry a much greater proportion of the axial loads in shaft friction, then the difference in the pile's surface roughness may become more important to the settlement response. This would be expected to be particularly evident in piles with a very large shaft area compared to the base area, of which H-piles would be a good example.

6.10   Choice of pile tip boundary condition

In the Introduction to this Chapter, it was highlighted that one of the techniques for inserting model piles into the model was to rigidly attach them to the base of the container, before sand pouring commenced. The settlement response of the pile groups in this Chapter has shown that at the start of an earthquake, piles which have been jacked are resistant to settlement until the pore pressures in the bulb of highly overconsolidated soil rise high enough to soften this zone of soil. This immediately raises the question of whether rigidly fixing the piles to the base of the model container provides an alternative method for investigating the behaviour of jacked piles at the start of an earthquake, since the container prevents settlement of the piles. However, as discussed by White & Bolton (2004), when a pile is jacked, the soil beneath the pile tip is being highly strained, resulting in zones of looser soil around the piles than is found in the free field. In addition, the jacking process leads to the formation of an interface zone of soil which is both very dense, and comprises highly crushed sand. In addition to these differences in the soil type and density around the piles, the jacking process creates a very different stress distribution around the piles, with very high lateral stresses near the pile tips. While it is possible that these initial differences become less important as high pore pressures develop in the bearing layer, these differences may affect the response in the initial stages of the earthquake. Finally, as shown in Section 6.7, while the pile group might not be settling at the start of the earthquake, the pile group may still be rocking from side to side, with the piles themselves still moving up and down. In this situation, rigidly connecting the piles to the base of the container will prevent this behaviour and therefore a different response will ensue.

6.11   Choice of earthquake motion

As discussed in Section 3.3.2, the earthquake loading applied with the SAM actuator might be considered to be a more severe loading condition than a real earthquake where only a couple of cycles of high amplitude shaking are typically encountered. It might then be argued that in a real earthquake, the pore pressures in the heavily overconsolidated soil beneath the tip of a jacked pile might not rise sufficiently high to soften the soil while the large accelerations are taking place. As a result, it is possible that the settlement response of a jacked pile during a more realistic earthquake will never enter the phase where it begins to develop settlement in a manner similar to a bored pile. However, this is beyond the scope of these tests, and further testing needs to be carried out to investigate this aspect.

6.12 Summary

In this Chapter, the axial response of a jacked pile foundation under earthquake has been investigated. The results from the pair of dynamic centrifuge tests which were carried out for this purpose have highlighted some interesting differences in the behaviour of both the pile group and the sand in the bearing layer during these tests:

- The heavily instrumented pile group was successfully jacked into a saturated soil model at the test acceleration, allowing the axial behaviour of a jacked pile foundation under earthquake loading to be investigated.

- Very large axial loads were mobilised during the jacking process. The reduction in axial load at the heads of the piles after the jacking process led to the axial loading reducing along the length of the pile. This reduction in load created a zone of highly overconsolidated sand beneath the piles.

- As a result of the large stresses during the jacking process, several gauges, especially those near the tips of the piles were observed to fail during the experiments.

- The pore pressure generation in the loose layer, as well as the accelerations in the loose and dense soil layers appear unaffected by the jacking of the piles.

- The pore pressures in the dense layer of the model appear to rise appreciably slower in the tests with the jacked piles compared with any of the tests with the bored piles.

- It was proposed that the bulbs of overconsolidated soil were responsible for the much slower build up of excess pore pressure observed in the tests with jacked piles, initially acting like a sink for the excess pore pressures in the dense layer.

- The pore pressures at the initial pile tip elevation were found to be larger between the piles than away from the piles. It was proposed that this did not reflect a hydraulic gradient from the piles to the free field, rather that it arose as a result of the soil between the piles being in a slightly looser state than the soil further from the piles. This zone of looser soil arises as a result of strong dilation during the jacking process.

- As a result of the lower pore pressures and the overconsolidated soil beneath the piles, the jacked piles did not begin to settle at the start of the first earthquake. Instead, the pile group rotates slightly about the leading pile, resulting in a small average heave of the pile group.

- Once the pore pressures in the dense layer had fully developed, the jacked piles began to accumulate very large absolute settlements. The rate of settlement of the pile group was observed to be similar to that of a bored pile.

- In the earthquake which followed the first, the settlement profile of the jacked pile group resembled that of a bored pile, and it was proposed that the settlement of the jacked pile accompanied by the high excess pore pressures in the dense layer of the first earthquake was responsible for the change in settlement behaviour of the pile group.

- As a result of the jacked piles not settling at the start of the first earthquake, a gap formed between the pile cap and the soil. This meant that the axial pile loads remained high at the start of the earthquake, with the pile groups essentially becoming "free-standing." With continued shaking, the degradation of the very stiff settlement response led to the axial loads on the piles transferring to the pile cap in a similar manner to the cap-supported bored piles.

- Post-earthquake settlement of the soil surface generated a gap beneath the pile caps of the jacked pile groups so that during the second earthquake, they remained free-standing throughout and resulted in the axial loading remaining large on these piles for the whole earthquake.

- The settlements of the pile groups with rough and smooth soil-pile interfaces were found to have very similar settlement responses as a result of the settlement response being controlled by the soil below the pile tips.

- A greater variation in shaft friction was observed with piles which had a roughened interface, which may indicate that the magnitude of shaft friction which can be mobilised by the piles during an earthquake is increased by a larger interface friction angle.

- While the pile groups did not settle at the beginning of the earthquake, the soil states around the jacked piles is complex meaning that installing the piles under 1g with vertical pile restraint is unlikely to be a useful way to study the behaviour of piled foundations during an earthquake.

- The earthquake motions during a real earthquake are not likely to be as sustained as those applied to the models in this Chapter, which may have implications for the settlement response of real jacked pile groups in the latter stages of an earthquake.

Chapter 7

Behaviour of piled foundations after an earthquake

7.1 Introduction

In the previous chapters, the axial behaviour of piled foundations during an earthquake has been investigated. As a consequence of the strong shaking, large inertial and kinematic loads are applied to the structure, leading to extremes in both the lateral and axial loads which are applied to the structure. After the strong shaking has ended, the axial loads which must be resisted by the ground simplify to those of the structure's dead weight. However, the strength and stiffness of the soil layers will be changing significantly in the moments after the earthquake, and as pointed out in Chapter 2, the axial behaviour of piled foundations after strong shaking remains poorly understood, with existing literature examining the case of free-standing pile groups.

The results of the preceding chapters have highlighted the differences in the behaviour of piles which are free-standing or cap-supported and whether the installation method represented bored or jacked piles. The differences in the axial load transfer which exist at the end of strong shaking on these different types of piles might be expected to have an effect on the behaviour of a piled foundation after an earthquake. Therefore, in this chapter, the results from the previously described tests will be examined from the period immediately following the end of strong shaking until the point where the excess pore pressures have completely dissipated, and no further changes in the loading or settlement of pile group would be expected.

Much of the work within this chapter can also be found in Stringer & Madabhushi (2011c).

7.2 Dissipation of excess pore pressures

In the preceding chapters, it was shown that the earthquake motions simulated on the models led to large excess pore pressures being generated across the full depth of the model soil profiles. However, once the earthquake ceases, additional pore pressures are no longer being generated and therefore the excess pore pressures must dissipate. This process is shown in Figure 7.1 for the first earthquake in each test. The dashed line in each plot indicates the full liquefaction pressure throughout the soil profile. Unshaded markers indicate the excess pore pressures recorded in the free field, while black-shaded markers denote those recorded beneath the pile tips at PB2.

7.2.1 Free field

Initially, pore pressures recorded throughout the loose layer, as well as those in the dense layer down to the initial depth of the pile tips, are very close to those estimated to cause full liquefaction. At the base of the model, excess pore pressures are also high, but generally do not indicate full liquefaction, especially in the tests with free-standing bored pile groups (MS06) and the jacked pile groups (MS10 and MS12). While the pore pressures from the bored pile group tests of MS01 and MS05 are not shown, similar results to those in MS06 were obtained.

The results shown in Figure 7.1 indicate that the differences in thickness and hydraulic conductivity of the dense layers used in the models affects the dissipation of excess pore pressures. In the tests where the relatively coarse Fraction C sand was used in the dense layer (all tests except MS08), excess pore pressures within the dense layer initially reduce rapidly after the earthquake, so that only small excess pore pressure differences across the bearing layer remained. Following this period of equalisation, remaining excess pore pressures in the bearing layer dissipate much more slowly. By contrast, in MS08, excess pore pressures dissipate much more gradually in the dense layer of the model. The difference in excess pore pressure dissipation is due to the disparity in hydraulic conductivity between the Fraction E and Fraction C silica sands. According to Hazen's equation, hydraulic conductivity scales with the square of the D_{10} particle size, as shown in Equation 3.1. Table 3.2 indicates that Fraction C has a D_{10} size approximately four times greater than Fraction E, meaning that its hydraulic conductivity estimated using Equation 3.1 is 16 times greater.

Since the bottom and side boundaries of the laminar container are impermeable, fluid can only drain through the top surface of the model. The rate of fluid flow in tests where the dense layer is constructed from Fraction C is therefore restricted by the rate at which
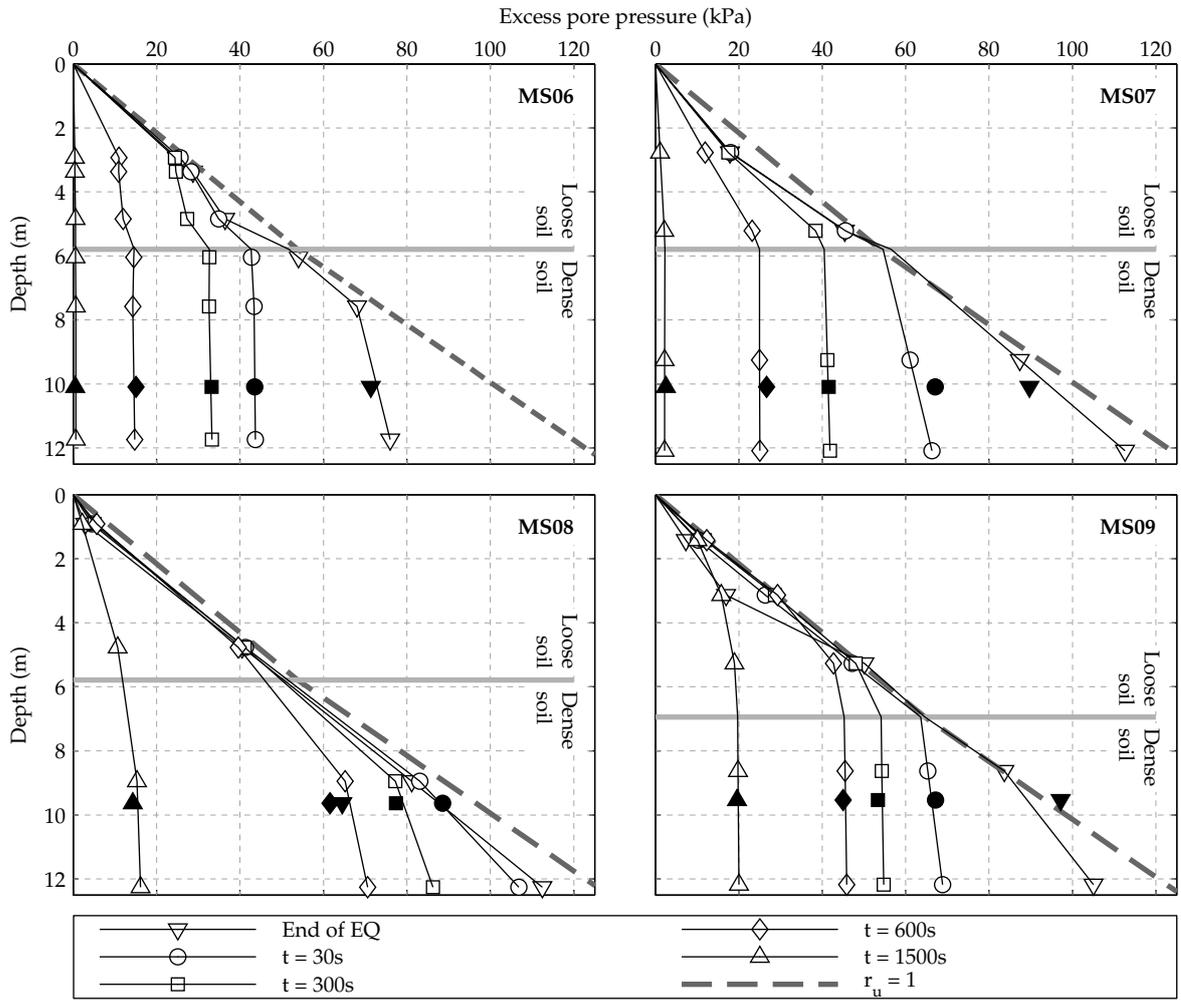
(a) Bored piles
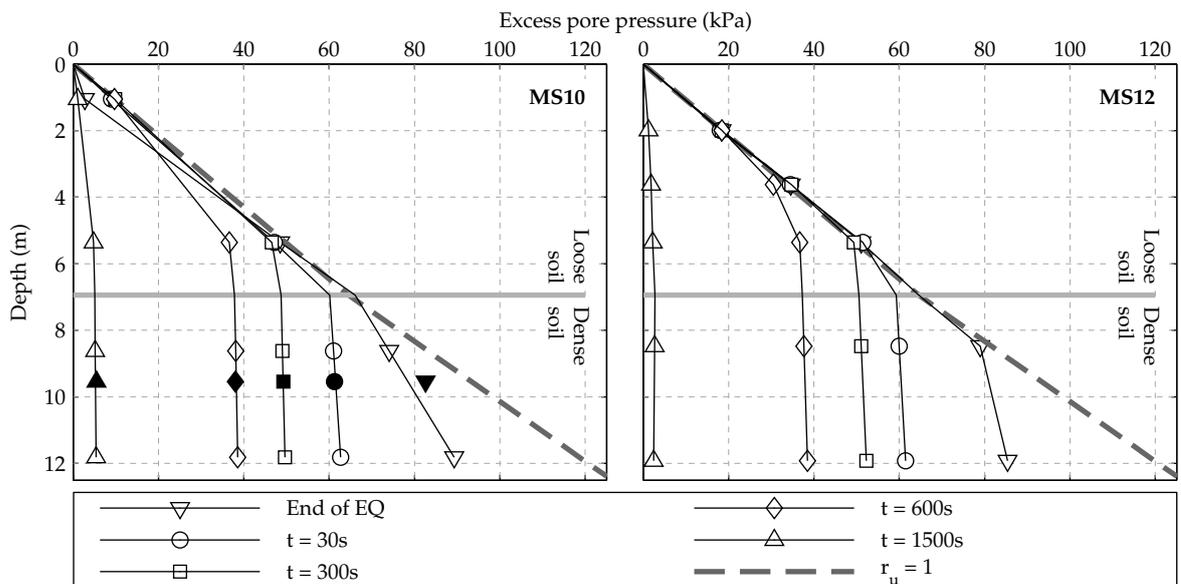
(b) Jacked piles

Figure 7.1: Dissipation of excess pore pressures after the first earthquake

it can drain through the liquefiable layer (which has the lower hydraulic conductivity), meaning that the hydraulic gradients in the Fraction C layer will be very low. Hence excess pore pressures rapidly equalise throughout these dense layers, as shown by the near-vertical sections in Figure 7.1.

7.2.2 Beneath the pile tips

It was noted in Section 3.7.2 that in the initial tests with the new pile group, no attempt was made to saturate the cavity containing the pile tip pore pressure transducers. As a result, very little dynamic response was recorded by the pile tip PPTs in MS06 or MS07. However, while the pore pressure information in these two tests was disregarded when discussing the behaviour of the pile group during the earthquakes, the measurements are assumed to faithfully record the pressures after the earthquake, where pore pressure changes occur slowly enough for the pressure in the cavity to remain in equilibrium. In attempting to improve the saturation further in MS12, the porous filters in front of the pile tip PPTs became blocked with a thick grease and as a result, no data is available for the pile tip pore pressures in this experiment.

7.2.2.1 Bored piles

In Figure 7.1(a), some differences were observed between the excess pore pressures measured at the tips of bored piles compared with those which are expected at the same depth in the free field (by interpolating between the PPT measurements above and below the pile tips). In the case of the free standing bored pile group (MS06), excess pore pressures beneath the pile tip were initially slightly below those in the free field, but then slightly rise above them for much of the remainder of the dissipation period. Similar, but more exaggerated patterns can be seen in MS07 and MS09, where the bored pile group was cap-supported and had Fraction C sand in the dense layer. In MS08, the cap-supported bored piles were embedded in a bearing layer of Fraction E and showed a different pattern; in this test, the pore pressure below the pile tip is initially much lower than the expected level in the free-field (≈ 23 kPa), but rises in the moments after the earthquake so that 30 s later it is close to the value expected in the free field. As the dissipation of excess pore pressures continues, the excess pore pressures below the pile tips again reduce and become lower than those expected in the free field for the remainder of the dissipation process.

The difference between the expected and observed excess pore pressures below the pile tips indicates that in addition to the dissipation of excess pore pressures, a further effect,

thought to be linked to the deviatoric stresses arising from the pile's axial load, is influencing the behaviour of this particular zone of soil. This effect will be discussed further in Section 7.7.

7.2.2.2 Jacked piles

The pore pressure response below the jacked piles in MS10 were found to be reasonably similar to that of MS06. As shown in Figure 7.1(b), the pore pressures below the pile tips in MS10 were initially greater than those in the free field. However, these rapidly reduced so that they remained close to the expected values for almost all of the dissipation process.

7.3 Axial loads after the earthquake

Figure 7.2 shows the changing axial load distribution with depth as the excess pore pressures dissipate, separated into the tests with the bored piles, and those with the jacked piles. Due to the difficulties encountered with the strain gauges in the tests with jacked piles highlighted in the previous chapter, only the axial loads from Leg 1 are shown in Figure 7.2(b).

7.3.1 Bored piles

In the free-standing bored pile group of MS06, significant axial loads exist at both the head and base of the pile at the end of the earthquake. As the pore pressures dissipate, the axial load at the pile head remains similar, but the loads along the remainder of the pile increase. It can be seen that the axial head load in MS06 has reduced slightly during the course of the earthquake. Since the pile group is free-standing, this reduction indicates some redistribution of axial load amongst the 4 piles within the group.

The behaviour of the free standing pile group of MS06 contrasts strongly with that of the cap-supported bored pile groups, where it can be seen that axial loads along the pile at the end of the earthquake are very close to zero, especially at the pile base. As the pore pressures dissipate, the axial loads along the length of the pile increase greatly. It can also be seen that when Fraction C was used in the dense layer (MS07 & MS09), the pile base load begins increasing immediately after the end of the earthquake. However, when Fraction E sand was used in the dense layer (MS08), the axial load remains zero for a period, after which the increases in base load occur more slowly and to lesser extent

(a) Bored Piles

(b) Jacked Piles
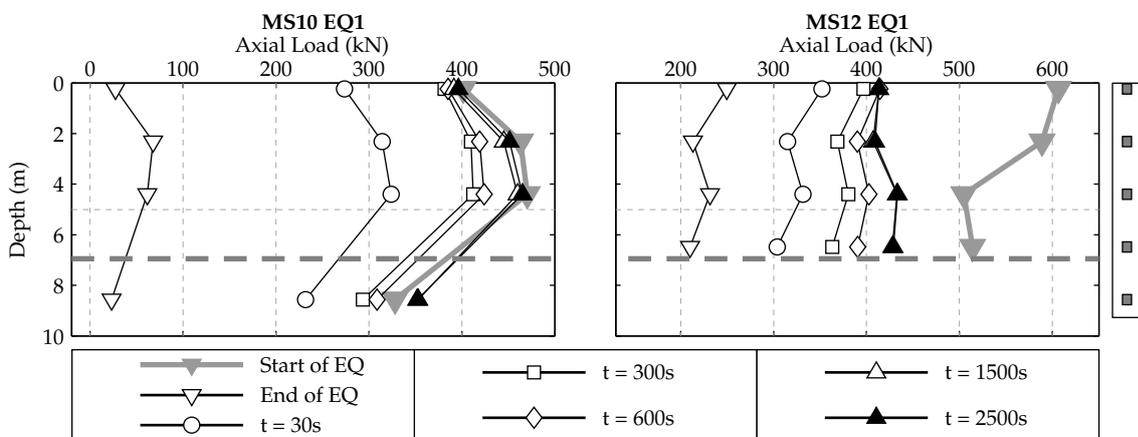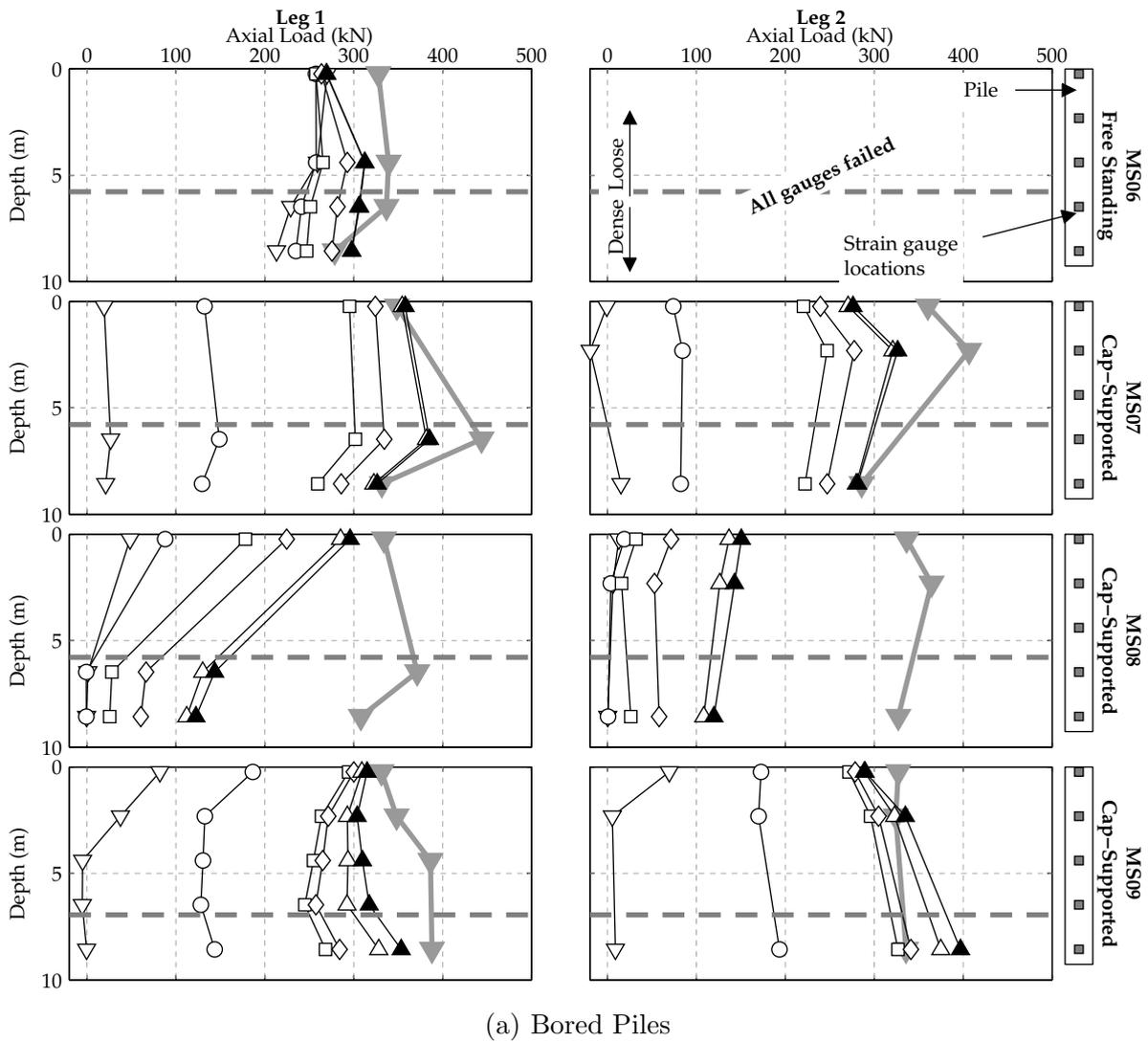
Figure 7.2: Axial loads measured after the end of the earthquake

compared with when Fraction C sand was used in the base layer of the model. Similar to the free-standing bored piles, in all data sets excepting Leg 1 of MS07, the axial head load at the end of the earthquake is generally lower than that at the start of the earthquake. In this case however, as well as the possibility for axial load distribution amongst the piles, it is possible that some of this difference in axial load is being carried by a small bearing pressure on the base of the pile cap.

7.3.2   Jacked piles

In the case of the jacked pile groups, it can be seen that in MS10, the axial loads again increased significantly after the earthquake had ended, with the final load distribution becoming very close to that at the start of the earthquake. In MS12, the axial loads were initially much higher on the pile shown than in the other tests, presumably due to an unfair loading distribution at the start of the earthquake. However, once again, it can be seen that after the earthquake has ended, significant increases in the axial load are observed.

7.4   Settlement

Figure 7.3 shows the absolute settlements of the pile groups (top half of the figure) after the first earthquake in each test. In each case, the settlements are shown relative to those at the end of the earthquake and were obtained by applying a low-pass filter (Butterworth filter with 0.1 Hz cut-off frequency) to the average of the settlements measured by the two potentiometers. Similar to the previous Chapters, these absolute settlements are assumed to be a good indicator of the movement of the piles relative to the dense layer. However, as discussed in Chapter 5, there are situations where the settlement of the pile cap relative to the ground's surface is of interest, since this relative settlement indicates whether vertical gaps develop between the foundation and the ground, or whether the building settles downward into the soil. The relative settlements between the pile cap and the free-field soil are therefore shown in the bottom half of Figure 7.3, using the LVDT shown in the model layouts (Figures 5.2 & 6.1). The settlements of the soil surface have been subjected to the same filtering as the pile cap settlement. In the figure, positive relative settlement indicates that the pile is advancing into the soil (i.e. pile group settlement is greater than soil settlement). As noted in Chapter 5, the LVDT in MS06 suffered very large settlements during the test, and therefore the relative settlements from this test are not available.

The absolute settlements of the free-standing bored pile group in MS06 indicate that almost no further settlement of the pile group occurred following the earthquake. Similarly,
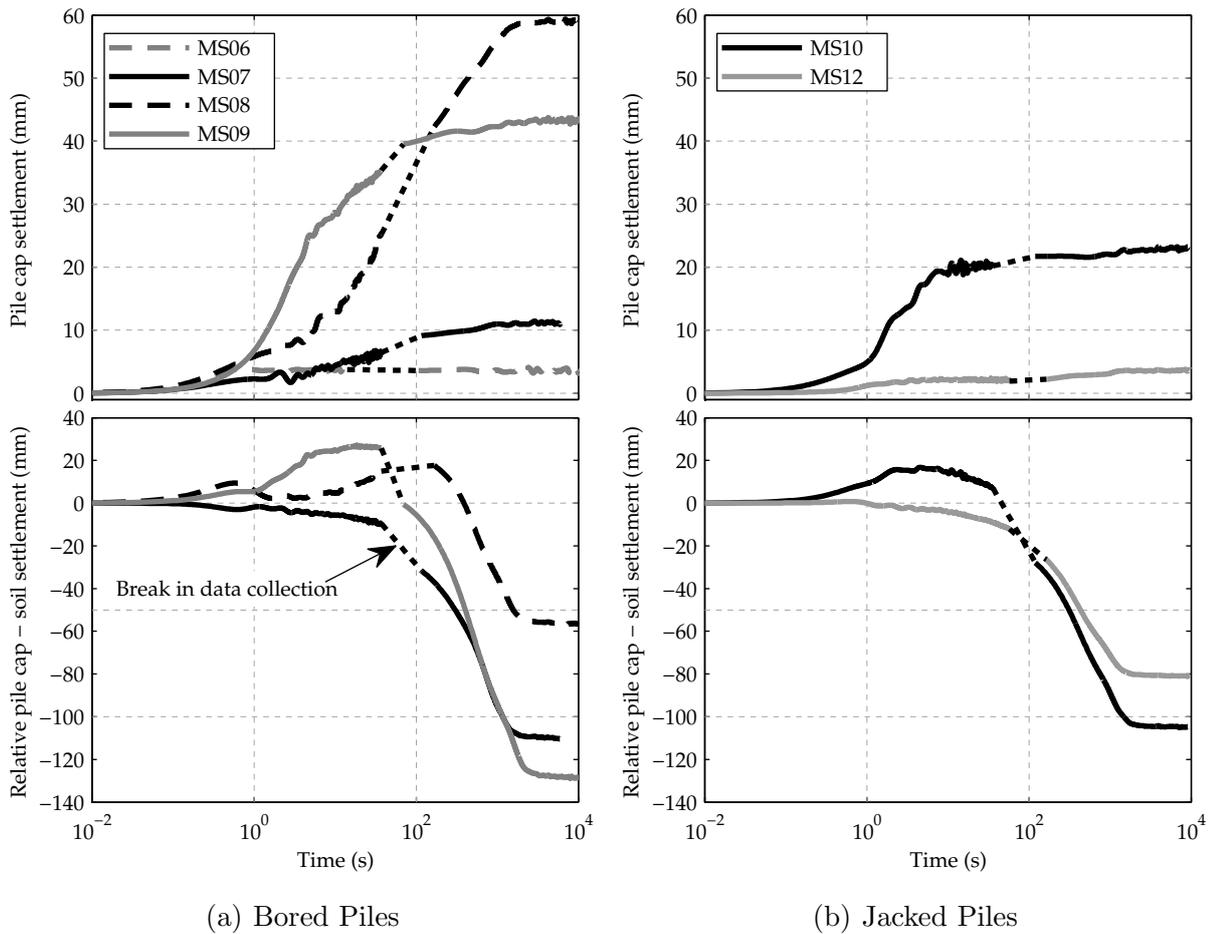
Figure 7.3: Absolute and relative soil-pile settlements after each earthquake

while not shown in Figure 7.3(a) the absolute settlements of the pile group in MS05 as well as those with the slightly longer pile group in MS01 were close to zero after the earthquake. However, this contrasts with the results of Knappett (2006) where the same pile group which was used in MS01 (JK-PG pile group) was embedded in a bearing layer of Fraction E sand. In this test (JK12), absolute post-earthquake settlements of 290 mm (quoted magnitude has been altered using the corrected g - level described in Section 4.2) were reported after the first earthquake. In the case of the cap-supported bored pile groups, the absolute settlement of MS07 is also relatively small, but in MS08 and MS09, larger absolute settlements of approximately 64 and 47 mm were recorded. Note that in the tests with Fraction C in the dense layer (MS06, MS07 and MS09), almost all of the absolute settlements occurring after the earthquake take place within the first 2 minutes of the dissipation phase. However, settlements in MS08 accumulate over 20 minutes.

The jacked pile groups in MS10 and MS12 show differing settlement responses after the earthquake. In MS10, where the axial load almost completely transfers to the pile cap at the end of the earthquake, post earthquake settlements of approximately 23 mm were recorded, indicating a stiffer response to the bored pile group of MS09. In MS12, where

174

the axial loading shown in Section 6.5.3 suggested that the pile cap did not make positive contact with the soil surface, the settlements are very low, similar to the free-standing pile group of MS06.

Although the soil surface settlement after the earthquake is not available in MS06, it can be inferred that since the pile group suffers only modest settlements in MS01, MS05 and MS06, these pile groups will show relative settlement profiles which start developing negative relative settlements immediately after the end of the earthquake.

The relative soil - pile cap settlements of the cap-supported bored pile groups indicate that when Fraction C sand was used in the dense layer of the model, the relative settlements approximately doubled in comparison with those where Fraction E sand was used. It is interesting that in MS07, the negative relative settlements occur from the beginning of the dissipation phase. In MS08 and MS09 however, there is an initial phase where the pile group moves downward relative to the soil, before the soil begins to settle faster than the pile. However, whereas in MS09 the change from positive to negative relative settlement occurs at approximately 20 s, in MS08 it occurs later, between 100 and 200 s after the earthquake. Finally, the relative settlements of the jacked pile groups again show some similarities with the bored pile groups. In MS10, it can be seen that similar to MS09, positive relative settlements develop initially, but after reaching a peak of 20 mm approximately 10 s after the earthquake, the relative settlements reduce and become progressively more negative with time. By contrast, the pile group of MS12 immediately develops negative relative settlement due to the low absolute settlement of the pile group after the earthquake.

The results in this section therefore highlight that the post-seismic settlements of the pile group have been influenced by whether the pile is cap-supported or free-standing at the end of the strong shaking as well as by the hydraulic conductivity of the bearing layer.

7.5 Shaft Friction

The evolution of shaft friction has been plotted for various time instants in Figure 7.4. Similar to previous chapters, shaft friction has been calculated as the difference in axial load between adjacent functioning strain gauges divided by the pile area between the gauges. The black brackets indicate the depth range over which the shaft friction in each graph has been calculated. As discussed in Chapter 6, the offsets in the axial load are particularly uncertain in the cases of the jacked pile groups. Since the shaft friction has been calculated as the difference in axial loads between two points, it is particularly vulnerable to errors in the overall level of axial load at each gauge. Inspection of the axial
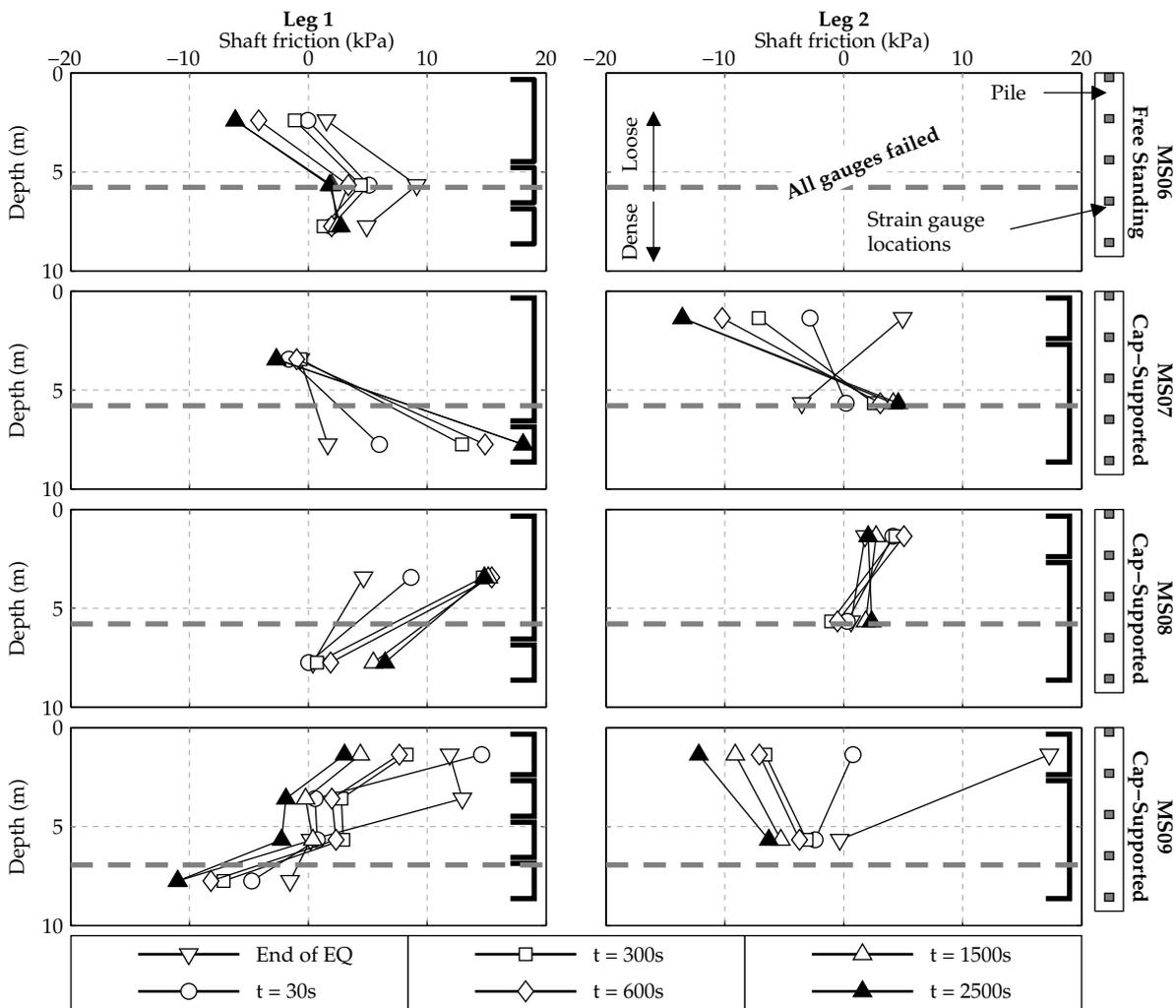
Figure 7.4: Evolution of shaft friction after the earthquake on bored piles

load distribution of MS12 in Figure 7.2(b) for example indicates that the shaft friction calculated would be positive at the top of the loose layer, while in the middle of the loose layer it is negative, and finally positive again at the bottom of the loose layer. For this reason, the evolution of shaft friction after the earthquake on jacked piles will not be discussed since the uncertainty in the axial load offsets renders the shaft friction values unreliable.

Large differences can be seen in the evolution of shaft friction on the bored piles after the earthquake in Figure 7.4. For the free-standing bored pile of MS06, the shaft friction becomes increasingly negative in the loose layer, while in the dense layer, the shaft friction remains positive throughout the dissipation period, but reduces in magnitude. When the pile group was cap-supported and embedded in a dense layer of Fraction C sand, the shaft friction in the loose layer again becomes increasingly negative with time, but within the dense layer, the shaft friction becomes increasingly positive. In MS08, with Fraction E in the dense layer, the shaft friction along the length of the pile actually remains positive throughout the dissipation period. The shaft friction on leg 1 between gauges E and B,

176

and on leg 2 between gauges 5 and 4 (at the head of the pile), increased to a peak at 900 s before reducing slightly until 2000 s where after it remained constant. In the dense layer, the shaft friction on both legs gradually increases with time. Finally, in MS09, the cap-supported pile group whose embedment within the dense Fraction C sand is less than that of MS07, the shaft friction near the head of the pile becomes increasingly negative on Leg 2, while on Leg 1, it reduces to a small value, but remains positive. Further down the pile, the shaft friction becomes negative on both pile legs, with increasing magnitude as the dissipation of excess pore pressures continues.

7.6   Axial load transfer

7.6.1   Pile head loads

The pile head loads shown in Figure 7.2 indicate two gross classes of axial loading condition while excess pore pressures are dissipating, which are sketched in Figure 7.5. In free-standing pile groups, the piles remain fully loaded throughout the earthquake since the pile cap is not in contact with the soil. This continues afterwards, and the axial pile head loads therefore remain constant.

By contrast, cap-supported pile groups show very low axial load at the pile head towards the end of the earthquake due to the pile cap settling into the soil. This results in the axial loads transferring from the piles to the pile cap as discussed in Chapter 5. During the dissipation phase, the piles begin to support axial loads again as the soil surface settles
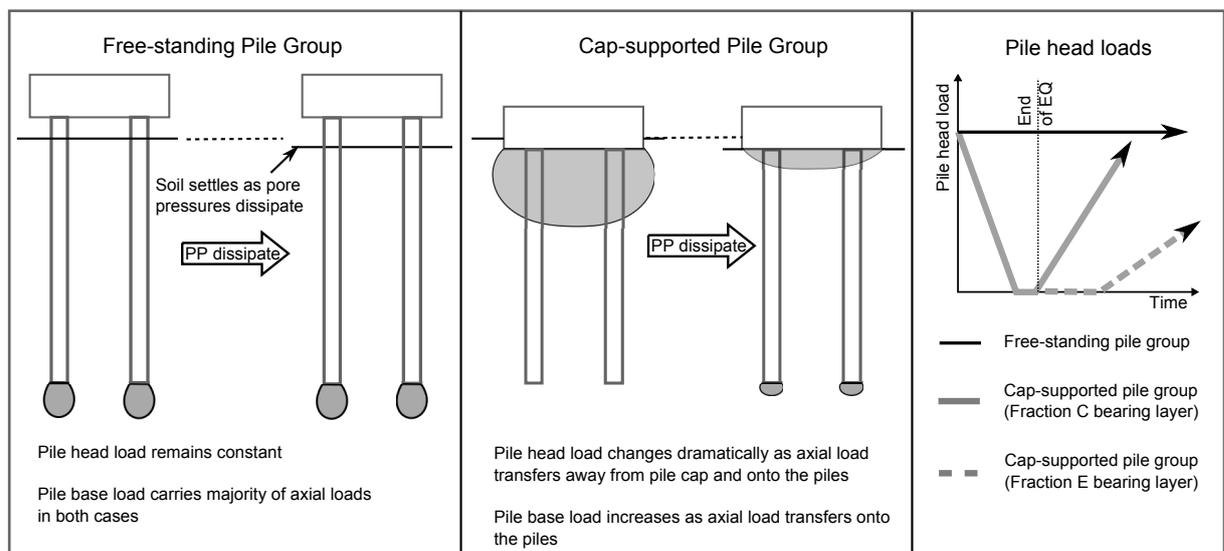
Figure 7.5: Schematic diagram showing how the pile head load is influenced by contact between the pile cap and soil surface

relative to the pile cap due to consolidation of the soil. The pile head axial loads therefore increase after the earthquake.

For axial loads to increase at the head of the pile, increasing axial resistance must also be mobilised on the piles to maintain equilibrium. The remobilisation of axial resistance is affected by the geometry and sands used in the soil profile, leading to differences in the re-loading of the piles in cap-supported pile groups shown in Figure 7.2 and the two paths shown in Figure 7.5.

7.6.2 Pile base loads

7.6.2.1 Free standing pile groups

The high base load at the end of the earthquake in MS06 shown in Figure 7.2(a) implies that at this time instant, large end bearing resistance is already mobilised. Knappett (2006) found that the stiffness of the soil near to free-standing pile groups increased during an earthquake, and suggested that the maintained base resistance during the earthquake arose as a result of dilation in the dense sand. Some evidence of this can be seen in Figure 7.1(a), where the pore pressures measured at the pile tips immediately after the earthquake in MS08 were observed to be significantly lower than those in the free field for a short period after the earthquake. However, since the large volume of soil surrounding the piles migration of pore pressure within the dense layer means that beneath the pile tips, the pore pressures increase close to those expected in the free field. It must however be remembered that in MS08, the pile group was cap-supported and as shown in Figure 7.2(a), the base resistance was not developed on these piles until much later. A similar, but smaller effect was observed at the tips of the free-standing piles of MS06. However, of greater importance to the post-earthquake behaviour of MS06 is the excess pore pressure at the deepest point in the model being significantly less than the liquefaction value. In the free-standing pile groups of MS05 and MS06, it was observed that at this deepest point, the pore pressures rose close to the level required for full liquefaction during the first few cycles of the earthquake, but as the earthquake progressed, the pore pressures at the base of the model already began to reduce, resulting in the excess pore pressure at the base of the model being significantly lower at the end of the earthquake than in the tests with the cap-supported pile groups. As a result, the soil directly beneath the pile tips has already regained significant stiffness, leading to the very small settlements after the earthquake observed in MS01, MS05 and MS06.

It was shown in Section 4.4.4 that when the pile group was embedded in a layer of sand with low hydraulic conductivity, the resulting co-seismic settlements were significantly higher. As noted in Section 7.4, the same appears to apply to the post earthquake

settlements. In JK-12, the post-earthquake excess pore pressures shown by Knappett (2006) indicated full liquefaction at the pile tip level for a significant period after the end of the earthquake. As a result, the dense soil will globally be at low effective stress and stiffness after the earthquake despite the high mobilised resistance at the pile tip. This suggests, assuming the cavity expansion solution of Yasufuku *et al.* (2001), that the bearing capacity of the piles in JK-12 would be very low for a period after the earthquake since this mechanism is governed by the global soil properties. This indicates that the piles would be suffering a bearing failure, resulting in the continued settlement reported by Knappett (2006).

Despite the distinct differences in the development of absolute pile group settlement between jacked and bored piles which was discussed in Section 6.7, it can be seen that after the earthquake, the absolute settlement of the pile group in MS12, which was thought to be largely free-standing, evolves in a similar manner to MS06, with very low additional settlements. This again can be attributed to the lower excess pore pressures deep in the dense layer at the end of the earthquake.

7.6.2.2 Cap-Supported pile groups

Soil beneath the piles regains strength and stiffness as excess pore pressures dissipate after the strong shaking has ended. As this happens, two extreme scenarios can be considered for the axial base load on a cap-supported pile. Firstly, axial loads continue to be supported by pile cap bearing pressure. The pile group therefore moves downwards with the soil surface. Secondly, the dense layer becomes infinitely stiff. The piles cannot settle further, meaning that axial loads rapidly transfer to the piles as the soil settles away from the pile cap. While the piles within the free-standing pile group in MS06 tend towards the latter scenario due to the large amount of base resistance mobilised at the end of the earthquake, the cap-supported pile groups show a large range in response.

Where the response lies between the two extremes is affected by how much axial resistance the piles can generate at a given moment. For the piles tested, the majority of the final axial resistance comes from pile end bearing. Figure 7.6(a) therefore indicates how the end bearing capacity of the piles, calculated according to Yasufuku *et al.* (2001), changes with the logarithm of time (in base 10) after the earthquake in each test. The solution assumes a cavity expansion mechanism for the piles in their ultimate limit state and is based on global soil parameters. The required effective stresses are therefore estimated based on the pore pressures observed in the free field. It was shown in Section 7.2.1 that the excess pore pressures within Fraction C sand equalised rapidly following the end of the earthquake and as a result, the difference in excess pore pressure across the depth of the layer was minimal. In these cases, the free field pore pressure at the pile tip level was
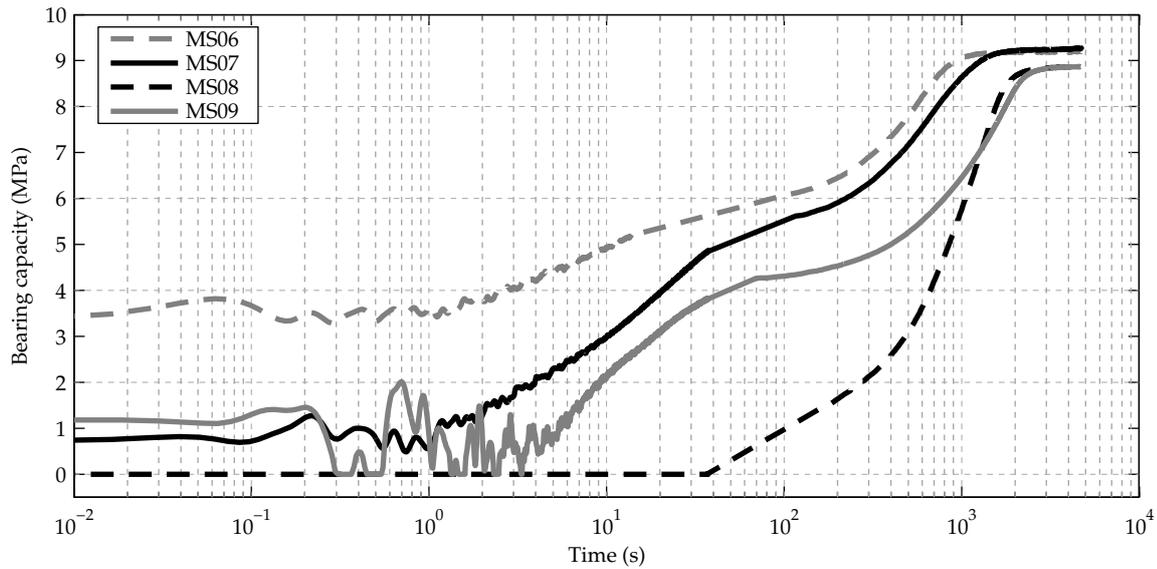
(a) Bearing capacity after the earthquakes, using Yasufuku *et al.* (2001)
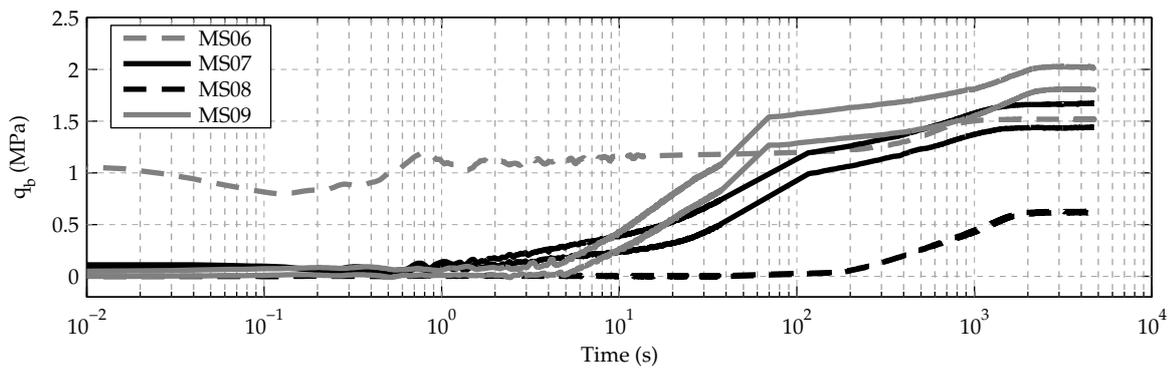
(b) End resistance mobilised by bored piles after the earthquake

Figure 7.6: Available and mobilised pile tip resistance after the earthquake

estimated using linear interpolation of the pore pressures measured at the deepest two pore pressure transducers in the model (i.e. P5 and P6 in test MS06). However, when Fraction E sand was used in the bearing layer (test MS08), the dissipation of excess pore pressures takes place much more gradually and the excess pore pressures vary significantly across the layer. It was found that for this scenario, the recorded pore pressures in the free field were well approximated using parabolic isochrone theory, described by Bolton (1979) with an initially triangular distribution of excess pore pressures.

Figure 7.6(b) shows measured pile base loads, and makes clear the role of pore pressure dissipation on the response of the pile group after the earthquake (The pile base loads in MS08 are very similar after the earthquake, hence only one line is shown in the figure). The rapid equalisation of pore pressures within the dense layers where Fraction C was used leads to the estimated base capacity increasing very quickly in the moments after the earthquake. Although Figure 7.6(a) showed that the piles in MS09 suffered large

settlements relative to the dense layer, approximately sixty percent of these settlements occur in the first 5 seconds after the earthquake, when the bearing capacity remains low, as shown in Figure 7.6(a). The base capacity in MS09 remains lower than in MS07 at any given time as the pore pressures remain slightly higher, owing to the deeper extent of the liquefiable layer (comprising of the finer Fraction E sand) in MS09. As a result, the end settlement of the piles relative to the dense layer are larger than those in MS07. Despite the high bearing capacity being available very soon after the end of the earthquakes in MS07 and MS09, the pile base loads remain much smaller than the estimated capacity. This is because mobilisation of base load requires an accompanying settlement. As increasing load is supported by the pile, the soil surface in the free field is able to settle relative to the pile cap, leading to ever increasing load transferring back to the piles, until the pile cap eventually becomes fully unloaded in the case of MS07. This process of remobilising end bearing resistance after the earthquake is thought to be responsible for the larger absolute settlement of the pile group after the earthquake in MS07 when compared with the free-standing pile group of MS06, as shown in Figure 7.7(a).

In MS08, the much lower rate of pore pressure dissipation within the dense layer leads the base capacity to remain zero until approximately 40 s after the end of the earthquake, after which base capacity increases, but more slowly than in MS07 and MS09. The lower base capacity in MS08 leads to the higher absolute pile settlement in Figure 7.3(a). The base loads remain very low until approximately 100 s, despite the base capacity rising steadily in this period. This again reflects the requirement for the piles to settle in order to mobilise a given amount of base capacity, which in this case means that the the pile cap continues to support the majority of load for much longer. This is also apparent in the bottom half of Figure 7.3(a), where the soil does not begin to settle relative to the pile cap until approximately 100 - 200 s after the earthquake.

While the post-earthquake absolute settlement of the cap-supported pile group was larger than that of a free-standing pile group in the case of a bearing layer with large hydraulic conductivity, the converse is true for the case where the hydraulic conductivity is low. This scenario is sketched in Figure 7.7(b). In this case, the excess pore pressures in the bearing layer remain high for a significant time after the earthquake. While in JK-12, this results in large settlements due to a bearing capacity failure at the base of the pile, in the case of MS08, the axial loads were completely transferred to the pile group during the earthquake and as a result the settlement of the pile group after the earthquake is controlled by the consolidation settlements of the soil surface, leading to the lower settlements of the cap-supported pile group.

The axial loads on the jacked pile group of MS10 were observed to increase in a similar manner to the cap-supported bored pile groups, with the difference that the resistance mobilised more quickly after the end of the earthquake, as shown in Figure 7.2(b). Similar

Free Standing

Cap-Supported

Pile cap initially carries
majority of axial loads

Loose, liquefiable layer | Low hydraulic conductivity

Pore pressures in dense soil reduce
rapidly after earthquake
-Bearing capacity greater than applied
load

Dense bearng layer | High hydraulic conductivity

End resistance already largely mobilised
at end of the earthquake
- Very little additional settlement

Axial loads at pile base very low at end of the earthquake
- settlement required to mobilise the base loads

(a) High hydraulic conductivity in the bearing layer

Free Standing

Cap-Supported

Pile cap supports axial load
until end bearing capacity
develops at pile base

Loose, liquefiable layer | Low hydraulic conductivity

Pore pressures in dense soil reduce
rapidly after earthquake
-Bearing capacity greater than applied
load

Dense bearng layer | High hydraulic conductivity

Resistance mobilised beneath the piles
at end of the earthquake, but bearing capacity
too low to support the resistance
- Large absolute settlements

End bearing resistance cannot be mobilised until
end bearing capacity begins to increase, so axial loads
remain supported by pile cap.
-Absolute settlements governed by settlement of the soil

(b) Low hydraulic conductivity in the bearing layer

Figure 7.7: Differences in the post-earthquake absolute settlement of free-standing and cap-supported pile groups due to the hydraulic conductivity of the bearing layer

to the free-standing pile groups, it can be seen in Figure 7.1(b) that at the end of the earthquake, the pore pressure deeper in the dense layer is significantly lower than that required for full liquefaction due to some dissipation during the earthquake. As a result, an increased bearing capacity is available to the piles in the moments after the earthquake, resulting in the lower absolute and relative settlements of the jacked pile group as the pore pressures dissipate.

7.7 Volumetric strains below the piles during the earthquake

It was shown in Figure 7.1 that excess pore pressures additional to those in the free field exist near the pile tips. The difference between the excess pore pressure in the free field and that below the pile tips is plotted against excess pore pressure in the free field in Figure 7.8, with arrows indicating the direction along the trace which corresponds to increasing time. When coarse Fraction C sand was present in the dense layer, the pore pressures below the pile tips were greater than expected, while when the finer Fraction E sand was present, the pore pressures were lower than expected. While the pore pressures are dissipating (leading to rising effective stresses in the free-field), Figure 7.2(a) showed that the pile base load increases monotonically in all tests (though to a lesser degree in MS06). This means that directly beneath the piles, the soil is subject to very large deviatoric stresses, which are also monotonically increasing since changes in pile base load result in large changes in vertical effective stress beneath the pile tips.
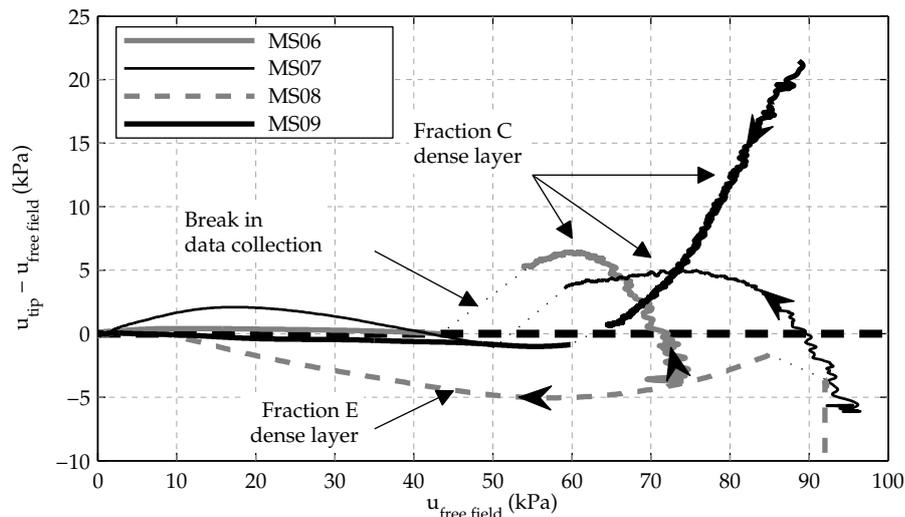
Figure 7.8: Difference in excess pore pressures at the pile tip horizon against dissipation of excess pore pressures in the free field after the earthquake

Start point	Undrained Path	Drained Path
D	-ve excess pp	dilation
L	+ve excess pp	contraction
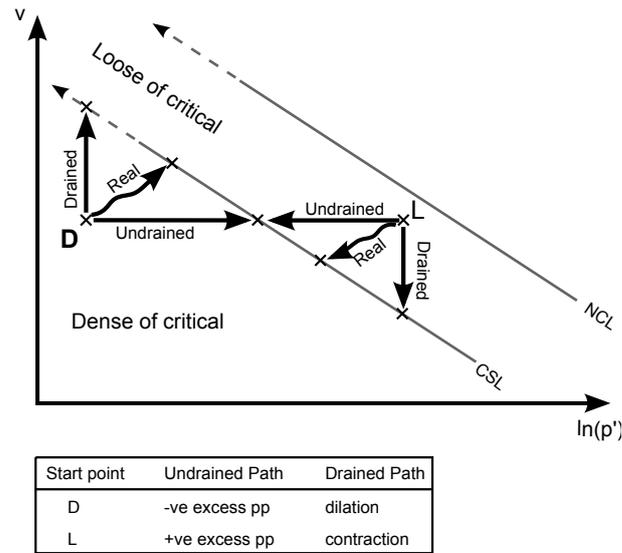
Figure 7.9: Paths to the critical state line for initially loose (L) and dense (D) soil states

Under very high deviatoric stresses, a soil element tends to shear until it reaches its critical state. Since the soil is saturated, it would be expected that this process would be accompanied by changes in pore pressures unless it took place very slowly. Using the Cam-clay model as a basic framework, soils which are on the contractile side of the critical state line would be expected to generate positive excess pore pressures during this process, while those on the dilatant side would be expected to generate negative excess pore pressures, as discussed in Section 2.2 and shown in Figure 7.9.

At present, earthquakes are often considered undrained events. However, any shearing event which takes place on a finite time scale can not be truly undrained, and the extent to which it represents an undrained event is defined by the hydraulic conductivity of the soil. In the case of a medium with infinite hydraulic conductivity, an earthquake event would be completely drained with all volume change taking place during the event.

Figure 7.10 displays hypothesised paths of specific volume and confining pressure below the pile tips during the testing sequence for the cases of Fraction E and Fraction C. Before the earthquake, the soil below the pile tips is at point A, under high confining pressure and low voids ratio. It was shown in Figure 5.5 that full liquefaction was reached within a few cycles at the pile tip level in every test where the MS-PG pile group was used. Additionally, in the case of cap-supported pile groups, the axial loads reduce to zero as the earthquake progressed. The soil element can therefore be considered to be in a state of very low confining pressure, but remaining in a very dense configuration and so moves to point B early in the earthquake.

Since the soil is very dense, it will be highly dilatant on shear. It was shown in Figure 5.9 that the pile caps suffered very large absolute settlements during the earthquake, and it is therefore assumed that the soil immediately below the pile tips attempts to

dilate during the earthquake. In the case where the dense layer comprises of Fraction E sand (relatively low hydraulic conductivity), the flow of fluid is relatively slow, and therefore volume change during the earthquake is correspondingly low and the soil moves to point E. However, when the dense layer comprises of Fraction C sand (large hydraulic conductivity), fluid can flow much faster, meaning that greater volume change can occur below the pile tips, potentially resulting in a much looser soil directly after the earthquake (point C).

After the earthquake, the mean confining pressure increases dramatically as excess pore pressures dissipate and in the case of cap-supported pile groups, the axial load transfers from the pile cap and onto the piles. This will move the soil state to points D and F in MS07 and MS08 respectively.

The high deviatoric stresses which exist when the piles become loaded are proposed to be high enough to cause the soil to attempt to deform, leading again to changes in excess pore pressures in an area close to the base of the pile. When Fraction E (low hydraulic conductivity) was used in the dense layer, the soil has remained below the critical state line (dilatant behaviour under shear), and therefore the pore pressures are slightly reduced. When Fraction C (large hydraulic conductivity) was used in the dense layer, the point lies above the critical state line, and therefore higher pore pressures are recorded.

The soil beneath the free-standing pile group (MS06) experiences different changes in soil state. Since the base of the pile continues to mobilise large resistance throughout the earthquake, the confining pressure must remain high below the pile tips throughout the experiment. In the free-standing configuration, the piles suffer large settlements relative to the dense layer, as shown in Figure 4.9(a). Similar to the cases of MS07 and MS09, fluid is able to flow rapidly in the dense layer and therefore the soil state moves to point G on or close to the critical state line. When the earthquake ends, there is a much smaller
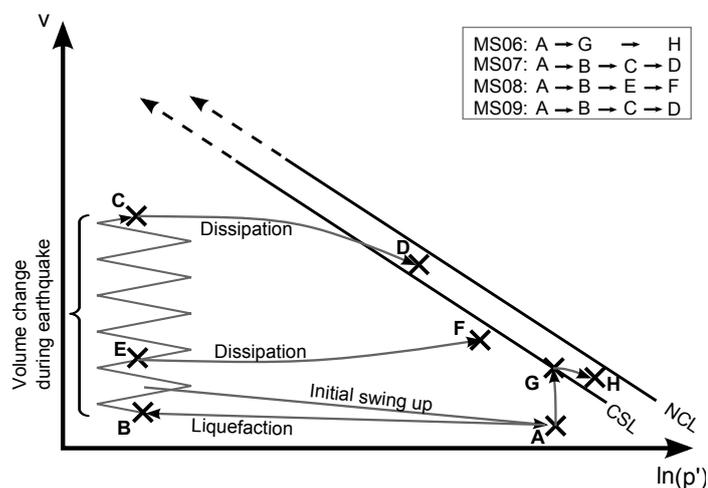
Figure 7.10: Schematic diagram showing changes in specific volume beneath the pile tips

increase in confining pressure below the pile base. This again potentially moves the soil state slightly to the right of the critical state line and into the contractile regime.

The excess pore pressures recorded at the pile tips suggest that, in a localised region of soil close to the pile tips, the difference in hydraulic conductivity of the two soils has led to the different soil types ending up on different sides of the critical state line immediately after the earthquake has ended.

7.8 Re-mobilisation of shaft friction

The development of pile shaft friction can be thought to depend on both the relative movements between the soil and pile (which mobilise the shaft friction) and the ultimate capacity at any given time. In the interpretation of the shaft friction which follows, it has been assumed that consolidation settlements after the earthquake only occur in the loose layer.

7.8.1 Influence of load application

In MS06, where the axial pile head load is constant, the absolute settlement of the pile group (shown in Figure 7.3(a)) was noted to cease almost immediately after the earthquake. At the pile head, the soil therefore begins moving downward relative to the pile immediately. This results in negative shaft friction being mobilised on the sections of the pile situated within the loose layer.

The increase in negative shaft friction while excess pore pressures dissipate is due to two effects. Firstly, the shaft friction capacity increases as the excess pore pressures dissipate. Secondly, the soil settlements at the surface are the accumulation of strain throughout the soil profile. Therefore, within the loose layer, the relative soil-pile settlements at depth will be much lower than those recorded near the surface. This means that as consolidation continues, greater shaft friction is being mobilised deep in the loose layer, while near the surface, the shaft friction capacity has already been reached, as sketched in Figure 7.11.

The downdrag forces just described lead to the axial loads increasing on the section of pile within the dense layer. However, as shown in Figure 7.4, the shaft friction in the dense layer did not increase. The rapid equalisation of pore pressures in the dense layer of the model (described in Section 7.2.1) leads to high shaft friction capacity being available almost immediately after the earthquake. However, the settlements in Figure 7.3(a) indicate that the section of the pile in the dense layer does not settle relative to the dense layer after the earthquake, meaning that shaft friction cannot be mobilised in
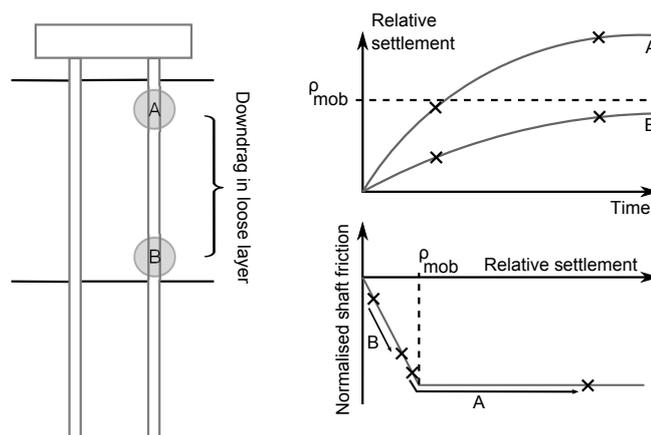
Figure 7.11: Mobilisation of shaft friction at different depths within the liquefiable layer

this layer to resist the increased axial loading. Instead, the extra axial loads are resisted by additional pile end bearing load.

The increasing pile head load on the cap-supported pile groups as the axial loads transfer from the pile cap to the piles after the earthquake leads to differences in the mobilised shaft friction. In MS07, the end bearing capacity during the dissipation of pore pressures far exceeded the axial loads applied to the piles. Since the axial loads are initially carried by the pile cap, the piles must settle (as shown in Figure 7.3(a) in order to mobilise base resistance. The larger absolute settlements lead to the much larger positive shaft friction observed in the dense layer of MS07 than MS06. In Figure 7.4, the shaft friction in the loose layer near the pile head again becomes increasingly negative with time due to the soil settling downward relative to the pile. While the magnitude of mobilised shaft friction is greater than that observed in MS06, it is thought that this arises due to the region over which the shaft friction was calculated. As shown in Figure 7.4, the shaft friction in MS07 is calculated at the head of the pile, where relative soil-pile displacements are greatest.

7.8.2 Influence of hydraulic conductivity

The influence of hydraulic conductivity on the base capacity of the piles in cap-supported pile groups after an earthquake was described in Section 7.6.2. This delay in regaining base capacity after the earthquake affects the subsequent development of shaft friction in MS08. In the dense layer, shaft friction remains near zero initially as the excess pore pressures remain high enough to keep the vertical effective stresses and therefore shaft friction capacity close to zero.

The much slower dissipation of excess pore pressures (shown in Figure 7.1(a)) means that the shaft friction capacity correspondingly increases slowly, hence shaft friction in the dense layer still remains very low 300 s after the earthquake despite the large downward

movement of the pile relative to the dense layer shown in Figure 7.3(a). Even though the shaft friction capacities of the piles in MS07 and MS08 would be expected to be very similar once all excess pore pressures have been dissipated, the recorded shaft friction in MS08 remains lower than in MS07. It is thought that this is due to the fact that the vast majority of the pile's settlement occurs while the effective stresses remain relatively low. Hence, in the latter stages of pore pressure dissipation when the shaft friction capacity is re-established, the pile does not settle enough to mobilise the available shaft friction capacity.

Figure 7.4 indicates that the shaft friction in the loose layer remained positive in MS08, in contrast to the downdrag forces observed in MS06 and MS07. It was shown in Figure 7.3(a) that the soil surface does not begin moving downward relative to the pile until approximately 100 - 200 s after the end of the earthquake. It would be expected that, as the soil accumulates increasing settlement relative to the pile, the shaft friction would first reduce to zero, and then become negative, as was the case in the other tests. This effect was partly observed on both instrumented piles, where the shaft friction began reducing slightly from 900 s until the pore pressures had finished dissipating. It remains surprising however that the shaft friction in the loose layer remains positive on both piles in the loose layer throughout the process of excess pore pressure dissipation. The axial loads in Figure 7.2(a) show that the pile cap continues to support axial load even after all excess pore pressures have finished dissipating since the final pile head loads are lower than those expected if the piles carried all of the superstructural load equally. This suggests that despite negative relative settlement between the free-field soil and the pile cap, some contact remains between the pile cap and soil surface, leading to a residual pile cap bearing pressure. In this case, the effective stresses below the pile cap will be higher than those in the free field and therefore downwards movement of the piles will generate positive shaft friction. Although the relative settlement shown in Figure 7.3(a) indicate that the soil surface begins settling relative to the pile at around t = 100 - 200 s after the earthquake, deeper in the loose layer, the reverse in relative settlement will happen at later times, resulting in positive shaft friction continuing to exist as the excess pore pressures dissipate.

7.9 Summary

In this chapter, the behaviour of piled groups after an earthquake has been discussed. While high accelerations and resulting dynamic load demands during the strong shaking might be thought to be the most vulnerable period for the structure, the post-earthquake phase remains important in determining the final relative settlements and axial load distributions.

This chapter has highlighted the differences in behaviour dependent on the manner in which axial load at the pile head develops, as well as the influence of the bearing layer's hydraulic conductivity. These differences are now summarised by considering the effects on the soil's behaviour and the behaviour of the different types of pile group separately.

7.9.1 Soil behaviour

- The dissipation of excess pore pressures within deep soil layers is greatly affected by its hydraulic conductivity. Where hydraulic conductivities are similar across the whole soil profile, parabolic isochrones provided a good fit to the observed dissipation of excess pore pressures. Where the deeper soil layer's hydraulic conductivity was larger than the overlying layer, then excess pore pressures throughout the layer equalise rapidly to the value at the bottom of the overlying layer. Remaining excess pore pressures dissipate in the same manner as the bottom of the overlying soil layer.

- Excess pore pressures measured below the pile tips suggest that in regions of intense shear, large volumetric strains can occur in soils of large hydraulic conductivity, leading to the initially dense soil crossing the critical state line as the effective stresses are regained following an earthquake and exhibiting a contractile response.

7.9.2 Free-standing piles

- Post earthquake settlements of the pile group are strongly influenced by the hydraulic conductivity of the bearing layer. Settlements were very limited when the bearing layer had a large hydraulic conductivity owing to the rapid increase in pile end bearing capacity. In bearing layers of low hydraulic conductivity, the piles experienced large settlements due to the bearing capacity remaining very low after the earthquake.

- Despite axial pile head loads remaining constant after the earthquake on free-standing pile groups, the consolidation of the soil profile led to an increase in axial loading on the piles due to negative shaft friction.

7.9.3 Cap-supported piles

- The axial head loads on cap-supported piles were observed to be low at the end of the earthquake due to the transfer of axial load from the piles to the pile cap which took place during the earthquakes. As the excess pore pressures dissipated, the axial loads being carried as pile cap bearing pressure returned to the piles, leading to large increases in axial pile head loads after the earthquake.

- In cases where the hydraulic conductivity of the base layer was large, it was found that the absolute post-seismic settlements of the cap-supported pile groups was larger than that of the free-standing pile groups due to the end bearing resistance needing to be remobilised.

- In cases where the hydraulic conductivity of the base layer was low, the absolute post-seismic settlements of the cap-supported pile groups are lower than those of a free-standing pile group, arising from the pile cap continuing to support the axial loads and prevent the plunging failure observed on the free-standing piles.

- Cap-supported pile groups in bearing layers of low hydraulic conductivity settled with the soil surface for a significant period due to the piles being unable to mobilise end bearing resistance. The settlement of these pile groups relative to the soil surface was therefore the smallest. Due to the small relative settlements, the shaft friction in the loose layer was also much smaller in this scenario. The more gradual dissipation of excess pore pressure responsible for the larger absolute pile group settlements, are also responsible for the apparent reduction in shaft friction mobilisation in the bearing layer.

7.9.4 Effect of installation

- Despite the differences in the behaviour of jacked and bored piles in Chapter 6, the behaviour of the jacked piles were found to be broadly in line with the bored piles in this phase of the tests, with their behaviour being largely dependent on whether the relative settlement during the earthquake had led to the pile groups becoming free-standing, or whether the axial load transfer to the pile cap which was apparent on cap-supported pile groups had occurred.

Chapter 8

Conclusions

8.1 Axial behaviour of piled foundations during earthquakes

In the opening chapter, the uncertainty surrounding the performance of piled foundations in liquefiable soils was highlighted, leading to the stated aim of clarifying the load transfer mechanisms which enable the axial loads on a piled foundation to be supported following the onset of liquefaction during a strong seismic event. The subsequent chapters have worked towards this singular aim, and have shown that the axial loads are carried in very different ways during an earthquake, depending largely upon whether the pile group was supported at its cap or whether the pile groups were "free-standing."

The following sections draw together the results from the research programme in order to make conclusions concerning the expected behaviour of pile groups during and after a strong earthquake. The effects of installation significantly affected the co-seismic axial behaviour of the pile groups and hence the conclusions will deal with nominally bored and jacked pile groups separately.

8.1.1 Axial load transfer of "bored" piles

In the scenario of free-standing pile groups in liquefied soil, the majority of axial load is transferred to the ground at the base of the piles, through the end bearing resistance. However, in the early phases of an earthquake, when the excess pore pressures are being generated, significant shaft friction was mobilised near the head of the piles. This effect arises from the induced dilation around the piles due to their lateral movement relative to the soil. However, this mobilised shaft friction near the pile head is a transient effect

191

8. CONCLUSIONS

and once the soil became fully liquefied, the shaft friction recorded in the loose soil became very small. In the dense soil, shaft friction capacity was sustained throughout the earthquake, despite low vertical effective stresses in the bearing layer as a result of the excess pore pressures. This observed shaft friction arises as a result of large lateral stresses being applied to the pile within the bearing layer, which are responsible for the horizontal acceleration of the pile caps.

The absolute settlement of the free-standing pile groups was strongly influenced by the hydraulic conductivity of the bearing layer. With large hydraulic conductivity the increments of excess pore pressure, caused by the increasing axial load on the piles each cycle, dissipate rapidly and hence allow the resistance in the sand to be mobilised at lower displacement, resulting in lower overall settlements.

The contribution of pile cap raft capacity is largely not considered in foundation design for normal working scenarios. However, this aspect significantly affects the behaviour of pile groups under seismic conditions in cases where liquefaction occurs and large pore pressures are generated at depth. Within the range of tests carried out, the absolute settlement of bored pile groups was always larger than that of the soil surface. While the absolute settlements of the pile group were affected by the hydraulic conductivity and thickness of the bearing layer, these parameters appear to have little influence on the magnitude of the pile group's vertical settlement relative to the soil surface. The zone of dilation proposed by Knappett & Madabhushi (2008b) developed as the pile caps settled vertically relative to the soil. The zone of stiffened soil resisted further settlement of the pile caps and led to the rapid unloading of the piles, such that the pile tips ultimately become unloaded, while the pile cap supports the majority of axial load. Despite the continued accumulation of absolute settlement after the piles had become unloaded, no mobilisation of pile end bearing resistance occurred. This effect arises from the softening of the soil beneath the piles occurring as a consequence of the reduction in the axial load on the piles.

However, contrary to the suggestion of Knappett (2006), shaft friction did not appear to be mobilised in the dense sand, but rather in the loose layer as a result of the dilation occurring beneath the pile cap.

In situations where short to medium length piles are to be used in areas where liquefaction could be a problem, it should be considered necessary to ensure that the pile caps and ground beams are suitably designed to support the axial loads from the building.

Where short to medium length piles have already been deployed in the foundation of a building in potentially liquefiable soils, then the ability of the ground beams and pile caps to support the axial loads from the structure must form a part of any assessment of the need to carry out retrofit work.

8.1.2   Axial response of jacked pile groups

While no consideration has previously been given to the influence of installation method on the axial behaviour of piled foundations, it has been shown that this is a critical factor in the dynamic behaviour of piled foundations. In contrast to the bored piles previously considered, jacked piles do not begin to develop absolute settlement until significantly after the beginning of the strong shaking.

The regions of overconsolidated and crushed soil beneath jacked piles leads to a more gradual development of excess pore pressures, such that unlike bored piles, the end bearing capacity of jacked piles is maintained for a significant period following the beginning of the earthquake.

The eventual migration of pore water to the soil below the pile tips leads to the softening of the response of the jacked piles, after which the piles behave in a similar manner to the bored pile groups, developing large settlements and reducing the vertical gap between the pile cap and the soil surface. Once this process occurs, the behaviour of a jacked pile in any future earthquake tends to be similar to that of a bored pile, accumulating settlements throughout the earthquake.

8.2 Post earthquake response of piled foundations

The response of the piled foundations in liquefied soil after the strong shaking has ended is largely dependent on the mobilisation of base capacity, which is strongly affected by the hydraulic conductivity within the bearing layer. If the hydraulic conductivity of the bearing layer is high, excess pore pressures rapidly equalise to the level at the top of the layer, bringing rapid increases in the available pile end bearing capacity. Consequently, axial loads can be fully supported by the pile tip very soon after the end of the strong shaking. Absolute settlements are then restricted to those required to mobilise the axial resistance. Post-earthquake absolute settlements of free-standing pile groups are therefore lower than a similar cap-supported pile group owing to the end bearing resistance remaining mobilised throughout the strong shaking in the former (at the expense of larger co-seismic settlement).

Furthermore, where the hydraulic conductivity of the bearing layer is large, negative shaft friction develops across all of the loose layer, as a result of the soil in this layer settling downwards relative to the pile. In the bearing layer, the larger absolute settlements of the cap-supported pile groups leads to larger positive shaft friction being mobilised in the bearing layer.

If the hydraulic conductivity of the bearing layer is relatively low, the increase in bearing capacity takes place more slowly. Free-standing pile groups therefore suffer large absolute settlements after the strong shaking as the pile group suffers a plunging type failure. By contrast, the absolute settlements of cap-supported pile groups are strongly reduced in comparison with free-standing pile groups since the axial loads do not need to be carried by the piles. The pile group's settlement is limited to that of the soil surface until such times that the bearing capacity is regained in the bearing layer.

Where the hydraulic conductivity of the bearing layer is low, the continuing absolute settlement of the pile group after strong shaking ends means that the downwards settlement of the soil relative to the pile in the loose layer remain low, leading to the shaft friction being positive on average across both the loose and dense soil layers.

8.3 Implications for practice

The experiments conducted in this research programme have highlighted some important aspects which need to be considered in the design of piled foundations for axial load during an earthquake.

- The large relative settlements of all of the bored pile groups in the experiments indicate that during an earthquake, regardless of the initial scenario, it can be expected that if large excess pore pressures are generated across the whole length of the pile, then the pile caps and base of the structure will begin to carry large axial loads. In these scenarios, the structural performance of the building will be improved by the use of large and robust pile caps, with well designed connections between the cap and piles.

- In scenarios where the end bearing capacity of a pile can be sustained for a significant period of the earthquake, such as jacked pile groups or piles which extend significantly in to competent base soils, then it must be expected that the soil will settle away from the pile caps, and the ensuing behaviour will resemble that of a free-standing pile group. In these scenarios, the piles must be designed to carry the additional axial loads which are required to resist the dynamic moments.

- The compressive stresses on the pile can be reduced significantly during an earthquake, either as the result of the piles countering the dynamic moments on the structure through a increase/decrease of axial load on different piles within the structure, or as a result of the axial loads transferring to the pile cap. In either scenario, concrete piles will become more vulnerable to tensile stresses set up as a result of bending moments in the piles. Therefore the design of piles in regions of high seismicity should not rely on compressive stresses from the structure's dead load when designing against the dynamic bending moments on the pile.

- Following an earthquake, in situations where the pile base capacity is either sustained throughout the strong shaking or regained rapidly afterwards, the settlements of the pile group will be small and therefore horizontal gaps, such as those shown in Chapter 1 will form and therefore, remedial work will likely be required.

- The hydraulic conductivity strongly influences the response of piles in the period following strong shaking. Particular care must be taken where the design of the building is such that the piles within the different groups supporting the building penetrate into different soil layers. In these scenarios, differential settlements between different pile groups may become an important issue if the dissipation of excess pore pressures does not occur equally in the different layers.

8.4 Directions for future work

8.4.1 Hybrid footings

The results of Chapter 5 demonstrated that during strong earthquakes where liquefaction becomes an issue, short to medium length piles can be expected to shed their axial loads to the connecting pile caps or ground beams. An alternative foundation may therefore be researched where the majority of axial load is carried by strong, stiff footings, but where the moment or shear capacity required under typical working conditions can be enhanced by a number of piles, or one large single pile, which need not have been designed to carry significant axial loading.

8.4.2 Installation effects

The results presented in Chapter 6 have shown that the dynamic response of the pile groups is significantly altered by the method of installation. However, the difficulties in measuring the axial loads during these tests means that the investigation presented was unable to fully clarify the load transfer which takes place on the jacked piles during the earthquake. The mechanisms discussed in Chapter 6 suggest that the hydraulic conductivity of the bearing layer may be a key parameter in determining the point at which the transition in axial behaviour of the jacked pile groups occurs. Further investigation is however required to determine the effect of hydraulic conductivity on the response of jacked pile groups, as well as determining other factors which play a key role in the response of jacked piles.

Additionally, the piles tested in Chapter 6 were tested in a closed-ended condition. However, in the field, jacked or driven piles are often tubular. As these piles are installed, a soil plug tends to form, with the shaft friction on the inside of the pile matching the resistance applied to the soil at the base of the pile. It is implicitly assumed in the tests of Chapter 6 that the soil plugs remain in place during an earthquake. However, the validity of this assumption needs to be investigated since failure of the soil plug will result in an extreme loss of axial capacity, regardless of the excess pore pressures in the base layer.

8.4.3 Response of structures to moderate earthquakes

In all of the tests carried out within this research programme and that of Knappett (2006), the axial response of piled foundations to very strong earthquakes has been considered, and in each case, full liquefaction was achieved within 2 - 3 cycles. However, in more moderate

earthquakes, the build up of excess pore pressures may take place much more slowly, in which case the axial behaviour of the piled foundations might be significantly changed, due to the slower degradation of axial capacity. Further research could therefore be carried out to investigate the axial behaviour of piled foundations in less severe earthquake earthquake conditions and where full liquefaction might not be reached. Such research would also be highly useful in clarifying the co-seismic settlement behaviour of piles at lower levels of excess pore pressure generation.

Additionally, it was discussed in Section 3.3.2 that the input motions applied by the SAM actuator might be subjecting the models to more severe loading than a real earthquake, where only a few cycles of high amplitude ground motion might be experienced. The results of Chapters 4 & 5 have focussed on the role of the lateral loads in the observed axial behaviour of the pile group. It is therefore necessary to investigate the effect of more "realistic" ground motions on the observed axial response of the foundations.

8.4.4   Effect of pile cap rotation

The experiments described within this thesis involved the behaviour of a single, isolated pile group. The settlement behaviour of the pile groups discussed in Chapter 6 as well as that described by Knappett & Madabhushi (2008a) involves a rocking of the pile group from side to side. An integral part of the mechanism involves the rotation of the pile cap as each leg experiences an increment of settlement when the axial loads are increasing once per cycle. However, in Chapter 1, it was noted that often piles and pile groups are not found in isolation, but form part of a larger foundation design. Figure 8.1 shows a hypothetical large building which is supported by multiple pile groups which are connected by ground beams. As shown in Figure 8.1, consideration must be given to whether the observed mechanisms are physically possible in real life - will the structure and ground beams act to prevent the rotation of the pile caps during an earthquake, and if so, to what extent will this affect the axial behaviour of the pile group? Will this remove the cyclic component of axial load during an earthquake, or will the cyclic component of axial load be applied to the pile group as a whole, as the dynamic moments are resisted by a number of pile groups within the structural system? The importance of considering the appropriate boundary conditions acting on the pile cap has been shown by Haskell *et al.* (2012), where consideration of the lateral restraint which acts on a pile cap in laterally spreading ground led to a different pile group failure mechanism being observed. Preventing the rotation of the pile cap, while allowing lateral and vertical translation will however be a difficult objective for a centrifuge experiment (though theoretically could be achieved with a series of guides which allow translation of the structure) and therefore it may be that this aspect would require the use of a numerical model to achieve. In

(a) Single pile group

(b) Integration of multiple pile groups within a larger building foundation system
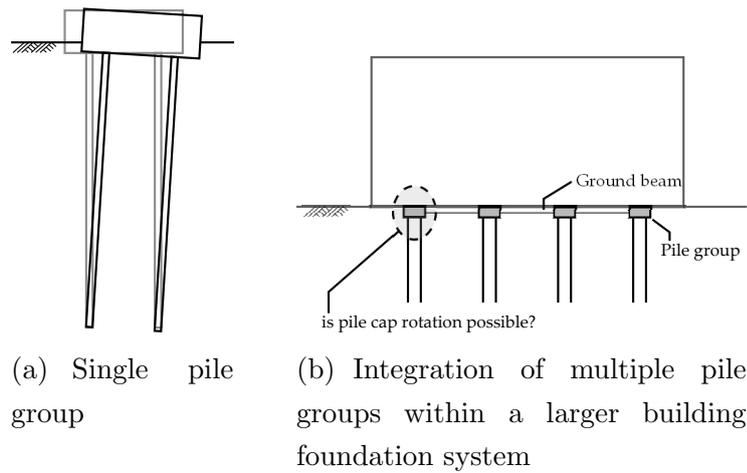
Figure 8.1: Pile cap boundary conditions

this scenario, the results from the centrifuge experiments obtained during this research programme could be used initially to validate the results from a numerical model where the pile cap is not restrained. If the model is able to replicate the behaviour of the pile group, then further analyses could be carried out where rotational fixity is applied to the pile cap.

References

ABBIREDDY, C.O.R. & CLAYTON, C.R.I. (2009). 'A review of modern particle sizing methods'. *Proceedings of the ICE - Geotechnical Engineering*, **162**(4):193–201.

ABDOUN, T., DOBRY, R., O'ROURKE, T.D. & GOH, S.H. (2003). 'Pile response to lateral spreads: Centrifuge modeling'. *Journal of Geotechnical and Geoenvironmental Engineering*, **129**(10):869–878.

ALONSO, E.E., JOSA, A. & LEDESMA, A. (1984). 'Negative Skin Friction on Piles - a Simplified Analysis and Prediction Procedure'. *Geotechnique*, **34**(3):341–357.

AMIRA, M., YOKOYAMA, Y. & IMAIZUMI, S. (1995). 'Friction Capacity of axially loaded model pile in sand'. *Soils and Foundations*, **35**(1):75–82.

BEREZANTZEV, V., KHRISTOFOROV, V. & GOLUBKOV, V. (1961). 'Load bearing capacity and deformation of piled foundations'. In *5th International Conference on Soil Mechanics and Foundation Engineering*, vol. 2, 11–15, Dunod Press, Paris, France.

BERRILL, J.B., CHRISTENSEN, S.A., KEENAN, R.P., OKADA, W. & PETTINGA, J.R. (2001). 'Case study of lateral spreading forces on a piled foundation'. *Geotechnique*, **51**(6):501–517.

BHATTACHARYA, S. (2003). *Pile instability during earthquake liquefaction*. Ph.D. thesis, University of Cambridge.

BHATTACHARYA, S., MADABHUSHI, S.P.G. & BOLTON, M.D. (2004). 'An alternative mechanism of pile failure in liquefiable deposits during earthquakes'. *Geotechnique*, **54**(3):203–213.

BOLTON, M. (1979). *A guide to soil mechanics*. Macmillan, London.

BOULANGER, R.W. & BRANDENBERG, S.J. (2004). 'Neutral plane solution for liquefaction-induced down-drag on vertical piles'. In M.K. Yegian & E. Kavazanjian, eds., *Geotechnical Engineering for Transportation Projects*, vol. 1 of *Geotechnical Special Publication 126*, 470–478, ASCE, New York.

REFERENCES

BOULANGER, R.W., KUTTER, B., BRANDENBERG, S., SINGH, P. & CHANG, D. (2003). 'Pile foundations in liquefied and laterally spreading ground during earthquakes: centrifuge experiments and analyses'. Tech. Rep. UCD/CGM-03/01, University of California at Davis.

BRADLEY, B. (2011). 'Comparing the ground motion of the Feb 2011 quake to the September 2010 quake, Version 4'. Tech. rep., New Zealand Society for Earthquake Engineering.

BRANDENBERG, S.J., BOULANGER, R.W., KUTTER, B.L. & CHANG, D.D. (2005). 'Behavior of pile foundations in laterally spreading ground during centrifuge tests'. *Journal of Geotechnical and Geoenvironmental Engineering*, **131**(11):1378–1391.

BRANDENBERG, S.J., BOULANGER, R.W., KUTTER, B.L. & CHANG, D.D. (2007). 'Liquefaction-induced softening of load transfer between pile groups and laterally spreading crusts'. *Journal of Geotechnical and Geoenvironmental Engineering*, **133**(1):91–103.

BRAY, J.D. & FROST, D. (2010). 'Geo-engineering Reconnaissance of the 2010 Maule, Chile Earthquake'. Tech. Rep. GEER-022, GEER.

BRENNAN, A.J., THUSYANTHAN, N.I. & MADABHUSHI, S.P.G. (2005). 'Evaluation of shear modulus and damping in dynamic centrifuge tests'. *Journal of Geotechnical and Geoenvironmental Engineering*, **131**(12):1488–1497.

BRENNAN, A.J., MADABHUSHI, S.P.G. & HOUGHTON, N.E. (2006). 'Comparing laminar and equivalent shear beam (ESB) containers for dynamic centrifuge modelling'. In C.W.W. Ng, L.M. Zhang & Y.H. Wang, eds., *6th International Conference on Physical Modelling in Geotechnics (ICPMG 2006)*, 171–176, Taylor & Francis Ltd, Hong Kong.

BROWN, D., MORRISON, C. & REESE, L. (1988). 'Lateral load behaviour of pile group in sand'. *Journal of Geotechnical Engineering*, **114**(11):1261–1276.

CARNEVALE, R. & ELGAMAL, A. (1993). 'Experimental results of RPI centrifuge Model No. 4b'. In K. Arulanandan & R. Scott, eds., *Verifications of numerical procedures for the analyses of soil liquefaction problems*, vol. 1, 691–700, Balkema, Davis, USA.

CASAGRANDE, A. (1936). 'Characteristics of cohesionless soils affecting the stability of slopes and earth fills'. *Journal of the Boston Society of Civil Engineers*, **23**(1):13–32.

CASTRO, G. (1975). 'Liquefaction and cyclic mobility of saturated sands'. *Journal of the Geotechnical Engineering Division*, **101**(GT6):551–569.

CHAKRABORTTY, P., POPESCU, R. & PHILLIPS, R. (2011). 'Liquefaction of heterogeneous sand: Centrifuge study'. *Geotechnical Testing Journal*, **34**(3):227–237.

CHARLIE, W.A., ALLARD, D.J. & DOEHRING, D.O. (2009). 'Pile Settlement and Uplift in Liquefying Sand Deposit'. *Geotechnical Testing Journal*, **32**(2):147–156.

CHIAN, S., STRINGER, M.E. & MADABHUSHI, S.P.G. (2010). 'Use of automatic sand pourers for loose sand models'. In S. Springman, J. Laue & L. Seward, eds., *Physical Modelling in Geotechnics*, vol. 1, 117–121, Taylor & Francis, Zurich, Switzerland.

COELHO, P. (2007). *In situ densification as a liquefaction resistance measure for bridge foundations*. Phd, University of Cambridge.

COELHO, P.A.L.F., HAIGH, S.K., GOPAL MADABHUSHI, S.P. & O'BRIEN, T.S. (2007). 'Post-earthquake behaviour of footings employing densification to mitigate liquefaction'. *Ground Improvement*, **11**(1):45–53.

CRESSWELL, A., BARTON, M.E. & BROWN, R. (1999). 'Determining the maximum density of sands by pluviation'. *Geotechnical Testing Journal*, **22**(4):324–328.

CUBRINOVSKI, M. & ISHIHARA, K. (1999). 'Empirical correlation between SPT N-value and relative density for sandy soils'. *Soils and Foundations*, **39**(5):61–71.

CUBRINOVSKI, M., KOKUSHO, T. & ISHIHARA, K. (2006). 'Interpretation from large-scale shake table tests on piles undergoing lateral spreading in liquefied soils'. *Soil Dynamics and Earthquake Engineering*, **26**(2-4):275–286.

DE ALBA, P.A. (1983). 'Pile settlement in liquefying sand deposit'. *Journal of Geotechnical Engineering*, **109**(9):1165–1180.

DEEKS, A.D., WHITE, D.J. & BOLTON, M.D. (2005). 'A comparison of jacked, driven and bored piles in sand'. In *16th International Conference on Soil Mechanics and Geotechnical Engineering*, vol. 4, 2103–2106, Millpress Science Publishers, Osaka, Japan.

DEWOOLKAR, M.M., HO, H.Y. & PAK, R.Y.S. (1998). 'Suitability of total stress gages for soil pressure measurements'. In T. Kimura, O. Kusakabe & J. Takemura, eds., *Centrifuge 98*, vol. 1, 129–134, Balkema, Tokyo.

DOBRY, R. & ABDOUN, T. (2011). 'An investigation into why liquefaction charts work: A necessary step toward integrating the states of art and practice'. In *5th International Conference on Earthquake Geotechnical Engineering*, 13–44, Santiago, Chile.

DUNGCA, J.R., KUWANO, J., TAKAHASHI, A., SARUWATARI, T., IZAWA, J., SUZUKI, H. & TOKIMATSU, K. (2006). 'Shaking table tests on the lateral response of a pile buried in liquefied sand'. *Soil Dynamics and Earthquake Engineering*, **26**(2-4):287–295.

REFERENCES

ELGAMAL, A., YANG, Z.H., LAI, T., KUTTER, B.L. & WILSON, D.W. (2005). 'Dynamic response of saturated dense sand in laminated centrifuge container'. *Journal of Geotechnical and Geoenvironmental Engineering*, **131**(5):598–609.

ELLIS, E.A., SOGA, K., BRANSBY, M.F. & SATO, M. (2000). 'Resonant column testing of sands with different viscosity pore fluids'. *Journal of Geotechnical and Geoenvironmental Engineering*, **126**(1):10–17.

FARRELL, T. & KUTTER, B. (1993). 'Experimental results of Model No. 12'. In K. Arulanandan & R.F. Scott, eds., *Verifications of numerical procedures for the analysis of soil liquefaction problems*, vol. 1, 1027–1035, Balkema, Davis, USA.

FELLENIUS, B.H. (1972). 'Down-drag on piles in clay due to negative skin friction'. *Canadian Geotechnical Journal*, **9**(4):323 – 337.

FELLENIUS, B.H. (1984). 'Negative skin friction and settlement of piles'. In *2nd International Seminar on Pile Foundations*, Nanyang Technical Institute, Singapore.

FELLENIUS, B.H. & SIEGEL, T.C. (2008). 'Pile drag load and downdrag in a liquefaction event'. *Journal of Geotechnical and Geoenvironmental Engineering*, **134**(9):1412–1416.

FIEGEL, G.L. & KUTTER, B.L. (1994). 'Liquefaction-induced lateral spreading of mildly sloping ground'. *Journal of Geotechnical Engineering*, **120**(12):2236–2243.

FIORAVANTE, V. (2002). 'On the shaft friction modelling of non-displacement piles in sand'. *Soils and Foundations*, **42**(2):23–33.

FLEMING, W.G.K. (1992). 'A New Method for Single Pile Settlement Prediction and Analysis'. *Geotechnique*, **42**(3):411–425.

FLEMING, W.G.K., WELTMAN, A., RANDOLPH, M. & ELSON, W. (2009). *Piling engineering*. Taylor & Francis, 3rd edn.

FLORIN, V. & IVANOV, P. (1961). 'Liquefaction of saturated sandy soils'. In *5th International conference on soil mechanics and foundation engineering*, vol. 1, 107–111, Dunod, Paris.

FORAY, P., BALACHOWSKI, L. & RAULT, G. (1998). 'Scale effect in shaft friction due to the localisation of deformations'. In T. Kimura, O. Kusakabe & J. Takemura, eds., *Centrifuge 98*, vol. 1, 211–216, Balkema, Tokyo.

FORAY, P., TSUHA, C., SILVA, M., JARDINE, R., YANG, Z. & RIMOY, S. (2011). 'Soil-pile interaction on an instrumented pile under cyclic axial loads in sand'. In *5th International Conference on Earthquake Geotechnical Engineering*, Santiago, Chile.

FUJII, S., ISEMOTO, N., SATOU, Y., KANEKO, O., FUNAHARA, H., ARAI, T. & TOKIMATSU, K. (1998). 'Investigation and analysis of a pile foundation damaged by liquefaction during the 1995 Hyogoken-Nambu Earthquake'. *Soils and Foundations*, **Special issue No.2 on geotechnical aspects of the January 17 1995 Hyogoken-Nambu earthquake**:179–192.

FUKUMURA, K., MATSUMOTO, T., OHNO, A. & HASHIZUME, Y. (2003). 'Experimental study on behaviour of model piled raft foundations in sand using shaking table at 1-g gravitational field'. In T. Newson, ed., *BGA International Conference on Foundations: Innovations, observations, design and practice*, 307–320, Thomas Telford, Dundee, UK.

GAVIN, K. & LEHANE, B.M. (2003). 'End bearing of small pipe piles in dense sand'. In T. Newson, ed., *BGA International Conference on Foundations: Innovations, observations, design and practice*, 321–330, Thomas Telford, Dundee, UK.

GONZALEZ, L., ABDOUN, T. & DOBRY, R. (2009). 'Effect of Soil Permeability on Centrifuge Modeling of Pile Response to Lateral Spreading'. *Journal of Geotechnical and Geoenvironmental Engineering*, **135**(1):62–73.

GUI, M.W. & BOLTON, M. (1998). 'Geometery and scale effects in CPT and pile design'. In Robertson & Mayne, eds., *1st International Conference on Site Characterisation*, 1063–1068, Balkema, Atlanta.

GUI, M.W., BOLTON, M.D., GARNIER, J., CORTE, J.F., BAGGE, G., LAUE, J. & RENZI, R. (1998). 'Guidelines for cone penetration tests in sand'. In T. Kimura, O. Kusakabe & J. Takemura, eds., *Centrifuge 98*, vol. 1, 155–160, Balkema Publishers, Tokyo.

HAIGH, S.K. (2002). *Effects of earthquake-induced liquefaction on pile foundations in sloping ground*. Ph.D. thesis, University of Cambridge.

HAIGH, S.K. & MADABHUSHI, S. (2011). 'Centrifuge modelling of pile-soil interaction in liquefiable slopes'. *Geomechanics and Engineering*, **3**(1):1–16.

HASKELL, J., MADABHUSHI, S. & CUBRINOVSKI, M. (2012). 'Boundary conditions in physical model tests   the influence of deck pinning on the response of piled bridge abutments in laterally spreading soils'. In *State of the Art and Practice in Geotechnical Engineering*, ASCE, San Francisco.

HERME, P. (2009). *Macaron (in French)*. agnes vienot, Paris.

HORIKOSHI, K., MATSUMOTO, T., HASHIZUME, Y. & WATANABE, T. (2003). 'Performance of piled raft foundations subjected to dynamic loading'. *International Journal of Physical Modelling in Geotechnics*, **3**(2):51–62.

REFERENCES

Hushmand, B., Scott, R.F. & Crouse, C.B. (1988). 'Centrifuge liquefaction tests in a laminar box'. *Geotechnique*, **38**(2):253–262.

Hyodo, M., Hyde, A.F.L. & Aramaki, N. (1998). 'Liquefaction of crushable soils'. *Geotechnique*, **48**(4):527–543.

Imamura, S., Hagiwara, T., Tsukamoto, Y. & Ishihara, K. (2004). 'Response of pile groups against seismically induced lateral flow in centrifuge model tests'. *Soils and Foundations*, **44**(3):39–55.

Inagaki, H., Iai, S., Sugano, T., Yamazaki, H. & Inatomi, T. (1996). 'Performance of caisson type quay walls at Kobe Port'. *Soils and Foundations*, **Special issue on geotechnical aspects of the January 17 1995 Hyogoken-Nambu earthquake**:119–136.

Ishihara, K. (1993). 'Liquefaction and Flow Failure during Earthquakes'. *Geotechnique*, **43**(3):351–415.

Ishihara, K. (1996). *Soil behaviour in earthquake geotechnics*. Oxford University Press, Oxford.

Ishihara, K. & Takatsu, H. (1979). 'Effects of overconsolidation and K_0 conditions on the liquefaction characteristics of sands'. *Soils and Foundations*, **19**(4):59–68.

Ishihara, K. & Yoshimine, M. (1992). 'Evaluation of settlements in sand deposits following liquefaction during earthquakes'. *Soils and Foundations*, **32**(1):173–188.

Ishihara, K., Tatsuoka, F. & Yasuda, S. (1975). 'Undrained deformation and liquefaction of sand under cyclic stresses'. *Soils and Foundations*, **15**(1):29–44.

Japanese Geotechnical Society (1996). 'Selected photographs on the 1995 Hyogoken-Nambu earthquake'. *Soils and Foundations*, **Special issue on geotechnical aspects of the January 17 1995 Hyogoken-Nambu earthquake**.

Klotz, E.U. & Coop, M.R. (2001). 'An investigation of the effect of soil state on the capacity of driven piles in sands'. *Geotechnique*, **51**(9):733–751.

Knappett, J. (2006). *Piled foundations in liquefiable soils: accounting for axial loads*. Ph.D. thesis, University of Cambridge.

Knappett, J. & Madabhushi, G. (2008a). 'Mechanism of pile group settlement in liquefiable soils'. In *Geotechnical Earthquake Engineering and Soil Dynamics IV*, Geotechnical Special Publication 181, Sacramento, CA.

Knappett, J. & Madabhushi, G. (2009a). 'Seismic bearing capacity of piles in liquefiable soils'. *Soils and Foundations*, **49**(4):525–536.

KNAPPETT, J.A. & MADABHUSHI, S.P.G. (2008b). 'Liquefaction-Induced Settlement of Pile Groups in Liquefiable and Laterally Spreading Soils'. *Journal of Geotechnical and Geoenvironmental Engineering*, **134**(11):1609–1618.

KNAPPETT, J.A. & MADABHUSHI, S.P.G. (2009b). 'Influence of axial load on lateral pile response in liquefiable soils. Part I: physical modelling'. *Geotechnique*, **59**(7):571–581.

KNAPPETT, J.A. & MADABHUSHI, S.P.G. (2009c). 'Influence of axial load on lateral pile response in liquefiable soils. Part II: numerical modelling'. *Geotechnique*, **59**(7):583–592.

KONIG, D., JESSBERGER, H.L., BOLTON, M., PHILLIPS, R., BAGGE, G., RENZI, R. & GARNIER, J. (1994). 'Pore pressure measurement during centrifuge model tests - experience of 5 laboratories'. In C. Leung, F. Lee & T. Tan, eds., *Centrifuge 94*, 101–108, Balkema, Singapore.

KRAMER, S. (1996). *Earthquake Geotechnical Engineering*. Prentice Hall, London.

KULASINGHAM, R. (2003). *Effects of void redistribution on liquefaction-induced deformations*. Ph.D. thesis, University of California.

KUO, M. (2011). *The influence of bacteria on the mechanical properties of deep-ocean clay sediments*. Ph.D. thesis, University of Cambridge.

KUTTER, B.L. & BALAKRISHNAN, A. (1998). 'Dynamic model test data from electronics to knowledge'. In T. Kimura, O. Kusakabe & J. Takemura, eds., *Centrifuge 98*, vol. 2, 931–943, Balkema, Tokyo.

KUTTER, B.L. & WILSON, D. (1999). 'De-liquefaction shock waves'. In T.D. O'Rourke, J. Bardet & M. Hamada, eds., *7th US-Japan Workshop on Earthquake Resistant Design of Lifeline Facilities and Countermeasures Against Liquefaction*, 295–310, MCEER, Seattle, WA.

KUTTER, B.L., GAJAN, S., MANDA, K.K. & BALAKRISHNAN, A. (2004). 'Effects of layer thickness and density on settlement and lateral spreading'. *Journal of Geotechnical and Geoenvironmental Engineering*, **130**(6):603–614.

LARSON, H. (1977). *Earth pressure around buried pipes*. Ph.D. thesis, University of Cambridge.

LEHANE, B.M. & WHITE, D.J. (2005). 'Lateral stress changes and shaft friction for model displacement piles in sand'. *Canadian Geotechnical Journal*, **42**(4):1039–1052.

REFERENCES

Lehane, B.M., Jardine, R.J., Bond, A.J. & Frank, R. (1993). 'Mechanisms of Shaft Friction in Sand from Instrumented Pile Tests'. *Journal of Geotechnical Engineering*, **119**(1):19–35.

Li, Z. (2010). *Piled foundations subjected to cyclic loads or earthquakes*. Ph.D. thesis, University of Cambridge.

Loukidis, D. & Salgado, R. (2008). 'Analysis of the shaft resistance of non-displacement piles in sand'. *Geotechnique*, **58**(4):283–296.

Luong, M. & Sidaner, J. (1981). 'Undrained behaviour of cohesionless soils under cyclic and transient loading'. In S. Prakash, ed., *1st International Conference on Recent Advances in Geotechnical Earthquake Engineering and Soil Dynamics*, vol. 1, 215–220, University of Missouri-Rolla, St Louis.

Madabhushi, S., Schofield, A.N. & Zeng, X. (1994). 'Complementary shear stresses in dynamic centrifuge modelling'. In R. Ebelhar, V. Drnevich & B.L. Kutter, eds., *Dynamic Geotechnical Testing II*, vol. 2 of *STP 1213*, 346–359, ASTM, San Francisco.

Madabhushi, S.P.G. (1992). *Response of tower structures to earthquake perturbations*. Ph.D. thesis, University of Cambridge.

Madabhushi, S.P.G. (1994). 'Effect of pore fluid in dynamic centrifuge modelling'. In C. Leung, F. Lee & T. Tan, eds., *Centrifuge 94*, 127–132, Balkema, Singapore.

Madabhushi, S.P.G., Schofield, A.N. & Lesley, S. (1998). 'A new Stored Angular Momentum (SAM) based earthquake actuator'. In T. Kimura, O. Kusakabe & J. Takemura, eds., *Centrifuge 98*, vol. 1, 111–116, Balkema, Tokyo.

Madabhushi, S.P.G., Patel, D. & Haigh, S.K. (2005). 'Geotechnical aspects of Bhuj Earthquake'. In *The Bhuj, India Earthquake of 26th January 2001*, Institute of Structural Engineers, London.

Madabhushi, S.P.G., Houghton, N.E. & Haigh, S.K. (2006). 'A new automatic sand pourer for model preparation at University of Cambridge'. In C.W.W. Ng, L.M. Zhang & Y.H. Wang, eds., *Physical Modelling in Geotechnics - 6th ICPMG '06*, 217–222, Taylor & Francis, Hong Kong.

Maheetharan, A. (1990). *Modelling the seismic response of piles and pile groups*. Ph.D. thesis, University of Cambridge.

Martin, G.R., Finn, W.D.L. & Seed, H.B. (1975). 'Fundamentals of liquefaction under cyclic loading'. *Journal of the Geotechnical Engineering Division*, **101**(5):423–438.

McVay, M., Zhang, L.M., Molnit, T. & Lai, P. (1998). 'Centrifuge testing of large laterally loaded pile groups in sands'. *Journal of Geotechnical and Geoenvironmental Engineering*, **124**(10):1016–1026.

Meyerhof, G. (1976). 'Bearing capacity and settlement of pile foundations'. *Journal of the Geotechnical Engineering Division*, **102**(GT3):197–228.

Mitchell, R.J. & Dubin, B.I. (1986). 'Pore Pressure Generation and Dissipation in Dense Sands under Cyclic Loading'. *Canadian Geotechnical Journal*, **23**(3):393–398.

Mitrani, H. (2006). *Liquefaction Remediation Techniques for Existing Buildings*. Ph.D. thesis, University of Cambridge.

Morris, D. (1979). *The centrifugal modelling of dynamic behaviour*. Ph.D. thesis, University of Cambridge.

Mortara, G., Ferrara, D. & Fotia, G. (2010). 'Simple Model for the Cyclic Behavior of Smooth Sand-Steel Interfaces'. *Journal of Geotechnical and Geoenvironmental Engineering*, **136**(7):1004–1009.

Motamed, R., Towhata, I., Honda, T., Yasuda, S., Tabata, K. & Nakazawa, H. (2009). 'Behaviour of pile group behind a sheet pile quay wall subjected to liquefaction-induced large ground deformation observed in shaking test in E-Defense project'. *Soils and Foundations*, **49**(3):459–475.

Muir Wood, D. (2004). *Geotechnical modelling*. Spon Press, London.

O'Rourke, T.D., Meyersohn, W., Shiba, Y. & Chaudhuri, D. (1994). 'Evaluation of pile response to liquefaction-induced lateral spread'. In T.D. O'Rourke & M. Hamada, eds., *Fifth U.S.-Japan workshop on earthquake resistant design of lifeline facilities and countermeasures against soil liquefaction*, 457–479, Buffalo, N.Y, USA.

Pamuk, A., Zimmie, T. & Abdoun, T. (2003). 'Pile group foundations subjected to seimically induced lateral spreading'. In T. Newson, ed., *BGA international conference on Foundations: innovations, observations design and practice*, 715–722, Thomas Telford, Dundee, UK.

Phillips, R. & Sekiguchi, H. (1991). 'Water wave trains in a drum centrifuge'. Tech. Rep. CUED/D-SOILS/TR249, University of Cambridge.

Poulos, H.G. (2001). 'Piled raft foundations: design and applications'. *Geotechnique*, **51**(2):95–113.

Randolph, M.F. (2003). 'Science and empiricism in pile foundation design'. *Geotechnique*, **53**(10):847–874.

REFERENCES

ROBERTSON, P.K. & CAMPANELLA, R.G. (1983). 'Interpretation of Cone Penetration Tests .1. Sand'. *Canadian Geotechnical Journal*, **20**(4):718–733.

ROLLINS, K. & STRAND, S. (2006). 'Downdrag forces due to liquefaction surrounding a pile'. In *8th US National Conference on Earthquake Engineering*, San Francisco, CA.

ROLLINS, K.M., OLSEN, R.J., EGBERT, J.J., JENSEN, D.H., OLSEN, K.G. & GARRETT, B.H. (2006). 'Pile spacing effects on lateral pile group behavior: Load tests'. *Journal of Geotechnical and Geoenvironmental Engineering*, **132**(10):1262–1271.

SCHNEIDER, J. (2007). *Analysis of piexocone data for displacment pile design*. Ph.D. thesis, University of Western Australia.

SCHOFIELD, A. (1981). 'Dynamic and earthquake geotechnical centrifuge modelling'. In S. Prakash, ed., *Recent Advances in Geotechnical Earthquake Engineering and Soil Dynamics*, vol. 3, 1081–1100, University of Missouri-Rolla, St Louis.

SCHOFIELD, A.N. (1980). 'Cambridge Geotechnical Centrifuge Operations'. *Geotechnique*, **30**(3):227–268.

SCHOFIELD, A.N. & WROTH, P. (1968). *Critical state soil mechanics*. European civil engineering series, McGraw-Hill, London, New York [etc.].

SEED, H. (1967). 'Slope stability during earthquakes'. *Journal of the Soil Mechanics and Foundations Division*, **93**(4):299–324.

SEED, H.B. & LEE, K. (1966). 'Liquefaction of saturated sands during cyclic loading'. *Journal of Soil Mechanics and Foundation Engineering*, **92**(SM6):105–134.

SHARP, M., DOBRY, R. & ABDOUN, T. (2003). 'Centrifuge modelling of liquefaction and lateral spreading of virgin, overconsolidated and pre-shaken sand deposits'. *International Journal of Physical Modelling in Geotechnics*, **3**(2):11–22.

SLADEN, J.A., DHOLLANDER, R.D. & KRAHN, J. (1985). 'The liquefaction of sands, a collapse surface approach'. *Canadian Geotechnical Journal*, **22**(4):564–578.

STEWART, D.P., CHEN, Y.R. & KUTTER, B.L. (1998). 'Experience with the use of methylcellulose as a viscous pore fluid in centrifuge models'. *Geotechnical Testing Journal*, **21**(4):365–369.

STONE, K. (1988). *Modelling of rupture development in soils*. Ph.D. thesis, University of Cambridge.

STRINGER, M.E. & MADABHUSHI, S.P.G. (2009). 'Novel computer-controlled saturation of dynamic centrifuge models using high viscosity fluids'. *Geotechnical Testing Journal*, **32**(6):1–6.

STRINGER, M.E. & MADABHUSHI, S.P.G. (2010a). 'Improving model quality in dynamic centrifuge modelling through computer controlled saturation'. In S. Springman, J. Laue & L. Seward, eds., *International Conference on Physical Modelling in Geotechnics*, vol. 1, 171–176, Taylor & Francis, Zurich, Switzerland.

STRINGER, M.E. & MADABHUSHI, S.P.G. (2010b). 'Measuring Shaft Friction During Earthquakes'. In S. Springman, J. Laue & L. Seward, eds., *International Conference on Physical Modelling in Geotechnics*, vol. 2, 1433–1438, Taylor & Francis, Zurich, Switzerland.

STRINGER, M.E. & MADABHUSHI, S.P.G. (2011a). 'The effect of pile installation method on dynamic pile response'. *International Journal of Physical Modelling in Geotechnics*, **11**(3):87–99.

STRINGER, M.E. & MADABHUSHI, S.P.G. (2011b). 'Importance of pile caps in liquefiable soils'. *Geotechnique*, **Under review**.

STRINGER, M.E. & MADABHUSHI, S.P.G. (2011c). 'Re-mobilisation of pile shaft friction after an earthquake'. *Soils and Foundations*, **Under Review**.

STRINGER, M.E. & MADABHUSHI, S.P.G. (2012). 'Axial load transfer in liquefiable soils for free-standing piles'. *Geotechnique*, **Accepted for publication on 19/04/2012**.

STRINGER, M.E., McMAHON, B. & MADABHUSHI, S. (2009). 'CAM-Sat: Computer controlled saturation for geotechnical modelling'. Tech. Rep. CUED/D-SOILS/TR348, University of Cambridge.

STRINGER, M.E., HERON, C. & MADABHUSHI, S.P.G. (2010). 'Experience using MEMS-based accelerometers in dynamic testing'. In S. Springman, J. Laue & L. Seward, eds., *Physical Modelling in Geotechnics*, vol. 1, 389 – 394, Taylor & Francis, Zurich, Switzerland.

SUN, H. (1990). *Ground deformation mechanisms for soil-structure interactions*. Ph.D. thesis, University of Cambridge.

TAKAHASHI, H., KITAZUME, M., ISHIBASI, S. & YAMAWAKI, S. (2006). '"Evaluating the saturation of model ground by P-wave velocity and modeling of models for a liquefaction study"'. *International Journal of Physical Modelling in Geotechnics*, **1**:13–15.

TAN, F. (1990). *Centrifuge and theoretical modelling of conical footings on sand*. Ph.D. thesis, University of Cambridge.

TAYLOR, R.N. (1995). *Geotechnical centrifuge technology*. Blackie Academic, London.

TEYMUR, B. (2002). *The significance of boundary conditions in dynamic centrifuge modelling*. Ph.D. thesis, University of Cambridge.

REFERENCES

TOKIMATSU, K. & SEED, H.B. (1987). 'Evaluation of settlements in sands due to earthquake shaking'. *Journal of Geotechnical Engineering*, **113**(8):861–878.

TOKIMATSU, K. & SUZUKI, H. (2004). 'Pore water pressure response around pile and its effects on P-Y behavior during soil liquefaction'. *Soils and Foundations*, **44**(6):101–110.

TOKIMATSU, K., MIZUNO, H. & KAKURAI, M. (1996). 'Building damage associated with geotechnical problems'. *Soils and Foundations*, **Special issue on geotechnical aspects of the January 17 1995 Hyogoken-Nambu earthquake**:219–234.

TSUCHIDA, H. (1970). 'Prediction and countermeasure against liquefaction in sand deposits'. In *Seminar of the Port and Harbours Research Institute, Ministry of Transport*, 3.1 – 3.33 (In Japanese), Yokosuka, Japan.

UESUGI, M. & KISHIDA, H. (1986). 'Frictional resistance at yield between dry sand and mild steel'. *Soils and Foundations*, **26**(4):139–149.

UZUOKA, R., SENTO, N. & KAZAMA, M. (2008). 'Seepage and inertia effect on rate-dependent reaction of a pile in liquefied soil'. *Soils and Foundations*, **48**(1):15–25.

VESIC, A. (1967). 'A study of bearing capacity of deep foundations'. Tech. Rep. B-189, Georgia Institute of Technology.

WHITE, D.J. (2003). 'PSD measurement using the single particle optical sizing (SPOS) method'. *Geotechnique*, **53**(3):317–326.

WHITE, D.J. & BOLTON, M.D. (2004). 'Displacement and strain paths during plane-strain model pile installation in sand'. *Geotechnique*, **54**(6):375–397.

WHITE, D.J. & BOLTON, M.D. (2005). 'Comparing CPT and pile base resistance in sand'. *Proceedings of the ICE - Geotechnical Engineering*, **158**(1):3–14.

WHITE, D.J. & LEHANE, B.M. (2004). 'Friction fatigue on displacement piles in sand'. *Geotechnique*, **54**(10):645–658.

WILSON, D. (1998). *Soil-pile-superstructure interaction in liquefying sand and soft clay*. Ph.D. thesis, UC Davis.

WONG, K. & TEH, C. (1995). 'Negative skin friction on piles in layered soil deposits'. *Journal of Geotechnical Engineering*, **121**(6):457–465.

YANG, Z.X., JARDINE, R.J., ZHU, B.T., FORAY, P. & TSUHA, C.H.C. (2010). 'Sand grain crushing and interface shearing during displacement pile installation in sand'. *Geotechnique*, **60**(6):469–482.

YASUFUKU, N. & HYDE, A.F.L. (1995). 'Pile end-bearing capacity in crushable sands'. *Geotechnique*, **45**(4):663–676.

YASUFUKU, N., OCHIAI, H. & OHNO, S. (2001). 'Pile end-bearing capacity of sand related to soil compressibility'. *Soils and Foundations*, **41**(4):59–71.

YETGINER, A.G., WHITE, D.J. & BOLTON, M.D. (2006). 'Field measurements of the stiffness of jacked piles and pile groups'. *Geotechnique*, **56**(5):349–354.

ZENG, X. & SCHOFIELD, A.N. (1996). 'Design and performance of an equivalent-shear-beam container for earthquake centrifuge modelling'. *Geotechnique*, **46**(1):83–102.

ZHAO, Y., GAFAR, K., ELSHAFIE, M., DEEKS, A.D., KNAPPETT, J.A. & MADABHUSHI, S.P.G. (2006). 'Calibration and use of a new automatic sand pourer'. In C.W.W. Ng, L.M. Zhang & Y.H. Wang, eds., *Physical Modelling in Geotechnics - 6th ICPMG '06*, vol. 1, 265–270, Taylor & Francis Ltd, Hong Kong.

Appendix A - Model Layouts

This appendix contains the model layouts with the nominal instrumentation positions given in mm.
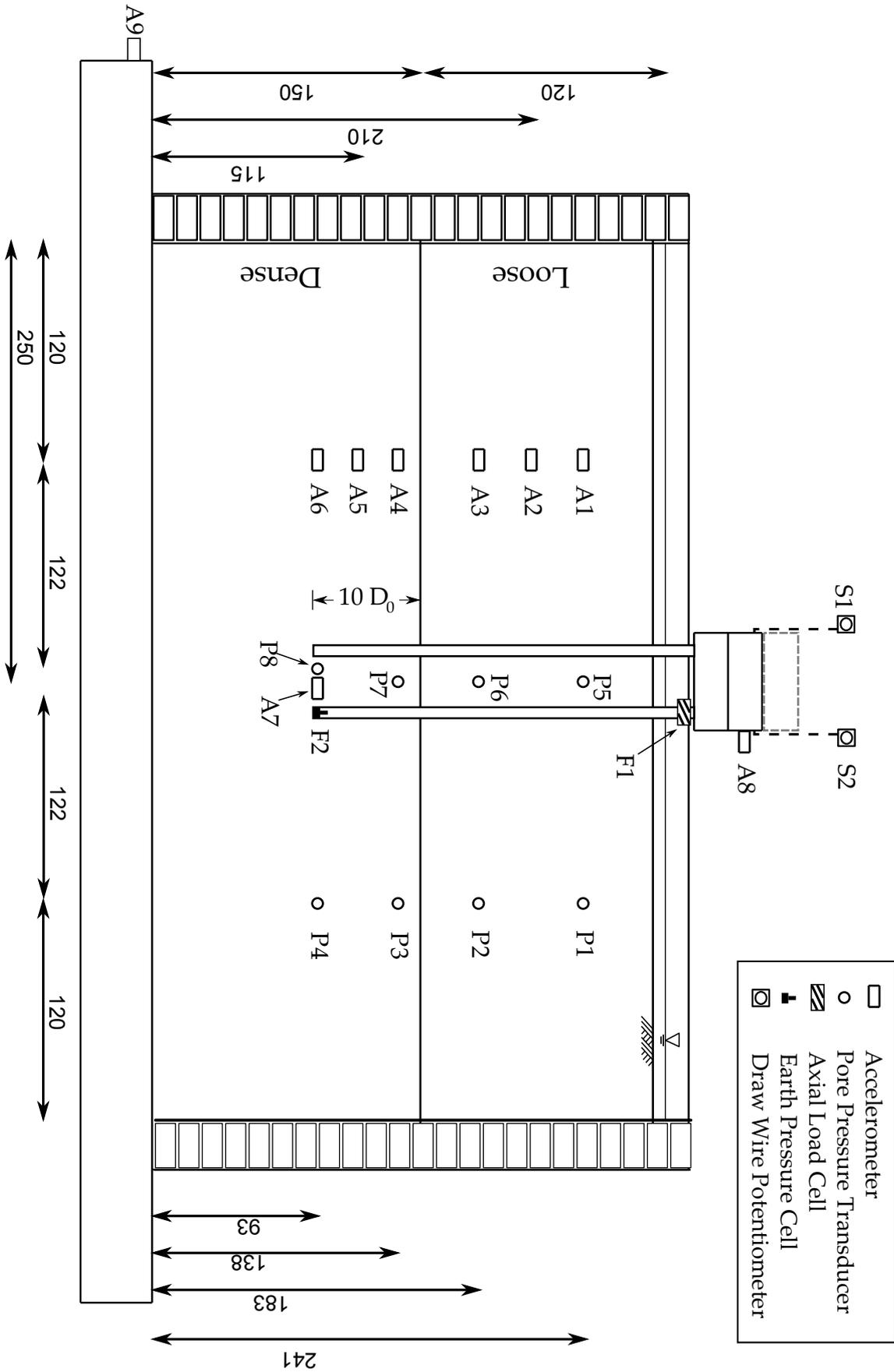
Figure A-i: Nominal instrumentation layout for MS01
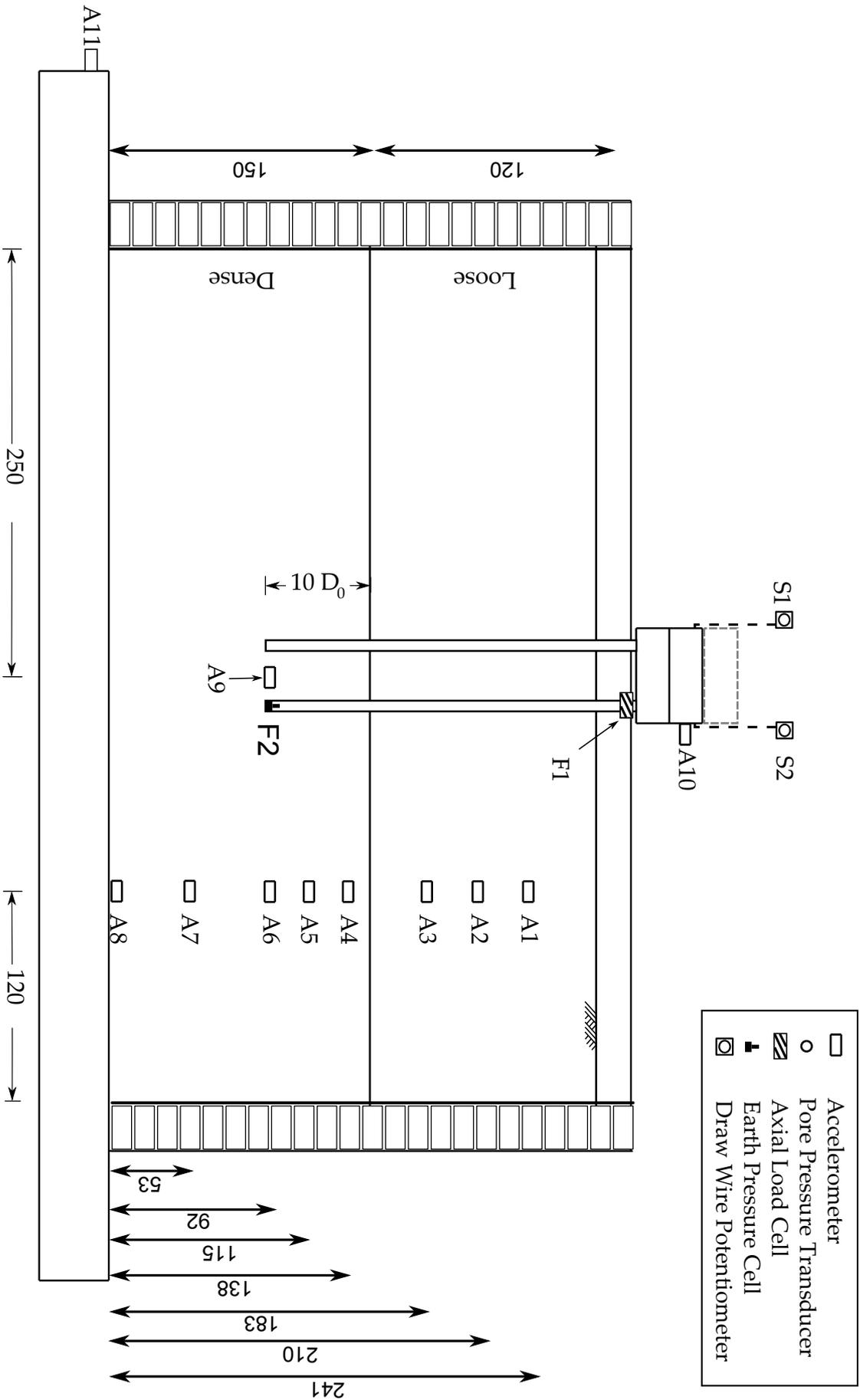
Figure A-ii: Nominal instrumentation layout for MS02
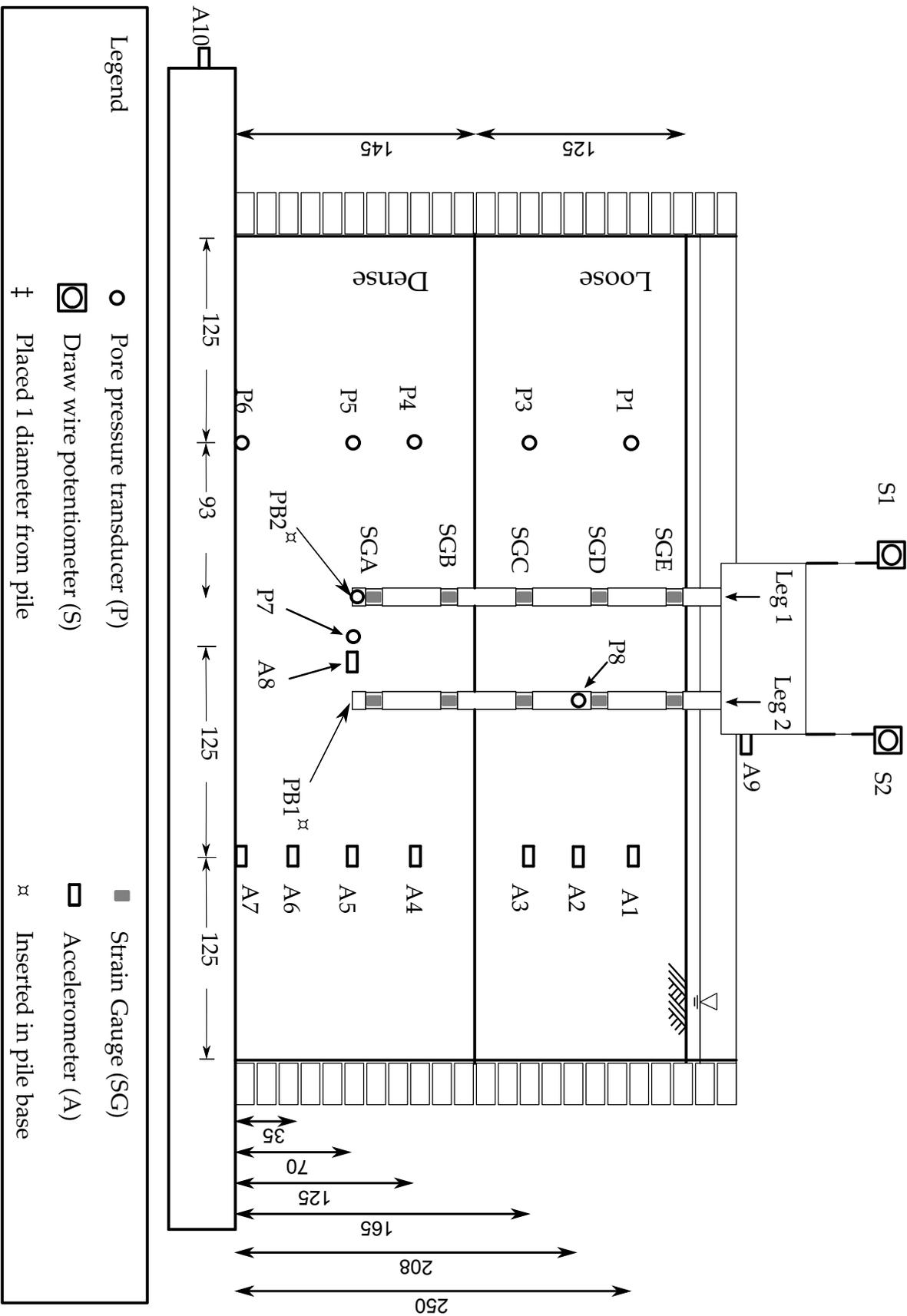
Figure A-iii: Nominal instrumentation layout for MS05
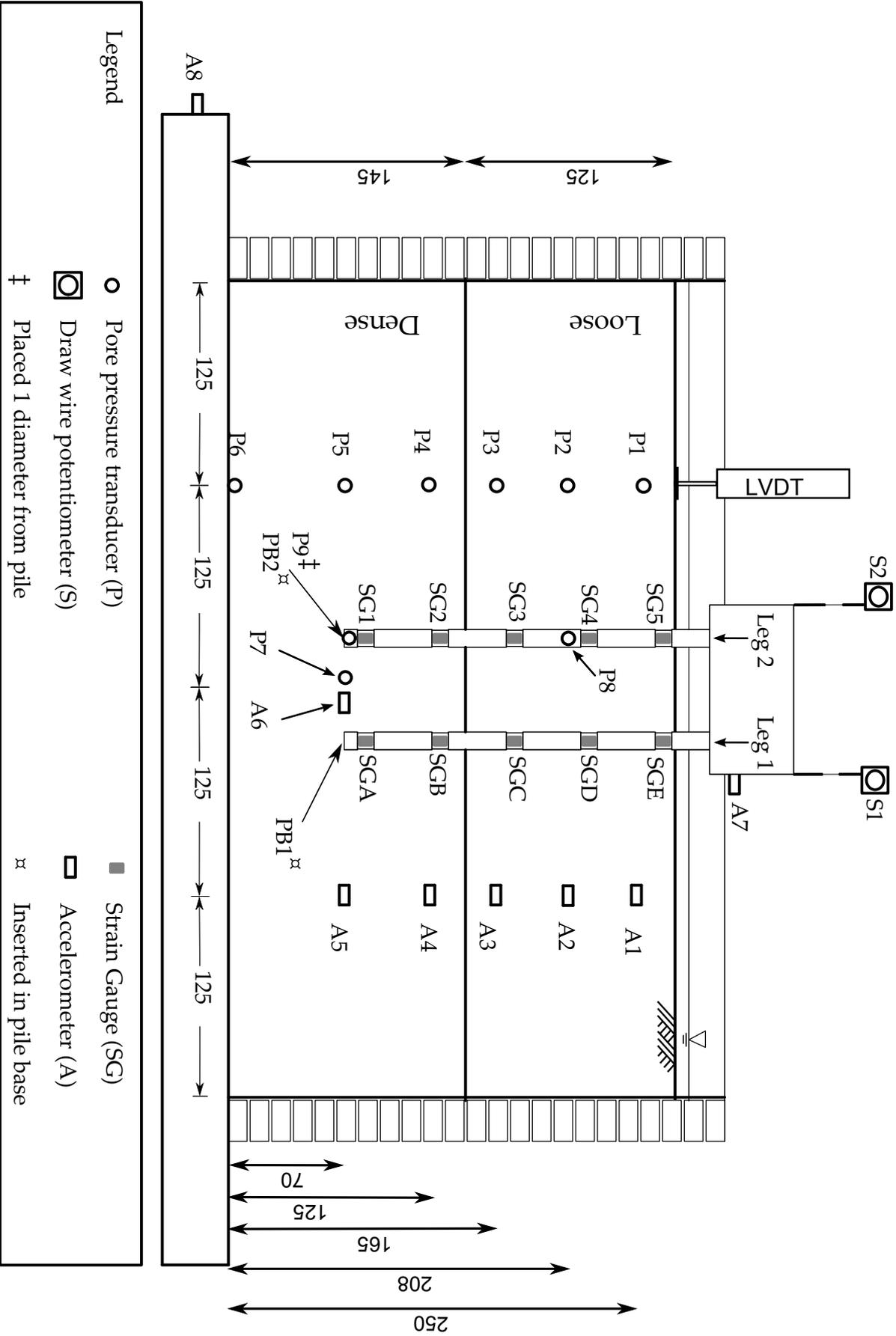
Figure A-iv: Nominal instrumentation layout for MS06
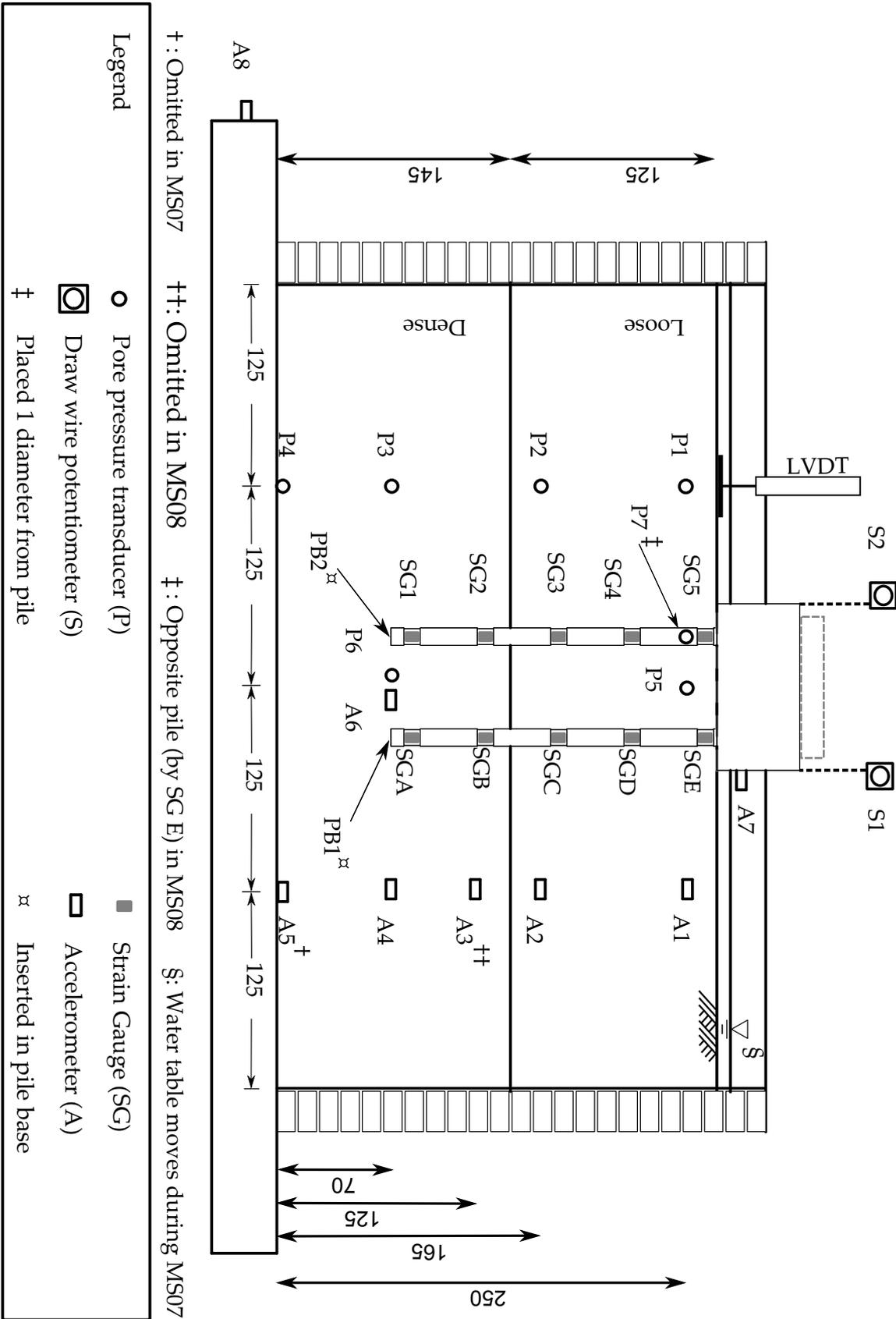
Figure A-v: Nominal instrumentation layout for MS07 and MS08
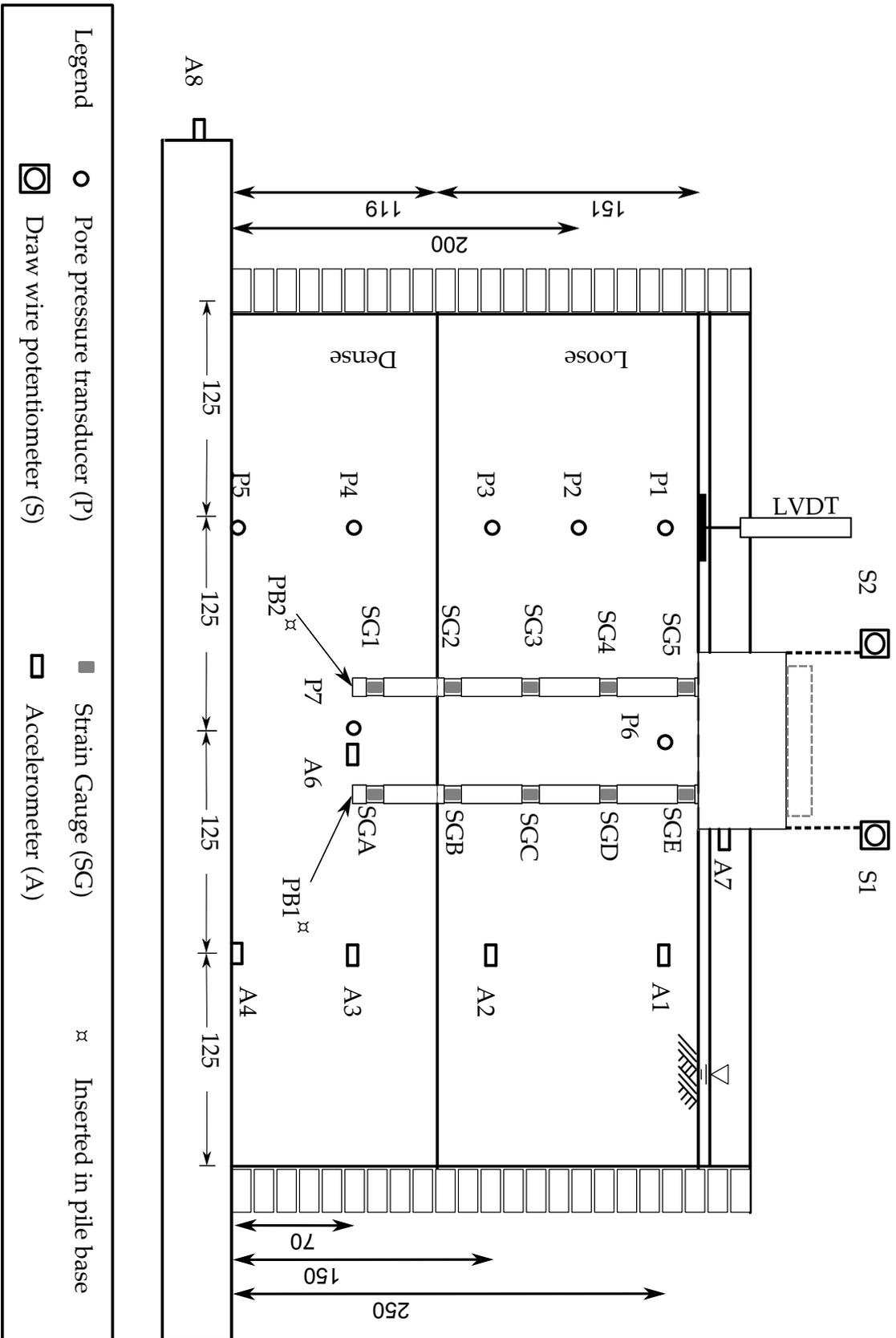
Figure A-vi: Nominal instrumentation layout for MS09
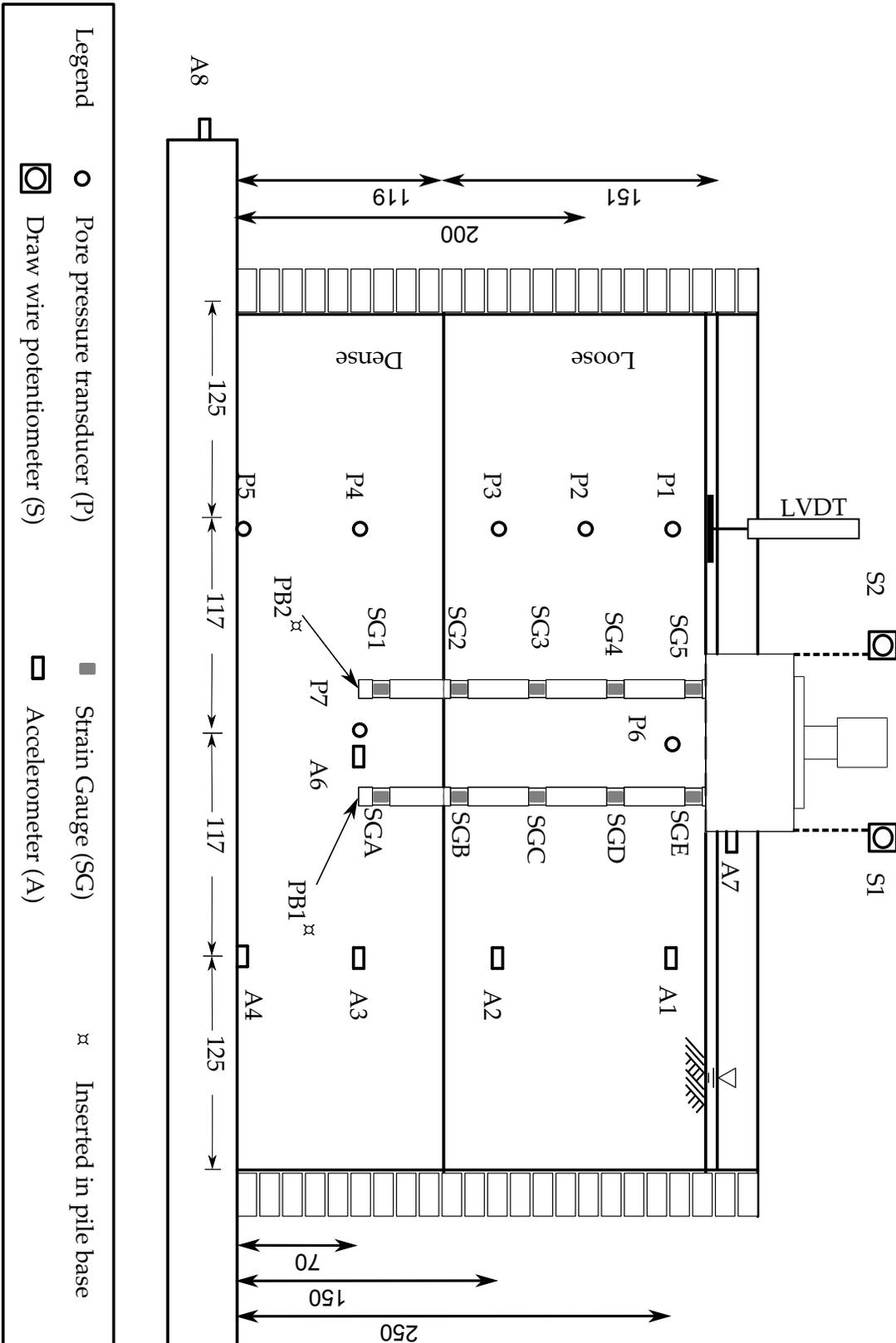
Figure A-vii: Nominal instrumentation layout for MS10 and MS12